NOTE TO USERS

THREE-DIMENSIONAL TURBULENCE MODELING FOR FREE SURFACE FLOWS

JUNYING QU

A Thesis

in

The Department

of

Building, Civil and Environmental Engineering

Presented in Partial Fulfillment of the Requirements
for the Degree of Doctor of Philosophy at
Concordia University
Montreal, Quebec, Canada

May 2005

Your file Votre référence
ISBN: 0-494-09965-8
Our file Notre référence
ISBN: 0-494-09965-8

ABSTRACT

Three-dimensional turbulence modeling for free surface flows

Junying Qu, Ph. D.

Concordia University

In engineering practice, some of the hydraulic structures encountered are used for distribution or collection of flows, measurement of flow rates or regulation of flows. It is very important to know the flow characteristics such as the mean flow pattern, the velocity distributions, and the pressure distribution in closed conduits or the water surface profiles in open channels. These flow characteristics can be obtained using experimental methods, exact theoretical methods or numerical methods.

Existing commercial codes have some limitations. For instance, the memory requirements and execution time are often excessive for solving hydraulic engineering problems. The boundary conditions to be used are rigidly specified in the software. The CFD software is also very expensive. It is beneficial to develop and validate a new numerical model that can speedily solve the specific problems in hydraulic engineering as mentioned earlier.

The present study develops and validates an efficient and accurate numerical turbulence model to simulate common hydraulic problems. The three-dimensional governing equations include the Reynolds-averaged Navier-Stokes (RANS) equations and the two–equation turbulence models such as the k-ω model and the k-ε model. The Volume of fluid (VOF) scheme is also incorporated to capture the free surface profiles in open

channel flows. For solving typical problems, the model developed presently needs much shorter execution time and requires less memory than the commercial code. For instance, to simulate open channel junction flows, the general-purpose commercial code (FLUENT) program required 30 days on the PC to reach the solution. The present model required about 4 days of execution time to solve the same problem.

To begin with, dividing and combining flows in rectangular closed conduits are simulated, as these flows are simpler than their counterparts in open channel flows. These simulations are later extended to two and three-dimensional flows that have free surfaces. The simulation results provide pressure distributions in closed conduits and water surface profiles in open channels besides velocity distributions and flow patterns. The results also yield zones of flow separations in expanding flows and stagnation zones in dividing and combining flows. The predictions of the simulations are validated using existing test data. Especially, for three-dimensional dividing flows in open channels, new test data are also obtained for the present model validation. For the lateral weir flows, the nonlinear partial least square method is used to obtain the functional relationship among the principle weir flow parameters.

The free surface turbulence model is developed and validated using the experimental data related to a number of flow situations encountered in hydraulic engineering practice. Hence, it is an efficient and useful tool to predict the flow characteristics of many such hydraulic flow systems. Due to their lower time demand and lower cost, the properly validated numerical models are preferred to experimental methods in predicting the characteristics of flows in which the range of flow variables can vary widely.

ACKNOWLEDGEMENTS

I would like to thank my supervisors, Dr. A.S. Ramamurthy and Dr. Diep Vo for suggesting the research topic. I would like to thank Dr. Sotiropoulos and Dr. Carballada for suggesting improvements to the thesis.

I also wish to thank Mr. N. Lang, B. Cooper and my colleagues for their assistance. Finally, I take the opportunity to thank my family and my friends for their support and interest throughout the research. Especially, I should thank to my wife Weifan Zhu and my father-in-law Wenqi Zhu and my mother-in-law Yuxian Zhang for their tremendous support during my stay at Concordia University.

TABLE OF CONTENTS

LIST OF FIGURES

LIST OF TABLES

NOTATIONS AND ABBREVIATIONS

1. Common notations

c = Void fraction;

F_r = Froude number;

g = Acceleration due to gravity;

p = Pressure;

Q = Discharge;

Q_r = Discharge ratio;

R = Hydraulic radius;

R_e = Reynolds number;

t = Time;

u = Axial velocity (parallel to the horizontal conduit wall);

u_τ = Resultant friction velocity;

U_i or V_i = Average flow velocity;

u_j = Average flow velocity (j = 1, 2 in two dimension, or j = 1, 2, 3 in three dimensions);

x_i = Cartesian coordinate (i=1, 2 in two dimension, or i=1, 2, 3 in three dimensions);

X, Y and Z = Coordinates at three dimensions;

y = Normal distance to the wall;

y_c = Critical depth;

y_e = End depth;

ρ = Density;

ν = Kinematic viscosity.

μ = Dynamic viscosity;

γ = Specific weight;

k = Turbulent kinetic energy;

ω = Specific dissipation rate;

ε = Dissipation rate;

2. Notations for the slot

B = Height of the main conduit;

C_d = Slot discharge coefficient;

D = Width (Span wise) of the main slot;

L = Width of the slot;

Q_1, Q_2, Q_3 = Discharges in the upstream main conduit, downstream main conduit and through the slot;

v = Vertical velocity;

V_1, V_2, V_3 = Mean axial velocities upstream of slot, downstream of slot and at the slot;

z = Distance in the span wise direction;

q = Discharges of the open channel upstream of the slot in unit width;

3. Notations for the free overfall

Fe = Froude number at end section;

q = Discharges for unit width;

U_e = Average horizontal velocity at the brink;

u_j = Average flow velocity (j = 1, 2 in two dimensions);

v = Vertical velocity component;

x = Longitudinal distance;

$X = x/y_e$ non-dimensional channel length in terms of y_e;

x_j = Cartesian coordinate (j = 1, 2 in two dimensions);

$Y = y/y_e$ non-dimensional flow depth in terms of y_e;

y^* = Local depth of the flow;

4. Notations for the side weir

a_{ij} = constants;

C_d = Discharge coefficient;

C_m = discharge coefficient (De Marchi 1934);

D = Diameter of the circular channel or width of the rectangular channel;

f = dependent variables;

F_1 = Froude number upstream;

g_i = polynomials;

L = Width of the side weir;

Q_s = Discharge of side weir;

q_s = Discharge over the side weir per unit length;

S = Height of the weir crest;

V_1 = Mean velocity upstream of the side weir;

x = Distance from the beginning of the side weir;

y = Flow depth at the section x;

Y_1 = Flow depth upstream;

η_0 = jet velocity parameters;

5. Notations for dividing and combining flows

A_1, A_2, A_3 = Cross section area at sections 1 (upstream of the main channel), 2 (downstream of the main channel) and 3 (the branch channel), respectively;

B= Width of the main channel (conduit);

Cc = Contraction coefficient;

E_1, E_2, E_3 = Total energy at sections 1, 2 and 3, respectively;

F_u = Froude number at upstream section of the main channel;

K_{12} = Loss of energy from section 1 to section 2;

K_{32} = Loss of energy from section 3 to section 2;

K_p = Loss of power from combining flows;

L = Width of the branch conduit;

p_1, p_2, p_3 = Pressure at sections 1, 2 and 3, respectively;

Q_1, Q_2, Q_3 = Discharge at sections 1, 2 and 3, respectively;

Q_b = Discharge of the branch channel;

Q_d = Discharge of the downstream main channel;

Q_u = Discharge of the upstream main channel;

Q_{rd} = Main-channel upstream-to-downstream discharge ratio Q_d/Q_u;

V_1, V_2, V_3 = Average flow velocity at sections 1, 2 and 3, respectively;

u, v and w = Velocity components in the X, Y and Z direction, respectively;

u*, v* and w* = Dimensionless velocity components in the X*, Y* and Z* directions, respectively;

V = Mean velocity;

X*, Y* and Z* = Coordinates at three dimensions in dimensionless units;

Y_b = Flow depth in the branch channel;

Y_d = Flow depth in the downstream of the main channel;

Y_u = Flow depth in the upstream of the main channel;

δ = Average Entry Angle.

6. Common abbreviations

1D – One-dimensional

2D - Two-dimensional

3D – Three-dimensional

CDS - Central difference scheme

CFD - Computation fluid dynamics

CV – Control volume

DCS - Deferred correction scheme

FVM - Finite volume method

PISO - Pressure implicit splitting of operator

PLS - Partial least squares

QUICK - Quadratic upwind interpolation for convective kinematics

RANS - Reynolds averaged Navier-Stokes

SIMPLE – Simi-implicit method for pressure-linked equation

UDS - Upwind difference scheme

VOF - Volume of fluid

CHAPTER 1

INTRODUCTION

1. 1 GENERAL REMARKS

In engineering practice, some of the hydraulic structures encountered are used for distribution or collection of flows, measurement of flow rates or regulation of flows. Dividing and combining flows are usually seen in the design of open channels and closed conduits in water and wastewater treatment plants, water distribution networks and irrigation units. The free overfall is the simplest flow-measuring device used in irrigation units. Lateral weirs are commonly used to regulate flows in open channels.

It is very important to know the flow characteristics such as the mean flow pattern, the velocity distributions, as also the pressure distribution in closed conduits or the water surface profiles in open channels. These flow characteristics can be obtained using experimental methods and numerical methods. Earlier due to the limitations of the computing hardware, only simple hydraulic problems were solved using numerical methods. Due to the advances in computer hardware and computing techniques, more complex problems in hydraulic engineering can be solved numerically.

Most flows in hydraulics are turbulent, highly unsteady and three-dimensional (3D). The Navier-Stokes equations are part of the governing equations for turbulent flow. Numerical methods are very important ways to investigate the flow characteristics of turbulent flow. Turbulence modeling is frequently used now to solve hydraulic problems. Computational fluid dynamics (CFD) deals with general procedure to solve fluid flow problems.

1. 2 LITERATURE REVIEW

1.2.1 Numerical models

Because Navier-stokes equations are high-order, nonlinear and multivariate, we cannot get the general solution. Usually, numerical solutions are sought for specific problems. Most flows encountered in engineering practice are turbulent. Because of the complications in turbulent flows, a simplified turbulent model is developed and applied to solve practical problems.

The most accurate numerical model is the direct numerical simulation (DNS) method in which the Navier-stokes equations are solved for all scales of motions in a turbulent flow field (Wilcox 2000). The results of the DNS contain very detailed information about the flow. But it requires a huge storage of data. The DNS is too expensive to be employed.

The second most accurate numerical model is the large eddy simulation method, which solves for the large-scale motions of the flow while modeling only the small scales of motions. The storage demands for LES are less than those for DNS. But, LES still needs high-efficiency computers. LES holds the promise as a future design tool, especially as computers continue to increase in speed and memory.

The most popular turbulence model is the Reynolds averaged Navier-Stokes (RANS) model. Based on the Boussinesq approximation, the two-equation models (k-ε and k-ω models) are applied. Beyond the Boussinesq approximation, stress transport model is used. Although stress transport model includes the anisotropic turbulence quantities, only a few investigators (Lasher and Taulbee 1994, Sotiropoulos and Patel 1995) have used

this model in hydraulic engineering. Many researchers prefer to two-equation RANS models.

For unsteady flows, the time dependent or unsteady Reynolds averaged Navier-Stokes (URANS) equations should be considered. Here the averaging time is greater than the characteristics timescale of turbulence and smaller than the characteristics period for the time evolution of the mean properties (Deck et al 2002). For flows with large separation, boundary layers are simulated based on RANS and separation zones are based on LES. This hybrid technique denoted as detached eddy simulation (DES) is proposed Spalart et al. (1997). However, UANS and DES will be more commonly used in the future after achieving higher computer hardware improvements.

1.2.2 Floor slots in closed conduits

The flow past a floor slot located in a closed rectangular conduit is found applications for distributing flows in engineering practices. Mitchell (1890) used the ideal flow theory to study the behavior of slot flows. McNown and Hsu (1951) studied the slot discharge coefficient using existing hydrodynamic models. Ramamurthy and Carballada (1979) studied the characteristics of closed conduit flow past a slot fitted with a barrier. Ramamurthy et al. (1994) experimentally investigated the flow characteristics of floor slots in rectangular closed conduits and obtained experimental data related to typical velocity distributions in the closed conduit at sections upstream and downstream of the slot. However, the numerical study of the floor slots in closed conduits is not done until now.

1.2.3 Floor slots in open channels

A number of studies have been conducted to analyze the behavior of flow past a floor slot in open channels. Chow (1959) presented a summary of the earlier studies related to flow past a floor slot. Venkataraman (1977, 1978) studied the slot flow problem analytically and experimentally and presented free surface profiles for various widths of the slot located in rectangular open channels. Nasser et al. (1980) determined the coefficient of discharge for the lateral outflow through a rectangular slot. Ramamurthy and Satish (1986) experimentally studied the effect of the ratio of slot width to flow depth on the slot discharge and obtained the pressure and velocity distributions at different locations. Recently, Mohapatra et al. (2001) presented a numerical study of open channel floor slot flows based on inviscid flow assumption. Compared to the existing experimental data (Ramamurthy and Satish 1986), they provided a good prediction of the pressure distribution. However, the model was not able to predict the velocity distribution very well.

1.2.4 Free overfall

The free overfall in a rectangular open channel serves as a discharge-measuring device. Rouse (1936) presented the classical result that the end depth ratio (EDR) $y_e/y_c = 0.715$. Rajaratnam and Muralidhar (1968) experimentally investigated the free overfall in rectangular channels and provided the free surface profile, the distributions of velocity and pressure in the upstream region of the brink depth. Hager (1983) and Marchi (1993) obtained the surface profiles for the free overfall in a rectangular channel. Ferro (1999) theoretically obtained the end-depth-discharge relationship for flow in rectangular, triangular and trapezoidal channels. Khan and Steffler (1996) studied the flow

characteristics of free overfall in a rectangular open channel using the depth-averaged momentum equation. Again, Mohapatra et al. (2001) presented a numerical study of free overfall in open channels based on inviscid flow assumption.

For commonly used trapezoidal channels, the end depth-discharge relation has been studied by only a very few investigators. In the discussion of a paper by Diskin (1961), Replogle (1962) studied the end depth–discharge relation. Rajaratnam and Muralidhar (1970) experimentally investigated the relation between end depth and discharge rate in trapezoidal channels for varying slopes. Keller and Fong (1989) firstly considered the end depth pressure force in the momentum equation. Recently, Ramamurthy et al. (2004) and Zhai (2003) provided flow velocity, pressure head and surface profiles for free overfall flows in trapezoidal channels.

1.2.5 Combining flows in closed conduits

Based on experimental data, various energy loss coefficients have been proposed for flow past junctions of circular closed conduits (McNown 1954; Gardel 1957; Blaisdell and Manson 1963; Ito and Imai 1973) and rectangular closed conduits (Ramamurthy and Zhu, 1997). Bajura's (1971) concept of pressure recovery factor is useful in analyzing dividing and combining flow problems of practical significance. Very recently, Huang et al. (2002) simulated combining flows in open channels and validated the 3D numerical model using the existing experimental data provided by Weber et al. (2001).

1.2.6 Dividing flows

Dividing flows are encountered often in environmental engineering and hydraulic engineering. Popp and Sallet (1983) used LDV to obtain the velocity field data for dividing flows past rectangular tee junctions. Fu et al. (1992) studied the dividing flows

in manifolds using the k-ε model and verified the predictions using test data in which laser Doppler Anemometry (LDA) was used. Ramamurthy and Zhu (1996) provided experimental data for dividing flows in 90° junctions of rectangular closed conduits.

The first detailed experimental study of dividing flows in open channels was done by Taylor (1944). Grace and Priest (1958) presented experimental results for the division of flow at different width ratios of the branch channel orientation to the main channel. Law and Reynolds (1966) investigated the problem of dividing flows using analytical and experimental methods. Ramamurthy et al. (1990) obtained an expression for the momentum transfer rate from the main to the branch channel. Hager (1984, 1992) studied the energy-loss coefficient for branch channel flows. Neary and Odgaard (1993) examined the effects of bed roughness on the three-dimensional structure of dividing flows. For low Froude number flows, they presented detailed velocity-vector and particle-trace plots in the initial part of the separation zone. Their measurements indicated no depth variations in the junction (Neary and Odgaard 1995). Neary et al. (1996) presented the numerical simulation of dividing flows under laminar flow conditions. Also, Neary et al. (1999) numerically investigated the lateral-intake inflows using two-equation turbulence model without considering the water surface effects. Hsu et al. (2002) presented a depth-discharge relationship and energy-loss coefficient for dividing flows in a narrow aspect ratio channel. Till now, experimental and numerical studies related to 3D mean velocity components and water surface profiles for dividing flows in open channels are not available.

1.2.7 Side weirs

Rectangular side weirs are used usually in irrigation and urban sewer systems for the purpose of flow regulation. De Marchi (1934) firstly studied side weir problems and defined the discharge coefficient C_m, which is called De Marchi's coefficient. Following De Marchi's idea, many investigators (Subramanya and Awasthy 1972, Nadesmoorthy and Thomson 1972, Yu-Tech 1972, Ranga Raju et al. 1979, Hager 1987, Singh et al. 1994 and Borghei et al. 1999) provided empirical equations for C_m. Ramamurthy and Carballada (1980) obtained the new discharge coefficient for side weirs in rectangular channels using a different way. Muslu (2001, 2002 and 2003) investigated the weir flow characteristics.

However, only Uyumaz and Muslu (1985) and Ramamurthy et al. (1995) have presented the theoretical and experimental study for flow over a side weir in circular channels.

1. 3 RESEARCH OBJECTIVES

The primary objective of this study is to develop, validate and demonstrate an efficient and accurate numerical turbulence model to simulate several common hydraulic problems. The Reynolds-averaged Navier-Stokes (RANS) equations and the two–equation turbulence models are used in the development of the model. The Volume of fluid (VOF) scheme is adopted to capture the free surface profiles in open channel flows. The flow characteristics of these flows include the velocity distributions besides the pressure distributions in conduits and the free surface profiles in open channel. These are obtained using the present numerical methods. Specifically, the following topics are studied in this thesis:

Numerical model for flow past a slot in a rectangular conduit (chapter 3): The 3D two-equation k-ω turbulence model is applied to obtain the characteristics of flow past a rectangular floor slot located in a rectangular closed conduit and the predictions are validated using existing experimental data.

3D simulation of dividing flows in 90° rectangular closed conduits (chapter 4): The 3D k-ω model based on RANS equations is used to find the mean flow characteristics of dividing flows in 90° rectangular conduit junctions and the results are validated using experimental data.

3D simulation of combining flows in 90° rectangular closed conduits (chapter 5): For combining flows in 90° rectangular conduit junctions, the 3D k-ω model based on RANS equations is used to find the mean flow characteristics and the results are validated using test data.

2D simulation of flow past an open channel floor slot (chapter 6): The free surface turbulence model is applied to obtain the flow characteristics and the predictions are validated using previous experimental data.

2D VOF model for numerical simulation of a free overfall (chapter 7): The VOF (VOF) turbulence model is applied to obtain the flow parameters of free overfall in rectangular channels. The predictions of the proposed numerical model are validated using existing experimental data for both subcritical and supercritical flow conditions. Base on the path followed by a fluid particle leaving the brink, the equations for nappe profiles in supercritical flows are obtained in terms of the end depth.

3D VOF model for simulation of a free overfall in trapezoidal channels (chapter 8): The VOF model is applied to obtain the flow characteristics of 3D open channel flows involving free surfaces. The predictions of the proposed model are validated using existing experimental data.

Experimental studies of dividing flows in open channels (chapter 9): Dividing flows in open channels are commonly encountered in hydraulic engineering. These flows are inherently 3D in character. In this study, experimental results are obtained for flow characteristics of dividing flow in a 90°, rectangular open-channel junction formed by channels of equal width. Depth measurements were made using point gages while velocity measurements were obtained using a 2D Dantec laser Doppler Anemometer (LDA) over grids defined throughout the junction region. This study presents the details of the experimental procedures and the flow characteristics.

3D modeling of dividing flows in open channels (chapter 10): The numerical model for dividing flows in open channels is developed. The 3D k-ω free surface turbulence model is applied to determine the mean flow characteristics of dividing flows in 90° rectangular open channel junctions. The predicted results are compared with the present experimental data.

Side weir flows (chapter 11): The multivariable nonlinear PLS method is adopted to determine the accurate functional relationship between the weir discharge coefficient and several of the weir flow parameters for flow past side weirs in rectangular channels and circular channels. A very brief study related to the simulation of flow past a side weir in a rectangular channel is presented.

CHAPTER 2

NUMERICAL METHODS

2.1 INTRODUCTION

For turbulent and incompressible fluid flows, the governing equations including the Reynolds-averaged Navier-Stokes (RANS) equations and the two–equation turbulence model are presented in this chapter. The boundary conditions for the free surface model and the wall function are described. Details of the numerical algorithm are shown in the following sections.

2. 2 RANS MODEL

In the Reynolds-averaged approaches to turbulence, all the unsteadiness is averaged out assuming that the unsteadiness is regarded as part of turbulence. The Reynolds averaged Navier-Stokes equation (RANS) is shown,

$$\frac{\partial U_i}{\partial t} + U_j \frac{\partial U_i}{\partial x_j} = -\frac{\partial p}{\partial x_i} + \frac{\partial}{\partial x_j}(2\nu S_{ji} - \overline{u_j' u_i'}) \tag{2.1}$$

where p = pressure, t = time, U_i = velocity in x_i direction, the subscript i=1, 2, 3 and j=1, 2, 3.

Also, the continuity equation is: $\frac{\partial U_i}{\partial x_i} = 0$ (2.2)

The two-equation models are the most popular turbulence models in the numerical simulation of turbulent flows. The two-equation models are based on the Boussinesq eddy-viscosity approximation, which assumes that the principal axes of the Reynolds stress tensor τ_{ij} are coincident with those of the mean strain-rate tensor s_{ij} at all of the

points in a turbulent flow. The coefficient of proportionality between τ_{ij} and s_{ij} is the eddy viscosity ν_T. The specific Reynolds stress tensor based on the Boussinesq assumption is:

$$\tau_{ij} = -\overline{u_i' u_j'} = \nu_T S_{ij} - \frac{2}{3} k \delta_{ij} \tag{2.3}$$

In the two-equation models, both the k–ε model and the k-ω model are most widely used.

2. 2. 1 Wilcox (1998) *k*-ω model:

Kinetic Eddy Viscosity: $\nu_T = k/\omega$ (2.4)

Turbulence kinetic energy:

$$\frac{\partial k}{\partial t} + U_j \frac{\partial k}{\partial x_j} = \tau_{ij} \frac{\partial U_i}{\partial x_j} - \beta^* k\omega + \frac{\partial}{\partial x_j}\left[(\nu + \sigma^* \nu_T)\frac{\partial k}{\partial x_j}\right] \tag{2.5}$$

Specific dissipation rate:

$$\frac{\partial \omega}{\partial t} + U_j \frac{\partial \omega}{\partial x_j} = \alpha \frac{\omega}{k} \tau_{ij} \frac{\partial U_i}{\partial x_j} - \beta \omega^2 + \frac{\partial}{\partial x_j}\left[(\nu + \sigma \nu_T)\frac{\partial \omega}{\partial x_j}\right] \tag{2.6}$$

Closure coefficients and auxiliary relations:

$$\alpha = \frac{13}{15}, \quad \beta = \beta_0 f_\beta, \quad \beta^* = \beta_0 * f_{\beta^*}, \quad \sigma = \frac{1}{2}, \quad \sigma^* = \frac{1}{2} \tag{2.7}$$

$$\beta_0 = \frac{9}{125}, \quad f_\beta = \frac{1 + 70 x_\omega}{1 + 80 x_\omega}, \quad x_\omega = \left|\frac{\Omega_{ij}\Omega_{jk}S_{ki}}{(\beta_0 * \omega)^3}\right| \tag{2.8}$$

$$\beta_0^* = \frac{9}{100}, \quad f_{\beta^*} = \begin{cases} 1, & x_k \le 0 \\ \dfrac{1 + 680 x_k^2}{1 + 400 x_k^2}, & x_k > 0 \end{cases}, \quad x_k \equiv \frac{1}{\omega^3}\frac{\partial k}{\partial x_j}\frac{\partial \omega}{\partial x_j} \tag{2.9}$$

$$\varepsilon = \beta^* \omega k \qquad \text{and} \qquad l = k^{1/2} / \omega \tag{2.10}$$

$$\Omega_{ij} = \frac{1}{2}\left(\frac{\partial U_i}{\partial x_j} - \frac{\partial U_j}{\partial x_i}\right), \qquad S_{ij} = \frac{1}{2}\left(\frac{\partial U_i}{\partial x_j} + \frac{\partial U_j}{\partial x_i}\right) \tag{2.11}$$

2. 2. 2 Standard $k - \varepsilon$ model:

Kinetic Eddy Viscosity: $\nu_T = C_\mu k^2 / \varepsilon$ (2.12)

Turbulence kinetic energy:

$$\frac{\partial k}{\partial t} + U_j \frac{\partial k}{\partial x_j} = \tau_{ij} \frac{\partial U_i}{\partial x_j} - \varepsilon + \frac{\partial}{\partial x_j}\left[(\nu + \nu_T / \sigma_k)\frac{\partial k}{\partial x_j}\right] \tag{2.13}$$

Dissipation rate:

$$\frac{\partial \varepsilon}{\partial t} + U_j \frac{\partial \varepsilon}{\partial x_j} = C_{\varepsilon 1} \frac{\varepsilon}{k} \tau_{ij} \frac{\partial U_i}{\partial x_j} - C_{\varepsilon 1} \frac{\varepsilon^2}{k} + \frac{\partial}{\partial x_j}\left[(\nu + \nu_T / \sigma_\varepsilon)\frac{\partial \omega}{\partial x_j}\right] \tag{2.14}$$

Closure coefficients and auxiliary relations:

$$C_{\varepsilon 1} = 1.44, \quad C_{\varepsilon 2} = 1.92, \quad C_\mu = 0.09, \quad \sigma_k = 1.0, \quad \sigma_\varepsilon = 1.3 \tag{2.15}$$

$$\omega = \varepsilon / (C_\mu k) \quad \text{and} \quad l = C_\mu k^{3/2} / \varepsilon \tag{2.16}$$

2. 3 BOUNDARY CONDITIONS

2. 3. 1 Wall functions

At the wall boundary, the wall-function approach proposed by Launder and Spalding (1974) is used for the two-equation turbulence modeling. The universal logarithmic law

of the wall with smooth surfaces that is applicable to the fully turbulent region outside the viscous sublayer is expressed as

$$\frac{u}{u_\tau} = \frac{1}{\kappa} \ln \frac{u_\tau y}{\nu} + C \qquad (2.17)$$

where, u = resultant velocity parallel to the wall at the first cell, u_τ = resultant friction velocity, $k = 0.41$, y = normal distance to the wall, ν = Kinematic viscosity and $C = 5.0$ for smooth surfaces. For rough surfaces, one has to consider the effects of roughness of the wall surface and the constant C should be changed. For fully rough wall, Eq. (2.18) must be considered,

$$\frac{u}{u_\tau} = \frac{1}{\kappa} \ln \frac{y}{k_s} + 8.5 \qquad (2.18)$$

Here k_s denotes the average height of surface roughness.

Eq. (2.19) should be considered while dealing with the k-w model (Wilcox 1994 and 2000, Neary et al. 1999).

$$\omega = S_R \frac{u_\tau^2}{\nu} \qquad (2.19)$$

where,

$$S_R = \begin{cases} \left(\frac{50}{k_s^+}\right), & k_s^+ < 25 \\ \left(\frac{100}{k_s^+}\right), & k_s^+ \geq 25 \end{cases} \quad \text{and} \quad k_s^+ = \frac{u_\tau k_s}{\nu}$$

The near wall values of turbulent kinetic energy k and the specific dissipation rate are specified assuming local equilibrium of turbulence (Wilcox 2000):

$$k = \frac{u_\tau^{\,2}}{\sqrt{\beta_o^*}}, \quad \omega = \frac{u_\tau}{\sqrt{\beta_o^*}\kappa y}, \varepsilon = \left(\beta_o^*\right)^{3/4} \frac{k^{3/2}}{\kappa y} \quad \text{where } \beta_0^* = \frac{9}{100} \tag{2. 20}$$

It is noted that during the numerical simulation the grid cells next to the wall boundary are constructed well within the turbulent region $30 < y^+ \equiv \frac{u_\tau y}{\nu} < 130$ (Rameshwaran and Naden 2003).

2. 3. 2 Free surface boundaries

For numerical simulations related to open channel flows, the free surface condition should be considered. The free surface elevation can be assumed horizontal if the water surface deformation is not large. This is the solid lid approximation. In most cases, it is necessary to know the shape of the free surface. Many methods have been used to find the shape of a free surface. They can be simply classified into two major groups (Ferziger and Peric, 2002).

Interface-Tracking Scheme

This method defines the free surface as a sharp interface. The motion of the free surface has to be traced in the computation. Boundary-fitted grids are used, and they are readjusted each time the free surface is moved. In order to get trace of a sharp interface, very small time steps and grids should be used.

At the free surface, the boundary for the vertical velocity, however, is determined by satisfying the free-surface kinematic condition (in Cartesian coordinates), i.e.,

$$u_z = \frac{\partial H}{\partial t} + u_x \frac{\partial H}{\partial x} + u_y \frac{\partial H}{\partial y} \tag{2. 21}$$

where u_x, u_y, and u_z denote flow velocity in x-direction, y-direction, and z-direction, respectively. H denotes the water depth, and t denotes time.

The pressure variable p is defined as a deviation from the hydraulic pressure, that is,

$$p = p_0 + gH \tag{2. 22}$$

where p_0 denotes the pressure of free surface, and g denotes the specific gravity. This scheme is applied in the numerical simulation of some flow cases (Meselhe and Sotiropoulos 2000, Huang et al. 2002).

Interface-Capturing Scheme

This interface-capturing method does not define a sharp boundary. The computation is performed on a fixed grid. The motions of the water surface are limited in the grid geometry. The shape of the free surface is determined by cells that are partially filled.

The interface-capture method is easier than the interface-tracking method for computation. One need not change the grid during the simulation, which saves lots of times. The typical scheme in the interface-capture method is the volume of fluid (VOF) scheme. This scheme is used by many researchers (Mohapatra et al. 2001, Chen et al. 2002 and Maronnier et al. 2003). Here, the VOF scheme is introduced.

For the VOF scheme, one has to introduce a new variable c, which is called the void fraction. The void fraction c is defined by the quantity ratio of water to air in a cell. Generally, c = 1 when the cell is filled fully by water and c = 0 when the cell is filled fully by air. The governing equation of c is follow (Ferziger and Peric 2002):

$$\frac{\partial c}{\partial t} + \frac{\partial (U_i c)}{\partial x_i} = 0 \tag{2.23}$$

Also c must satisfy the condition

$$0 \leq c \leq 1 \tag{2.24}$$

Therefore, for free surface problems, one has to solve the equation for the void fraction besides the conservation equation for mass and momentum.

Alternatively, near the free surface boundary, one can treat both fluids as a single fluid, whose properties vary in space according to the volume fraction of each phase, i.e.:

$$\phi = \phi_1 c + \phi_2 (1 - c) \tag{2.25}$$

where ϕ = density, molecular viscosity and turbulence quantities. Subscripts 1 and 2 denote the two fluids (e.g. water and air).

For the velocity components near the free surface boundary, it is assumed that the velocity of air is equal to the velocity of water. Far from the free surface boundary, the velocity is equal to zero in the air. The pressure near the free surface boundary is obtained using linear extrapolation method from the interior of the water domain.

2. 3. 3 Inlet boundaries

At the inflow boundary, the zero derivative condition is applied to velocity components and turbulence parameters. In some cases, at inflow boundary, the uniform flow condition for flow velocities and turbulence quantities is used simply. The pressure at the inlet boundary is linearly extrapolated from the interior of the domain. The water surface level can be specified or obtained using the liner extrapolation method.

2. 3. 4 Outlet boundaries

The pressure is prescribed, and is usually set to zero. The flow related data for flow velocities and turbulence quantities are obtained by using the linear extrapolation of computed values in the two adjacent interior points that are just above the exit plane. This boundary condition is also termed as the zero diffusion flux condition.

At the outlet boundary for open channel, the water surface level can be specified or obtained using the liner extrapolation method.

2. 4 NUMERICAL ALGORITHM

2. 4. 1 Finite volume methods

Finite volume method (FVM) is usually used in computational fluid dynamics. The integral forms of those governing equations as mentioned earlier, are transformed onto the computational domain and they are then discretized with the finite-volume method. The computational domain is subdivided into a finite number of small control volumes (CVs) by grids. The computational node is usually assigned to the CV center. The integral forms of those governing equations apply to each CV, as well as to the solution domain as a whole. If one sums equations for all CVs, one can obtain the global conservation equation, since the surface integral over inner CV faces cancel out. To obtain an algebraic equation for each CV, the surface and volume integrals need be approximated.

2. 4. 2. Discretization of the convective terms

Numerous forms of interpolation are available. Some are less efficient and some are less stable in the course of iteration. It is very important to choose a right interpolation

scheme. Usually, first order or second order schemes are used. Higher-order schemes, such as QUICK (Quadratic Upwind Interpolation for Convective Kinematics) and second-order upwind schemes, are possible options for high precision requirements. The upwind difference scheme (UDS) is the only approximation that unconditionally satisfies the boundedness criterion (Ferziger and Peric 2002). It is however a first order scheme, numerically diffusive, and requires very fine grids to obtain accurate solutions. The central difference scheme CDS is a second order scheme. It is more accurate, but it may produce oscillatory solutions and the convergence rate is usually slower (Ferziger and Peric 2002). The deferred correction scheme (DCS) combines the advantages of both UDS and CDS. DCS utilizes the UDS in implicit method, and the difference between UDS and CDS is calculated explicitly using values from the previous iteration.

$$F_e = F_e^{UDS} + (F_e^{CDS} - F_e^{UDS})^{old} \tag{2.26}$$

Here F represents the convective term. DCS was also mentioned by Huang (2000).

2. 4. 3 Grid generation

For a regular geometry, it is simple to choose the grid. The grid lines follow the coordinate directions. However, most flows in engineering practice involve complex geometries, which cannot be readily fitted with Cartesian grids. In order to apply such a simple grid to solution domains with inclined or curved boundaries, the boundaries have to be approximated to staircase-like steps. If this approach is used, it results in errors in the solution. Boundary-fitted-orthogonal grids and curvilinear coordinates are most often used to calculate flows in complex geometries (most commercial codes use such grids). They can be structured, block-structured, or unstructured. The advantage of such grids is

that they can be adapted to any geometry. Since the grid lines follow the boundaries, the boundary conditions are easier to implement than with the stepwise approximation of the curved boundaries. In this study, a multiblock grid method is used, which is one type of the boundary-fitted-orthogonal grids. For the multiblock grid method, the complex geometry is decomposed into several blocks. Each block is meshed with a power law function, which generates a fine mesh in the vicinity of the boundary or in the flow region where the flow changes rapidly. As mentioned in section 2.3.1, grids near the wall boundary have to satisfy the requirement of the wall function.

2. 5 DEVELOPMENT OF THE NUMERICAL MODEL

2.5.1 Discretization details

The momentum and turbulence closure equations can be typically written in general form in Cartesian Coordinates (Figs. 2.1 and 2.2),

$$\frac{\partial \Phi}{\partial t} + \frac{\partial (u\Phi)}{\partial x} + \frac{\partial (v\Phi)}{\partial y} + \frac{\partial (w\Phi)}{\partial z} - \{\frac{\partial}{\partial x}[(\nu + \nu_T)(\frac{\partial \Phi}{\partial x})] + \frac{\partial}{\partial y}[(\nu + \nu_T)(\frac{\partial \Phi}{\partial y})] + \frac{\partial}{\partial z}[(\nu + \nu_T)(\frac{\partial \Phi}{\partial z})]\} = S \tag{2.27}$$

Here,

in u-momentum equation, $\Phi = u$, $S = -\frac{\partial p}{\partial x}$

in v-momentum equation, $\Phi = v$, $S = -\frac{\partial p}{\partial y}$

in w-momentum equation, $\Phi = w$, $S = -\frac{\partial p}{\partial z}$

in k-equation, $\Phi = k, S = \tau_{ij} \frac{\partial U_i}{\partial x_j} - \beta^* k\omega$

in ω-equation, $\Phi = k, S = \alpha \frac{\omega}{k} \tau_{ij} \frac{\partial U_i}{\partial x_j} - \beta\omega^2$

in ε-equation, $\Phi = k, S = C_{\varepsilon 1} \frac{\varepsilon}{k} \tau_{ij} \frac{\partial U_i}{\partial x_j} - C_{\varepsilon 1} \frac{\varepsilon^2}{k}$

in c-equation (Eq. 2.23), $\Phi = c, S = 0$

The program employs a control-volume approach using a collocated grid. In the collocated grid, all variables are stored at the center of the control volume. In the program developed, only regular grid (cubic) is used. In brief, k -ω model is only presented.

Unsteady terms (Discretization –continued)

$$A_P|_U = \frac{1}{\Delta t}, \quad S_P|_U = \frac{1}{\Delta t} \Phi^n \tag{2.28}$$

Convective terms (Deferred Correction Schemes)

East face (Figs. 2.1 and 2.2): $A_E|_C = \frac{\min(u_e, 0)}{\Delta x}$

West face: $A_W|_C = -\frac{\max(u_w, 0)}{\Delta x}$

North face: $A_N|_C = \frac{\min(v_n, 0)}{\Delta y}$

South face: $A_S|_C = -\frac{\max(v_s, 0)}{\Delta y}$

Top face: $A_T|_C = \dfrac{\min(\ v_t,0)}{\Delta z}$

Bottom face: $A_B|_C = -\dfrac{\max(\ v_b,0)}{\Delta z}$

At central point P:

$$A_P|_C = \frac{[-\min(\ u_w,0) + \max(\ u_e,0)]}{\Delta x} + \frac{[-\min(\ v_s,0) + \max(\ v_n,0)]}{\Delta y} + \frac{[-\min(\ v_b,0) + \max(\ v_t,0)]}{\Delta z}$$

$$\begin{aligned} S_P|_C = &-\{u_e[(1-ge)\Phi_P + ge\cdot\Phi_E] - (\max(u_e,0)\cdot\Phi_P + \min(u_e,0)\cdot\Phi_E)\}/\Delta x \\ &+\{u_w[(1-gw)\Phi_P + gw\cdot\Phi_W] - (\max(u_w,0)\cdot\Phi_W + \min(u_w,0)\cdot\Phi_P)\}/\Delta x \\ &-\{v_n[(1-gn)\Phi_P + gn\cdot\Phi_N] - (\max(v_n,0)\cdot\Phi_P + \min(v_n,0)\cdot\Phi_N)\}/\Delta y \\ &+\{v_s[(1-gs)\Phi_P + gs\cdot\Phi_S] - (\max(v_s,0)\cdot\Phi_S + \min(v_s,0)\cdot\Phi_P)\}/\Delta y \\ &+\{v_t[(1-gt)\Phi_P + gt\cdot\Phi_T] - (\max(v_t,0)\cdot\Phi_P + \min(v_t,0)\cdot\Phi_T)\}/\Delta z \\ &+\{v_b[(1-gb)\Phi_P + gb\cdot\Phi_B] - (\max(v_b,0)\cdot\Phi_B + \min(v_b,0)\cdot\Phi_P)\}/\Delta z \end{aligned}$$

in which

$$ge = \frac{\Delta_y\cdot\Delta_z}{\Delta xe},\quad gn = \frac{\Delta_x\cdot\Delta_z}{\Delta yn},\quad gt = \frac{\Delta_x\cdot\Delta_y}{\Delta zt}$$

$$gw = \frac{\Delta_y\cdot\Delta_z}{\Delta xw},\quad gs = \frac{\Delta_x\cdot\Delta_z}{\Delta ys},\quad gb = \frac{\Delta_x\cdot\Delta_y}{\Delta zb}$$

Stress terms

$$A_W|_S = -(\nu+\nu_T)_w\cdot\Delta y\cdot\Delta z\frac{1}{\Delta xw},\quad A_E|_S = -(\nu+\nu_T)_e\cdot\Delta y\cdot\Delta z\frac{1}{\Delta xe}$$

$$A_S|_S = -(\nu+\nu_T)_s\cdot\Delta x\cdot\Delta z\frac{1}{\Delta ys},\quad A_N|_S = -(\nu+\nu_T)_n\cdot\Delta x\cdot\Delta z\frac{1}{\Delta yn}$$

$$A_B\,|_S = -(\nu + \nu_T)_b \cdot \Delta x \cdot \Delta y \frac{1}{\Delta zb}\ , \quad A_T\,|_S = -(\nu + \nu_T)_t \cdot \Delta x \cdot \Delta y \frac{1}{\Delta zt}$$

$$A_P\,|_S = -(A_W\,|_S + A_E\,|_S + A_S\,|_S + A_N\,|_S + A_B\,|_S + A_T\,|_S)$$

$$S_P\,|_S = 0$$

Source terms: (CDS)

For u-momentum $S_P\,|_O = -(p_e - p_w)\cdot \Delta y \cdot \Delta z$

For v-momentum $S_P\,|_O = -(p_n - p_s)\cdot \Delta_x \cdot \Delta_z$

For w-momentum $S_P\,|_O = -(p_t - p_b)\cdot \Delta_y \cdot \Delta_x$

For k-equation $S_P\,|_O = (P)_P$, $A_P\,|_O = (\beta * \omega)_P$

For ω-equation $S_P\,|_O = (\alpha \frac{\omega}{k} P)_P$, $A_P\,|_O = (\beta\omega)_P$

Add all term together

$$A_E\,|_e = \min(u_e, 0)\cdot \Delta y \cdot \Delta z - (\nu + \nu_T)_e \cdot \Delta y \cdot \Delta z \frac{1}{\Delta xe} \tag{2.29}$$

$$A_W\,|_w = -\max(u_w, 0)\cdot \Delta y \cdot \Delta z - (\nu + \nu_T)_w \cdot \Delta y \cdot \Delta z \frac{1}{\Delta xw} \tag{2.30}$$

$$A_N\,|_n = \min(v_n, 0)\cdot \Delta x \cdot \Delta z - (\nu + \nu_T)_n \cdot \Delta x \cdot \Delta z \frac{1}{\Delta yn} \tag{2.31}$$

$$A_S\,|_s = -\max(v_s, 0)\cdot \Delta x \cdot \Delta z - (\nu + \nu_T)_s \cdot \Delta x \cdot \Delta z \frac{1}{\Delta ys} \tag{2.32}$$

$$A_T|_t = \min(w_t, 0)\cdot\Delta y\cdot\Delta x - (\nu+\nu_T)_t\cdot\Delta x\cdot\Delta y\frac{1}{\Delta zt} \tag{2.33}$$

$$A_B|_b = -\max(w_b, 0)\cdot\Delta y\cdot\Delta x - (\nu+\nu_T)_b\cdot\Delta x\cdot\Delta y\frac{1}{\Delta zb} \tag{2.34}$$

$$A_P = A_P|_U + A_P|_C + A_P|_S + A_P|_O \tag{2.35}$$

$$S_P = S_P|_U + S_P|_C + S_P|_S + S_P|_O \tag{2.36}$$

2. 5. 2 Pressure-correction methods (SIMPLE method)

In order to solve the RANS equations and obtain the variables u, v, w and p, the semi-implicit method for pressure-linked equation (SIMPLE) algorithm is employed.

The Prediction Step

When solving the momentum equation, one assumes that the pressure field P^0 from the previous iteration is known. Velocity field U^* is then predicted by solving the momentum equation, which can also be expressed as:

$$U_{iP}^* + \frac{1}{A_P}\sum A_L U_{iL}^* + \frac{1}{A_P}S_{iP} + \frac{1}{A_P}\frac{\partial p^0}{\partial x_i} = 0 \tag{2.37}$$

where the third term is the source term from the unsteady, convective and stress terms in momentum equations, and the fourth term is the original source term from the pressure gradient in the momentum equations.

The Correction Step

At this point, the velocity field with the given pressure field does not satisfy the continuity. Pressure and velocity need to be corrected to satisfy both continuity and momentum equations:

$$\frac{\partial U_i^{**}}{\partial x_i} = 0 \tag{2.38}$$

$$U_{iP}^{**} + \frac{1}{A_P}\sum A_L U_{iL}^{*} + \frac{1}{A_P} S_{iP} + \frac{1}{A_P}\frac{\partial p^{*}}{\partial x_i} = 0 \tag{2.39}$$

By substituting Eq. (2.37) from Eq. (2.39), one gets the corrected velocity, written as:

$$U_{iP}^{**} = U_{iP}^{*} - \frac{1}{A_P^i}\frac{\partial p'}{\partial x_i} \tag{2.40}$$

where p' is the pressure correction, defined by

$$p' = p^{*} - p^{0} \tag{2.41}$$

and the corresponding velocity correction can be introduced similarly

$$U' = U_i^{**} - U_i^{*} \tag{2.42}$$

By substituting Eq. (2.40) into Eq. (2.38), one gets the corrected pressure, written as:

$$\frac{1}{A_P^u}\frac{\partial^2 p'}{\partial x^2} + \frac{1}{A_P^v}\frac{\partial^2 p'}{\partial y^2} + \frac{1}{A_P^w}\frac{\partial^2 p'}{\partial z^2} = -\left(\frac{\partial u_P^{*}}{\partial x} + \frac{\partial v_P^{*}}{\partial y} + \frac{\partial w_P^{*}}{\partial z}\right) \tag{2.43}$$

The final discretized pressure-correction equation is written as:

$$A_W^p p'_W + A_W^p p'_W + A_P^p p'_P + A_S^p p'_S + A_N^p p'_N + A_B^p p'_B + A_T^p p'_T = S_P \tag{2.44}$$

$$A_W^p|_S=\frac{1}{\Delta x\cdot\Delta xw\cdot A_P^u},\quad A_S^p|_S=\frac{1}{\Delta y\cdot\Delta ys\cdot A_P^v},\quad A_B^p|_B=\frac{1}{\Delta z\cdot\Delta zb\cdot A_P^w}$$

$$A_E^p|_S=\frac{1}{\Delta x\cdot\Delta xe\cdot A_P^u},\quad A_N^p|_S=\frac{1}{\Delta y\cdot\Delta yn\cdot A_P^v},\quad A_T^p|_T=\frac{1}{\Delta z\cdot\Delta zt\cdot A_P^w}$$

$$A_P^p|_S=-(A_W^p|_W+A_E^p|_E+A_S^p|_S+A_N^p|_N+A_B^p|_B+A_T^p|_T)$$

$$S_P^p|_S=\frac{1}{dx}(u^*{}_e-u^*{}_w)+\frac{1}{dy}(v^*{}_n-v^*{}_s)+\frac{1}{dz}(w^*{}_t-w^*{}_b)$$

Using the SIP method, the p' is obtained. Then, one can correct u, v and w by Eq. (2.40) and get u^{**}, v^{**}, w^{**} and p^* as following,

$$U_{iP}^{**}=U_{iP}^{*}-\frac{1}{A_P^i}\frac{\partial p'}{\partial x_i} \tag{2.45}$$

$$p^*=p^0+p' \tag{2.46}$$

2. 5. 3 Solution convergence and grid sensitivity

In this study, steady flows are simulated using iteration methods. The iteration convergence is required to determine the numerical accuracy. Generally, the iteration convergence error is defined as the deference between the exact and the iterative solutions of the discretized equations. In fact, the difference between successive iterates is usually used as a measure of the error in the converged solution (Wilcox 2000). Therefore, the convergence criterion is defined to determine when to stop the process. In this study, the error of the relative residual for the iteration process is controlled at 0.1%.

A good grid is very important to reduce the discretization errors. For each simulation case, one has to check the grid sensitivity or grid independence. The most common way

to demonstrate grid sensitivity is to refine a grid with twice or half as many grid points for computation. However, the grid size is limited by some other factors such as the wall function. In order to satisfy the wall function, one has to ensure the first grid near the wall boundary in the log-low layer ($30 < y^+ \equiv \frac{u_\tau y}{\nu} < 130$) as mentioned in section 2.3.1. That is to say, for a flow with the mean water velocity U = 1.0 m/s, the size of the first grid y near the wall boundary is approximately 0.6 mm < y < 2.6 mm.

In this study, the grid independence is checked based on the convergence criterion for the region outside the wall boundary condition. Generally speaking, the discretization errors are large for a coarse grid. The grid chosen is also considered the other researchers for the similar simulation cases such as Huang et al. (2002).

For instance, the grid independence was checked for the simulation of dividing flows in closed conduits (chapter 4). The grid chosen is listed in table 4.1. If one choose half of the grid point listed in table 4.1, the error of the relative residual for the iteration process is greater than 0.8%, which is much more than the required convergence criterion (0.1%). The difference for the value of pressure and velocity between these two computations is around 5%. If one choose half of the grid point listed in table 4.1 only in Y and Z direction, the error of the relative residual for the iteration process is greater than 0.6%. The difference for the value of pressure and velocity compared to the grids (table 4.1) is around 3%. If one chooses double of the grid listed in table 4.1, the error of the relative residual for the iteration process is greater than 0.05% and the difference for the value of pressure and velocity between these two computations is around 0.5%.

2. 5. 4 Solution procedures

The solutions procedures are summarized as following:

1) Set flow parameters and choose models
2) Generate grids.
3) Set boundary conditions and initial conditions
4) Calculate the free surface for open channel flows.
5) Calculate velocities.
6) Calculate pressures.
7) Calculate turbulent quantities.
8) Repeat steps 4-7 until convergence is reached.

2. 6 DEVELOPED PROGRAMS

The program developed in this study includes the free surface model and the two-equation turbulence models. The physical source code is developed using C++ language and compiled under Visual C++ platform. It can be applied to laminar flows, turbulent flows in unsteady or steady states.

At first, the program was developed for 2D case based on the simple example program provided by Ferziger and Peric (2002). Then, the developed 2D program was used to simulate combining flows and dividing flows in closed conduits and validated with the existing experimental data.

At the second step, the program was upgraded from 2D to 3D. The numerical algorithm is mentioned in the earlier part of this chapter. The program has included the k-ω model

and $k - \varepsilon$ model. The developed 3D program was used to simulate floor slot flows, combining flows and dividing flows in closed conduits and validated the 3D program with the existing experimental data.

Based on the developed 3D program for closed conduit boundaries, the VOF scheme was added in the program for free surface boundaries. The free surface model is validated using the experimental data from Weber (2001). Then the program is used to simulate dividing flows in open channels.

Right now, many types of commercial software are used in the computation fluid dynamics (CFD) area, such as FLUENT and PHOENICS. FLUENT is widely used in engineering practice. The details of FLUENT can be obtained from the help file of FLUENT or the website www.fluent.com. The program developed in this study is compared with the result obtained from FLUENT. In most cases, they are in good agreement. However, FLUENT is used for general purposes (good for hydraulics, fluid mechanics, chemical engineering, environmental engineering etc.). It includes applications to a large number of flow configurations (hydraulic applications, fluid mechanics applications such as subsonic, supersonic and hypersonic flows, two-phase flows including cavitation, contaminant transport, mass transfer, heat transfer, pollution reactive gas flows, etc.). There are only a few boundary conditions available in FLUENT. Those boundary conditions are not satisfied for all the flow cases. For instance, for free surface flow, there is no boundary condition that can be used for the inlet boundary if the flow discharge is known and the free surface is unknown at the inlet.

The present study has developed the 3D free surface turbulence model for a specific class of hydraulic problems (regulating, controlling and measuring incompressible flows). As

such it is more efficient, less memory and execution time. It also supports more flexible boundary conditions.

For instance, the numerical study of combining flows in open channel was used to compared between using the present program and FLUENT. At the same grid geometry, same flow configurations and the same computer, it took around 30 days using FLUENT and it took 4 days using the present developed program.

However, by the time limit, the program developed in this study cannot simulate the flow problems with the multiple free surfaces in the present form. FLUENT can simulate the multiple free surfaces very well. Therefore, in this study, FLUENT is used to simulate only the problems with the multiple free surfaces as in the case of the free overfall and the lateral weirs. All the other simulations are based on the model developed in the present study.

CHAPTER 3

NUMERICAL MODEL FOR FLOW PAST A SLOT IN A RECTANGULAR CONDUIT

3. 1 INTRODUCTION

The flow past a lateral slot of length L (Fig. 3.1) located in the wall of a closed rectangular conduit of depth B finds applications in the design of equipment used for distributing flow in engineering practice (Benefield et al. 1984). Mitchell (1890) used the ideal flow theory to study the behavior of slot flow. Existing hydrodynamic models relate the slot discharge coefficient C_d with parameters such as L/B, the slot discharge Q, the total energy E ($E = V^2/2g + p/\gamma$), the jet angle and the ratio of the flow velocity (V_1) upstream of the slot to the flow velocity (V_2) downstream of the slot (McNown and Hsu 1951). Hence, the slot discharge coefficient can be expressed as $C_d = Q/(LB\sqrt{2gE})$. Ramamurthy and Carballada (1979) studied the characteristics of closed conduit flow past a slot fitted with a barrier. Based on the concept of the pressure recovery factor (Bajura 1971), several practical dividing flow models have been developed to characterize many aspects of flows through lateral outlets in open channels (Ramamurthy and Satish 1988). Experimental data related to typical velocity distributions in the closed conduit at sections upstream and downstream of the slot are presented by Ramamurthy et al. (1994).

In this chapter, the present model developed is applied to flow past a slot in a closed rectangular conduit. The 3D two-equation k-ω turbulence model is adopted for the

numerical simulation. The results of the simulation are validated using the experimental data (Ramamurthy et al. 1994).

3. 2 BOUNDARY CONDITIONS

At the conduit boundary, the standard wall-function is used (chapter 2). At the inlet, known flow velocities and turbulent quantities for a uniform flow are prescribed and pressures are linearly extrapolated from the interior of the domain. At the outlet boundaries, the zero diffusion flux condition is used for velocities and turbulent quantities. At the slot outlet, the pressure is set to zero at the corner "b" (Fig. 3.1) and the rest is obtained by extrapolation method. At the outlet of the main channel, the pressure is obtained by extrapolation method while the discharge is fixed.

3. 3 EXPERIMENTAL DATA

For flow past a floor slot in a rectangular conduit, Ramamurthy and Zhu (1994) used a closed rectangular Plexiglas conduit 41.3mm x 91.5mm in cross section. It was nearly 4 m long upstream of the slot to provide a fully developed flow in the approach section. The downstream edge "*c*" (Fig. 3.1) of the slot was sharp. It was beveled to a very small angle to let the jet emerge freely. For the fixed value of conduit height B = 91.5mm, the geometry of the slots used yielded L/B = 0.11, 0.78, and 1.0. The Dantec Laser Doppler anemometry (LDA) unit permitted the measurements of the velocities in the test section. Very closely spaced 1.5 mm diameter wall taps were used to measure the pressure. The experimental data related to velocity and pressure were collected along the central line of the conduits, as the flow was assumed to be two-dimensional. However, this assumption of two dimensionality of the flow was partly verified by taking velocity profiles at

additional span wise locations (Ramamurthy et al. 1994). Details of the experimental data are available in a related publication (Zhu, 1995).

3. 4 RESULTS

Three meshes SM1 to SM3 are generated for 3 different L/B ratios (table 3.1). The flow domain is meshed with a power law function, which generates a fine mesh in the vicinity of the conduit boundary. The grid cells next to the wall boundary are constructed well within the log layer region. By specifying inlet and outlet conditions, the solution procedure is continued until convergence is achieved. To this end, the error reduction in successive steps has to be at least three order-of-magnitude.

In the present study, both the 2D and 3D models were developed. This 2D model is able to predict the velocity data of the experiments (Zhu 1995) reasonably well. However, it under predicts the pressure loss along the length of the conduit. Consequently, the available test data are compared only with the 3D simulation. It should be noted that the 3D simulation includes the frictional losses occurring at all the four sides of the conduit. As such, it agrees better with the experimental data. Although test data are available for three slot width ratios, for brevity, only data for two typical width ratios (L/B = 1.0 and L/B = 0.11) are used for validation.

3. 4. 1 Pressure distribution near the slot

Fig. 3.2 compares the computed pressure distribution for $Q_r = Q_3/Q_1 = 0.65$ and L/B = 1.0 with the test data (Ramamurthy et al. 1994). Clearly, both the computed and the experimental pressure data indicate that the model faithfully captures the acceleration along "*ab*" and the deceleration along "*cd*" and the existence of a separation zone in the

expanding flow region downstream of the slot section. Unfortunately, the experimental pressure data was not available for the region spanning the slot (Insert of Fig. 3.2). The downstream end "*c*" of the slot is considered to be the stagnation point in the computational model. In the theoretical model, the stagnation point occurs at a point slightly downstream of "*c*" (Michell 1890). The stagnation pressure at "*c*" (Insert of Fig. 3.2) recorded by the present model is close to the stagnation pressure computed on the basis of the approach flow conditions in the experiment.

Fig. 3.3 shows the comparison between the computed data and test data for the distribution of pressure when $Q_r = 0.10$ and L/B=0.11. Because the slot is very narrow in this case, the test data is less plentiful (insert Fig. 3.3) in the slot section "*bc*" (Fig. 3.1).

3. 4. 2 Profiles of velocities

Fig. 3.4 shows the comparison of the computed and experimentally determined axial and vertical velocity profiles for the slot ratio L/B = 1.0 and the discharge ratio $Q_r = 0.65$. Fig. 3.4a, and Fig. 3.4d to Fig. 3.4l refer to the velocity distribution along the conduit central line (z/D = 0.5). Test data validate the numerical model predictions.

For the conditions shown in Fig. 3.4, both Q_r and L/B are large. Hence, at the region "*cd*" on the wall opposite to the slot, the existence of the flow reversal in the expanding flow is clearly discernible in the axial velocity profiles (Figs. 3.4h to 3.4*l*). According to the experimental data, a very small reversal of flow occurs also at the point "*c*". This is not observed in the computed data for the axial velocity (u), since "*c*" is the designated stagnation point in the simulation. In reality, as stated earlier, the stagnation point in real flows is at a location slightly downstream of "*c*". The downstream slot corner "*c*" is located at X/L = 1.

Further, the axial velocity distribution for span wise locations of z/D = 0.5, z/D = 0.35 and z/D = 0.65 are also shown (Figs 3.4a, 3.4b and 3.4c) at location "*b*" (Fig. 3.1). The close agreement among the 3 profiles indicates that the approach flow conditions for the test were nearly two-dimensional.

The vertical velocity (v) increases from the location "*b*" to the location "*c*" and gets reduced in the section downstream of the slot (X/L = 1). This aspect of the flow is seen in both the experimental and the computed data except at location X/L = 0.98 (Fig. 3.4i). This disagreement between the model prediction and the test data for the vertical velocity at X/L = 0.98 is again attributed to the fact that the stagnation point is slightly downstream of c in real flows. Fig. 3.5 shows the comparison between the computed velocity profile and experimental velocity profiles for $Q_r = 0.10$ and L/B = 0.11 and the agreement is good.

3. 5 CONCLUSIONS

For flow past a slot in rectangular closed conduit, the present 3D two-equation turbulence model can reproduce the flow characteristics including flow separation. In particular, the model predictions agree well with the experimental data related to measured pressure and velocity components. The location of the stagnation point occurs just downstream of slot as predicted by the theoretical analysis (Michell 1890).

CHAPTER 4

3D SIMULATION OF DIVIDING FLOWS IN 90° RECTANGULAR CLOSED CONDUITS

4. 1 INTRODUCTION

Dividing flows in closed conduits (Fig. 4.1) are encountered often in environmental engineering and hydraulic engineering, while dealing with water and wastewater treatment plants, water distribution networks and irrigation systems. There are many variables that influence the performance of these systems. In the past, the study of dividing flows has been restricted to physical models, one-dimensional theoretical analysis or one-dimensional numerical solutions. Several studies (McNown 1954; Gardel 1957; Blaisdell and Manson 1963; Bajura 1971; Ito and Imai 1973) have provided the various energy loss coefficients for flow past junctions of circular closed conduits. Popp and Sallet (1983) used LDV to obtain the velocity field data for dividing flow past a rectangular tee junction for which the area ratio L/B = 1 (Fig. 4.1). Fu et al. (1992) studied the flows in manifolds using the k-ε model and verified the predictions using data of tests in which laser Doppler Anemometry (LDA) was used. Ramamurthy and Zhu (1996) provided experimental data for dividing flows in 90° junctions of rectangular closed conduits. Neary and Odgaard (1993) examined the effects of bed roughness on the 3D structure of a dividing flow. Neary et al. (1996) presented the numerical simulation of dividing flows under laminar flow conditions. Also, Neary et al. (1999) numerically investigated the lateral-intake inflows with rough wall using two-equation turbulence model without considering the water surface effects.

In this chapter, the present model developed is used to obtain the flow characteristics for dividing flows in 90° rectangular conduit junctions. These characteristics include the energy loss coefficients, pressure profiles, velocity profiles and the mean flow pattern. The results are validated using experimental data of Ramamurthy and Zhu (1996).

4. 2 EXPERIMENTAL DATA

The experimental data for dividing flows in 90° closed conduit junctions are presented by Ramamurthy and Zhu (1996) involving a range of area ratios and discharge ratios. Their test conduits consisted of a main conduit 6.3m long and a branch conduit 1.25 m long. The inner dimensions of the main conduit were 91.5 mm x 41.2 mm. The flow depth in the main conduit and the branch conduit were the same. For the rectangular branch conduits, three different cross sections were used to get the area ratios L/B of 1.0, 0.77, and 0.22. Here, L and B, respectively, denote the widths of the branch and main conduits (Fig. 4.1). The Dantec Laser Doppler Anemometry (LDA) unit was used to measure velocities in the test section. Very closely spaced 1.5 mm diameter wall taps were used to measure the wall pressure (Ramamurthy and Zhu 1996).

The experimental data related to mean velocities and pressure were mainly collected along the central line of the conduits, as the flow was assumed to be 2D in the test program (Ramamurthy and Zhu 1996). Details of the experimental data are available in related publications (Zhu 1995).

4. 3 BOUNDARY CONDITIONS

For the main conduit, at the inlet, known flow velocities and turbulent quantities at zero gradient condition are prescribed. At the outlet of the main conduit, the pressure is

specified as zero. Further, for mean flow velocities and turbulence quantities, the zero-gradient along the conduit flow direction is applied. At the outlet of the branch conduit, the flow parameters are obtained using the extrapolation method. At the conduit boundary, the standard wall-function is used as mentioned in chapter 2.

4. 4 SOLUTION PROCEDURES

Body fitted coordinates are used in the Cartesian frame. Mesh SM1 is generated for the chosen area ratio L/B = 0.77 (Table 4.1). The flow domain is meshed with a power law function, which generates a fine mesh in the vicinity of the conduit boundary. The grid cells adjacent to the boundary region are constructed within the fully turbulent region.

The solution procedure is continued until convergence is achieved. To this end, the error reduction in successive steps has to be at least three order-of-magnitude.

4. 5 RESULTS AND DISCUSSIONS

The model developed presently also includes the 2D version of the numerical simulation. The 2D model is able to predict the velocity data of the experiments (Ramamurthy and Zhu 1996) reasonably well. However, it slightly under predicts the pressure loss along the length of the conduit. Consequently, the available test data are compared with the 3D model. The 3D simulation includes the frictional losses occurring at all sides of the conduits. As such, it agrees better with the experimental data, where frictional losses do occur on all sides of the conduits. Although test data are available for three area ratios, for brevity, only the data for one typical area ratio (L/B = 0.77) are used for validation.

4. 5. 1 Energy loss coefficients

The coefficients K_{12} and K_{13} denoting the loss of energy from section 1 to 2 and from section 1 to 3, respectively, (Fig. 4.1) are presented below. Thus,

$$E_1 = \frac{p_1}{\rho g} + \frac{V_1^2}{2g}, \quad E_2 = \frac{p_2}{\rho g} + \frac{V_2^2}{2g}, \quad E_3 = \frac{p_3}{\rho g} + \frac{V_3^2}{2g} \tag{4.1}$$

$$K_{12} = \frac{E_1 - E_2}{\frac{V_1^2}{2g}}, \quad K_{13} = \frac{E_1 - E_3}{\frac{V_1^2}{2g}} \tag{4.2}$$

Here, ρ = density of water and g = acceleration due to gravity. The total energy, pressure, discharge, and velocity of flow are, respectively, *E, p, Q*, and *V*. Suffixes 1, 2, and 3 refer to sections 1, 2, and 3 in Fig. 4.1.

For validation, test data (Ramamurthy and Zhu 1996) related to L/B = 0.77 are used. The agreement between predicted data and test data is similar for other L/B ratios. For the rectangular conduit (L/B = 0.77), Figs. 4.2a and 4.2b show the variation of the energy loss coefficients K_{12} and K_{13} with $Q_r = Q_3/Q_1$. They indicate that the predicted values of K_{12} and K_{13} agree with the experiment data (Ramamurthy and Zhu 1996).

4. 5. 2 Pressure distributions

As stated earlier, the test data (Ramamurthy and Zhu 1996) were mainly obtained along the central line of the conduits, as the flow was assumed to be 2D in the test program. Figs. 4.3 to 4.5 present the comparison of test data with the predicted data for dividing conduit flows (L/B = 0.77 and Q_r = 0.57).

The measured wall pressure profiles along the main conduit and the branch conduit agree reasonably well with the predicted wall pressure profiles (Fig. 4.3a and 4.3b). Due to the

acceleration of the flow entering the lateral, the pressure along the near wall *ab* (Fig. 4.1) of the main conduit drops drastically at the corner *b*. Along the main conduit wall, the stagnation pressure near the corner *h* of the near wall decreases to the value of the pressure along the far wall *lm* in a short distance *hn* (Fig. 4.3a). In general, the simulation also faithfully predicts the pressures along the walls of the branch conduit (Fig. 4.3b). The recovery of pressure in the branch is slightly lower than the measured pressure (Fig. 4.3b). The predicted and the experimental wall pressure data agree well for other area ratios and discharge ratios.

4. 5. 3 Velocity profiles

Fig. 4.4a indicates that the simulation can predict the profiles of the velocity components *u* and *v* reasonable well in the main conduit. Outside the junction section, the *v*-component is relatively weak compared to the *u*-component. Again in Fig. 4.4b, there is a reasonable agreement between the predicted and experimental values of the velocity components in the branch including the existence of reverse flow. However, the simulation indicates a reverse flow in the branch up to Y/B = 3.5, while the test data (Ramamurthy and Zhu 1996) shows a reverse flow only up to Y/B = 2.5.

4. 5. 4 Mean flow patterns

Flow separation occurs when there is an abrupt change in the wall alignment away from the direction of the flow as at point *b* or when the flow encounters the adverse pressure gradient due to flow expansion as in the main conduit region *lm*, downstream of the junction (Fig. 4.5). The shape of the simulated zone of separation compares qualitatively with the separation zone of the experiment data (Ramamurthy and Zhu 1996). The

simulation clearly predicts the very low velocities along the far wall region *lm* of the main conduit. The reattachment appears to be somewhat longer in the simulation.

4. 6 CONCLUSIONS

The present turbulence model faithfully reproduces the mean flow characteristics of dividing flows of 90° junctions of rectangular closed conduits. These characteristics include the energy loss coefficients, pressure profiles, velocity profiles and the mean flow patterns. The zone of flow separation predicted by the model qualitatively agrees with the experimental data.

CHAPTER 5

3D SIMULATION OF COMBINING FLOWS IN 90° RECTANGULAR CLOSED CONDUITS

5.1 INTRODUCTION

Combining flows are encountered often in environmental engineering and hydraulic engineering, while dealing with water and wastewater treatment plants and irrigation systems. There are many variables that influence the performance of these systems. Therefore, it is very important to know the characteristics of combining flows (Fig. 5.1) in closed conduits. In the past, the study of combining flows has been restricted to physical models, one-dimensional theoretical analysis or one-dimensional numerical solutions. Based on experimental data, various energy loss coefficients have been proposed for flow past junctions of circular closed conduits (McNown 1954; Gardel 1957; Blaisdell and Manson 1963; Ito and Imai 1973) and rectangular closed conduits (Ramamurthy and Zhu, 1997). Bajura's (1971) concept of pressure recovery factor is useful in analyzing dividing and combining flow problems of practical significance. Very recently, Weber et al. (2001) preformed an extensive experimental study of 90° open channel junction flows for the purpose of providing comprehensive data needed for numerical code validation (Huang et al. 2002).

In this chapter, the present model developed is applied to combining flows in a 90° rectangular conduit junctions. The energy loss coefficients and the mean flow pattern in terms of the contraction coefficients and the mean entry angle of the branch flow into the

main were obtained for combining flows in rectangular closed conduits. The results were validated using experimental data of Ramamurthy and Zhu (1997).

5. 2 EXPERIMENTAL DATA

The experimental data for combining flows in 90° closed conduit junctions are presented by Ramamurthy and Zhu (1997) involving a range of area ratios and discharge ratios. Their test conduit consisted of a main conduit 6.3 m long and a side conduit 1.25 m long. The inner dimensions of the main rectangular conduit were 91.5 mm x 41.2 mm. For the rectangular branch conduits, three different cross sections were used to get the area ratios L/B of 1.0, 0.77, and 0.22. Here, L and B respectively denote the widths of the branch and main conduits (Fig. 5.1). The Dantec Laser Doppler Anemometry (LDA) unit was used to measure velocities in the test section. Very closely spaced 1.5 mm diameter wall taps were used to measure the wall pressure (Ramamurthy and Zhu 1997 and Zhu 1995).

The experimental data related to velocities and pressures were collected along the central line of the conduits, as the flow was assumed to be two-dimensional. Details of the experimental data are available in a related publication (Zhu 1995).

5. 3 BOUNDARY CONDITIONS

At the conduit boundary, the standard wall-function is used. At the inlet, known flow velocities and turbulent quantities for fully developed conduit flow are prescribed. At the outlet, the pressure is fixed as zero and the zero-gradient along the conduit flow direction is applied for flow velocities and turbulence quantities.

5. 4 SOLUTION PROCEDURES

Body fitted coordinates are used in the Cartesian frame. The origin "*s*" (Fig. 5.1) is chosen to be x = 0, y = 0 and z = 0. Here, z = 0 coincided with the plane of symmetry of the conduit. Three meshes SM1 to SM3 are generated for different L/B ratios (Table 1). In table 1, $X_{upstream}$ denotes the main conduit length upstream of "*b*" (x = 0, y = B) shown in Fig. 1. $X_{downstream}$ denotes the main conduit length downstream of "*e*" (x = L, y = B). $Y_{main\ conduit}$ denotes the main conduit width "*bs*". X_{branch} denotes the branch conduit width "*be*". Y_{branch} denotes the branch conduit length upstream of "*b*". The number of the grid in the Z direction is 12 (Table 5.1). For grid generation, the multi-block procedure is applied. Huang et al. (2002) present an excellent description of the general procedure to use the multi-block algorithm. The flow domain is meshed with a power law function. A very fine mesh is generated very near the conduit boundary. The grid cells adjacent to the wall boundary region are constructed within the fully turbulent region.

By specifying inlet and outlet conditions, the solution procedure is continued until convergence is achieved for all of the flow variables. To this end, the convergence (error reduction) in successive steps has to be at least three order-of-magnitudes. The results of numerical modeling were also checked for grid independence, while keeping the first grid cells within the fully turbulent region.

5. 5 RESULTS AND DISCUSSIONS

The model developed presently also includes the 2D version of the numerical simulation. The 2D model is able to predict the velocity data of the experiments (Ramamurthy and Zhu 1997) reasonably well. However, the 2D simulation under predicts the pressure loss

along the length of the conduit. Consequently, the available test data are compared only with the 3D model. The 3D simulation includes the frictional losses occurring at all the four sides of the conduits. As such, it agrees better with the experimental data, where frictional losses do occur on all the four sides of the conduits. The 2D simulation (not shown) in fact slightly under estimates the frictional losses.

5. 5. 1 Energy loss coefficients

The coefficients K_{12} and K_{32} denoting the loss of energy from section 1 to 2 and from section 3 to 2 respectively (Fig. 5.1), are presented below,

$$E_1 = \frac{p_1}{\rho g} + \frac{V_1^2}{2g}, \quad E_2 = \frac{p_2}{\rho g} + \frac{V_2^2}{2g}, \quad E_3 = \frac{p_3}{\rho g} + \frac{V_3^2}{2g} \tag{5.1}$$

$$K_{12} = \frac{E_1 - E_2}{\frac{V_2^2}{2g}}, \quad K_{32} = \frac{E_3 - E_2}{\frac{V_2^2}{2g}} \tag{5.2}$$

where, ρ = density of water and g = acceleration due to gravity. The total energy, pressure, discharge, and velocity of flow are, respectively, *E, p, Q*, and *V*. Suffixes 1, 2, and 3 refer to sections 1, 2, and 3 in Fig. 5.1. The procedure to obtain the energy loss through extrapolation of pressure profiles is described in an early publication (Ramamurthy and Zhu, 1997).

For validation, test data (Ramamurthy and Zhu, 1997) related to L/B = 0.22, 0.77 and 1.0 are used (Figs. 5.2, 5.3 and 5.4). The agreement between predicted data and test data is reasonable. For the rectangular conduit (L/B = 0.22), Figs. 5.2a and 5.2b show the variation of the energy loss coefficients K_{12} and K_{32} with $Q_r = Q_3/Q_2$. They indicate that the predicted values of K_{12} and K_{32} agree with the experiment data. Even the data for circular pipes related to junctions (Ito and Imai, 1973) has a qualitative agreement with

the predicted value of K_{12} and K_{32} (Figs. 5.4a and 5.4b). For circular pipes, the area ratios of the branch to the main conduit are used in place of L/B in Fig. 5.4.

5. 5. 2 Mean flow patterns

Figs. 5.5, 5.6 and 5.7 respectively present the comparison of pressure head data plots for combining conduit flows for various area ratios and discharge ratios. In all cases, the measured wall pressure profiles along the main conduit agree well with the predicted wall pressure profiles.

In fig. 5.5 for L/B = 0.22 and Q_3/Q_2 = 0.50, the confluence of the branch flow and the main flow leads to an increase in the pressure near the upstream junction corner "*b*" (Fig. 5.5a). The stagnation point is very close to this corner. The large drop in the pressure that occurs across section "*be*" (Fig. 5.5a) can be attributed to the increasing curvature of the streamlines from "*b*" to "*e*" (Fig. 5.8) of the branch flow that enters the main conduit. Downstream of section "*e*", the wall pressure variation is negligible (Fig. 5.5a) in the separation zone (Fig. 5.8), where velocities are very small. The simulation also captures the merging of the two wall pressure profiles along the main conduit in the region "*hmi*" and "*ef*" (Fig. 5.5a). The predictions of pressure profiles are in general very close to the test pressure data along the branch conduit walls "*cb*" and "*de*" (Fig. 5.5b). Similar observations can be made for the two other cases (Figs. 5.6 and 5.7).

For brevity, the flow patterns of the predicted data are compared with the tested data only for L/B = 0.22 and Q_3/Q_2 = 0.50 (Fig. 5.8). At corner "*e*" of the junction (Fig. 5.8b), the flow separates while entering the main conduit to form a separation region bounded by "*ek*" in the section downstream of the junction.

The lines "*ek*" and"*bl*" in the contracting section were determined by calculating the streamline boundaries for the main and branch flows assuming the flow to be two-dimensional. However, in the expanding region, the flow rapidly becomes three-dimensional. As such, the dash lines shown in Fig. 5.8 denote only the approximate streamline locations. The predicted flow pattern (Fig. 5.8b) qualitatively agrees well with the experimental flow pattern (Fig. 5.8a) in terms of the contraction coefficients and the width of the separation zone.

For further validation of the model, the velocities for L/B = 0.22 and Q_3/Q_2 = 0.50 derived from the simulation are also compared with the test data (Fig. 5.9). The predicted distributions of the velocity components u and v agree very well with the measured velocity data at various sections of X/L. Near X/L = 12, the velocity component v is quite small.

5. 5. 3 The expansion loss and contraction coefficient C_c

Most of the energy loss due to mixing occurs in the expanding section downstream of the section "*m*" in Fig. 1. The value of expansion loss K_p and C_c can be computed from Eq. (5.3) below,

$$K_p = (1-\frac{Q_3}{Q_2})K_{12} + \frac{Q_3}{Q_2}K_{32} = (\frac{1}{C_c}-1)^2 \qquad (5.3)$$

where, K_p also denotes the loss of power (Ramamurthy and Zhu, 1997) in combining flows (Fig. 5. 1). Table 5.2 lists the experimental data and the numerical results related to the contraction coefficient C_c. The agreement between the two is reasonable.

5. 5. 4 Momentum transfer and average entry angle δ

The momentum transferred by the branch to the main was determined by three independent methods (Ramamurthy and Zhu 1997). Table 5.2 shows the exit angle δ (Fig. 5.1) obtained from the experiments and from the numerical model. The result shows that the numerical data has a good agreement with the experimental data. For small A_3/A_2 and large Q_3/Q_2 values, the branch conduit essentially enters the main conduit as a jet at a large value of δ at the entry section "*eb*" (Fig. 5.8). While entering the main conduit, the lateral flow along the wall "*de*" separates at "*e*", runs parallel to the wall "*de*" for a short distance, and turns later. The lateral conduit flow along wall "*cb*" separates ahead of corner "*b*", bends to the right and enters the main at an angle (Fig. 5.8).

5. 6 CONCLUSIONS

The present 3D two-equation turbulence model faithfully reproduces the mean flow characteristics of combining flows for 90° junctions of rectangular closed conduits. The numerical results agree well with the experimental data related to pressure and velocity fields. The zone of flow separation predicted by the model qualitatively agrees with the experimental data.

CHAPTER 6

SIMULATION OF FLOW PAST AN OPEN CHANNEL FLOOR SLOT

6. 1 INTRODUCTION

Floor outlets or bottom racks are frequently used to divert flow from one stream to another stream (Fig. 6.1). Applications of floor slots also include their use as horizontal trash-racks in hydro power plants and curb outlets in streets (Brune et al. 1975 and Venkataraman 1977). An understanding of the flow behavior over bottom or floor outlets is very important for the proper design and performance of flow diversion works. A number of studies have been conducted to analye the behavior of flow in such outlets, which form part of a drainage system. Venkataraman (1977, 1978) studied the slot flow problem analytically and experimentally. For the slot flow, he obtained an expression for the angle of the diverted jet and the ratio of the upstream and downstream water depths. He also presented free surface profiles for various widths of the slot located in a 0.3 m wide rectangular channel. Nasser et al. (1980) determined the coefficient of discharge for the lateral outflow through a rectangular slot. Ramamurthy and Satish (1986) experimentally studied the effect of the ratio of slot width to flow depth on the slot discharge, and measured the pressure and velocity distributions at different locations. Chow (1959) provides a summary of the earlier studies related to flow past a floor slot.

Recently, Mohapatra et al. (2001) presented an interesting study of open channel floor slot flow using numerical simulation. They used Young's volume of fluid (Y-VOF) surface-tracking technique to predict the pressure and velocity distributions and validate

the model using the existing experimental data (Ramamurthy and Satish 1986). It provided a good prediction of the pressure distribution. However, the model based on the inviscid flow was not able to predict the experimental velocity distribution very well.

In this chapter, the RANS equations are applied to flow past a floor slot in a rectangular open channel. The 2D two-equation k–ε turbulence model is adopted for the numerical simulation. The fractional volume of fluid (VOF) method is used, which is an efficient method for treating the complicated free-surface problem. The results of simulation are validated using the experimental data (Ramamurthy and Satish 1986 and Venkataraman 1977) pertaining to surface profiles, velocities and pressure heads.

6. 2 EXPERIMENTAL DATA

For flow past a 2D floor slot, Ramamurthy and Satish (1986) used a rectangular channel that was 25.4 cm wide and 12 m long. It was made of polished stainless steel plates. Transverse rectangular slots fixed in the channel were obtained from machined Plexiglas inserts. A gradual channel transition along with screens at the channel entrance ensured stable and smooth flow in the approach section. The discharge through the slot and the main channel were measured by previously calibrated standard V-notches. The velocity and pressure distributions across the channel section were recorded at regular intervals. A 3 mm diameter Pilot tube was used to obtain the total head and a screwdriver static probe with a flattened end section was used to get the static pressure head. The experimental data related to velocity and pressure head were collected along the central line of the channels, as the flow was assumed to be two-dimensional. Details of the experimental data are available in a related publication (Satish, 1986). As stated earlier, Venkataraman

(1978) experimentally obtained the water surface profile for flow past a floor slot located in a 0.3 m wide smooth open channel.

6. 3 TURBULENCE MODEL

The proposed model solves the standard 2D Reynolds averaged continuity and Navier-Stokes equations for turbulent unsteady flow based on the two-equation k–ε model. The control volume technique is used to convert the governing equations to algebraic equations that can be solved numerically. It employs the collocated-grid approach. The pressure-velocity coupling is achieved using the PISO algorithm (Issa, 1986).

6. 4 BOUNDARY CONDITIONS

At the wall boundary, the standard wall-function is used. At the inlet (Fig. 6.2), known flow velocities and turbulent quantities are prescribed. The outlet HI far downstream from the slot section BO and the outlet TF of the slot (Fig. 6.2) are defined as pressure boundaries. This allows the water to flow out freely. All the air boundaries are defined as pressure boundaries with zero pressure head. For the free surface boundary, the VOF scheme is used as mentioned in Chapter 2.

6. 5 SOLUTION PROCEDURE

The computational domain is shown in Fig. 6.2. The channel upstream of the slot AB is 3.0 m long in the x - direction. The channel downstream of the slot QH is 1.2m long. The channel bed, ABQH (Fig. 6.2) is located at a height of 0.08m above the bottom of the computational domain. Hence, ST = GF = 0.08 m. The slot width L is set equal to 0.0192m, 0.04m, 0.055m and 0.074m. Body fitted coordinates are used in the Cartesian frame. Four meshes SM1 to SM4 are generated for various slot widths (table 6.1). The

flow domain is meshed with a power law function that generates a fine mesh in the vicinity of the channel boundary. The grid cells next to the boundary are constructed well within the turbulent region. Flow parameters for different computational cases are also shown in table 6.1. The flow mode is supercritical. Through the time-dependent simulation, the water flows on the open channel and constitutes the free surface between air and water for the specified inlet and outlet conditions.

6. 6 RESULTS

6. 6. 1 Pressure and axial velocity distribution near the slot

Fig. 6.3 compares the computed pressure and axial velocity distributions for the slot width L= 0.0192 m with the test data (Ramamurthy and Satish, 1986). The locations of stations (STNs) 1 to 5 are shown in Fig. 6.1. The deviation of the pressure head from the hydrostatic distribution (Fig. 6.3) is caused by the streamline curvature. For the sections upstream of the slot, the predicted vertical pressure head distribution is similar to the experimental pressures heads at stations 1 to 3 upstream of the slot (Fig. 6.3). The simulated pressure head at stations 4 and 5 downstream of the slot also follow the general trend of the measured pressure head except in the regions very close to the wall. The simulated axial velocity profiles at all the stations agree very well with the measured value (Fig. 6.3). The acceleration of the flow and the resulting reduction in the thickness of the boundary layer just ahead of the slot are well captured by both the test data and the simulation (STNs 2 to 3, Fig. 6.3).

6. 6. 2 Surface profile

Fig. 6.4 shows the comparison of the computed and experimentally determined surface profiles for various slot widths. For the slot width L = 0.0192m (Fig. 6.4a), the predicted surface profile compares well with the surface profile determined experimentally by Satish (1986). Figs. 6.4b, 6.4c and 6.4d compare the simulated surface profiles with the surface profile measured by Venkataraman (1978) on the basis of a large number of experiments. He used three slot widths (L = 0.040m, 0.055m and 0.740m). The comparison is very good. As expected, for the supercritical flow present in his test, the water surface decreases with the discharge per unit width in the section downstream of the slot.

6.7 CONCLUSIONS

The 2D two-equation k–ε turbulence model with the VOF method simulates faithfully the flow past a floor slot in a rectangular open channel. The existing experimental data validates the predictions of the numerical model. The data include water surface profile besides distribution of pressure head and axial velocity. The predicted water depth along the open channel can provide guidance for the design of the wall height in diversion works related to drainage systems and power channels used in hydroelectric development.

CHAPTER 7

VOF MODEL FOR A FREE OVERFALL IN RECTANGULAR CHANNELS

7. 1 INTRODUCTION

Solutions to open channel flow problems can be obtained on the basis of theoretical analysis or the analysis of experimental data. Theoretical analysis can lead to exact solutions or approximate solutions that meet the needs of practicing engineers. The recent trend is to seek solutions to open channel flow problems with the help of numerical simulation. To this end, one can use the fractional volume of fluid (VOF) method to simulate two- dimensional flow problems involving a free surface. In the present note, the free overfall in a rectangular open channel is chosen to apply the VOF procedure. The simulation predicts the surface profile and the distributions of the velocity and the pressure head at the end section and at sections upstream of the end section.

The free overfall in a rectangular open channel serves as a discharge-measuring device (Fig. 7.1). A large number of theoretical and experimental studies have been carried out to know its characteristics. Rouse (1936) presented the classical result that the end depth ratio (EDR) $y_e/y_c = 0.715$, where y_e denotes the end depth and y_c denotes the critical depth. Replogle (1962) has conducted some exploratory tests to find the flow characteristics of an overfall at the end of a rectangular channel. Rajaratnam and Muralidhar (1968) investigated the free overfall in rectangular channels and provided the experimental relations for EDR at various channel slopes. They also determined the free

surface profile, the distributions of velocity and pressure in the upstream region of the brink depth.

Hager (1983) used the extended energy and momentum equations to obtain the surface profiles for the free overfall in a rectangular channel. Marchi (1993) got an expression for the free surface profile upstream of the brink depth and the lower profile of the nappe downstream of the brink depth. Ferro (1999) theoretically obtained the end-depth-discharge relationship for flow in rectangular, triangular and trapezoidal channels.

Khan and Steffler (1996) used the depth-averaged momentum equation to determine the flow characteristics of the free overfall in a rectangular open channel. Their procedure based on the finite element method yielded a very good representation of the water surface profiles for the flow over an overfall. They assumed a linear distribution of the axial velocity. Recently, Mohapatra et al. (2001) presented an interesting study of the free overfall using numerical simulation. They used Young's volume of fluid (Y-VOF) surface-tracking technique to predict the flow characteristics. It provided a good prediction of the pressure distribution. As they used the inviscid flow relations and the free-slip boundary condition, some errors were present in the simulated velocity profiles.

In this chapter, the RANS equations are applied to solve the free overfall problem in a rectangular open channel. The 2D two-equation k–ε turbulence model is adopted for the numerical simulation. The fractional volume of fluid (VOF) method is an efficient method for treating the complicated free-surface problem. The results of simulation are validated using the experimental data (Rajaratnam and Muralidhar 1968; Rouse 1936) pertaining to surface profiles, velocities and pressure heads. The predicted surface

profiles also agree well with the theoretical results (Hager 1983; Marchi 1993) and the simulated results (Khan and Steffler 1996).

7. 2 TURBULENCE MODEL

The proposed model solves the standard equations for turbulent unsteady flow based on the two-equation k-ε model. The control volume technique is used to convert the governing equations to algebraic equations that can be solved numerically. It employs the collocated-grid approach. The pressure-velocity coupling is achieved using the PISO algorithm (Issa, 1986).

7. 3 BOUNDARY CONDITIONS

At the wall boundary, the standard wall-function (Chapter 2) is used. At the inlet BA (Fig. 7.1), known flow velocities and turbulent quantities are prescribed. Here, the uniform flow condition for the horizontal velocity is provided. The outlet HG and JG downstream from the end depth (Fig. 7.1) are defined as pressure boundaries. This allows the water to flow out freely. All the air boundaries are defined as pressure boundaries with zero pressure. For the free surface boundary, the VOF model is used as mentioned in chapter 2.

7. 4 SOLUTION PROCEDURE

The computational domain is shown in Fig. 7.1. The channel BC upstream of the end depth CD is 6.0 m long in the x - direction. The channel JG downstream of the end depth DC is 1.0 m long. The step CJ is 0.2 m high. Body fitted coordinates are used in the Cartesian frame. The flow domain is meshed with a power law function that generates a fine mesh in the vicinity of the channel boundary. The grid cells next to the boundary are

constructed well within the turbulent region. Table 7.1 provides additional details related to the grid used.

Flow parameters for different computational cases are also shown in table 7.2. Through the time-dependent simulation, the water flows on the open channel and constitutes the free surface between air and water for the specified inlet and outlet conditions.

7. 5 DISCUSSION OF RESULTS

7. 5. 1 Supercritical flows

7. 5. 1. 1 Velocity and pressure head distribution near the end depth

Figure 7.2 shows the predicted distribution of velocity and pressure head in the vicinity of the brink for the supercritical approach flow in a rectangular channel (case 2A in table 7.2). Due to the difficulties associated with accurate measurements in supercritical approach flows, the available experimental data for supercritical flows are very limited.

Figure 7.2a shows the simulated axial velocity distribution agrees well with the test data (Rajaratnam and Muralidhar 1968), although the vertical velocity distribution and the pressure head distribution data at the brink are not in very good agreement with the test results (Figs. 7.2a and 7.2b).

7. 5. 1. 2 Surface profiles

For supercritical approach flows, Fig. 7.3 shows the non-dimensional water surface profile y/y_c as a function of the channel length x/y_c. The simulated surface profiles ADF and CE agree very well with the experimental profiles (Rajaratnam and Muralidhar 1968), and the theoretical profiles (Hager 1983; Marchi 1993). Hager (1983) and Marchi (1993) provided the equation for the lower nappe profile CE. Since the horizontal

velocity u remains almost unchanged after the flow crosses the brink, the vertical distance between the upper profile DF and lower profile CE will be equal to the end depth ratio y_e/y_c. As such, the equation to the upper profile DF is also known.

One can obtain the nappe profiles DF and CE in terms of the end depth y_e. Using particle dynamics, one can obtain Eqs. 7.1 and 7.2 to denote the lower and upper nappe profiles.

$$-Y = aX^2 + bX \tag{7.1}$$

$$-Y = aX^2 + bX + 1 \tag{7.2}$$

Here, $Y = y/y_e$, $X = x/y_e$. Based on the path followed by a fluid particle leaving the point C (Fig. 7.1), one can show that $a = \frac{1}{2F_e^2}$, where $F_e = \frac{U_e}{\sqrt{gy_e}}$ and U_e = average horizontal velocity at the brink. The fitted curves for the simulated nappe profiles indicated that the coefficient b is very close to a. Hence, $a = b = \frac{1}{2F_e^2}$. Fig. 7.4 shows that the profiles based on Eqs. 7.1 and 7.2, agree well with the simulated profiles.

7. 5. 2 Subcritical flows

7. 5. 2. 1 Velocity and pressure head distribution near the end depth

For subcritical approach flow in a rectangular channel (case 1A in table 2), the predicted distributions of the axial velocity component u and the vertical velocity component v near the end depth are shown in Fig. 7.5. In Fig. 7.5, the velocity component u and v are plotted against the non-dimensional flow depth above the channel bed y/y^*. Here y^* = the local depth of the flow and $y^* = y_e$ at the brink. The results of the simulation are in very good agreement with the experimental data (Rajaratnam and Muralidhar 1968). Figures

7.5b, c and d show the distribution of the axial velocity component u for various sections upstream of the brink. The axial velocities are slightly higher in the lower regions at the brink (Fig. 7.5a). For x/y_c □ -2.23, it is seen that the streamlines curvature increases and this is reflected in the development of the v component of the flow (Figs. 7.5d to 7.5a) as x/y_c varies from 0 to -2.23.

Figure 7.6 shows the distribution of the non-dimensional vertical pressure head $p/\gamma y^*$ at various sections close to the brink with y/y^*. In Fig. 7.6, the pressure distribution obtained by the present simulation is compared with the experimental data of Rajaratnam and Muralidhar (1968). With the development of the streamline curvature beyond x/y_c = -2.23, the hydrostatic distribution of the pressure head (Fig. 7.6d) gradually changes over to the lens-like distribution at the brink (x/y_c = 0). The predicted distribution of the pressure head at the brink agrees well with the test data (Rajaratnam and Muralidhar 1968).

7. 5. 2. 2 Surface profiles

Figure 7.7 shows the non-dimensional flow depth y/y_c as a function of the non-dimensional distance x/y_c for subcritical approach flows. In Fig. 7.7, the surface profile obtained by the present simulation is compared with the theoretical profiles obtained by Hager (1983) and Marchi (1993). This figure also includes the experimental profiles determined by Rajaratnam and Muralidhar (1968), Rouse (1936), and the simulated surface profiles obtained by Khan and Steffler (1996). All these are found to agree very well with the present simulated profiles.

For a free overfall in a rectangular channel, for all subcritical approach flows, the surface profiles upstream AD of the brink collapse to a single curve (Fig. 7.7). Further, the upper

and lower nappe profiles collapse respectively to single curves DF and CE (Fig. 7.7). Lastly, the lower nappe profiles downstream of the brink also collapse to a single non-dimensional curve CE (Fig. 7.7). The vertical distance between the curves DF and CE is essentially equal to the end depth ratio. Fig. 7.7 also shows the critical depth occurs when x/y_c is close to – 4. This is in agreement with the experimental results of Kandaswamy and Rouse (1957).

7. 6 CONCLUSIONS

The 2D two-equation k-ε turbulence model together with the VOF tracking technique faithfully simulates the characteristics of flow past a free overfall in a rectangular open channel. The free overfall flow in a rectangular open channel serves as a good example of a 2D open channel flow problem for simulation. The predictions of the VOF based numerical model are validated using the existing experimental and theoretical results related to water surface profiles and distributions of the pressure head and velocity components.

Based on the path followed by a fluid particle leaving the brink, the equations for the nappe profiles in supercritical flows are obtained in terms of the end depth y_e. The predicted water surface profiles for the overfall can provide guidance for the design of the wall heights in irrigation systems.

CHAPTER 8

SIMULATION OF A FREE OVERFALL IN TRAPEZOIDAL CHANNELS

8. 1 INTRODUCTION

The free overfall in an open channel serves as a discharge-measuring device in irrigation systems. For the commonly used trapezoidal channel, the end depth-discharge relation has been studied by only a very few investigators. In the discussion of a paper by Diskin (1961), Replogle (1962) provided significant insight to the study of the end depth–discharge relation. For varying slopes, based on a comprehensive experimental program, Rajaratnam and Muralidhar (1970) experimentally determined the relation between end depth and discharge rate in a trapezoidal channel. In the analysis of the end depth problem of trapezoidal channels, Keller and Fong (1989) were the first to include the contribution of the end depth pressure force in the momentum equation and validate the results with the test data. They used the widely accepted end depth related pressure head data of Replogle (1962). Based on a statistical analysis of empirical data, Gupta et. al (1993) provided a calibration curve relating Q and y_e in trapezoidal channels. Litsa and Evangelos (1995) presented a quadratic relation between y_e and y_c that was simple in form and useful in practice. Khan and Steffler (1996) used the vertically averaged continuity equation and moment equations to obtain the characteristics of flow past rectangular free overfalls and sharp-crest weirs. Their results agreed well with the test data. Recently, Ramamurthy et al. (2004) and Zhai (2003) provided flow velocity, pressure head and surface profiles for a free overfall flow in a trapezoidal channel.

In this chapter, the 3D two-equation k-ε turbulence model is adopted for the numerical simulation of the free overfall problem in a trapezoidal open channel. The fractional volume of fluid (VOF) method is used to capture the free surface. The results of simulation are validated using experimental data (Rajaratnam and Muralidhar 1970, Zhai 2003) pertaining to surface profiles, velocities and pressure heads.

8. 2 TURBULENCE MODEL

The proposed model solves the standard 3D Reynolds averaged continuity and Navier-Stokes equations for turbulent unsteady flow based on the two-equation k-ε model. The control volume technique is used to discretize the governing equations that can be solved numerically. It employs the collocated-grid approach. PISO method is used for pressure and velocity coupling calculation.

8. 3 BOUNDARY CONDITIONS

At the wall boundary, the wall-function approach proposed in chapter 2 is used. At the inlet, known flow velocities and turbulent quantities are prescribed. Here, the uniform flow condition for the horizontal velocity is provided. The outlet far downstream from the end depth is defined as pressure boundaries. This allows the water to flow out freely. All the air boundaries are defined as pressure boundaries with zero pressure. For the free surface boundary, the VOF model is used (chapter 2).

8. 4 SOLUTION PROCEDURE

The computational domain is shown in Fig. 8.1. The channel BC upstream of the end depth CD is 6.0 m long in the x - direction. The channel JG downstream of the end depth DC is 1.0 m long. The step CJ is 0.2 m high. Body fitted coordinates are used in the

Cartesian frame. The flow domain is meshed with a power law function that generates a fine mesh in the vicinity of the channel boundary. The grid cells next to the boundary are constructed well within the turbulent region (Fig. 8.2). Through the time-dependent simulation, the water flows on the open channel and constitutes the free surface between air and water for the specified inlet and outlet conditions.

8. 5 DISCUSSION OF RESULTS

8. 5. 1 Velocity and pressure head distribution near the end depth section

Figs. 8.3a to 8.3c show the experimental (Zhai, 2003) and the predicted distributions of the axial velocity in the plane of channel symmetry at 3 sections (x/y_c = - 0.15, - 0.61 and - 1.23) upstream of brink. The flow is supercritical at sections J, I and H (Fig. 8.3). Here, the non-dimensional axial velocity (u/u_c) is plotted against the non-dimensional flow depth (y/y_c) above the channel bed. The predicted and experimental velocity distributions clearly capture the acceleration of the flow in the region upstream of the brink. The results of the simulation are in good agreement with the experimental data (Zhai, 2003).

Figs. 8.4a to 8.4d show the predicted distributions of the axial velocity at the end depth sections A, B, C and D (Fig. 8.4). The results of the simulation are in very good agreement with the experimental data (Zhai, 2003). Fig. 4a also includes the test data of Rajaratnam and Muralidhar (1970). They too follow the predicted trend of the velocity distribution. Figs. 8.4a to 8.4d also indicate that the velocity does not change very much in the lateral direction. However, in the vertical direction, the velocity near the channel bed increases due to the increased curvature of the streamlines near the bed.

Figs. 8.4e and 8.4h show the distribution of the non-dimensional vertical pressure head $p/(\gamma y_c)$ at various sections A, B, C and D (Fig. 8.4) close to the brink with y/y_c. In Figs. 8.4e and 8.4h, the pressure distribution obtained by the present simulation is compared with the experimental data (Zhai, 2003). The pressure distribution in the vertical direction at locations at A, B and C appear to be nearly identical.

8. 5. 2 Surface profiles

Fig. 8.5 shows the non-dimensional flow depth y/y_c as a function of the non-dimensional distance x/y_c for the subcritical approach flow. In Fig. 8.5, the surface profile obtained by the present simulation is compared with the experimental profiles determined by Rajaratnam and Muralidhar (1970) and Zhai (2003). All these profiles are found to agree very well with the present simulated profile. Fig. 8.5 also shows that the critical depth occurs when x/y_c is close to – 4. For the free overfall in rectangle channels, the experimental results of Kandaswamy and Rouse (1957) indicated that the critical depth occurs when x/y_c is close to – 4.

8. 6 CONCLUSIONS

The 3D two-equation k-ε turbulence model together with the VOF method simulates faithfully the characteristics of flow past a free overfall in a trapezoidal open channel. The predictions of the numerical model agree well with the existing experimental results related to water surface profiles and distributions of the pressure head and velocity components.

CHAPTER 9

EXPERIMENTAL INVESTIGATIONS OF DIVIDING FLOWS IN OPEN CHANNELS

9. 1 INTRODUCTION

In hydraulic engineering and environmental engineering, one commonly comes across branching channel flows. Some of the distinctive characteristics of a dividing flow in an open-channel are illustrated in Fig. 9.1. They include a zone of separation immediately near the entrance of the branch channel, a contracted flow region in the branch channel, a stagnation point near the downstream corner of the junction, and a possible region of flow separation at the far sidewall of downstream of the junction in the main channel due to flow expansion.

There are a great number of experimental and analytical studies dealing with dividing flows. The first detailed experimental study of dividing flows in an open channel was done by Taylor (1944). He proposed a graphical solution, which included a trial and error procedure. Grace and Priest (1958) presented experimental results for the division of flow at different width ratios of the branch channel orientation to the main channel. They also classified the division of flow into two regimes with and without the appearance of local standing waves near the branch. The regime without waves corresponded to the case where the Froude numbers were relatively small. The regime with the waves corresponded to the free over-fall conditions at sections downstream of the junction. Milne-Thomson (1949), Tanaka (1957) and Murotta (1958) have solved the problem of branch channels analytically using conformal transformation based on the assumption of

flow depth being constant in all the channels. Law and Reynolds (1966) investigated the problem of dividing flows using analytical and experimental methods. Hager (1984) proposed a simplified model for evaluating the energy loss coefficient for flow through branches neglecting variation of velocity at the entrance to the branch. Existing results (Krishnappa and Seetharamiah 1963, Law 1965, Sridharan 1966, Ramamurthy and Satish 1988) indicate that the flow condition at the entrance to the branch is generally not submerged when the Froude number F_r in the branch is greater than a threshold value (0.3 or 0.35). Ramamurthy et al. (1990) obtained an expression for the momentum transfer rate from the main to the branch channel. Hager (1992) derived an expression for the energy-loss coefficient for branch channel flows. He assumed critical flow at the contracted section and expressed the branch discharge coefficient as a function of F_u and Q_{rd}. Neary and Odgaard (1993) examined the effects of bed roughness on the three-dimensional structure of dividing flows. For low Froude number flows, they presented detailed velocity-vector and particle-trace plots in the initial part of the separation zone. Their measurements indicated no depth variations in the junction (Neary and Odgaard 1995). Further, Neary et al. (1999) numerically investigated the lateral-intake inflows using three dimensional two-equation turbulence models without considering the water surface effects.

Weber et al. (2001) preformed an extensive experimental study of combining flows in a 90° open channel for the purpose of providing a comprehensive data set comprising three velocity components, turbulence stresses and water surface mappings. Recently, assuming the velocities to be nearly uniform, Hsu et al. (2002) presented a depth-

discharge relationship and energy-loss coefficient for a subcritical, equal-width, right-angled dividing flow over a horizontal bed in a narrow aspect ratio channel.

Till now, the experimental data related to three-dimensional mean velocity components and water surface profiles for dividing flows in open channels are not available. The primary objective of the present experimental study is to obtain these flow characteristics of dividing flows in a 90°, sharp-edged, rectangular open-channel junction formed by channels of equal width. The data set presented in this study is composed of water surface mapping, 3D velocity in the vicinity of the channel junction region.

9. 2 EXPERIMENTAL DETAILS

The experiments are performed in a 90° dividing flow channels (Fig. 9.2). The main channel is 6.198 m long. The branch channel is 2.794 m long. The main channel and the branch channel are 0.305 m high and 0.610 m wide. They are made of 12.7 mm Plexiglas plates and rest on a steel frame. The branch channel is positioned at the distance of 2.794 m from the channel entrance (Fig. 9.2). The angle of the branch is 90°. The channel beds are horizontal. The flow enters the main channel after passing through the transition section that contains screens and honeycombs. This ensures properly developed flow with low turbulence in the flume. At the end of the main channel and branch channel, control gates are placed to regulate the flow depth.

The discharge from the main flume or the branch channel is measured using standard V-notches. The maximum error in the discharge measurement is estimated to be 3%. The point gage used to measure the water surface in the channels can record depths to the nearest 0.1mm. The laser Doppler Anemometry (LDA) unit is used to measure the mean

velocity components of the flow fields. The error of velocity measurement is estimated to be 1%. The water surface profile for a given flow condition is completely and continuously mapped in one day.

The coordinates system used to record data is shown in Fig. 9.2. All distances are non-dimensionalized by the channel width, B = 0.610 m. The non-dimensionalized coordinates are X*, Y* and Z* for X/B, Y/B and Z/B, respectively. All measurements are made with reference to the floor of the upstream lower corner O of the branch channel where X* = Y* = Z* = 0 (Fig. 9.3). The velocity components in the X, Y and Z direction are defined as u, v and w, respectively. The velocities u*, v*, w* are non-dimensionalized by the critical velocity $V_c = (\frac{Q_u^2}{gB^2})^{\frac{1}{3}}$ at the upstream of the main channel, where Q_u denotes the discharges of the upstream main channel.

Measurements are always made only after steady conditions are attained. The measuring locations are shown in Fig. 9.3. Test conditions ensure the Reynolds number of the flow $\mathrm{Re} = \frac{VR}{\nu}$ is generally high for both the main and the branch channels. Here R, V and ν denote hydraulic radius, mean velocity and kinematic viscosity, respectively.

The discharges of downstream main channel and branch channel flows are denoted as Q_d and Q_b, respectively. The discharge ratio Q_r denotes the ratio of Q_b to Q_u (Table 9.1). For brevity, only data for some Q_r and selected locations are shown in the discussion of results.

9. 3 EXPERIMENTAL RESULTS

9. 3. 1 Velocity component v*

Fig. 9.4 shows contour plots for the velocity component v* near the water surface (Z* = 0.27) for Q_r = 0.838 in the junction region. In this sketch, the narrow area of return flow near the entrance to the branch denotes the separation zone that envelopes the recirculating flow. For Q_r = 0.838, the largest velocities of v* occur just downstream of the branch near Y* = -1.0 (Fig. 9.4), where the maximum flow contraction occurs. In fact the largest velocities of v* appear to occur just downstream of the branch near Y* = -1.0 for all the 5 discharge ratios tested. Downstream of Y* = -0.1.0 for Q_r = 0.838, the separation zone begins to shrink. Further, the separation region ends at Y* close to –2.3 for Q_r = 0.838 and Z* = 0.27. From the experimental result, it is also observed that the recirculation region becomes smaller near the channel bottom corresponding to the lower values of Z* (Fig. 9.5a and 5b).

For the section at Y* = -1.0, Figs. 9.5a and 5b show the contour plot of the v* component for Q_r = 0.149 and 0.838 respectively. Here, the view shown is for an observer looking towards the positive Y* direction. The increase in the width of the separation with decreased values Q_r is clearly seen in these sketches. It is found that for the different flow conditions, the separation zone increases both in width and length as the discharge ratios decrease.

For combining flows in rectangular channels, at a fixed discharge ratio, it was noted (Weber et al 2000, Ramamurthy and Zhu 1997) that higher angles of entry of the lateral flow into the main channel resulted in the larger separation zones. In the present case of

the dividing flows, the mean exit angle of the streamlines for flow entering the branch, increases with an increase in Z* (surface streamlines) compared to the exit angles of the streamlines located at the lower Z* (bottom streamlines). Further, for a fixed Z*, the exit angle of the flow decreases when the discharge ratio Q_r increases.

9. 3. 2 Vector field u*-v*

Fig. 9.6 shows the plots for the vectors resulting from the velocity component u*and v* at Z* = 0.270 and Z* = 0.033 for Q_r = 0.838 in the junction region. As mentioned earlier, the wider and longer separation zone occurs at higher Z* value (Figs. 9.6a and 6b). Further, when Q_r decreases, the width of separation zone increases (Figs. 9.5a and 5b).

A second separation zone (Fig. 9.1) may occur in the section of the main channel downstream of the junction because of flow expansion in this region. The width and length of the separation zone increase when Q_r increases. When Q_r is very small, the separation zone wouldn't exist. As before, the separation zone near the surface layers is wider (Figs. 9.6a and 6b) than the separation zone near the channel bottom. The stagnation zone (Fig. 9.1) occurs at the downstream corner of the junction. The highest velocity u* occurs at the upstream corner of the junction.

9. 3. 3 Secondary flows

Secondary flows are very important in three-dimensional experimental investigation of open channel flows. Fig. 9.7 shows vector plots of u*-w* defining in the X*-Z* plane at various locations Y* = -0.29 to Y* = -2.5, for Q_r = 0.838 in the branch channel. The existence of a strong secondary current in the contracting region is clearly seen in Fig. 9.7a. The spiral motion in the anti-clockwise direction gets weakened as the flow moves

downstream. Still, the flow appears to have not recovered even at Y* = -2.5 since the u* is considerable. As one would expect, in the recirculation zone, the secondary flow is quite weak as shown by the short vectors in this zone. It is also observed that the secondary flow occurs even in the main channel as shown in the v*-w* vector plot of Fig. 9.8. The strongest spiral motion occurs near the downstream corner of the junction.

The main objective of the study was to know the details of the characteristics of dividing flows in the junction region. However, to get the true picture of the secondary flow, which is important, the length of the main channel and the branch channel downstream of the junction should be much longer. In the present case, the length of the branch channel was of the order of 5B and hence is considerable to be short.

9. 3. 4 Water surface profiles

The water surface profile is shown for $Q_r = 0.409$ and $Q_r = 0.838$ in Fig. 9.9. It shows that the flow depth in the main channel is higher than the flow depth in the branch channel. The lowest flow depth occurs at the contracted zone in the branch channel. Further downstream of this zone, the flow depth increases as the width of the separation zone decreases. As the speeds of the curved streamlines separating from the upstream corner h (Fig. 9.1) are very high, the corresponding flow depths are relatively smaller near h than the depth of the approaching main flow.

For a low value of $Q_r = 0.409$, Fig. 9.9a shows that the flow depth at the stagnation zone around b (Fig. 9.1) is higher than the depths at other regions in the junction. However, for a higher value of $Q_r = 0.838$, the recirculation zone existed in the far wall region of the

main channel just downstream of the junction (Fig. 9.6). Consequently, the flow depth in this region rst (Fig. 9.1) is slightly higher (≈ 2%) than the depth at the stagnation zone.

For all flow conditions, generally the flow depth Y_d in the main channel downstream of the junction was higher than the flow depth Y_u in the approaching flow. Also, both the flow depths Y_u and Y_d were higher than the flow depth Y_b in the branch channel. The flow depth ratio Y_u/Y_d and Y_b/Y_d decrease while the discharge ratio Q_r increases. In Fig. 9.10, the experimental values of Y_u/Y_d are plotted against the values of Y_u/Y_d predicted by the theoretical relation (Eq. 9.1) suggested by Hsu et al. (2002). The agreement appears to be reasonable.

$$\left(\frac{Y_u}{Y_d}\right)^3 - \left[1+\frac{1}{2}F_d\right]\left(\frac{Y_u}{Y_d}\right)^2 + \frac{1}{2(1-Q_r)^2}F_d^2 = 0 \qquad (9.1)$$

9. 4 CONCLUSIONS

The three mean velocity components and the water surface profiles for dividing flows in a 90°, sharp-edged, rectangular open-channel junction formed by channels of equal width open channels is obtained. The width and length of the separation zone in the branch channel decrease when the discharge ratio Q_r increases. The separation zone is smaller near the channel bottom corresponding to the lower values of Z* than the separation zone near the surface (higher values of Z*). The mean exit angle of the streamlines for flow entering the branch, increases with an increase in Z* (surface streamlines) compared to the mean exit angle of the streamlines located at the lower Z* (bottom streamlines). Further, for a fixed Z*, the exit angle of the flow decreases when the discharge ratio Q_r increases. The largest velocities of v* appear to occur just downstream of the branch near

$Y^* = -1.0$ for all the 5 discharge ratios tested, where the maximum flow contraction occurs.

A separation zone may also occur in the main channel downstream of the junction, because of the flow expansion. The width and length of this separation zone increase with the increase in the discharge ratio Q_r. The secondary flow (spiral motion in the anti-clockwise direction) in the branch channel is considerable in the contracted flow region. For subcritical flows, the depth Y_d is always higher than Y_u. The depths Y_u and Y_d are always higher than Y_b. The depth ratios Y_u/Y_d and Y_b/Y_d decrease when the discharge ratio Q_r increases. The lowest flow depth occurs in the region of flow contraction in the branch channel.

CHAPTER 10

3D MODELING OF DIVIDING FLOWS IN OPEN-CHANNELS

10. 1 INTRODUCTION

Dividing flows are commonly encountered in hydraulic engineering and environmental engineering. There are a great number of earlier experimental and analytical studies dealing with dividing flows (Taylor 1944, Grace and Priest 1958, Milne-Thomson 1949, Tanaka 1957, Murotta 1958 and Ramamurthy and Satish 1988). For dividing flows in open channels, Taylor (1944) proposed a graphical solution based on detailed test program. This included a trial and error procedure. Law and Reynolds (1966) investigated the problem of dividing flows using analytical and experimental methods. Ramamurthy et al. (1990) obtained an expression for the momentum transfer rate from the main to the branch channel. Hager (1984, 1992) provided a simple procedure to find the energy loss coefficient for flow through open channel branches. Neary and Odgaard (1993) examined the effects of bed roughness on the 3D structure of dividing flows at a fixed flow depth. Neary et al. (1996) presented the numerical simulation of dividing flows under laminar flow conditions. Also, Neary et al. (1999) numerically investigated the lateral-intake inflows using the two-equation turbulence model without considering the water surface effects. Hsu et al (2002) presented depth-discharge relationships and energy-loss coefficients for subcritical flows in a T-junction. The channel bed was horizontal and the channel was narrow. Recently, Huang et al. (2002) provided a comprehensive numerical study of combining flows in open-channel junctions using the

3D turbulence model. This numerical model was validated by experimental data (Weber et al. 2001).

In this chapter, the developed 3D free surface turbulence model is used to study the characteristics of dividing flows in open channels. The numerical model is compared with the present experimental data.

10. 2 NUMERICAL ALGORITHM

The developed model solves the standard equations for turbulent flow based on the two-equation k-ω model. The computational domain is shown in Fig. 10.1. The width B of the channel is equal to 0.610 m and the height H of channel is equal to 0.305 m. To apply the uniform inlet flow condition to begin with, the length of main channel upstream of the junction is extended to 6.1 m (= 10B). However, the length of the main channel downstream of junction and the length of the branch channel are 2.44 m (= 4B) since the main interest is to study the junction flow characteristics. This configuration corresponds to the channel length in the experimental setup. Normally, it is desirable to have a much longer channel than 4B in the experimental setup.

The multiblock algorithm is developed for grid generation and computation. The flow domain is meshed with a power law function that generates a fine mesh in the vicinity of the channel boundary (Fig. 10.2). The grid cells next to the boundary are constructed well within the turbulent region.

10. 3 BOUNDARY CONDITIONS

At the free surface, the volume of fluid (VOF) scheme is used, which is introduced in chapter 2. At the wall boundary, the standard wall-function is used (chapter 2). At the

inlet, the gradients of velocity quantities, turbulent quantities and void fractions in the axial direction are prescribed as zero. The total flow rate Q_u is known. Hence, assuming an initial depth at the inlet yields the initial inlet mean velocity. As calculation progresses, both the depth and the velocity at the inlet get altered. At the end of each iteration, only the new mean velocity at the inlet is adjusted to provide the same flow rate Q_u. The pressure heads at the inlet are obtained using linear extrapolation methods from the interior of the solution domain. At the start of calculations, hydrostatic pressure distribution is assumed in the solution domain. At the outlets of the main channel and the branch channel, the water surfaces are prescribed (given data based on the rating curves of the two channel outlet controls). The velocities and turbulent quantities at both outlets are obtained using the linear extrapolation method from the interior of the solution domain. At the end of each iteration, the new mean velocities at the two outlets are adjusted to ensure the prescribed flow rates Q_d in the main and Q_b in the branch. All the air boundaries are defined as zero pressure boundaries. The pressure heads at both two outlets are obtained using linear extrapolation methods from the interior of the solution domain.

10. 4 RESULTS AND DISCUSSIONS

The coordinate system (Fig. 10.1) is the same as the one stated in chapter 9. For brevity, only the experimental data for $Q_r = 0.838$ (chapter 9) is considered for comparing the predicted results with the test data.

10.4. 1 Velocity component v*

Fig. 10.3 shows the agreement between the experimental data and the model predictions for the contour plots of the velocity component v* near the water surface (Z* = 0.270) in the junction region. In the numerical results (Fig. 10.3b), the separation zone is obtained in the branch channel. The maximum flow contraction occurs near Y* = -1.0 in the branch (Figs. 10.3a and 10.3b). Further, both in the model prediction and in the test data, the recirculation region becomes smaller near the bottom corresponding to lower values of Z* (not shown).

The variation of v* at Y* = -1.0 in the branch channel is shown in Figs. 10.4a and 10.4b. The view shown is for an observer looking towards the positive Y* direction. The agreements between the experimental result and the numerical result are reasonable.

10. 4. 2 Vector field u*-v*

Fig. 10.5 shows vector plots for the velocity component u*-v* at Z* = 0.270 in the junction region. It shows that there are two separation zones in the junction region. One occurs in the branch channel and the reattachment point is close to Y* = -2.0 for the region close to the water surface. The other separation zone caused by the flow expansion is in the main channel downstream of the junction. The stagnation zone occurs near the downstream corner of the junction. As one would expect, the highest velocity u* occurs at the upstream corner of the junction. The predicated results and the test data are in good agreement (Fig. 10.5).

For a more quantitative comparison, test data and predicted data for the velocity component v* at a few locations in the branch channel are shown in Fig. 10.6. The

agreement between the two is reasonable. In the branch, for X* = -0.098 at the location Y* = -0.29 (Fig. 10.6a) and Y* = -1.0 (Fig. 10.6b), the values of v* are positive. This indicates that these points are in the flow separation zone. However, for X* = -0.098 and Y* = -1.62 (Fig. 10.6c), v* is negative near the channel bottom and positive near the water surface (high Z*). This shows that the separation zone is wider at the top as mentioned before. For X* = -0.787 at Y* = -1.0 denoting the maximum contracting zone (Fig. 10.6b), v* is higher than the value v* at an upstream section Y* = -0.29 (Fig. 10.6a) and Y* = -1.62 (Fig. 10.6c).

For sections X* = 0.0 and X* = -1.70 in the main channel, Fig. 10.7 shows the comparison of u* based on test data and predicted data. At the section X* = 0.0, u* is quite high at the location Y* = 0.098, which is near the upstream corner of the junction. The positive value of u* at Y* = 0.787 and X* = -1.7 (Fig. 10.7b) again indicates that there is a separation zone in the main channel.

10. 4. 3 Secondary flows

Figs. 10.8 and 10.9 show the comparison of the secondary flows at Y* = -0.29 and -0.73 respectively. They show that the two-equation turbulence model can capture the secondary flow. However, the vortex size of the secondary flow in the prediction is smaller than the vortex size in the experiment. Huang et al. (2002) remarks rightly that higher order turbulence models are needed to capture the secondary flow characteristics more faithfully.

10. 4. 4 Water surface profiles

Figs. 10.10a and 10.10b display the water surface profiles in the junction region. The water surface decreases in the branch channel compared to the main channel. There is very a sharp drop of the water surface at the upstream corner of the junction (Fig. 10.10b). This is also observed during the test (Fig. 10.10a). The flow depth at the downstream corner of the junction denoting the stagnation point is higher than the other neighboring regions (Fig. 10.10b). Since $Q_r = 0.838$, the axial velocity u* is reduced considerably as the flow cross the junction. This results in a large separation zone in the main channel. Hence, the variation of the flow depth in this region is very small (Fig. 10.10a). The maximum difference between the predicted results and the test data related to the flow depths in the junction region is less than 5%. The overall agreement of the water surface profiles is reasonable (Fig. 10.11).

10. 5 CONCLUSIONS

For dividing flows in 90° rectangular open-channel junctions, the 3D two-equation turbulence model faithfully reproduces the mean flow characteristics such as velocity profiles, water surface profiles and mean flow patterns. In particular, the separation zone near the entrance to the branch channel and the separation zone in the main channel downstream of the junction are also predicted by the model and the predictions qualitatively agree with experimental data. The predicted reattachment length on the branch wall of the separated flow is close to the test results. The overall validation of the model is reasonable. Since numerical modeling is relatively less expensive, a well-validated model can be used to predicted flow behavior in field situations encountered.

CHAPTER 11

SIDE WEIR FLOWS

11. 1 GENERAL REMARKS

This chapter presents two studies related to side weirs that one used for flow control. Side weir flows are truly 3D free surface flows. The weir flow characteristics depend on a large number of geometric and hydrodynamic variables. Solutions to such problems can be obtained based on numerical methods or partial least-squares (PLS) methods besides experimental methods.

Rectangular side weirs (Fig. 11.1) are used extensively by hydraulic engineers in irrigation and urban sewer systems for the purpose of flow regulation and diversion. In the past, the lateral weir flow problem has been studied experimentally or theoretically. Assuming the total energy along the side weir to be constant, De Marchi (1934) obtained the following equation for a side weir located in a rectangular channel

$$q_s = \frac{dQ_s}{dx} = \frac{2}{3} C_m \sqrt{2g}\,(y - S)^{3/2} \qquad (11.1)$$

in which, Q_s = discharge of side weir, x = the distance from the beginning of the side weir, q_s = the discharge over the side weir per unit length, g = specific gravity acceleration, S = the height of the weir crest and y = flow depth at the section x, C_m = discharge coefficient known as the De Marchi coefficient. In terms of main dimensionless parameters (De Marchi 1934), C_m can be expressed as follows,

$$C_m = f(F_1, \frac{L}{D}, \frac{s}{Y_1}) \qquad (11.2)$$

in which, F_1 denotes the Froude number upstream of the side weir and $F_1 = \frac{V_1}{\sqrt{gY_1}}$, Y_1 = the flow depth upstream of the side weir in the open channel, V_1 = the mean velocity in the upstream of the side weir, L = width of the side weir and D = the channel width.

F_1 is considered as the only flow parameter for weir flow (Subramanya and Awasthy 1972, Nadesamoorthy and Thomson 1972, Yu-Tech 1972, Ranga Raju et al. 1979, Hager 1987). The additional parameters L/D and S/Y_1 were included in the weir flow analysis by Ramamurthy and Carballada (1980). They also presented a different version of Froude number $F_0 = \frac{V_1}{\sqrt{g(Y_1 - s)}}$. Singh et al. (1994) considered the influence of S/Y_1 to be more than that of L/D and provided the (empirical) linear dependence of C_m on F_1 and S/Y_1. Borghei et al. (1999) presented an empirical equation relating C_m with F_1, S/Y_1 and L/D. Muslu (2001) obtained the weir flow characteristics including the variation of the flow depths along the span of the weir.

Using De Marchi's equation, one has to generally go through complicated steps to calculate the discharge of the side weir after obtaining C_m (Subramanya and Awasthy 1972). In most of the earlier studies, De Marchi's equation was the starting point.

For flow over a sharp-crested side weir in circular channels, Uyumaz and Muslu (1985) have presented the theoretical and experimental study. According to them,

$$Q_s = C_d L \sqrt{2g}\,(Y_1 - s)^{3/2} \tag{11.3}$$

Dimensional analysis indicates the following relationship,

$$C_d = f(F_1, \frac{L}{D}, \frac{S}{Y_1}) \tag{11.4}$$

in which D = diameter of the circular channel.

Ramamurthy et al. (1995) provided a theoretical expression to relate the mean weir discharge coefficient C_d with the jet velocity parameter η_0 $\left(= \frac{V_1}{\sqrt{2gD}} \sqrt{\frac{V_1^2}{2gD} + \frac{Y_1}{D} - \frac{S}{D}} \right)$ and L/D for rectangular side weirs located on the side of circular channels.

11. 2 PLS METHOD FOR SIDE WEIR FLOWS

At first, PLS approximation (Wold 1966) is a powerful technique for process modeling and multivariate statistical process control. In particular, the nonlinear PLS method is widely used for dealing with a dependent variable and several independent variables that have a highly nonlinear correlation (Lakshminaraynan et al. 1997 and Malthouse et al. 1997). However, this method has received less attention in hydraulic engineering practice. In this section, the multivariable non-linear PLS method is used to determine the discharge coefficient of side weirs in terms of the various weir flow variables.

11. 2. 1 Theoretical consideration

In general, the relation among variables pertaining to experiments is non-linear. The dependent variable could be related to many independent variables. In the following section, the multivariable nonlinear PLS method is described briefly. One assumes the dependent variable f to be a function of several independent variables x_i (i = 1, …, n),

$$f = f(x_1, x_2, ..., x_n) \tag{11.5}$$

In order to express the relationship between f and x_i, fitting polynomials can be used to relate f with the other variables as follows.

$$f = g_1(x_1) \cdot g_2(x_2) \cdot \ldots \cdot g_n(x_n) = \prod_{i=1}^{n} g_i(x_i) \tag{11.6}$$

in which, $g_i(x_i)$ is a high degree polynomial equation (Eq. 11.7),

$$g_i = a_{i0} + a_{i1}x_i + a_{i2}x_i^2 + \ldots + a_{im}x_i^m = \sum_{j=0}^{m} a_{ij}x_i^j \tag{11.7}$$

Here, a_{ij} is a constant (j = 0, …, m). Thus,

$$f = \prod_{i=1}^{n} (\sum_{j=0}^{m} a_{ij}x_i^j) \tag{11.8}$$

Assuming that s samples are obtained in the experiment, if one uses f_k to represent the experimental value corresponding to x_{ik}, with x_{ik} free of error, the sum of the square errors are defined by

$$\delta^2 = \sum_{k=1}^{s} (f - f_k)^2 \tag{11.9}$$

Here, k denotes the sample number and k = 1, …, s.

By the least-square method, one obtains the partial derivatives with respect to the a_{ij}. Thus, for i =1, …, n, j = 0, 1, …, m and k = 1, …, s,

$$\frac{\partial}{\partial a_{ij}} \left[\sum_{k=1}^{s} (f - f_k)^2 \right] = 0 \tag{11.10}$$

Eq. 11.10 can be reduced to the following form.

$$\sum_{k=1}^{s}\left[(f-f_k)\frac{\partial f}{\partial a_{ij}}\right]=0 \tag{11.11}$$

Considering Eqs. 11.6 and 11.7, one can get,

$$\frac{\partial f}{\partial a_{ij}}=\prod_{\substack{i=1\\ i\neq t}}^{n} g_i\frac{\partial g_t}{\partial a_{ij}}=\prod_{\substack{i=1\\ i\neq t}}^{n} g_i x_t^j \qquad (j=1,\ldots,\ n) \tag{11.12}$$

After Eq. 11.12 is substituted into Eq. 11.11, Eq. 11.11 becomes,

$$\sum_{k=1}^{s}\left[(f-f_k)(\prod_{\substack{i=1\\ i\neq t}}^{n} g_i x_t^j)\right]=0 \tag{11.13}$$

Using Eqs. 11.6 and 11.7 in Eq. 11.13 and simplifying Eq. 11.13. Eq. 11.14 is obtained,

$$a_{ij}=\frac{\sum_{k=1}^{s}\left\{(f_k)\left[(\prod_{\substack{i=1\\ i\neq t}}^{n} g_i)x_t^j\right]_k-\left[(\prod_{\substack{i=1\\ i\neq t}}^{n} g_i)^2(\sum_{\substack{p=0\\ p\neq j}}^{m} a_{tp}x_t^p)x_t^j\right]_k\right\}}{\sum_{k=1}^{s}\left[(\prod_{\substack{i=1\\ i\neq t}}^{n} g_i)x_t^j\right]_k^2} \tag{11.14}$$

where t = 1, …, n; j = 0, 1, …, m.

Solving Eq. 11.14 iteratively, the constants a_{ij} can be obtained. Hence, the relationship among the variables is established.

11. 2. 2 Applications

In this chapter, the mean discharge coefficient C_d of side weir flows in a rectangular open channel and in a circular open channel is defined as follows

$$Q_s = C_d L\sqrt{2g}(Y_1 - s)^{3/2} \tag{11.15}$$

Knowing C_d, the weir discharge can be directly obtained. From Eqs. 11.2 ans 11.4, considering the channel width or the circular diameter D, $C_d = f(F_1, \frac{L}{D}, \frac{s}{Y_1})$.

The objective is to determine the dependence of C_d on the three other variables F_1, S/Y_1 and L/D using the nonlinear PLS method. Generally, the higher accuracy is obtained with the higher degree of polynomials for each independent variable. One has to analyze the importance for each independent variable and use many trials until the square error is reduced to a specified value (Gerald and Wheatley 1994). In this section, the flow is considered to be subcritical and $L/D \leq 1$. In this range of L/D, C_d is weakly dependent on L/B. However, C_d is strongly influenced by F_1 and S/Y_1. After a few trials, the second-degree polynomial function is chosen for L/D, and the fourth degree polynomial functions are chosen for F_1 and S/Y_1. Thus,

$$C_d = g_1\left(\frac{L}{D}\right)\cdot g_2\left(\frac{S}{Y1}\right)\cdot g_3(F_1) \tag{11.16}$$

in which,

$$g_1\left(\frac{L}{D}\right) = a_{10} + a_{11}\left(\frac{L}{D}\right) + a_{12}\left(\frac{L}{D}\right)^2 \tag{11.17}$$

$$g_2\left(\frac{S}{Y_1}\right) = a_{20} + a_{21}\left(\frac{S}{Y_1}\right) + a_{22}\left(\frac{S}{Y_1}\right)^2 + a_{23}\left(\frac{S}{Y_1}\right)^3 + a_{24}\left(\frac{S}{Y_1}\right)^4 \tag{11.18}$$

$$g_3(F_1) = a_{30} + a_{31}(F_1) + a_{32}(F_1)^2 + a_{33}(F_1)^3 + a_{34}(F_1)^4 \tag{11.19}$$

where $a_{10}, a_{11}, a_{12}, a_{20}, a_{21}, a_{22}, a_{23}, a_{24}, a_{30}, a_{31}, a_{32}, a_{33}$ and a_{34} are constants.

Case 1: Side weirs in rectangular open channels

The experimental data for side weirs in rectangular open channels are obtained from Carballada (1979) as all details of the experimental data are available. A program is developed to compute these constants. After computations, one obtains,

$$C_d = \left[1.0 + 0.33\left(\frac{L}{D}\right) - 0.105\left(\frac{L}{D}\right)^2\right] \times \left[1.0 + 0.034\left(\frac{S}{Y_1}\right) - 0.491\left(\frac{S}{Y_1}\right)^3 + 0.421\left(\frac{S}{Y_1}\right)^4\right] \times \left[0.348 + 0.022\,(F_1) - 0.203\,(F_1)^2 + 0.303\,(F_1)^3 - 0.168\,(F_1)^4\right] \quad (11.20)$$

The computed discharge Q_{wc} is based on Eqs. 11.15 and 11.20 using the corresponding experimental values of F_1, S/Y_1 and L/D (Carballada 1979). The correlation between Q_{wc} and the measured discharge Q_{wm} (Carballada 1979) is shown in Fig. 11.2. The maximum difference between the predicted results and the test data is less than 10%. The details (F_1, S/Y_1 and L/D) of the original data for other investigators were not available. Using the corresponding experimental values of F_1, S/Y_1 and L/D (Carballada 1979), the computed discharges based on the empirical equations for C_m proposed by other investigators against the measured discharge Q_{wm} (Carballada 1979) are also shown in Fig. 11.2. Singh et al. (1994) and Borghei et al. (1999) provided the (empirical) linear dependence of C_m on F_1 and S/Y_1. This may have resulted in the overestimation of the measure discharge in some cases (Fig. 11.2). It may also be noted that the flow is close to critical and is generally undulatory at very high Froude numbers and this may be the course for the slight data scatter under this condition. The predicted discharge Q_{wc} based on the present equations (Eqs. 11.15 and 11.20) is in good agreement with the experimental data Q_{wm} (Carballada 1979). It would be beneficial to obtain the original

weir flow data of all previous studies and apply the nonlinear PLS method to improve the discharge prediction.

Case 2: Side weirs in circular open channels

The experimental data for side weirs in circular open channels are obtained from the studies of Zhu (1995). As described in case 1, after computations, the following results are obtained,

$$C_d = \left[1.0 - 0.191\left(\frac{L}{D}\right) + 0.284\left(\frac{L}{D}\right)^2\right] \times \left[1.0 + 0.871\left(\frac{S}{Y_1}\right) - 4.070\left(\frac{S}{Y_1}\right)^2 + 2.969\left(\frac{S}{Y_1}\right)^3 + 3.294\left(\frac{S}{Y_1}\right)^4\right] \times \left[0.4241 - 0.124\,(F_1) + 0.922\,(F_1)^2 - 1.463\,(F_1)^3 + 0.709\,(F_1)^4\right] \quad (11.21)$$

The computed discharge Q_{wc} is based on Eqs. 11.15 and 11.21. Fig. 11.3 displays the correlation between the measured discharge Q_{wm} (Zhu 1995) and Q_{wc}. The computed discharges based on the empirical equations of C_d proposed by Uyumaz and Muslu (1985), and Ramamurthy et al. (1995) against the measured discharge Q_{wm} (Zhu 1995) are also shown in Fig. 11.3. The computed discharges using Eq. 11.21 are in good agreement with the experimental data (Zhu 1995).

11. 2. 3 Conclusions

The functional relations between the discharge coefficient C_d and the weir flow parameters F_1, S/Y_1 and L/D in a rectangular open channel and in a circular open channel are obtained on the basis of the multivariable nonlinear partial least-square (PLS) method. For subcritical approach flows and $L/D \leq 1$, this relationship can be used to predict the weir discharge. The mean discharge coefficient C_d defined in Eq. 15 directly

yields the weir discharge for side weirs in rectangular and circular channels. The predicted results for the side weir discharge are in good agreement with the experimental results. Compared to the previous study, the calculation procedures for the discharge of the side weirs are simplified. The nonlinear PLS method can also be applied to many other cases characterized by a large number of variables.

11. 3 NUMERICAL STUDY OF SIDE WEIR FLOWS

In this section, the flow past a side weir in a rectangular channel is simulated using the 3D free surface turbulence model. The numerical results are compared with the experimental data (Subramanya and Awasthy 1972).

11. 3. 1 Solution procedures

The plan view of the computational domain is shown in Fig. 11.4. The channel is 9 m long in x-direction (TP = 9.0 m) and 0.1 m high in z-direction. The width of the channel D is 0.248 m in y-direction (MT = PN = 0.248 m). The length of side weir L is 0.0996 m (AE = 0.0996 m). The height of the weir crest S is 0.0 m. The channel bed is horizontal. The side weir (AE) is situated at a distance of 6.0 m from the inflow section (MA = 6.0 m). To compare the predicted data with the experimental data (Subramanya and Awasthy 1972), this weir geometry is chosen.

The k-ω turbulence model is used to simulate the mean flow characteristics and the VOF method is used to capture the free surface. More details of this model are mentioned in chapter 2. For the inflow boundary, the uniform longitudinal velocity and a fixed flow depth are used. For the outlet boundaries at the downstream of the channel and at the side weir section, the assumed pressure is zero. The flow domain is meshed with a power law

function that generates a fine mesh in the vicinity of the channel boundary or near the side weir region. The grid in y-direction is 24. The grid in z-direction is 14. The grid in x direction is 200 totally. The grid details near the weir region are shown in Fig. 11.5.

11. 3. 2 Discussion of results

Little information about the water surface profiles and velocity distributions is available. Only, Subramanya and Awasthy (1972) have provided some test results that can be used to validate the model. Even, in this case, all the details related flow conditions were not available. Hence, only part of the test results presented are used for comparison with the predicted data. Specifically, for the inlet boundary, the discharge is 5.556 *l/s*. the inflow depth is 0.04 m. these values are chosen for the simulation to match the experimental conditions (Subramanya and Awasthy 1972).

Figs. 11.6a, 11.6b and 11.6c show the non-dimensional flow depth z/H_0 as a function of the non-dimensional distance y/D at three cross sections near the weir outlet region. Here H_0 = 0.035 m and D denotes the channel width. Figs. 11.6d and 11.6e show the non-dimensional flow depth z/H_0 versus the non-dimensional distance x/L at two sections near the weir outlet region. Here L denotes the length of the side weir. In Fig. 11.6, the surface profile obtained by the present simulation is compared with the experimental profiles determined by Subramanya and Awasthy (1972) and the agreement is reasonable. One should note that the flow depth in the test was extremely small (0.035 m) and the Froude number was close to critical for the approach flow, which results in undular flow. As such, the measurement of the flow depth in tests is difficult under such conditions. The three dimensionality of the weir flow (Fig. 11.6) is clearly discernable. The point S in Fig. 11.6e just downstream of the weir edge E (Fig. 11. 4b) is in the stagnation zone.

Fig. 11.7 shows that the stagnation zone corresponding to the high flow depths occurs just downstream of the weir edge E (Fig 11. 4b).

Fig. 11.8 shows the predicted distributions of the velocity component u/u_0 (axial) and v/u_0 (lateral) in z direction near the weir outlet. Here $u_0 = 0.748$ m/s. No test results are available for comparison with the predicted data for the specific flow conditions considered above. For this particular flow condition (discharge $Q_r = 0.11$), the lateral velocity component (v) is close to zero at X/L = 2.0. This tends to indicate that the flow is recovering quickly in the channel section downstream of the weir. However, when the weir discharge is large, corresponding to large values of Q_r, the expansion of the flow in the section downstream of the weir will be considerable. This leads to a large recirculation zone. Hence, the flow recover occurs in the relatively long distance downstream of the weir.

11. 3. 3 Conclusions

The 3D free surface model predicts the surfaces profiles reasonable well. The simulation captures the flow characteristics such as the location of the stagnation zone near the downstream edge of the weir.

CHAPTER 12

CONCLUSIONS AND SCOPES FOR FURTHER STUDIES

12. 1 CONCLUSIONS

12. 1. 1 The numerical model

An efficient and accurate turbulence model is developed. It can solve the 3D free surface turbulent flow problems. The model is developed for a number of flow configurations and validated using the existing or newly tested data. As such, the model is considered to be very reliable. Unlike commercial code, addressed to solve all types of CFD problems encountered in engineering principles, the present model is focused on serving the specific hydraulic engineering problems. Hence, the program developed is efficient from a point view of memory and time required for program execution. Unlike the experimental procedures, with less effort the well-validated numerical model can be used to easily obtain the flow characteristics of those flows including velocity distributions, pressure head distribution in conduits and free surface profiles in open channels.

1. Flow past a slot in a rectangular closed conduit: The model developed faithfully reproduces the flow characteristics such as the flow separation and the distributions of pressure and velocity. In particular, the location of the stagnation point occurs just downstream of slot, as predicted by the theoretical analysis.

2. Dividing flows in rectangular closed conduits: The model yields the mean flow characteristics of dividing flows at 90° junctions of rectangular closed conduits. These characteristics include the energy loss coefficients, pressure profiles, velocity profiles and the mean flow patterns including the recirculation zone.

3. Combining flows in rectangular closed conduits: The model faithfully predicts the mean flow characteristics of combining flows for 90° junctions of rectangular closed conduits. The predicted results agree well with the existing experimental data related to pressure and velocity fields. Further, the zone of flow separation predicted by the model qualitatively agrees with the experimental data.

4. Dividing flows in open channels: For dividing flows in 90° rectangular open-channel junctions, the model provides the velocity profiles, the water surface profiles and the mean flow patterns. The separation zone in the branch channel and the separation zone in the main channel downstream of the junction are predicted by the model. The predictions qualitatively agree with the experimental data. The model is validated using the present experimental data.

12. 1. 2 Use of FLUENT

1. Flow past an open channel floor slot: For flow past a floor slot in a rectangular open channel, the results of the model prediction agree well with the existing test data. The results include water surface profile besides distribution of pressure head and axial velocity. The predicted water depth along the open channel provides guidance for the design of the wall height in diversion works related to drainage systems and power channels.

2. The free overfall: For a free overfall in a rectangular open channel, the numerical model is used to obtain the water surface profiles and distributions of the pressure head and velocity components. The results predicted agree well with the existing experimental and theoretical results.

The theoretical equations for the nappe profiles in supercritical flows are obtained in terms of the end depth y_e. The theoretical predictions agree well with the test data.

3. Free overfall in trapezoidal channels: The model provides the water surface profiles and the distributions of the pressure head and velocity components for 3D flow past a free overfall in a trapezoidal open channel. The predictions of the model agree well with the existing experimental results.

12. 1. 3 Experimental results

For dividing subcritical flows in a 90° rectangular open-channel junction, the experimental studies provide the three mean velocity components and the water surface profiles in the junction region. The width and length of the separation zone in the branch channel decrease when the discharge ratio Q_r increases. The observed separation zone is smaller near the channel bottom corresponding to the lower values of Z* than the separation zone near the surface (higher values of Z*). For a fixed Z*, the exit angle of the flow decreases when Q_r increases. The width and length of the separation zone in the main channel due to flow expansion increase with the increase in Q_r. The depth ratios Y_u/Y_d and Y_b/Y_d decrease when Q_r increases.

12. 1. 4 Side weir flows

The multivariable nonlinear partial least-square (PLS) method provides the accurate functional relations between the mean discharge coefficient C_d and the weir flow parameters F_1, S/Y_1 and L/D in a rectangular open channel and in a circular open channel. For subcritical approach flows and $L/D \leq 1$, this relationship precisely predicts the weir discharge. C_d directly yields the weir discharge for side weir flows. This procedure is

simpler than the earlier procedures to compute the weir discharge based on C_m. The predicted results are in good agreement with the experimental data.

The predicted results of the flow characteristics of the side weir in a rectangular channel agree with the available experimental data. The side weir flow is truly 3D free surface flow.

12. 2 SCOPES FOR FURTHER STUDIES

1. Models developed may be extended to other hydraulic engineering practice like curvilinear flows, supercritical flows, jet flows and wake flows.
2. The model may be extended to open channel flows with multiple free surfaces. Advanced turbulence models may be developed to get the various turbulence characteristics.
3. The length of the branch channel and the length of the downstream of the main channel should be extended longer to obtain better characteristics for secondary flows. The turbulence characteristics may be measured.
4. It would be beneficial to obtain the original rectangular and circular lateral weir flow data of all previous studies and apply the nonlinear PLS method to improve the discharge prediction.

APPENDIX 1 REFERENCES

1. Bajura, R. A. (1971). "A model for flow distribution in manifolds," J. Engg. For Power, ASME, 7-12.
2. Benefield, J. R., Judkins, J. K., and Parr, A. D. (1984). "Treatment plan hydraulics for environmental engineers", Prentice-Hall, Englewood Cliffs, New Jersey.
3. Borghei, S. M., Jalili, M. R., and Ghodsian, M. (1999). ''Discharge coefficient for sharp-crested side weirs in subcritical flow.'' Journal of Hydraulic Engineering, ASCE, 125(10), 1051–1056.
4. Blaisdell, F. W. and Manson, P. W. (1963). "Loss of energy at sharpe-edge pipe junction in water conveyance systems," Tech. Bull 1283, US Dept. of Agric. Washington D.C.
5. Brune, A. W., Graf, W. H., Appel, E., and Yee, P. P. (1975). "Performance of pennsylvania highway drainage inlets," Journal of the Hydraulics Division, ASCE, 101(12), 1519-1537.
6. Carballada, L. B. (1979). "Some characteristics of lateral flow," Ph. D thesis. Concordia University, Montreal, Canada.
7. Chen Q., Dai G. and Liu H. (2002). "Volume of fluid model for turbulence numerical simulation of stepped spillway overflow of plane free overfall," Journal of Hydraulic Engineering, ASCE, 128(7), 683-688.
8. Chow, V. T. (1959). Open channel hydraulics, McGraw-Hill, New York.

9. Deck, S., garnier, E. and Guillen, P. (2002). "Turbulence modeling applied to space launcher configurations," Journal of Turbulence, 3, 1-21.

10. De Marchi, G. (1934). "Saggio di teoria di funzionamente degli stramazzi laterali," L'Energia Elettrica, Milano, Italy, 11, 849–860 (in Italian).

11. Diskin, M. H. (1961). "End depth at a drop in trapezoidal channels." Journal of the Hydraulics Division, ASCE, 87(4), 11-32

12. Ferro, V. (1999). "Theoretical end-depth-discharge relationship for free overfall," Journal of Irrigation and Drainage Engineering, ASCE, 125(1), 40–44.

13. Ferziger, J. H. and Peric M. (2002). "Computational method for CFD," 3rd edition, Springer.

14. Fu, H., Watkins, A. P. and Yianneskis, M. (1992). " Computation of 3D turbulent flows in a pipe junction with reference to engine inlet manifolds," I. Mech. E. Proc. Instn. Mech. Engrs. 206(6), 285-295.

15. Gardel, A. (1957). "Les pertes de charge dans les ecoulements au travers de branchments en Te," ["Pressure drops in flows through T-shaped pipe fittings,"] Bull. Tech. Suisse Rom. 83(9), 123-130, and 83(10), 143-148.

16. Gerald, C. F. and Wheatley, P. O. (1994). "Applied numerical analysis," 5th edition, Addison-Wesley Publishing Company.

17. Grace, J. L., and Priest, M. S. (1958). "Division of flow in open channel junctions." Bulletin No. 31, Engineering Experimental Station, Alabama, Polytechnic Institute.

18. Gupta, R. D., Jamil, M., Mohsin, M. (1993). "Discharge prediction in smooth trapezoidal free overfall (positive, zero and negative slopes)," Journal of Irrigation and Drainage Engineering, ASCE, 119(2), 215-224.

19. Hager, W. H. (1983). "Hydraulics of plane free overfall," Journal of Hydraulic Engineering, ASCE, 109(12), 1683-1697.

20. Hager, W. H. (1984). "An approximate treatment of flow in branches and bends," Proc. Instn. Mech, Engrs., 198C(4), 63–69.

21. Hager, W. H. (1987). "Lateral outflow over side weirs," Journal of Hydraulic Engineering, ASCE, 113(4), 491–504.

22. Hager, W. H. (1992). "Discussion of 'Dividing flow in open channels,' By A. S. Ramamurthy, D. M. Tran, and L. B. Carballada.'' Journal of Hydraulic Engineering, ASCE, 118(4), 634–637.

23. Hsu, C., Tang, C.; Lee, W. and Shieh, M. (2002). "Subcritical 90° equal-width open-channel dividing flow," Journal of Hydraulic Engineering, ASCE, 128(7), 716–720.

24. Huang, J. (2000). "Development and validation of a three-dimensional numerical model for application to river flow." Ph. D thesis, University of Iowa, Iowa, U.S. A.

25. Huang, J., Weber, L. J and Lai, Y. G. (2002). "3D numerical study of flows in open-channel junctions," Journal of Hydraulic Engineering, ASCE, 128(3), 268-280.

26. Issa, R. I. (1986). "Solution of implicitly discretized fluid flow equations by operator splitting," Journal of Computational Physics, 62, 40–65.

27. Ito, H. and Imai, K. (1973). "Energy losses at 90 degree pipe junctions," Journal of the Hydraulics Division, ASCE, 99(9), 1353-1368.

28. Kandaswamy, P. K. and Rouse, H. (1957). "Characteristics of flow over terminal weirs and sills," Journal of the Hydraulics Division, ASCE, 83(4), 11-32.

29. Keller, R. J. and Fong, S. S. (1989). "Flow measurement with trapezoidal free overfall." Journal of Irrigation and Drainage Engineering, ASCE, 115(1), 125-136.

30. Khan, A. A., and Steffler P. M. (1996). "Modeling overfalls using vertically averaged and moment equations," Journal of Hydraulic Engineering, ASCE, 122(7) 397-402.

31. Krishnappa, G., and Seetharamiah, K. (1963). "A new method of predicting the flow in a 90° branch channel," La Houille Blanche, assn. Pour la Diffusion de la Documentation of Hydraulique, Grenoble, No. 7.

32. Lakshminaraynan, S., Shah, S. and Nandakumar, K. (1997). "Modeling and control of multivariable processes: dynamic PLS approach," AICHE Journal, 43(9), 2307–2322.

33. Lander, B. E., and Spalding, D. B. (1974). "The numerical computation of turbulent flows," Computational Methods for Applied Mechanical Engineering, 3, 269-289.

34. Lasher, W. C. and Taulbee, D. B. (1994). "Reynolds stress model assessment using round jet experimental data," International Journal of Heat and Fluid Flow, 15(5), 357-363.

35. Law, S. W. (1965). "Dividing flow in an open channel," Ph. D Thesis, McGill University, Montreal, Canada.

36. Law, S. W., and Reynolds, A. J. (1966). "Dividing flow in an open channel," Journal of the Hydraulics Division, ASCE, 92(2), 4730-4736.

37. Litsa, A. P. and Evangelos, H. (1995). "General end-depth-discharge relationship at free overfall in trapezoidal channel," Journal of Irrigation and Drainage Engineering, ASCE, 121(2), 143-151.

38. Malthouse, E., Tamhane, A. and Mah, R. (1997). "Nonlinear partial least squares," Computers and Chemical Engineering, 21(8), 875–890.

39. Marchi, E. (1993). "On the free overfall," Journal of Hydraulic Research, IAHR, 31(6), 777-790.

40. Maronnier, V., Picasso, M. and Rappaz, J. (2003). "Numerical simulation of three-dimensional free surface flows," International Journal for Numerical Methods in Fluids, 42, 697–716.

41. McNown, J. S. and Hsu, E., (1951). "Application of conformal mapping to dividing flow," Proc. Midwestern Conf. On Fluid Dynamics, J. W. Edwards, Ann Arbor, Mich., 143-155.

42. McNown, J. S. (1954). "Mechanics of manifold flow," Trans, ASCE, 110, 1103-1142.

43. Meselhe, E. A. and Sotiropoulos, F. (2000). "Three-dimensional numerical model for open channels with free-surface variations," Journal of Hydraulic Research, IAHR, 38(2), 115-121.

44. Milne-Thomson, M. (1949). "Theoretical hydrodynamics," MacMillan and Co. Ltd.

45. Mitchell, J. M. (1890). "On the theory of the free stream lines," Philosophical Trans. of the Roy. Soc., (London), A 181, 389-431.

46. Mohapatra, P. K., Bhallamudi, S. M. and Eswaran, V. (2001). "Numerical study of flows with multiple free surfaces, " International Journal for Numerical Methods in Fluids, 36, 165–184.

47. Murota, A. (1958). "On the flow characteristics of a channel with a distributory," Technology Reports of the Osaka University, 6 (198).

48. Muslu, Y. (2001). "Numerical analysis for lateral weir flow," Journal of Irrigation and Drainage Engineering, ASCE, 127(4), 246–253.

49. Nadesamoorthy, T., and Thomson, A. (1972). "Discussion of 'Spatially varied flow over side weirs', " Journal of Hydraulic Division, ASCE, 98(12), 2234–2235.

50. Nasser, M. S., Venkataraman, P. and Ramamurthy A. S. (1980) "Flow in a channel with a slot in the bed," Journal of Hydraulic Research, IAHR, 18(4), 359–367.

51. Neary, V. S. and Odgaard, A. J. (1993). "Three-dimensional flow structure at open channel diversions," Journal of Hydraulic Engineering, ASCE, 119(11), 1223–1230.

52. Neary, V. S., and Odgaard, A. J. (1995). Closure to "Three-dimensional flow structure at open channel diversions," Journal of Hydraulic Engineering, ASCE, 121(11), 88–90.

53. Neary, V. S. and Sotiropoulos, F. (1996). "Numerical investigation of laminar flows through 90-degree divisions of rectangular cross-section," Computers and Fluids, 25(2), 95–118.

54. Neary, V. S., Sotiropoulos, F. and Odgaard, A. J. (1999). "Three-dimensional numerical model of lateral-intake inflows," Journal of Hydraulic Engineering, ASCE, 125(2), 126–140.

55. Popp, M. and Sallet, D. W. (1983). "Experimental investigation of one- and two-phase flow," Intl. Conf. On the Physical Modeling of Multi-Phase Flow, BHRA Fluid Engg., 67-90.

56. Rajaratnam, N. and Muralidhar, D. (1968). "Characteristics of the rectangular free overfall," Journal of Hydraulic Research, IAHR, 6(3), 233–258.

57. Rajaratnam, N. and Muralidhar, D. (1970). "The trapezoidal free overfall," Journal of Hydraulic Research, IAHR, 8(4), 419-447.

58. Ramamurthy, A. S. and Carballada, L. B. (1979). "Lateral flow past a barrier", Journal of Fluid Engineering, ASME, 101(4), 449-452.

59. Ramamurthy, A. S., and Carballada, L. (1980). ''Lateral weir flow model.'' Journal of Irrigation and Drainage Division, ASCE, 106(1), 9–25.

60. Ramamurthy, A. S. and Satish M. G. (1986). "Discharge characteristics of flow past a floor slot," Journal of Irrigation and Drainage Engineering, ASCE, 112(1), 20–27.

61. Ramamurthy, A. S. and Satish, M. G. (1988). "Division of open channel flow in short branches", Journal of Hydraulic Engineering, ASCE, 114(4), 428-438.

62. Ramamurthy, A. S., Tran, D. M., and Carballada, L. B. (1990). "Dividing flow in open channels," Journal of Hydraulic Engineering, ASCE, 116(3), 449–455.

63. Ramamurthy, A. S., Zhu weimin, and Carballada, L. B. (1994). "Flow past a 2D lateral slot", Journal of Environmental Engineering, ASCE, 120(6), 1632-1638.

64. Ramamurthy, A. S., Zhu, W. and Vo, D. (1995). "Rectangular lateral weirs in circular open channels." Journal of Hydraulic Engineering, ASCE, 121(8), 608–612.

65. Ramamurthy, A. S. and Weimin Zhu. (1996). " Dividing flows in 90° junctions of rectangular closed conduits." Journal of Hydraulic Engineering, ASCE, 122(12), 687-691.

66. Ramamurthy, A. S. and Weimin Zhu. (1997). " Combining flows in 90° junctions of rectangular closed conduits." Journal of Hydraulic Engineering, ASCE, 123(11), 1012-1019.

67. Ramamurthy, A. S., Zhai, C. and Qu J. Y. (2004). " End depth-discharge relation at free overfall of trapezoidal channels, " Journal of Irrigation and Drainage Engineering, ASCE, 130(5), 432-436.

68. Rameshwaran, P. and Naden, P. S. (2003). "Three-dimensional numerical simulation of compound channel flows," Journal of Hydraulic Engineering, ASCE, 129(8), 645-652.

69. Ranga Raju, K. G., Prasad, B., and Gupta, S. K. (1979). "Side weir in rectangular channel," Journal of Hydraulic Division, ASCE, 105(5), 547–554.

70. Replogle, J. A. (1962). "Discussion of the end depth at a drop in trapezoidal channels by M. H. Diskin". Journal of Hydraulic Division, ASCE, 88(2), 161–165.

71. Reynolds, O. (1895). "On the dynamical theory of incompressible viscous fluids and the determination of the criterion," Phil. Tans. Roy. Soc. London Ser. A, 186, 123-164.

72. Rouse, H. (1936). "Discharge characteristics of the free overfall," Civil Engineering, ASCE, 6, 257-260.

73. Satish M. G. (1986). "Discharge characteristics of flow past a floor slot," Ph. D thesis. Concordia University, Montreal, Canada.

74. Serre, M. and Odgaard, A. J. (1994). "Energy loss at combining pipe junction," Journal of Hydraulic Engineering, ASCE, 120 (7), 808-830.

75. Singh, R., Manivannan, D., and Satyanarayana, T. (1994). "Discharge coefficient of rectangular side weirs," Journal of Irrigation and Drainage Engineering, ASCE, 120(4), 814–819.

76. Sotiropoulos, F. and Patel, V. C. (1995). "Application of Reynolds-stress transport models to stern and wake flows," Journal of Ship Research, 39(4), 263-283.

77. Spalart, P.R., Jou, W.H. Strelets, M. and Allmaras, S.R. (1997). "Comments on the feasibility of LES for wings, and on a hybrid RANS/LES approach. In: Liu, C., Liu, Z. (Eds.) 'Advances in DNS/LES', " Greden Press, Columbus, 137-148.

78. Sridharan, K. (1966). "Division of flow in open channels," thesis, Indian Institute of Science, Bangalore, India.

79. Subramanya, K., and Awasthy, S. C. (1972). "Spatially varied flow over side weirs," Journal of Hydraulic Division, ASCE, 98(1), 1–10.

80. Tanaka, K. (1957). "The improvement of the inlet of the power canal," Transactions of the Seventh General Meeting of IAHR, Lisbon, 1, 17.

81. Taylor, E. H. (1944). "Flow characteristics at rectangular open-channel junctions," Trans. ASCE, 109, 893–902.

82. Uyumaz, A., and Muslu, Y. (1985). "Flow over side weirs in circular channels," Journal of Hydraulic Engineering, ASCE, 111(1), 144–160.

83. Venkataraman P. (1977). "Divided flow in channels with bottom openings," Journal of Hydraulics Division, ASCE, 103(2), 190–194.

84. Venkataraman P. (1978). "Spatially varied flow in open channels," Ph. D thesis Venkateshwara University, Tirupati, India.

85. Weber, L. J., Schumate, E. D., and Mawer, N. (2001). "Experiments on flow at a 90° open-channel junction," Journal of Hydraulic Engineering, ASCE, 127(5), 340–350.

86. Wilcox, D. C. (1994). "Simulation of transition with a two-equation turbulence model, " AIAA J., 32(2), 247-255.

87. Wilcox, D. C. (2000). "Turbulence modeling for CFD". 3rd edition, DCW Industries, Inc.

88. Wold, H. (1966). "Non-linear estimation by iterative least-squares procedures," In: David, F. (Ed.), Research Papers in Statistics. Wiley, New York.

89. Yu-Tech, L. (1972). "Discussion of 'Spatially varied flow over side weirs' by Subramanya, K. and Awasthy, S.C.," Journal of Hydraulic Division, ASCE, 98(1), 2046-2048.

90. Zhai. C. (2003). "Hydrodynamic principles applied to flow measurement." M. A. Sc thesis. Concordia University, Montreal, Canada

91. Zhu, W. M. (1995). "Characteristics of dividing and combining flows," Ph. D thesis. Concordia University, Montreal, Canada.

APPENDIX 2

THE DESCRIPTION OF THE DEVELOPED PROGRAM

GENERAL MARKS

The developed program includes the three-dimensional free surface turbulence model. C++ programming language is used under Microsoft visual studio C++.

The governing equations are as following:

Continuity equation.

Navier-Stokes equations for laminar flows

RANS equations for turbulence models

Governing equation for k-ω model (Wilcox 2000)

Governing equation for $k-\varepsilon$ model (Wilcox 2000)

Governing equation for VOF model (Ferziger, J. H. and Peric M. 2002)

It can be applied to laminar flows, turbulent flows in unsteady or steady states.

For turbulent flow, the program provides 1. k-ω model, 2 $k-\varepsilon$ model, 3 stress-transport model and 4. LES model (3 and 4 are partly completed and not yet validated.)

For the pressure-velocity coupling calculation, the SIMPLE method is used. Chapter 2 provides the details.

THE HISTORY OF THE DEVELOPED PROGRAM

Step 1. At first, the program was developed for 2D case based on the simple example program (2300 lines) provided by Ferziger and Peric (2002). I translated the program

(Ferziger and Peric 2002) from Fortran language to the more efficient C++ language (1200 lines). I also changed some sections of the numerical algorithm during the translation. Then I tested the modified program and verified this program yielded the same results as the original program (Ferziger and Peric 2002) for a straight duct flow.

Step 2. Based on the developed 2D program, I simulated more complex flows such as the slot flows in closed conduits (2D), combining flows and dividing flows in closed conduits (2D) and validated using existing experimental data.

Step 3. I upgraded the validated 2D program to 3D. I simulated the slot flows in closed conduits, combining flows and dividing flows in closed conduits and validated using existing experimental data.

Step 4. Based on the developed 3D program, I blended the VOF model to the program for 3D free surface flows. I validated the free surface model using the experimental data from Weber (2001) in IOWA University. For brevity, the validation details are not shown in the thesis.

Then I validated the program by the present experimental data for dividing flows in open channels (included in the thesis).

THE STRUCTURE OF THE PROGRAM

The main program:

chsMain.cpp: the main program control the whole computing procedures. (363 lines)

The header files:

chsMain.h: define the general variables, subroutines, functions. (160 lines)

chsAnalysis.h: define functions for the result analysis. (744 lines)

chsBasic.h: define the basic subroutines (defined arrays, etc.). (697 lines)

chsBC.h: define functions for the boundary conditions and initial conditions.(331 lines)

chsFiles.h: define functions for data input and output (save results). (438 lines)

chsGrid.h: define functions for the grid generation in power law ratios. (294 lines)

chsPressure.h: define functions for the pressure calculation. (638 lines)

chsSurface.h: define functions for the free surface calculations including VOF model.(1020 lines)

chsTurb.h: define functions for turbulence quantities calculations including $k-\varepsilon$ model, k-ω model, stress transport model and LES model (the stress transport model is not already).(1244 lines)

chsVelocity.h: define functions for the velocity component calculations. (458 lines)

The program has 6367 lines totally for dividing flows in open channels.

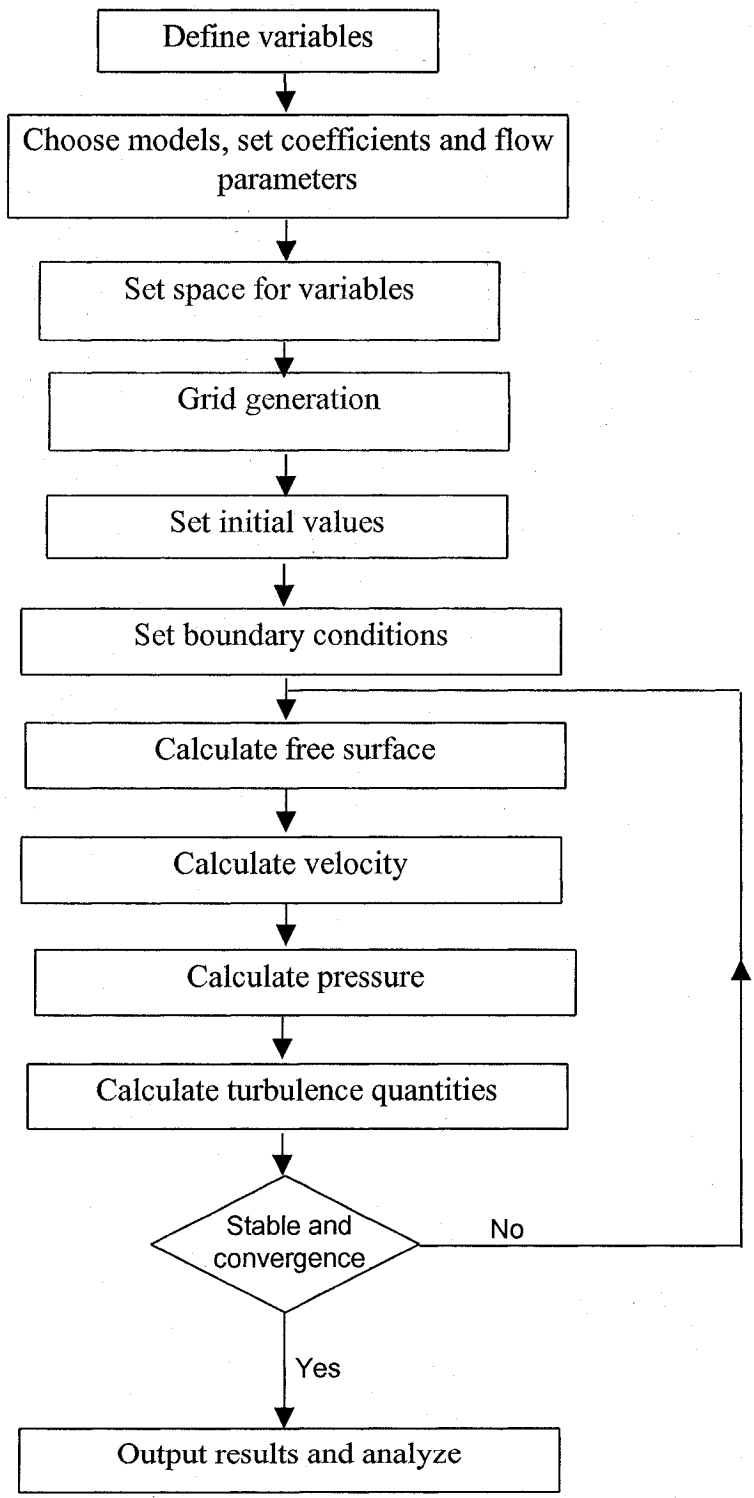

Fig. A.1 The flow chart of the developed program

APPENDIX 3 FIGURES

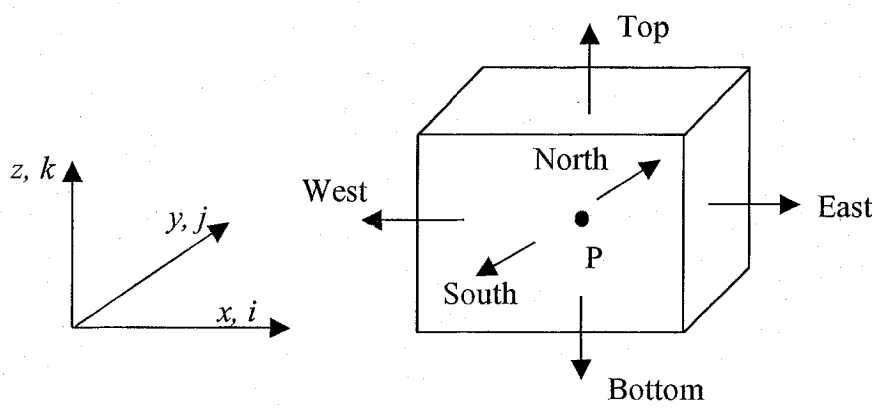

Fig. 2.1 A typical control volume (CV)

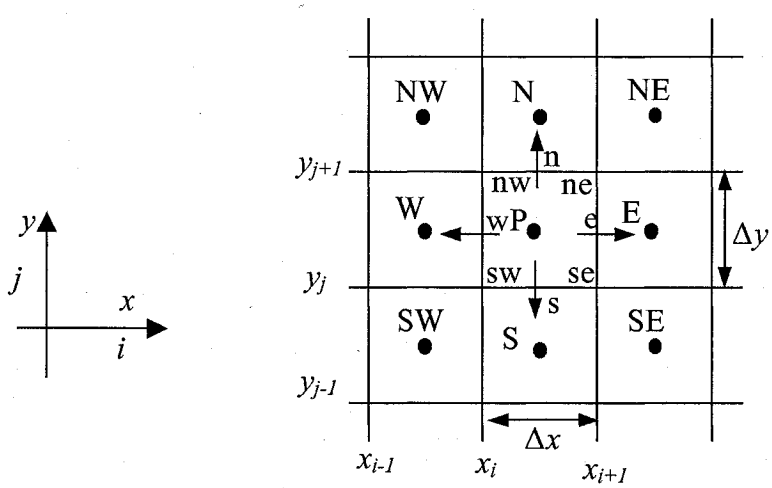

a) x-y plane

Fig. 2.2 A typical CV and the notation used for a Cartesian 3-D grid

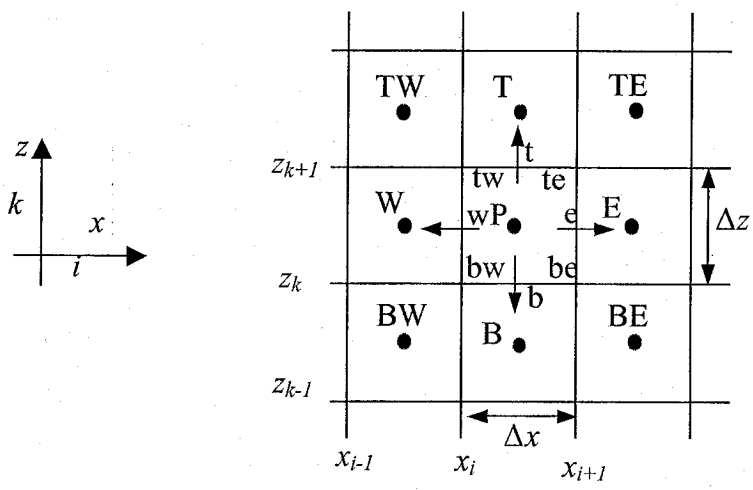

b) x-z plane

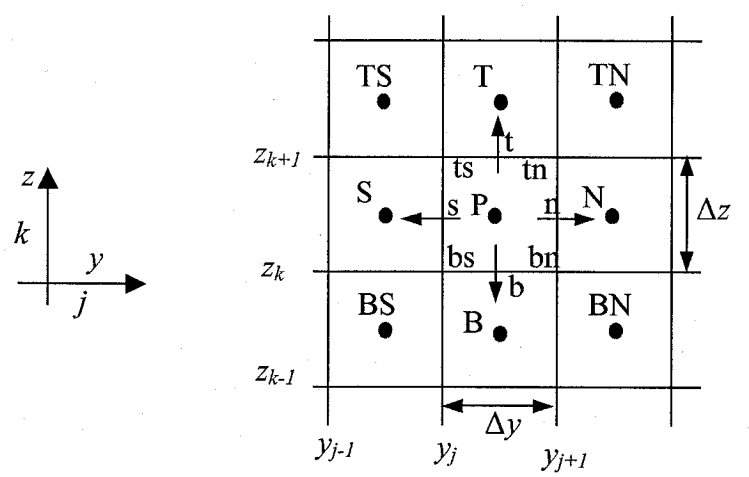

c) y-z plane

Fig. 2.2 A typical CV and the notation used for a Cartesian 3-D grid (continued)

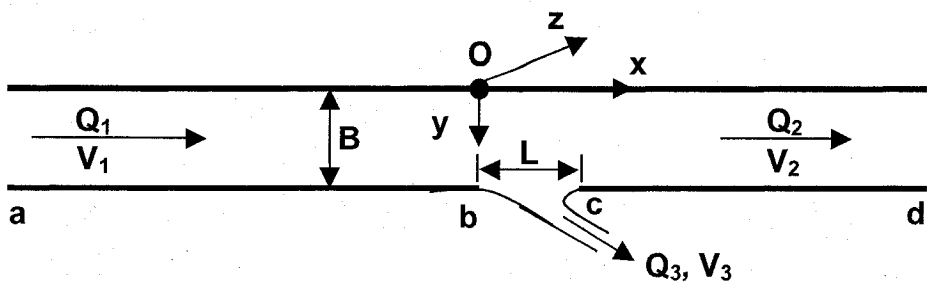

Fig. 3.1 Flow past a slot

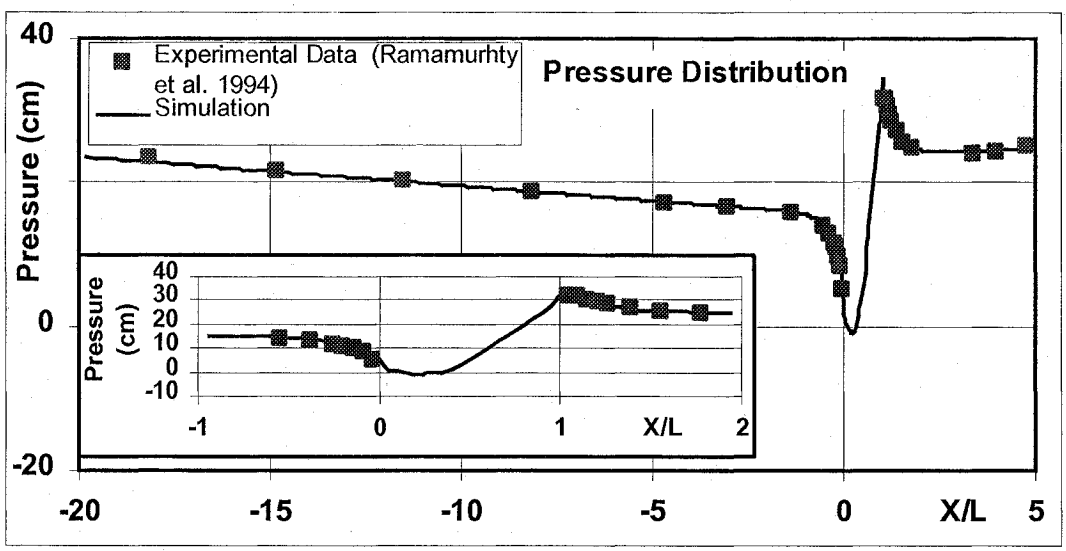

Fig. 3.2 Pressure distribution along the wall a-b-c-d (L/B=1.0, Q_3/Q_1=0.65)
Insert: Expended view in the region –1<X/L<2

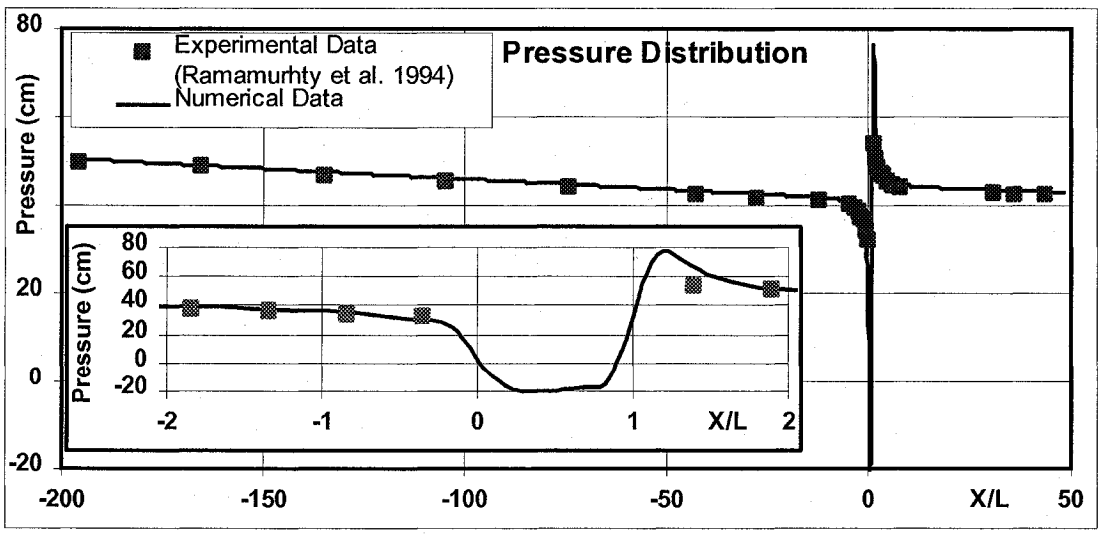

Fig. 3.3 Pressure distribution along the wall a-b-c-d (L/B=0.11, Q_3/Q_1=0.10)
Insert: Expended view in the region –2<X/L<2

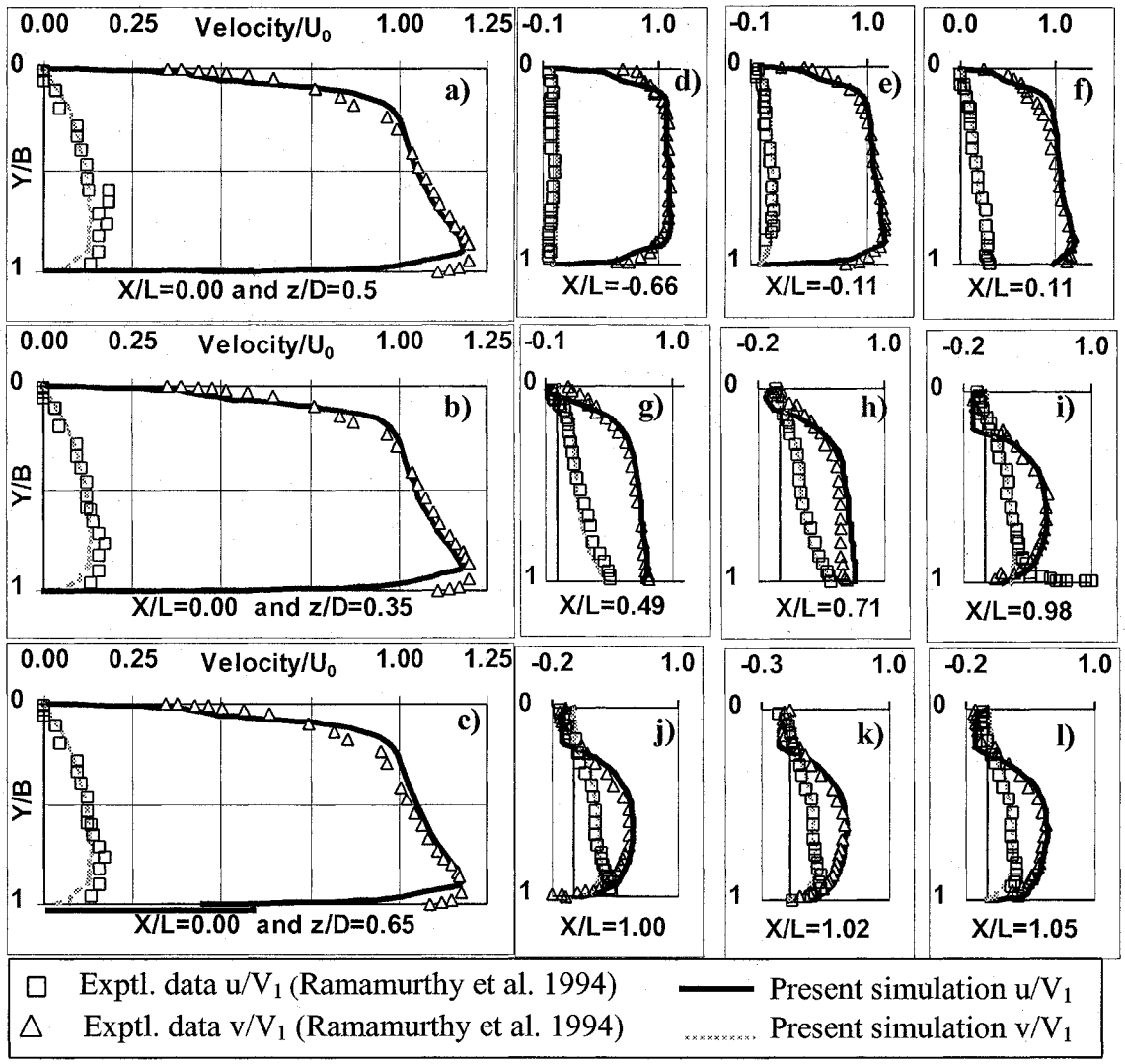

Fig. 3.4 Velocity distributions (L/B=1.0, Q_3/Q_1=0.65)

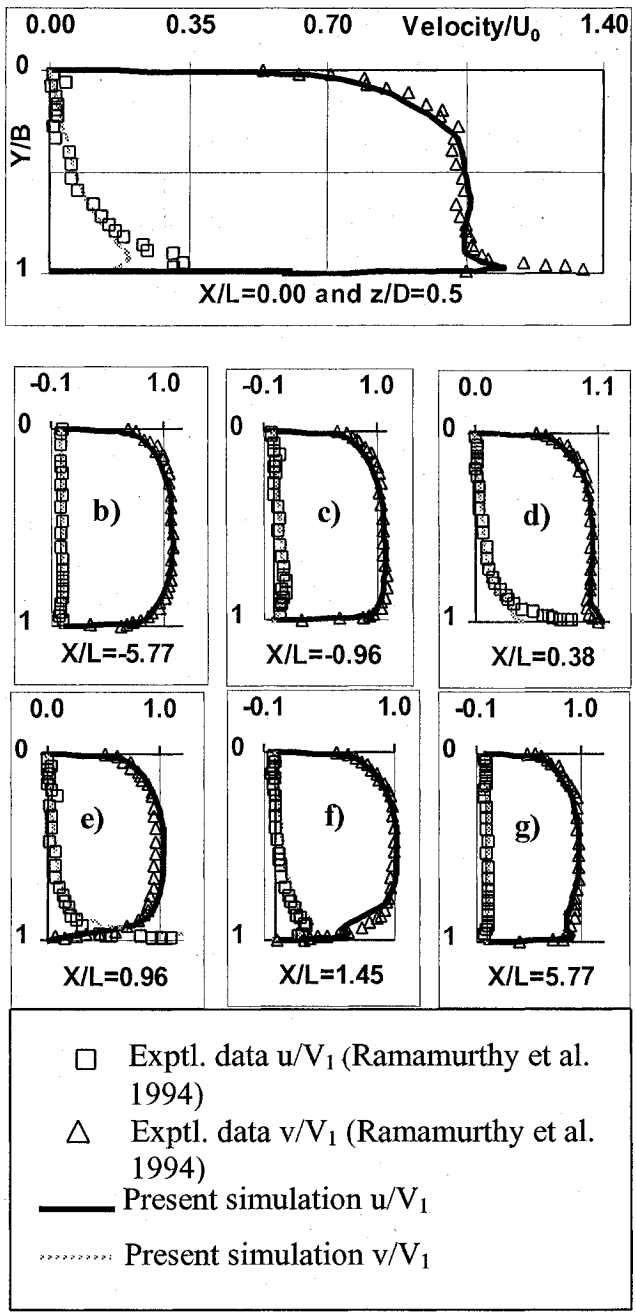

Fig. 3.5 Velocity Distribution (L/B=0.11, Q_3/Q_1=0.10)

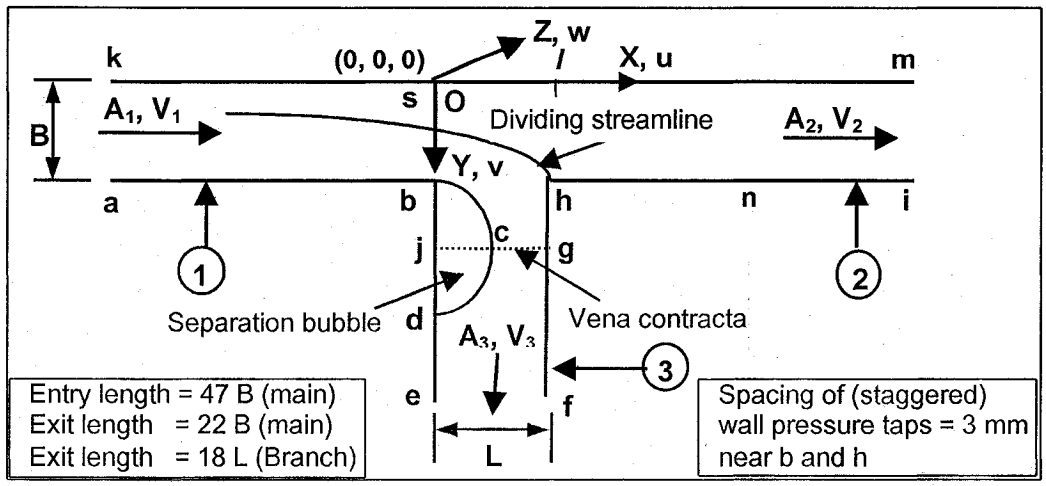

Fig. 4.1 Dividing flow in rectangular conduit junctions (O denotes the origin)

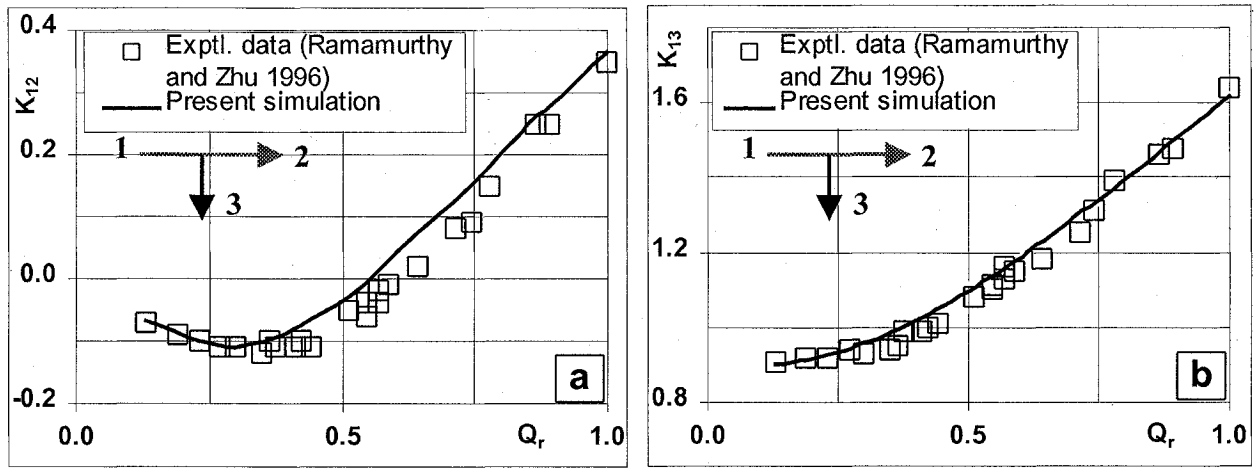

Fig. 4.2 Comparison of energy loss coefficients (L/B=0.77). a) K_{12}. b) K_{13}.

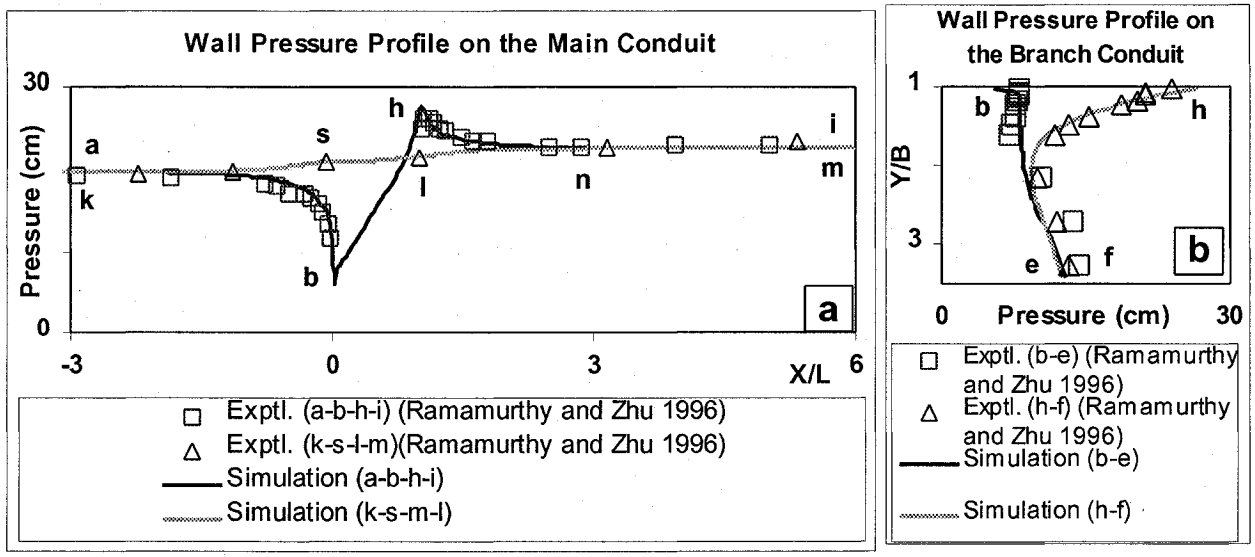

Fig. 4.3 Pressure profiles for L/B=0.77 and Q_3/Q_2=0.57

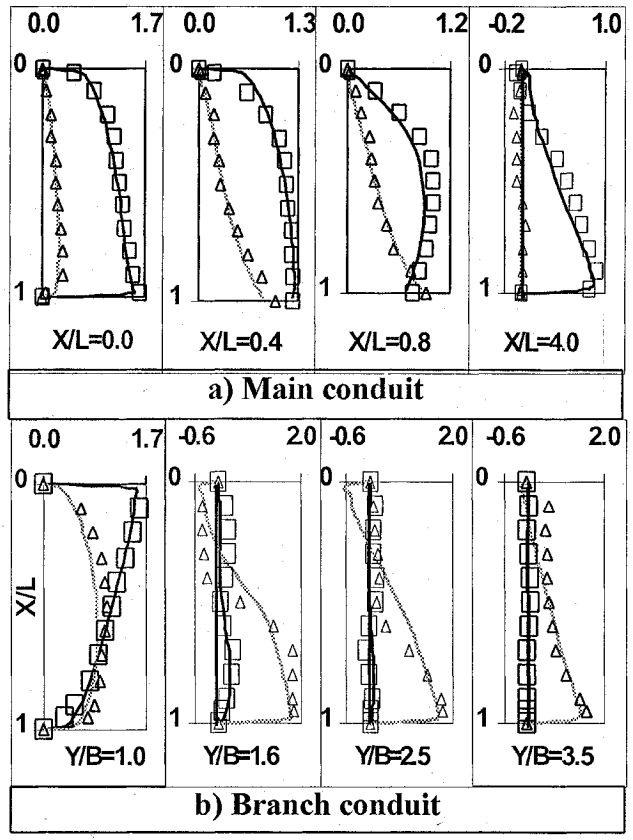

Fig. 4.4 Velocity distributions at sections of the main and the branch conduits

□ Exptl. data u/U_0 (Ramamurthy and Zhu 1996) —— Simulation u/U_0

△ Exptl. data v/U_0 (Ramamurthy and Zhu 1996) ····· Simulation v/U_0

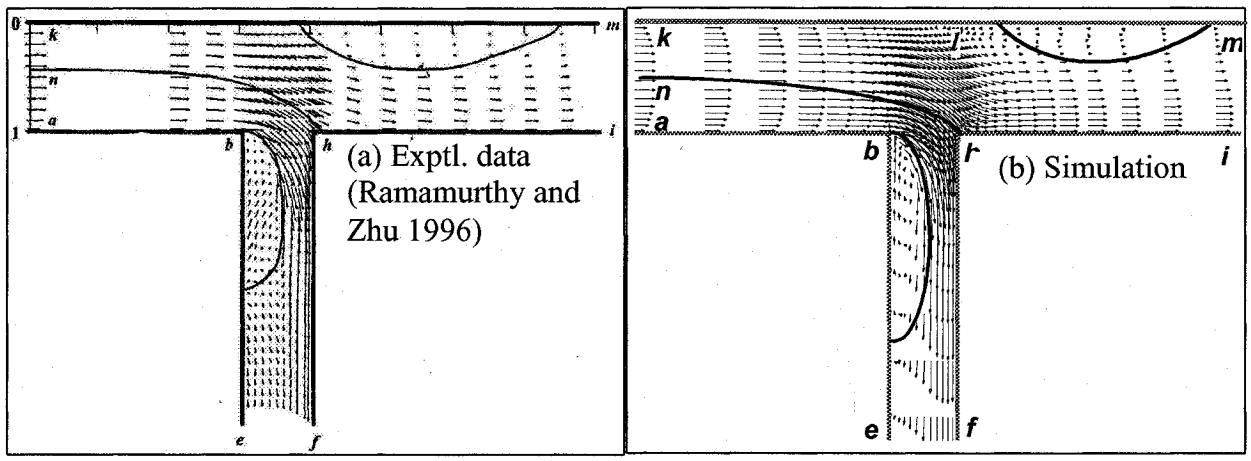

Fig. 4.5 Comparison of the mean flow pattern for L/B=0.77 and Q_3/Q_1=0.57

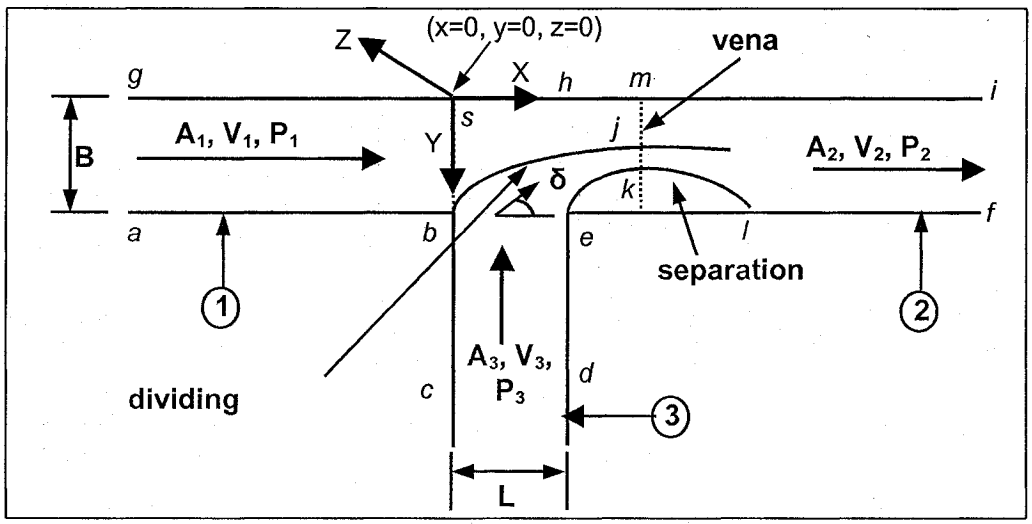

Fig. 5.1 Combining flow in rectangular conduit junctions

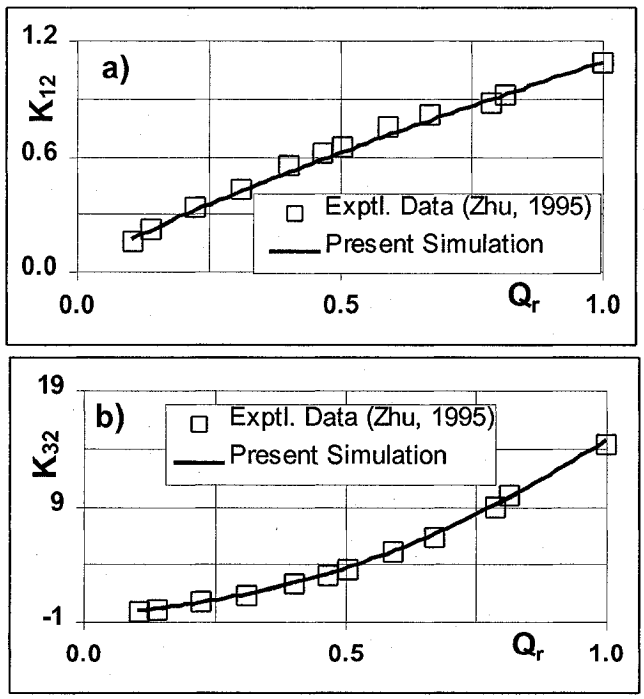

Fig. 5.2 Comparison of energy loss coefficients for L/B=0.22 a) K_{12}. b) K_{32}.

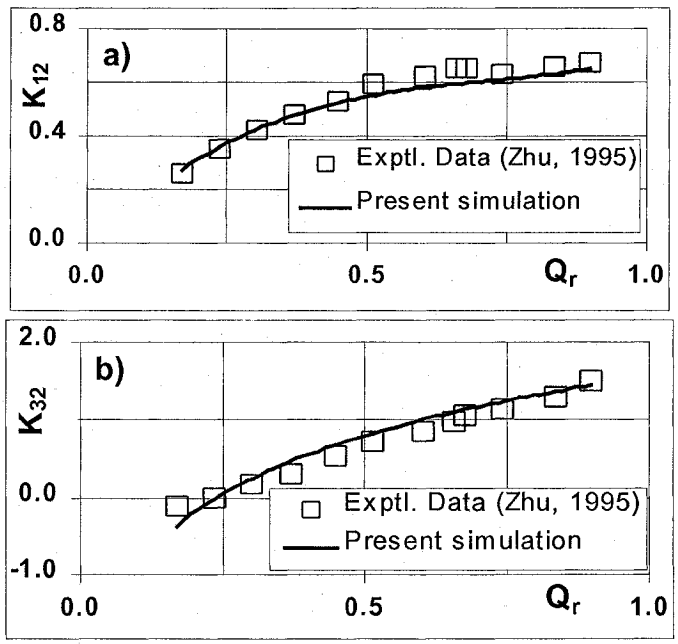

Fig. 5.3 Comparison of energy loss coefficients for L/B=0.77 a) K_{12}. b) K_{32}.

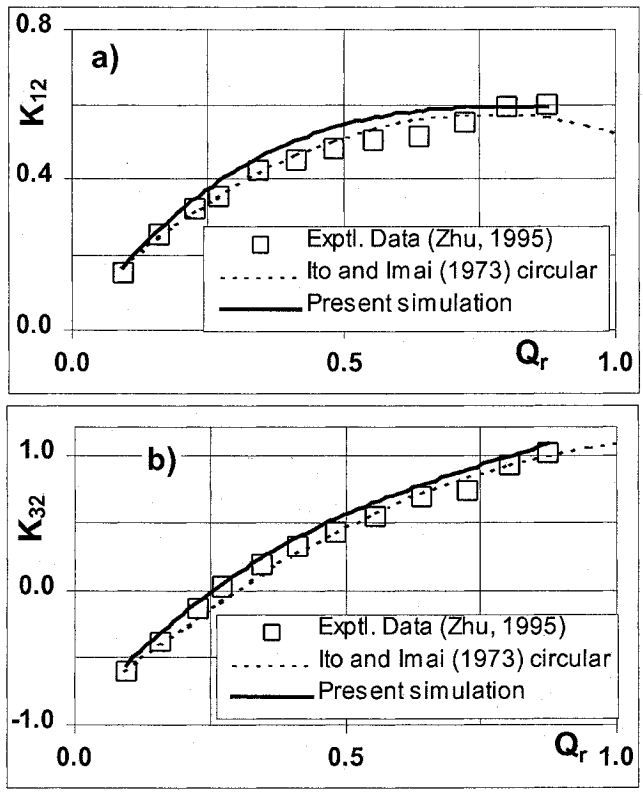

Fig. 5.4 Comparison of energy loss coefficients for L/B=1.0 a) K_{12}. b) K_{32}.

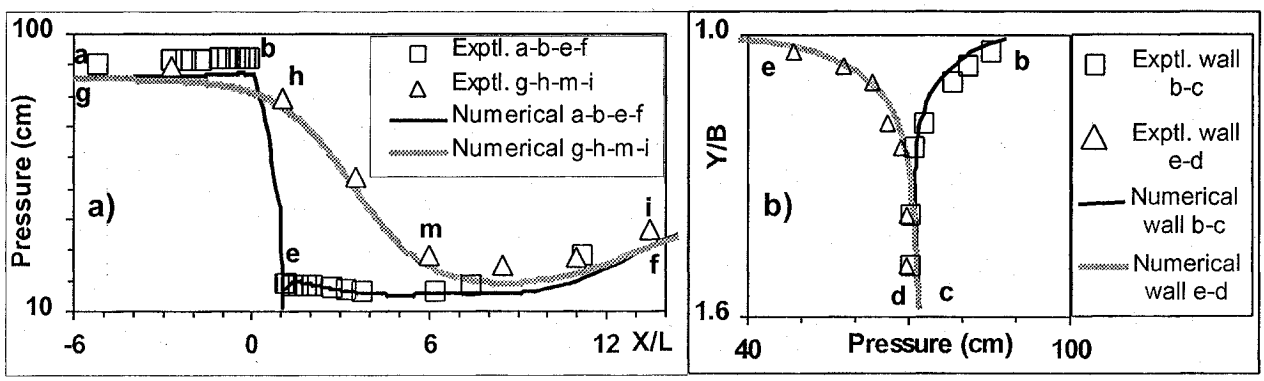

Fig. 5.5 Pressure Profile for L/B = 0.22 and $Q_3/Q_2 = 0.50$ a) main conduit b) branch conduit

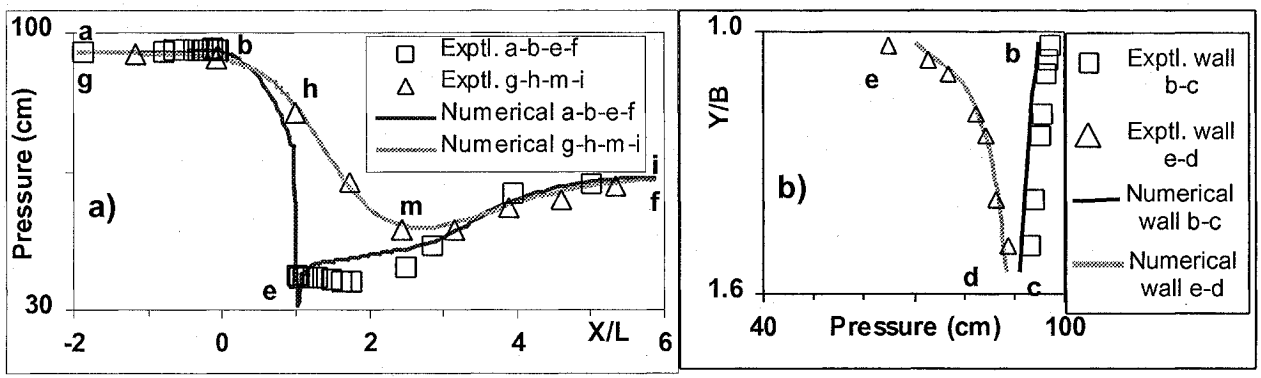

Fig. 5.6 Pressure Profile for L/B = 0.77 and $Q_3/Q_2 = 0.68$ a) main conduit b) branch conduit

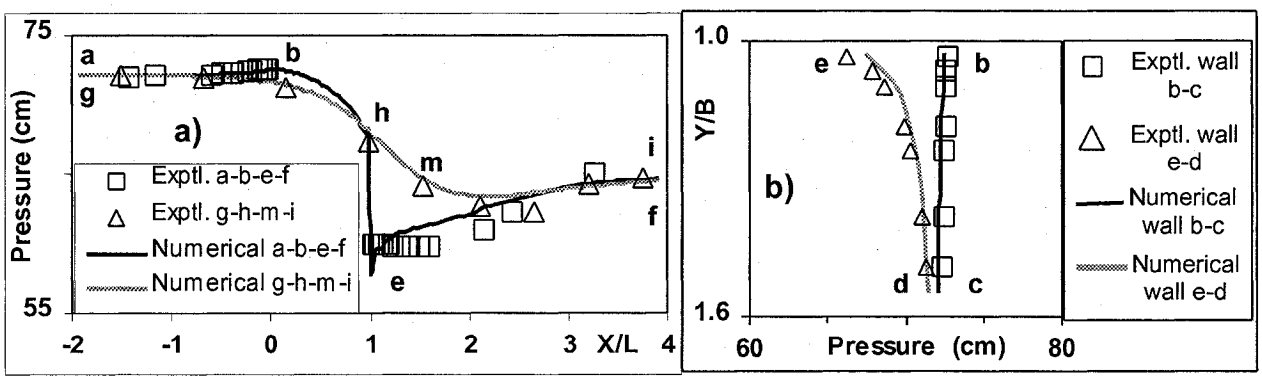

Fig. 5.7 Pressure Profile for L/B = 1.0 and $Q_3/Q_2 = 0.46$ a) main conduit b) branch conduit

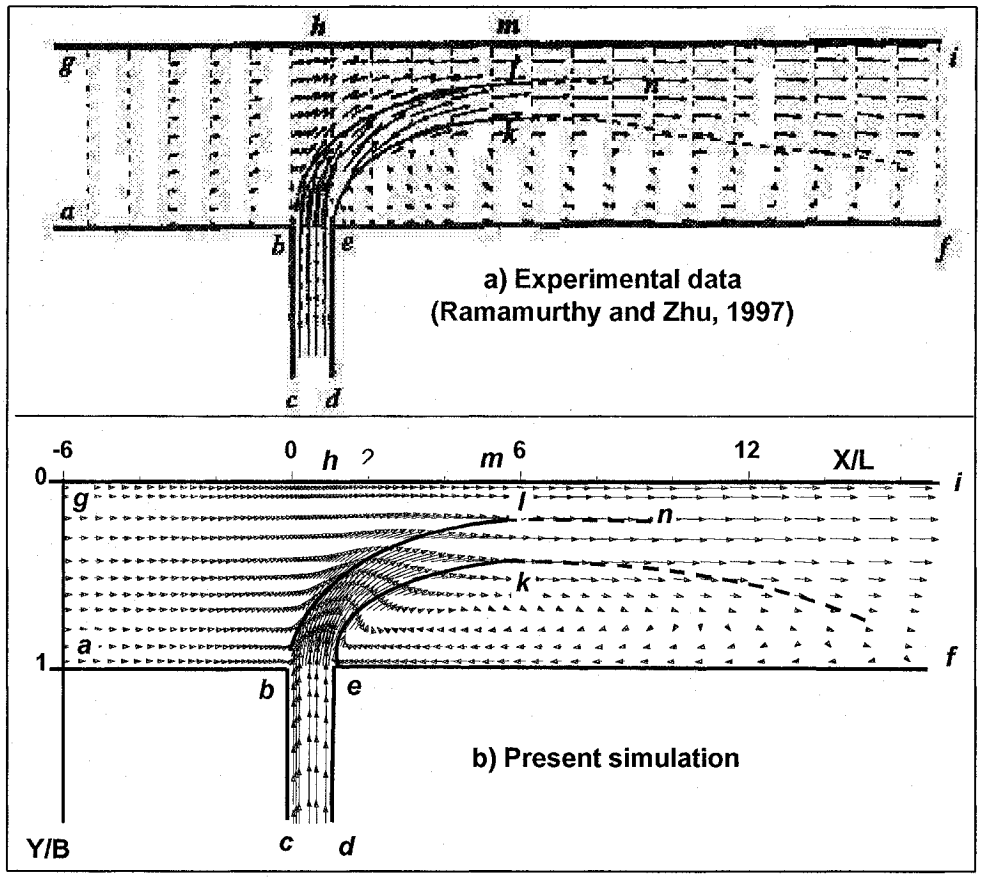

Fig. 5.8 Flow Pattern for L/B = 0.22 and $Q_3/Q_2 = 0.50$

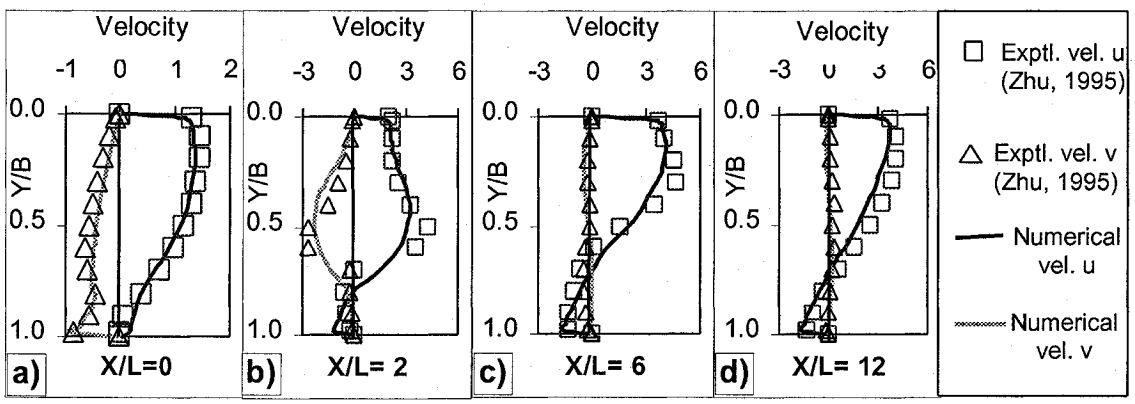

Fig. 5.9 Velocity distribution at various sections for L/B = 0.22 and $Q_3/Q_2 = 0.50$

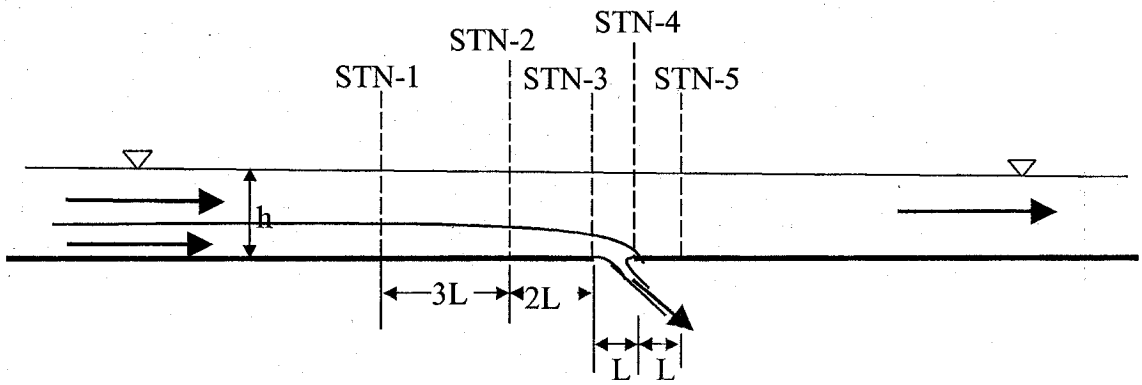

Fig. 6.1 Flow past a floor slot in an open channel

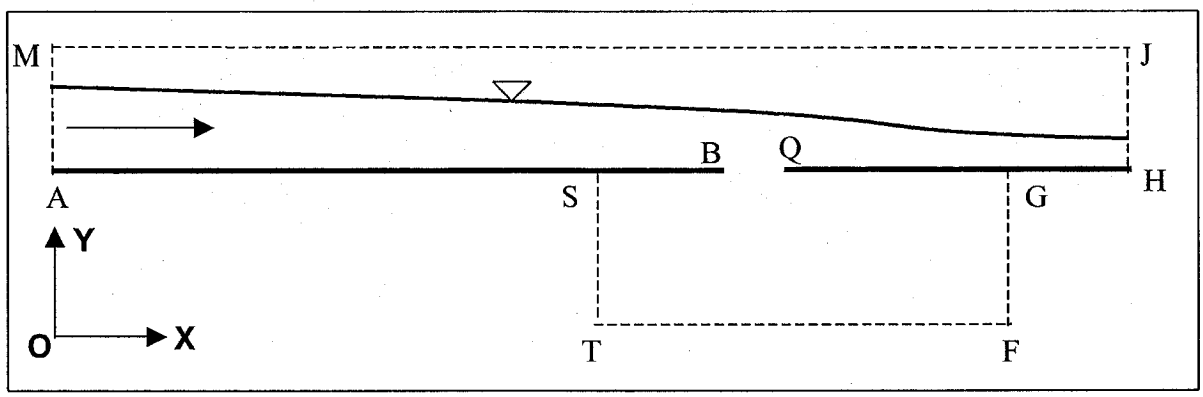

Fig. 6.2 Computational domain for flow past a floor slot

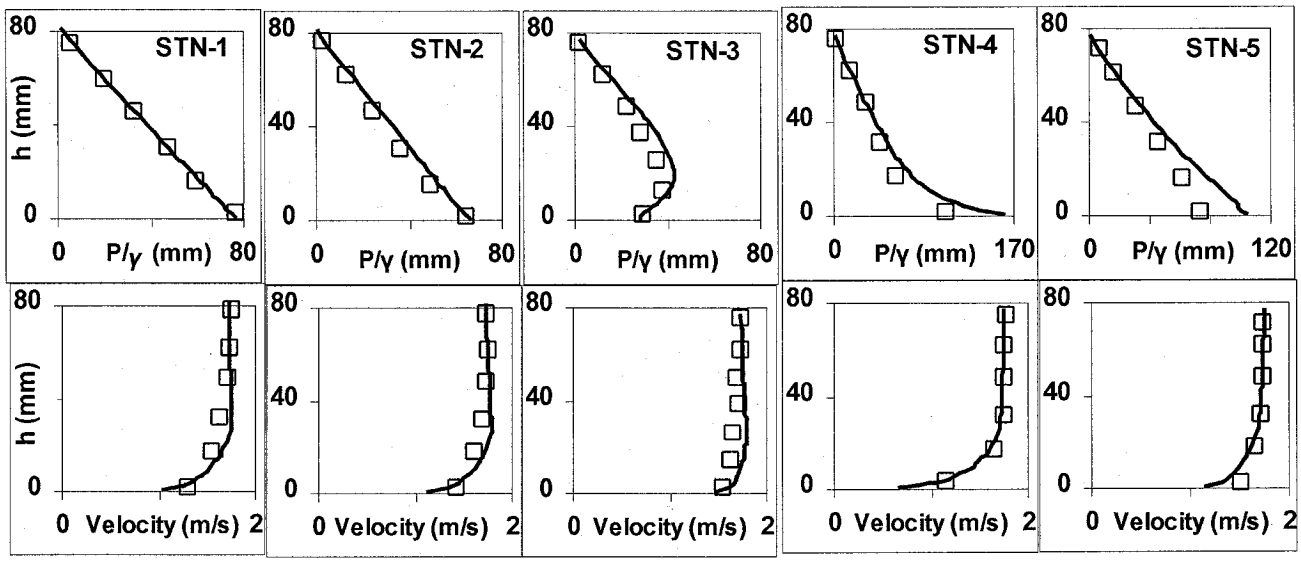

Fig. 6.3 Velocity and Pressure distribution at various sections.

□ Exptl. Data (Ramamurthy and Satish, 1986) —— Present Simulation

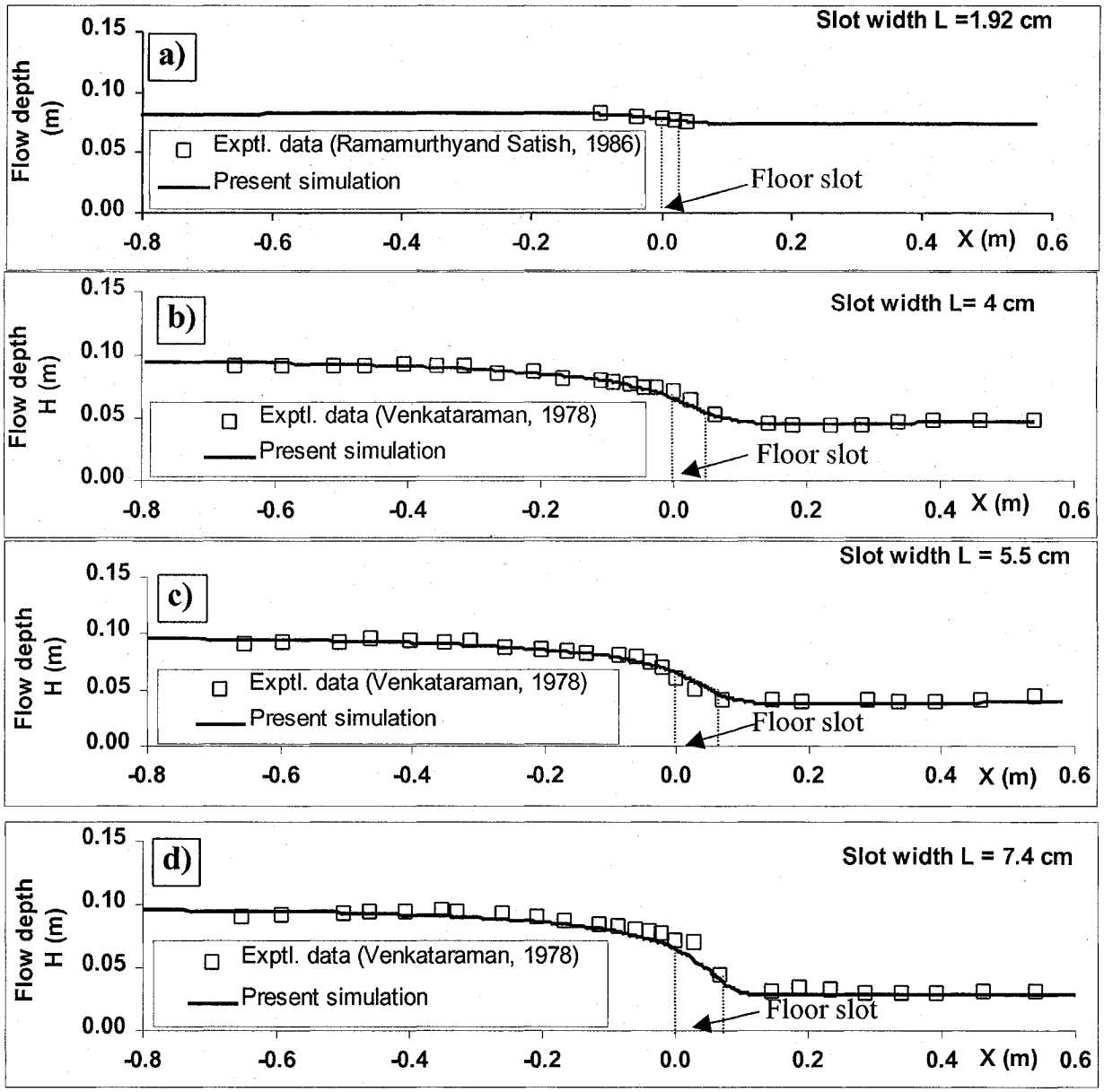

Fig. 6.4 Water surface profiles at various slot widths

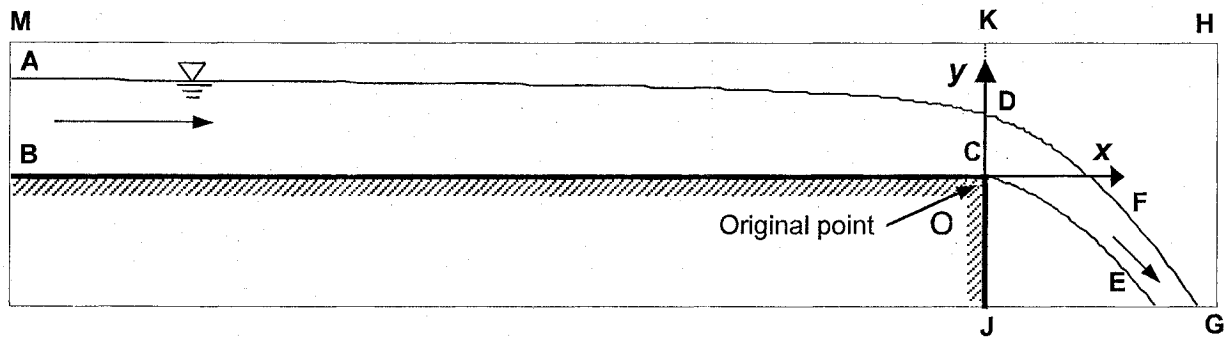

Fig. 7.1 Geometry at free overfall

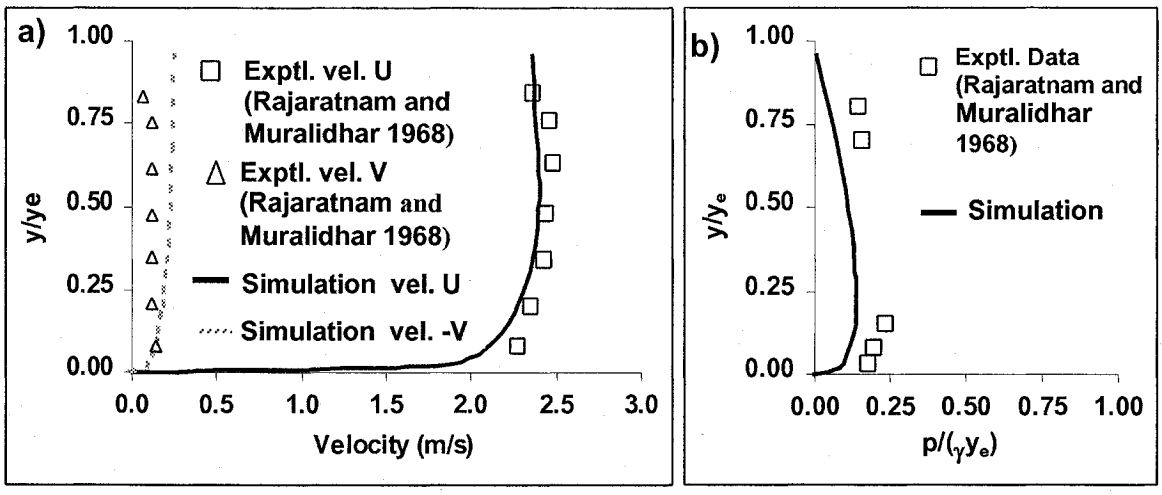

Fig. 7.2 Velocity and pressure distribution at end depth for supercritical flow ($Fr_0 = 2.4$)
a) Velocity distribution b) Pressure distribution

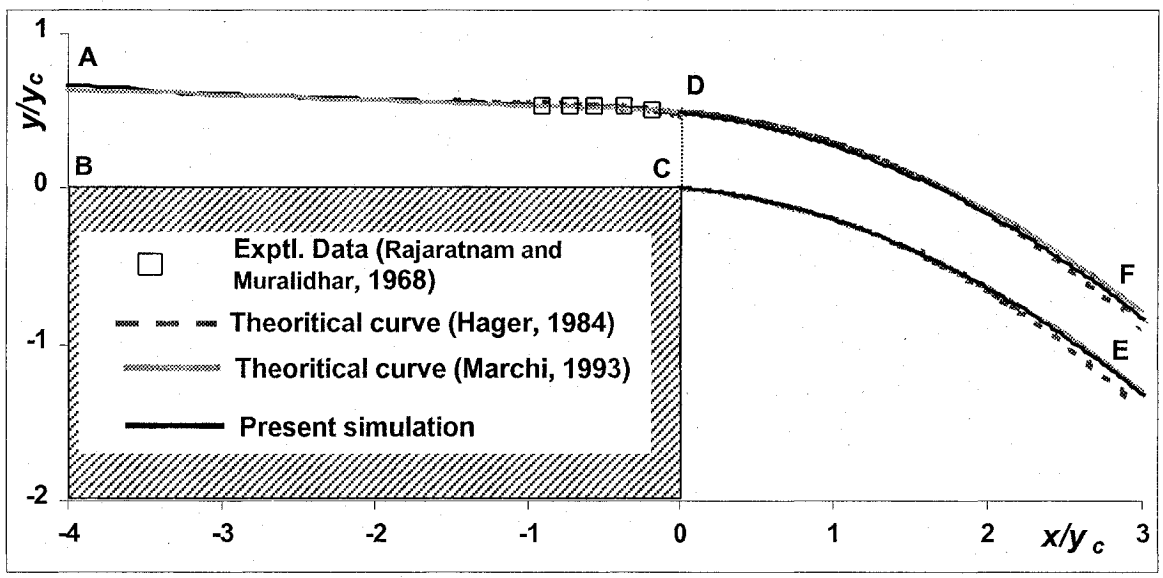

Fig. 7.3 Surface profiles of a free overfall for supercritical approach flow ($Fr_0 = 2.4$)

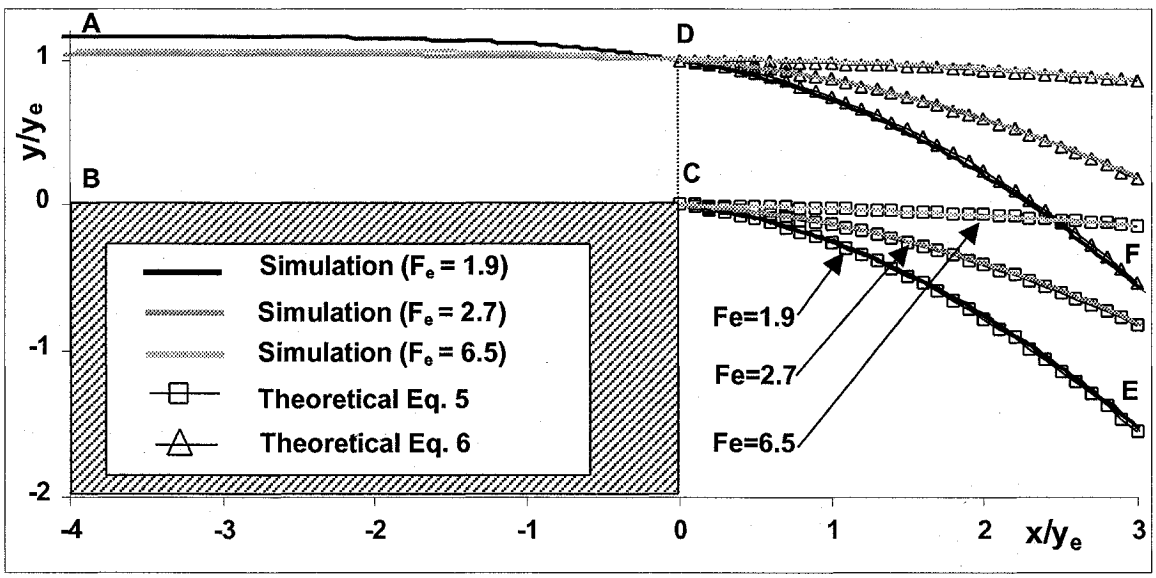

Fig. 7.4 Surface profiles of a free overfall for supercritical approach flow with Eqs.7.1 and 7.2

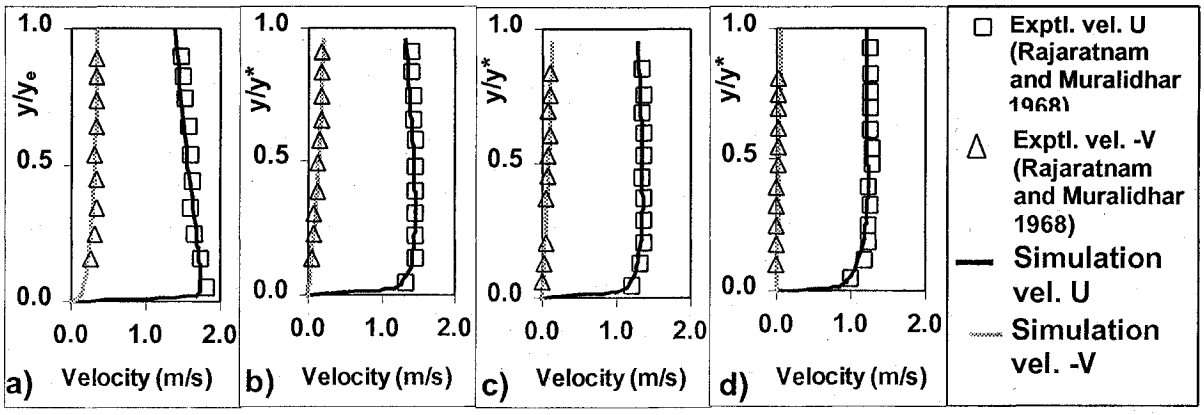

Fig. 7.5 Velocity distribution at various sections near end depth for subcritical flow
a) at x/y_c =0 b) at x/y_c = - 0.45 c) at x/y_c = - 0.89 d) at x/y_c = - 2.23

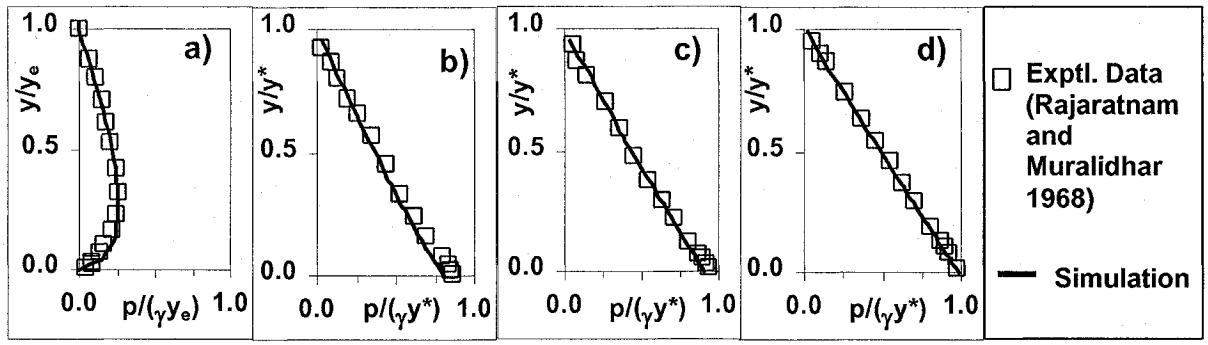

Fig. 7.6 Pressure distribution at various sections near end depth for subcritical flow
a) at x/y_c =0 b) at x/y_c = - 0.45 c) at x/y_c = - 0.89 d) at x/y_c = - 2.23

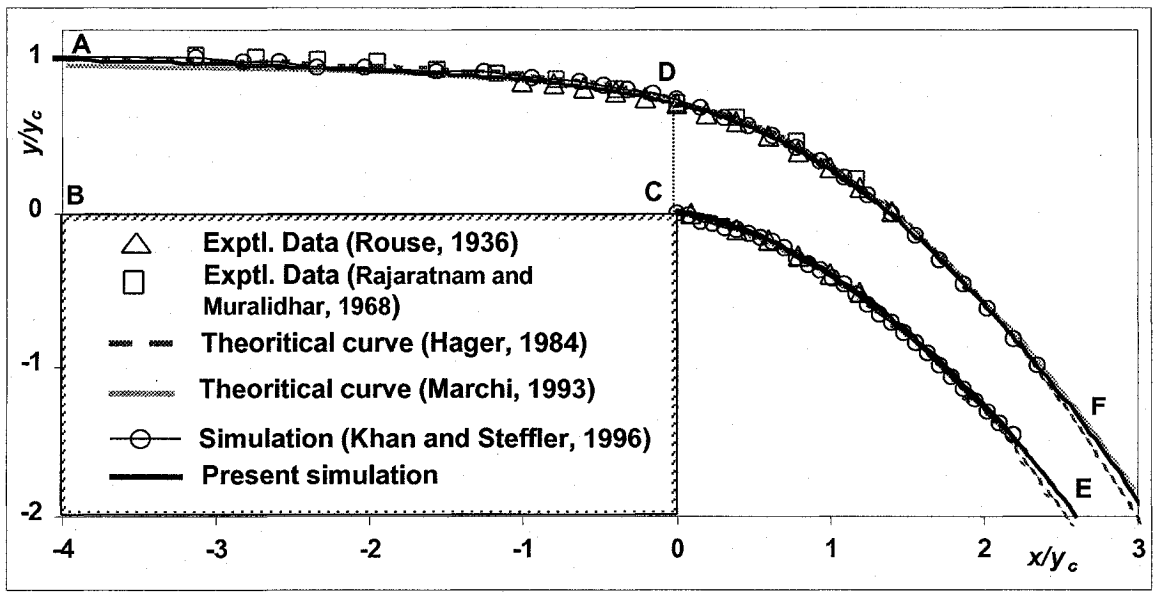

Fig. 7.7 Surface profiles of a free overfall of subcritical approach flow

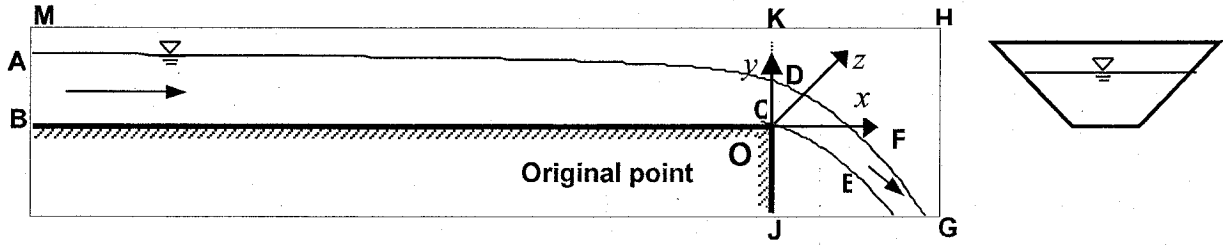

Fig. 8.1 Geometry at free overfall at a trapezoidal channel

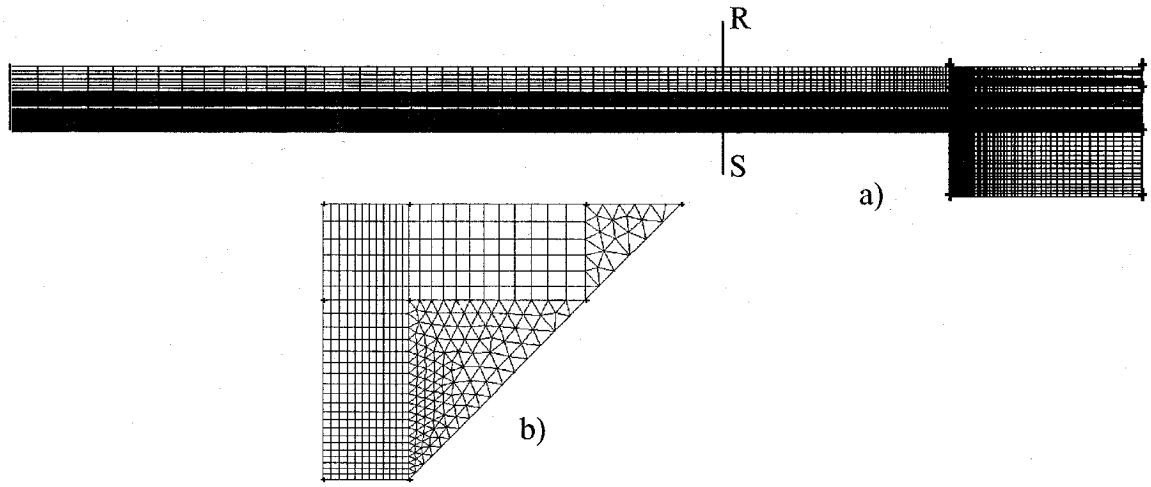

Fig. 8.2 Details of grid.
a) longitudinal section along the plane of symmetry
b) half-cross section across RS.

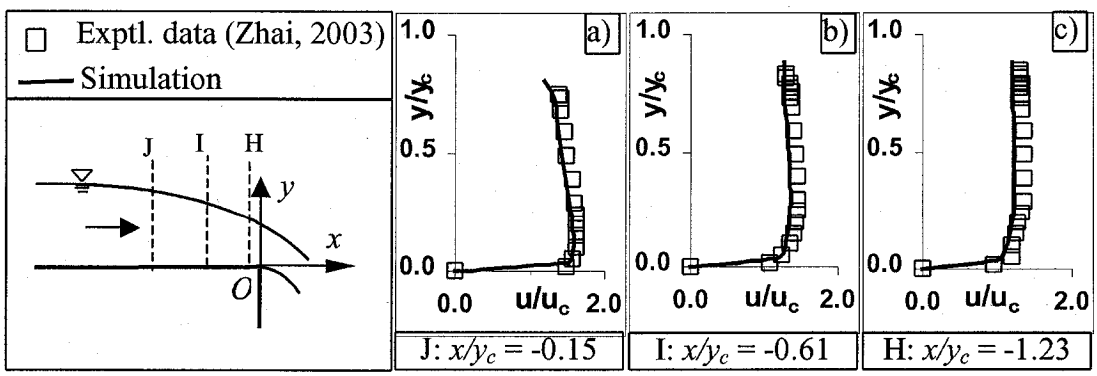

Fig. 8.3 Velocity distribution upstream of the brink

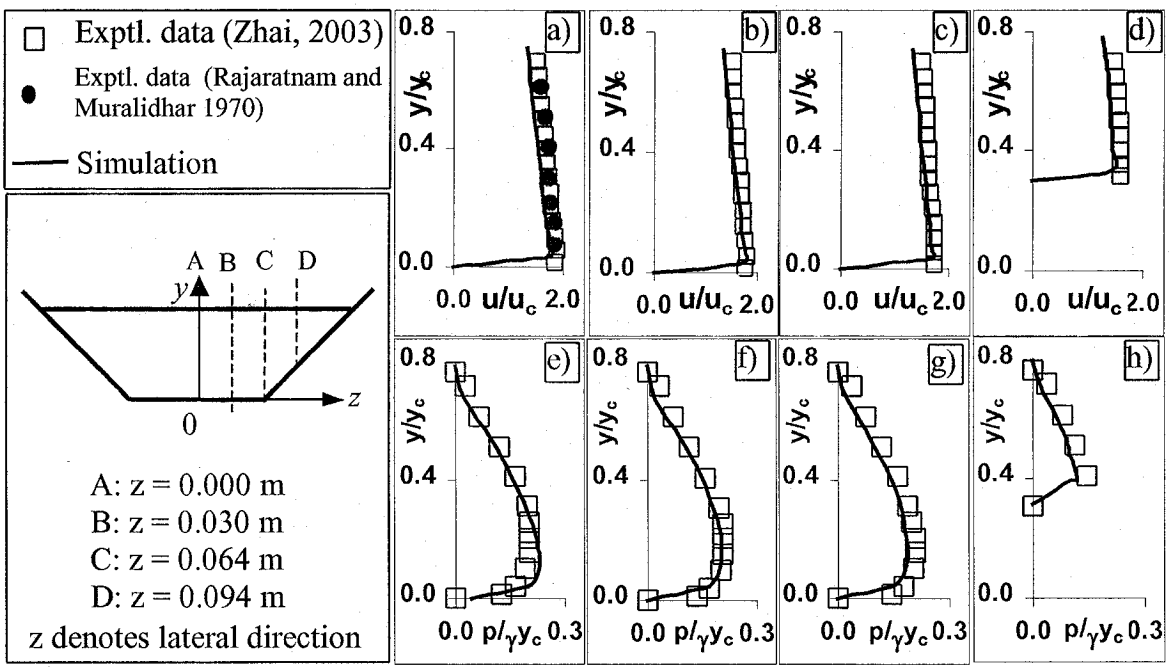

Fig. 8.4 Velocity and pressure distribution at the brink
(Channel bottom width = 0.127 m. Channel side slope: 1:1)

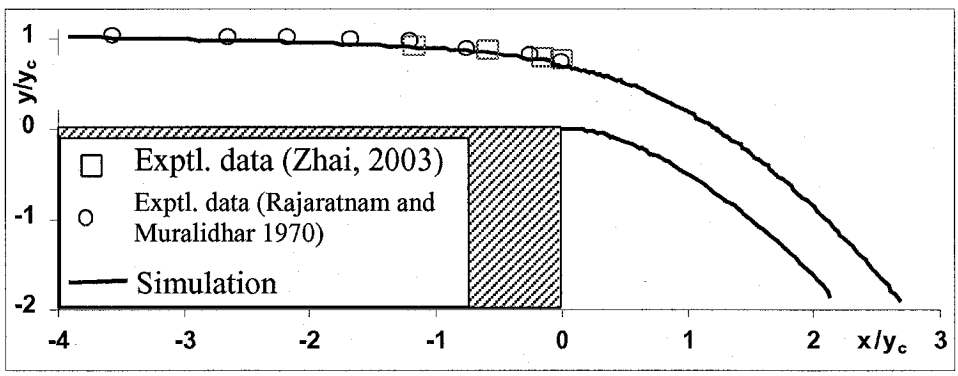

Fig. 8.5 Water surface profile of a free overfall at a trapezoidal channel

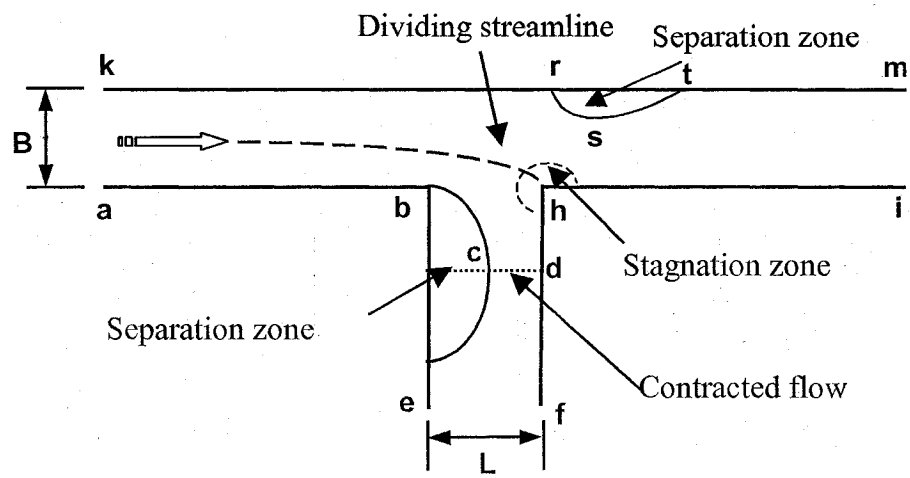

Fig. 9.1 Flow characteristics of a dividing flow in open channels

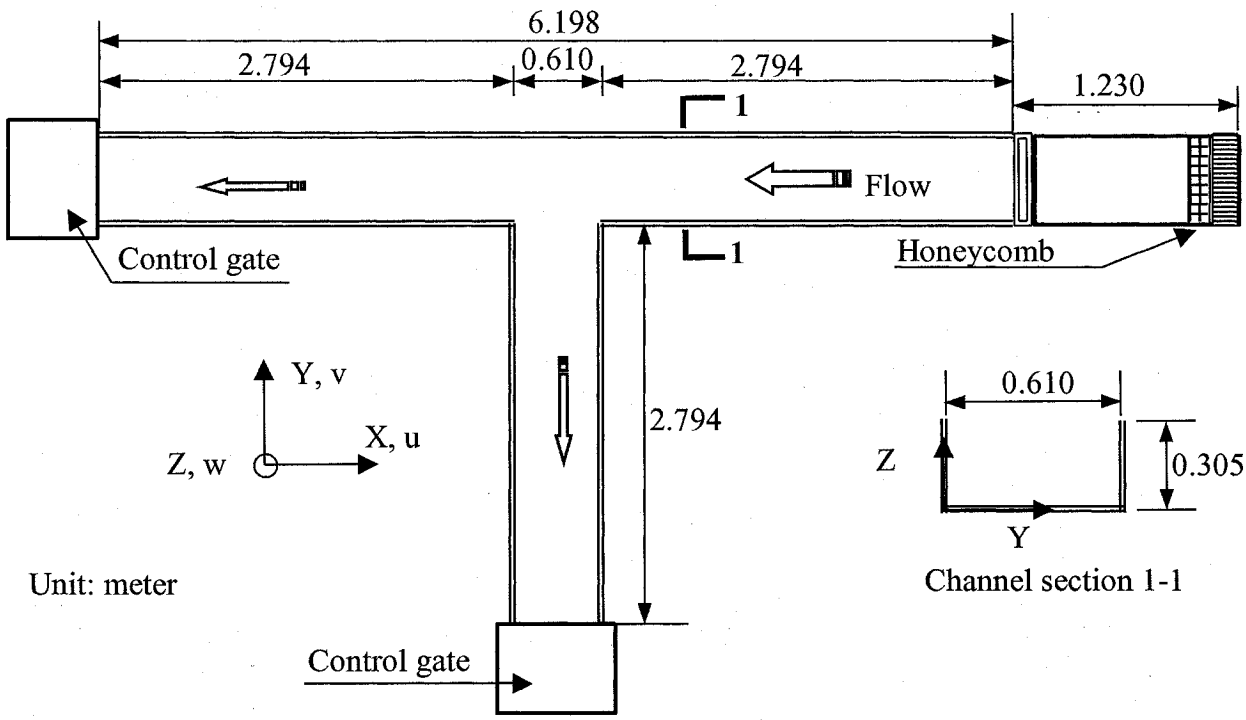

Fig. 9.2 Experimental Channel for dividing flow

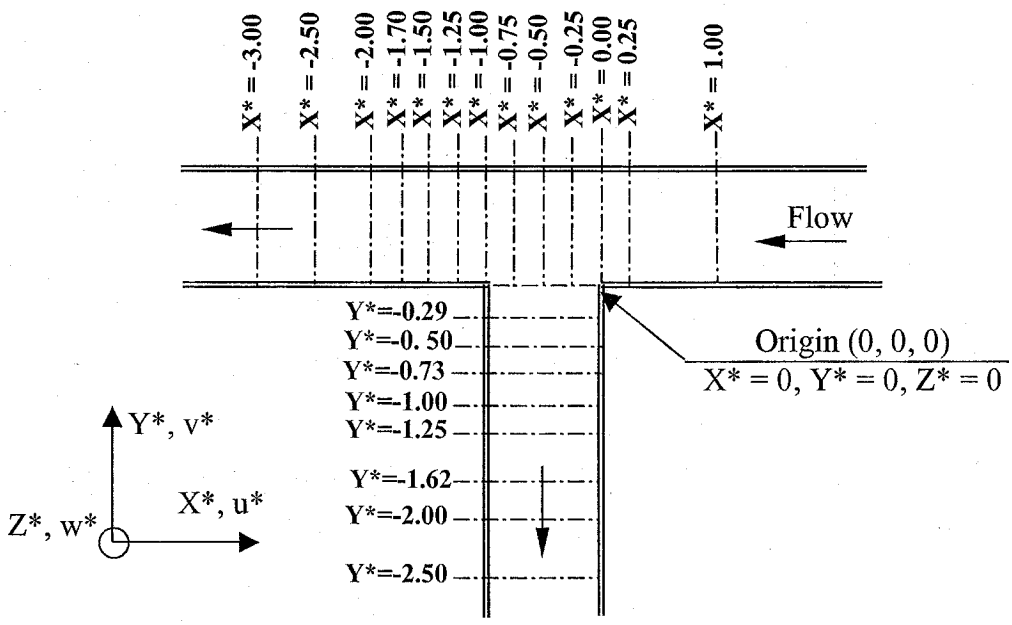

a) Data collection sections (plane view)

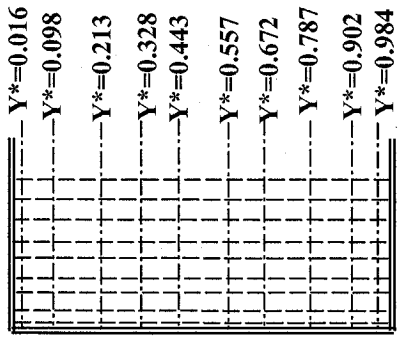

b) Data collection locations at cross section (looking downstream)

Fig. 9.3 Cross sections for measurements of the flow velocity

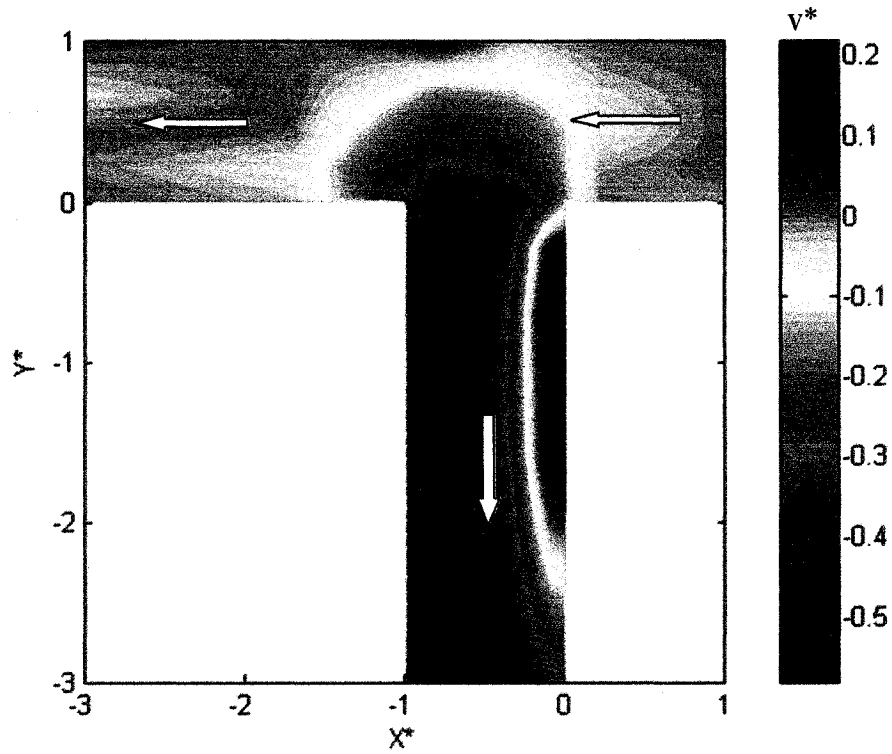

Fig. 9.4 Contours for velocity v* at the plane Z* = 0.27 for Q_r = 0.838

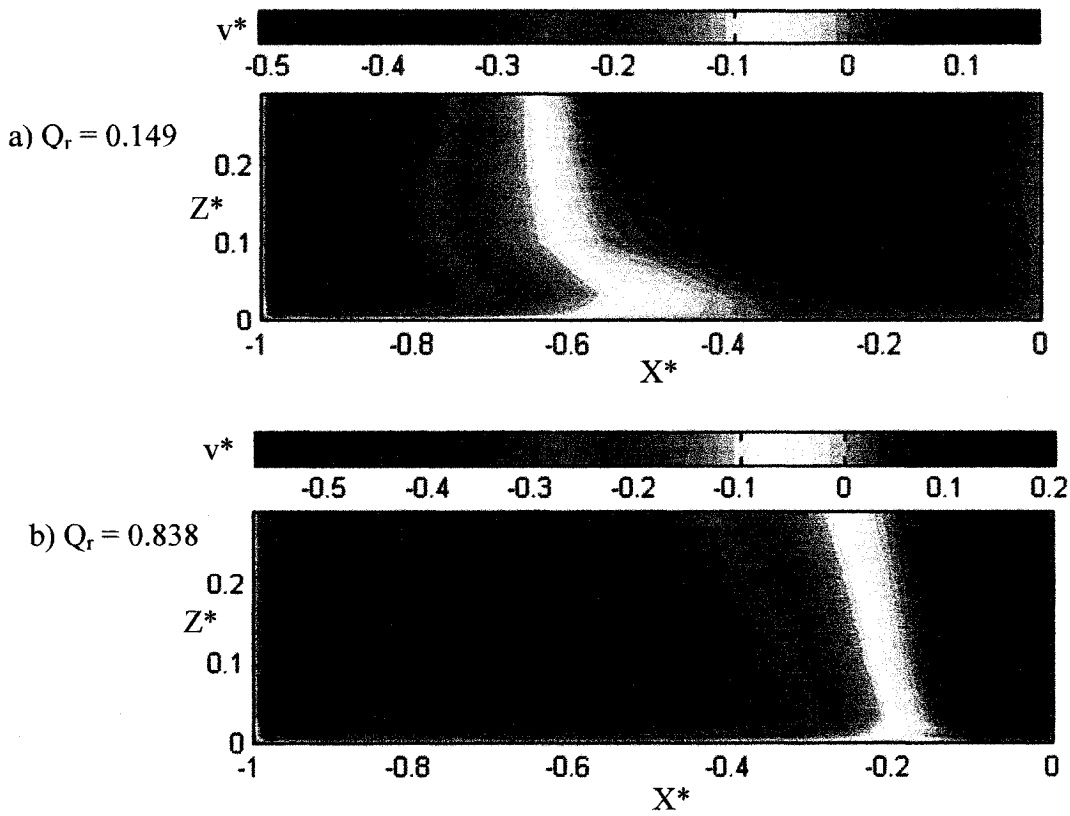

Fig. 9.5 Contours for velocity v* at cross section Y* = -1.0

a)

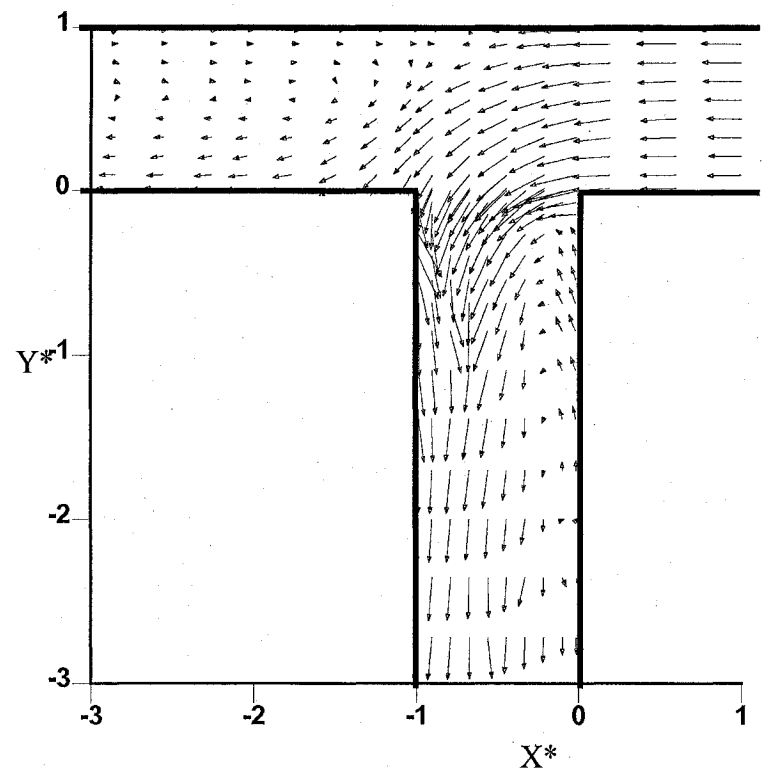

b)

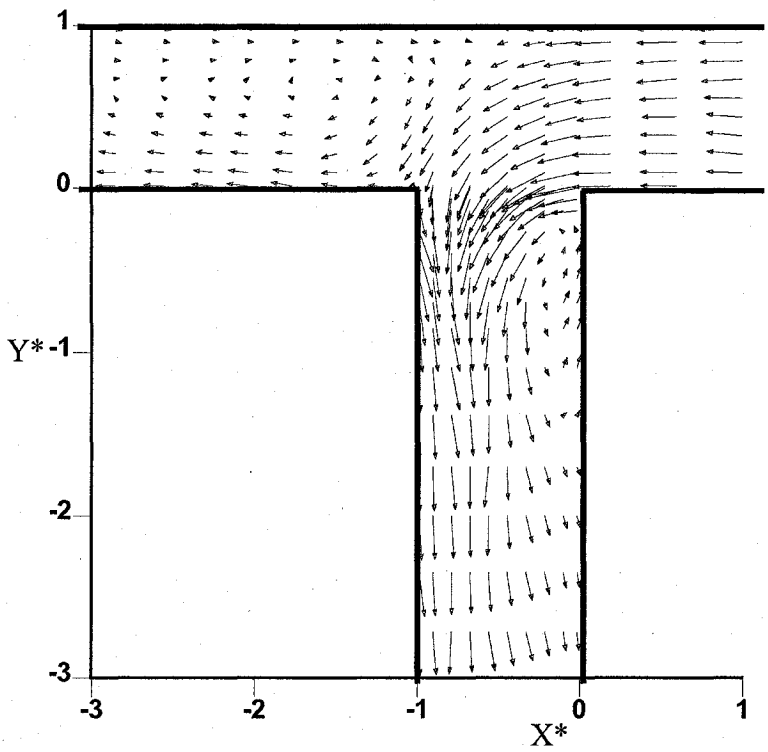

Fig. 9.6 Velocity u*-v* vector plot for $Q_r = 0.838$ at different level
a) Z* = 0.27 b) Z* = 0.033

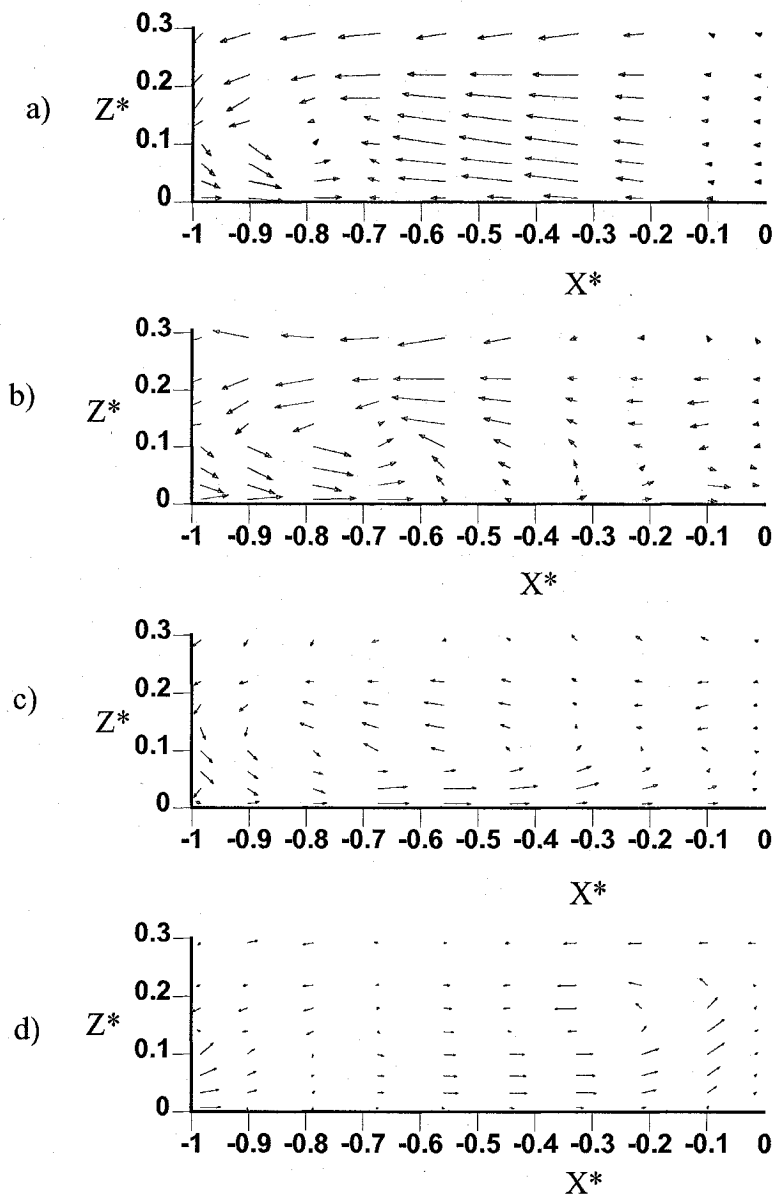

Fig. 9.7 Velocity u*-w* vector plot for $Q_r = 0.838$ at various locations (looking upstream) a) Y* = -0.29 b) Y* = -0.73 c) Y* = -1.0 d) Y* = -2.50

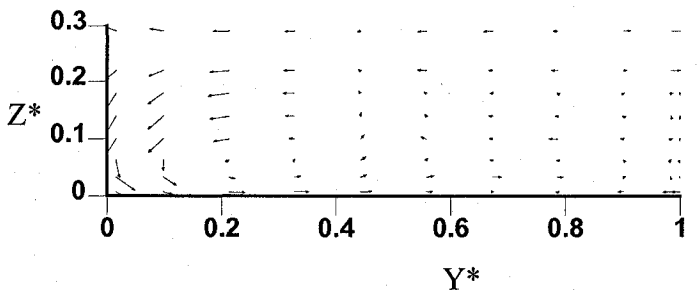

Fig. 9.8 Velocity v*-w* vector plot for $Q_r = 0.838$ at X* = -1.7

a)

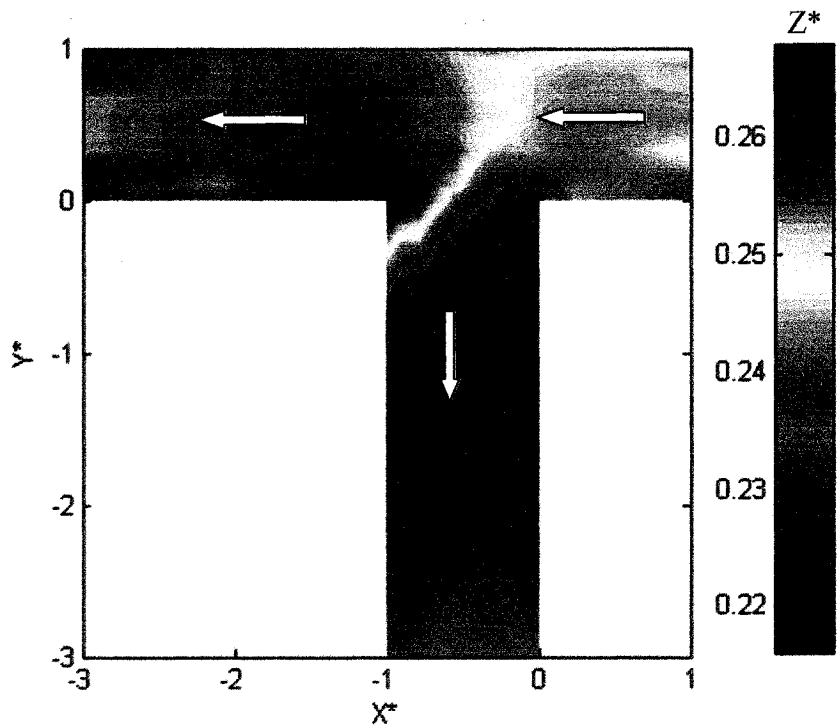

b)

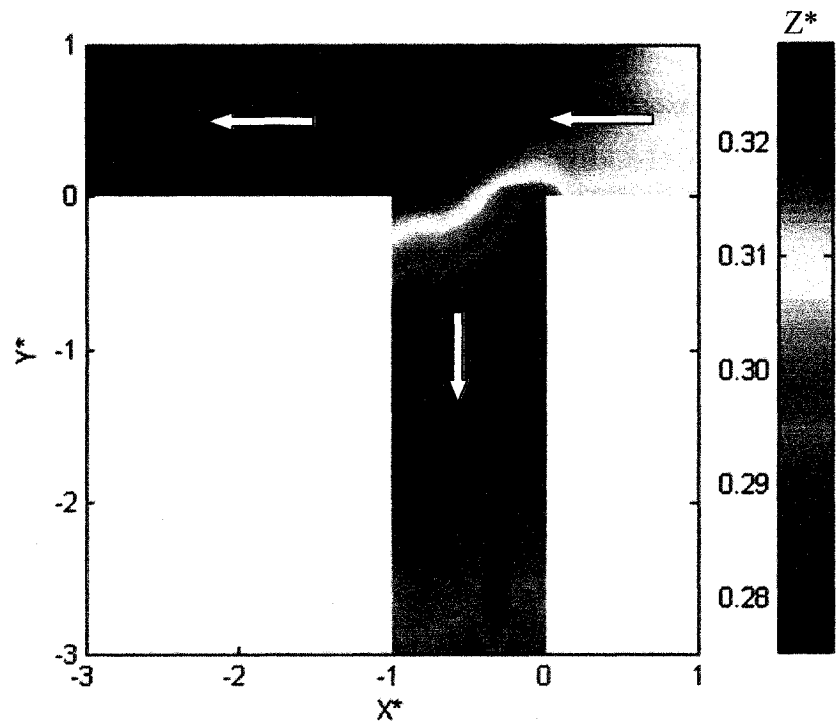

Fig. 9.9 Water surface profiles a) $Q_r = 0.409$ b) $Q_r = 0.838$

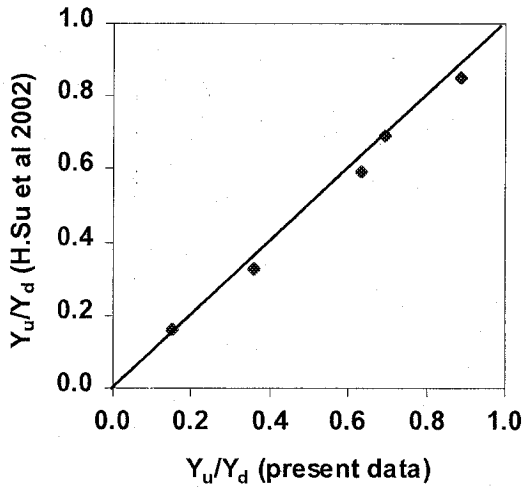

Fig. 9.10 Comparison of the flow depth ratio Y_u/Y_d

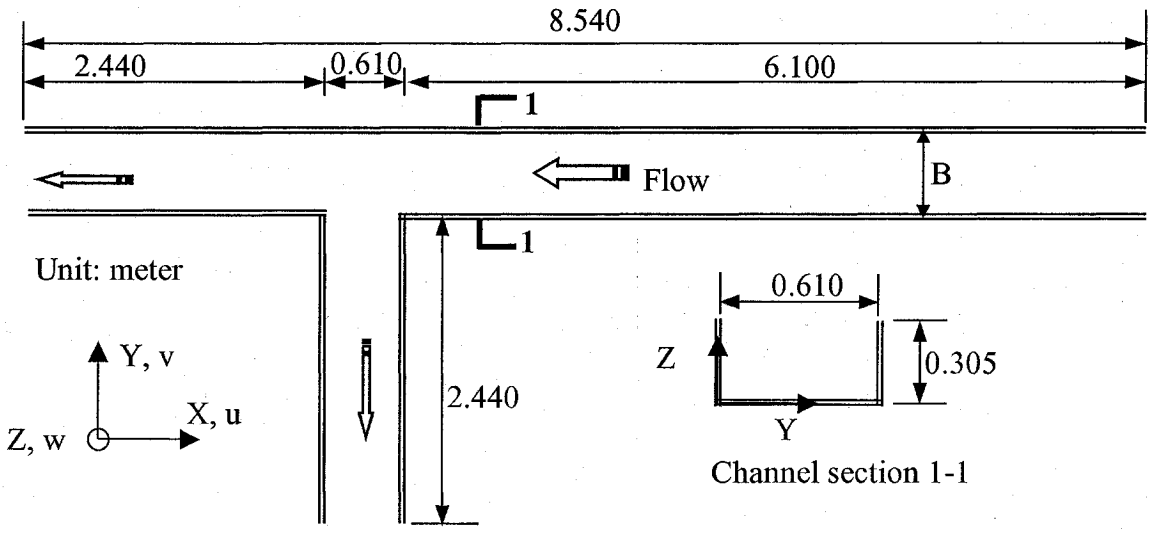

Fig. 10.1 Computational domain

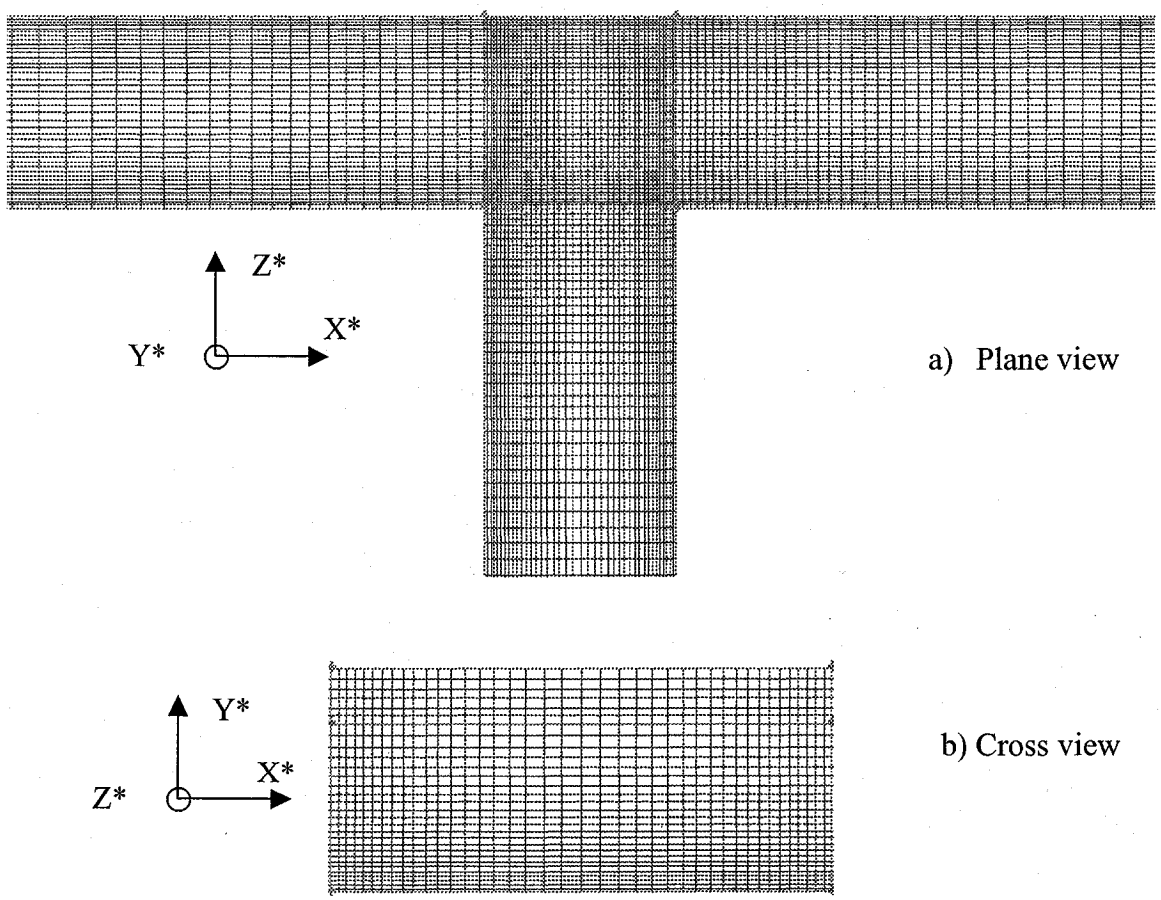

Fig. 10.2 Grid geometry near junction region

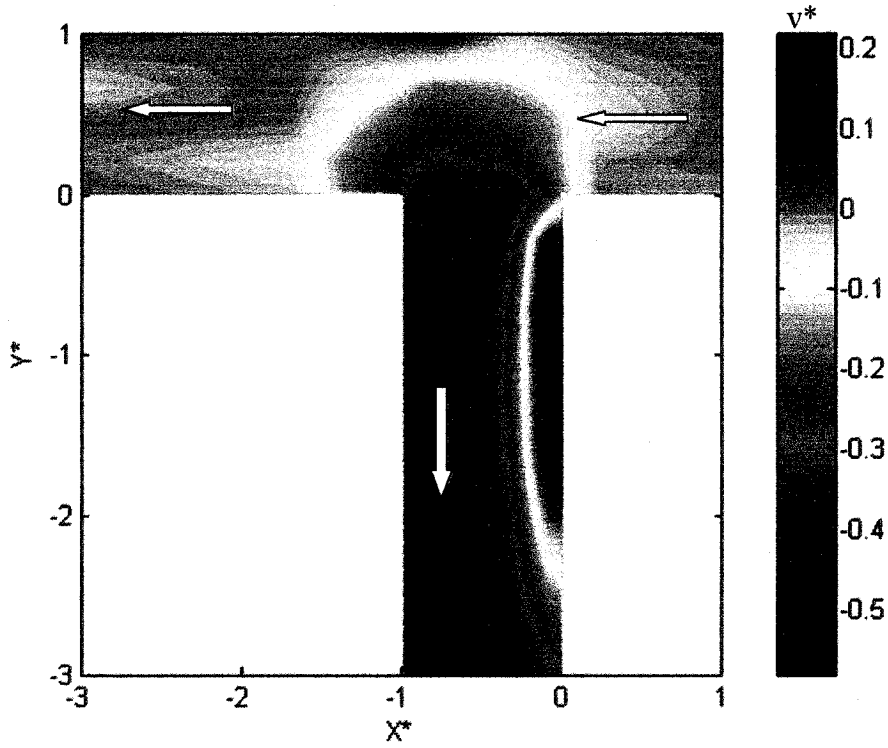

a) Experimental data

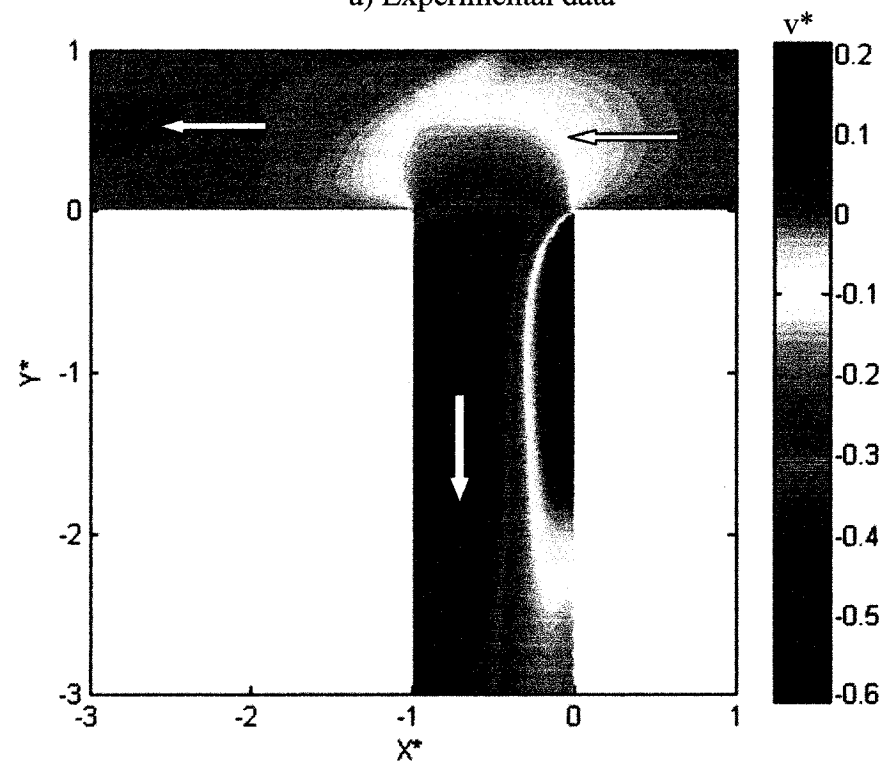

b) Numerical data

Fig. 10.3 Contours for velocity v* at the plane Z* = 0.27

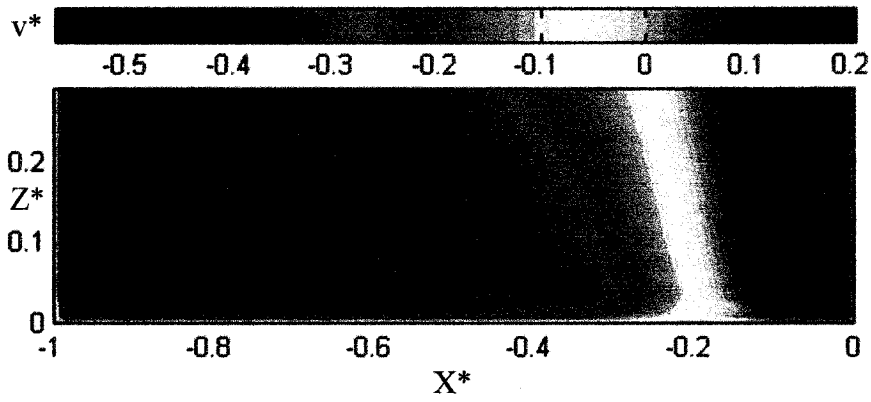

a) Experimental data

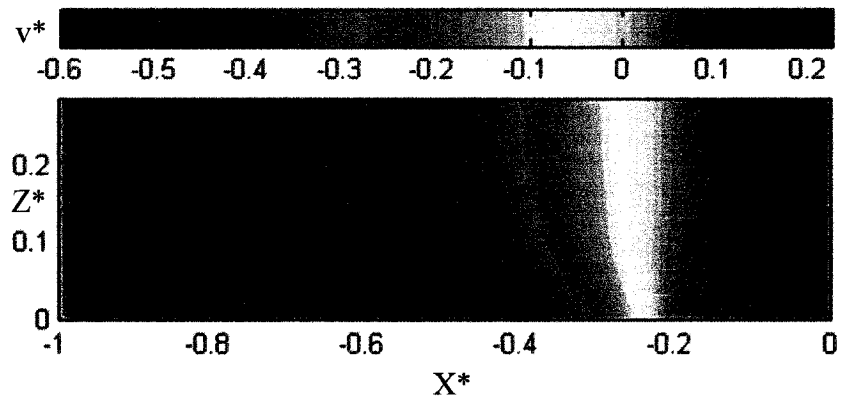

b) Numerical data

Fig. 10.4 Contours for velocity v* at cross section Y* = -1.0

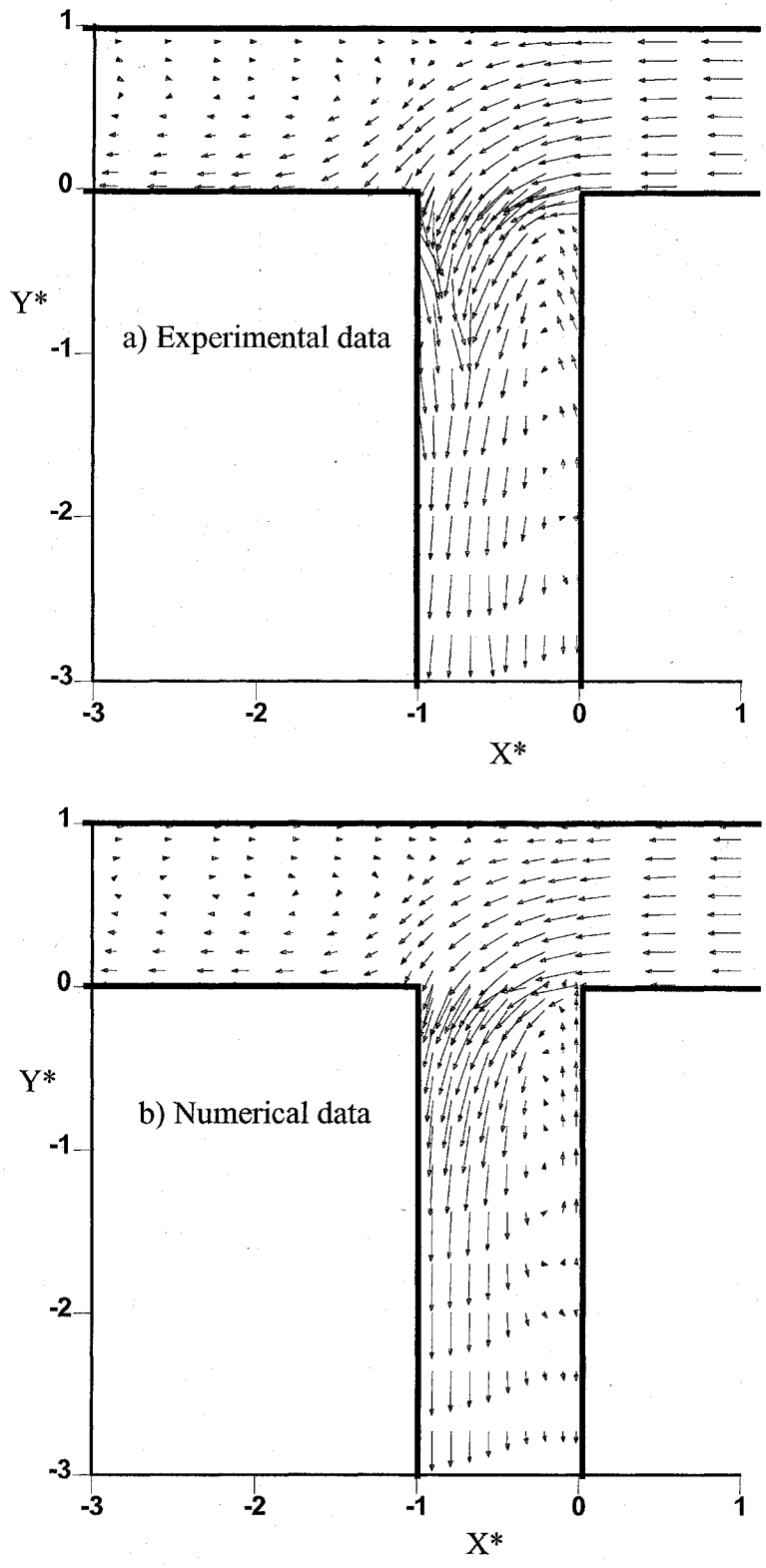

Fig. 10.5 Velocity u*-v* vector plot at Z* = 0.27

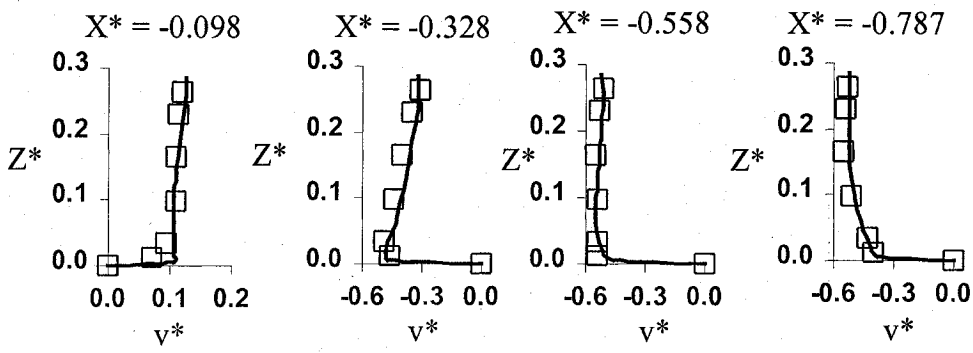

a) Y* = -0.29

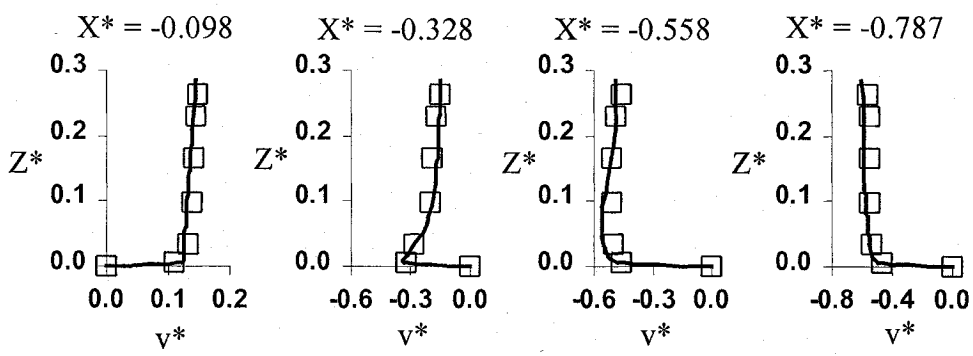

b) Y* = -1.0

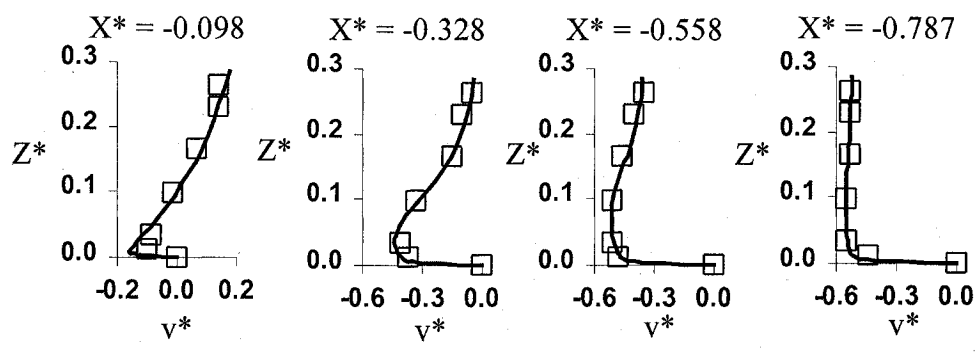

c) Y* = -1.62

Fig. 10.6 Comparison of velocity v* in the branch channel
(□ Experimental data —— Numerical data)

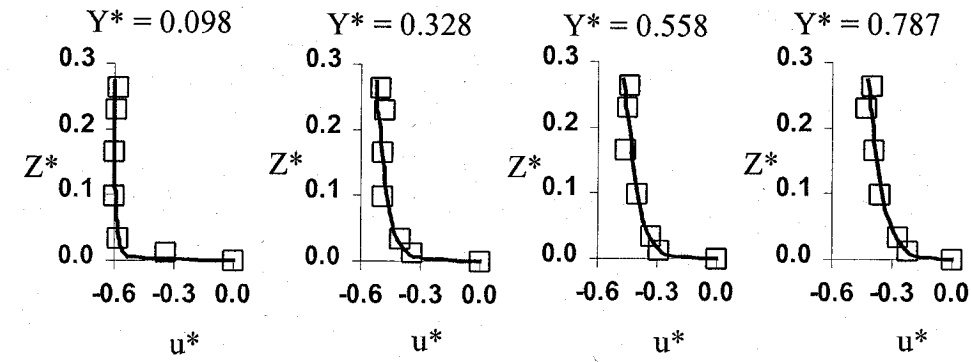

a) X* = 0.0

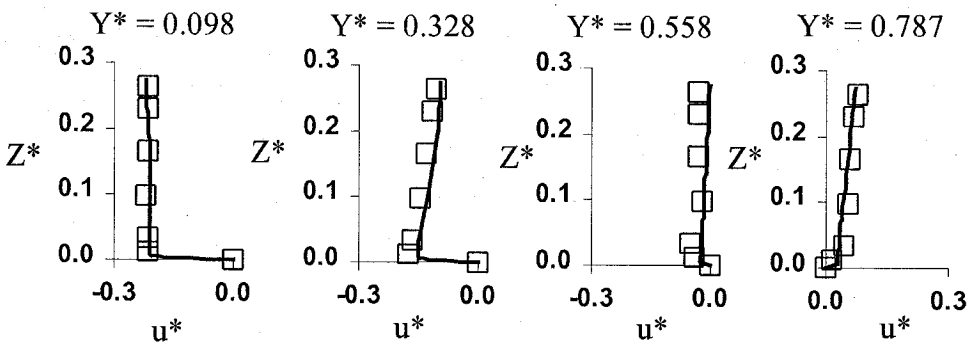

b) X* = -1.70

Fig. 10.7 Comparison of velocity u* in the main channel
(□ Experimental data —— Numerical data)

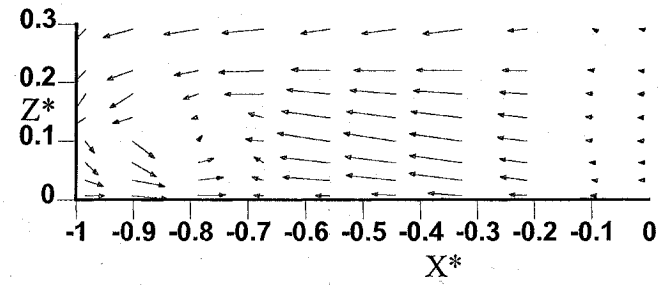

a) Experiment

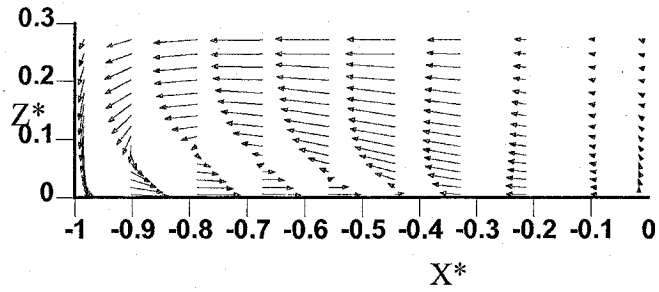

b) Simulation

Fig. 10.8 Velocity u*-w* vector plot at Y* = -0.29 (looking upstream)

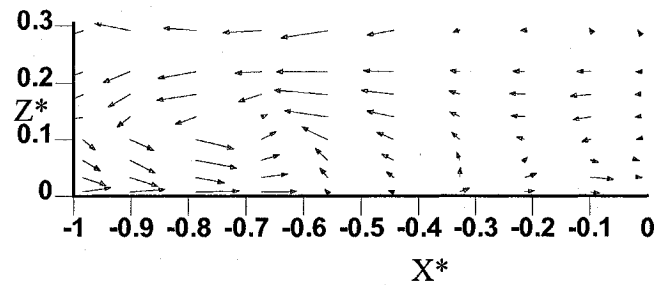

a) Experimental data

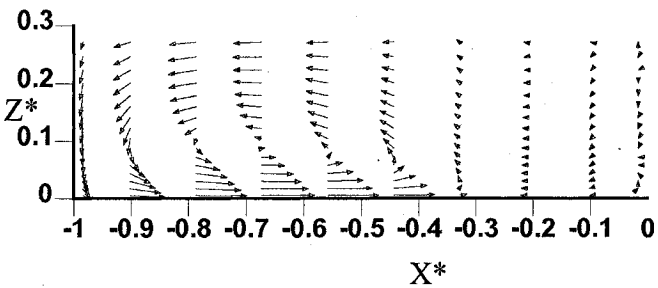

b) Numerical data

Fig. 10.9 Velocity u*-w* vector plot at Y* = -0.73 (looking upstream)

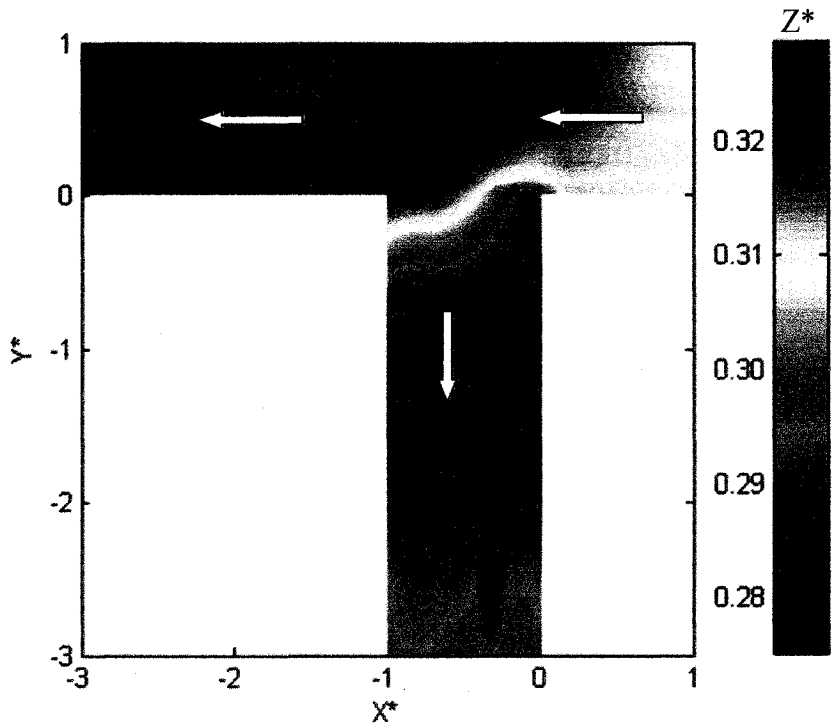

a) Experimental data

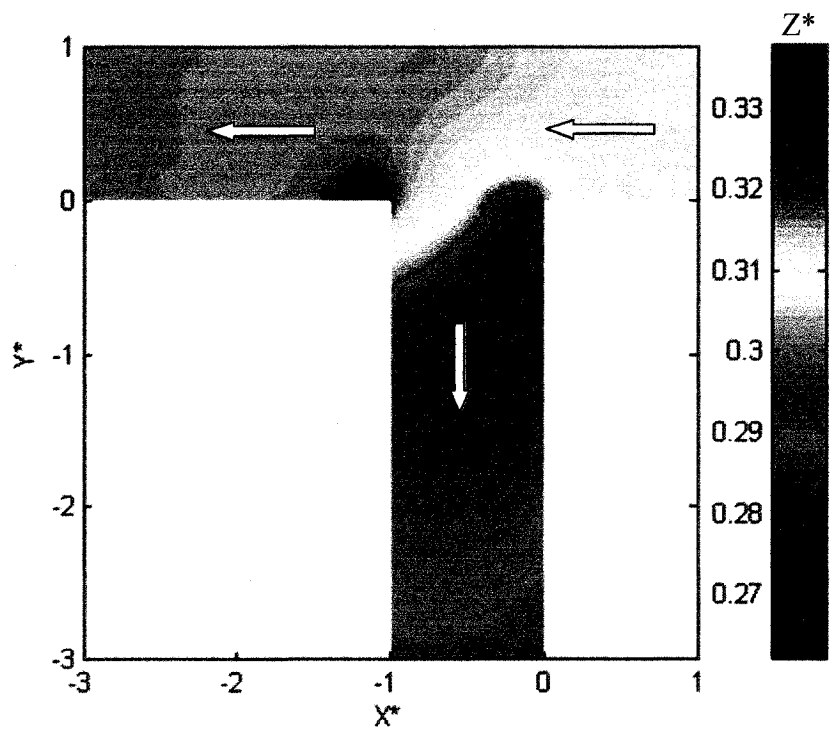

b) Numerical data

Fig. 10.10 Water surface profiles

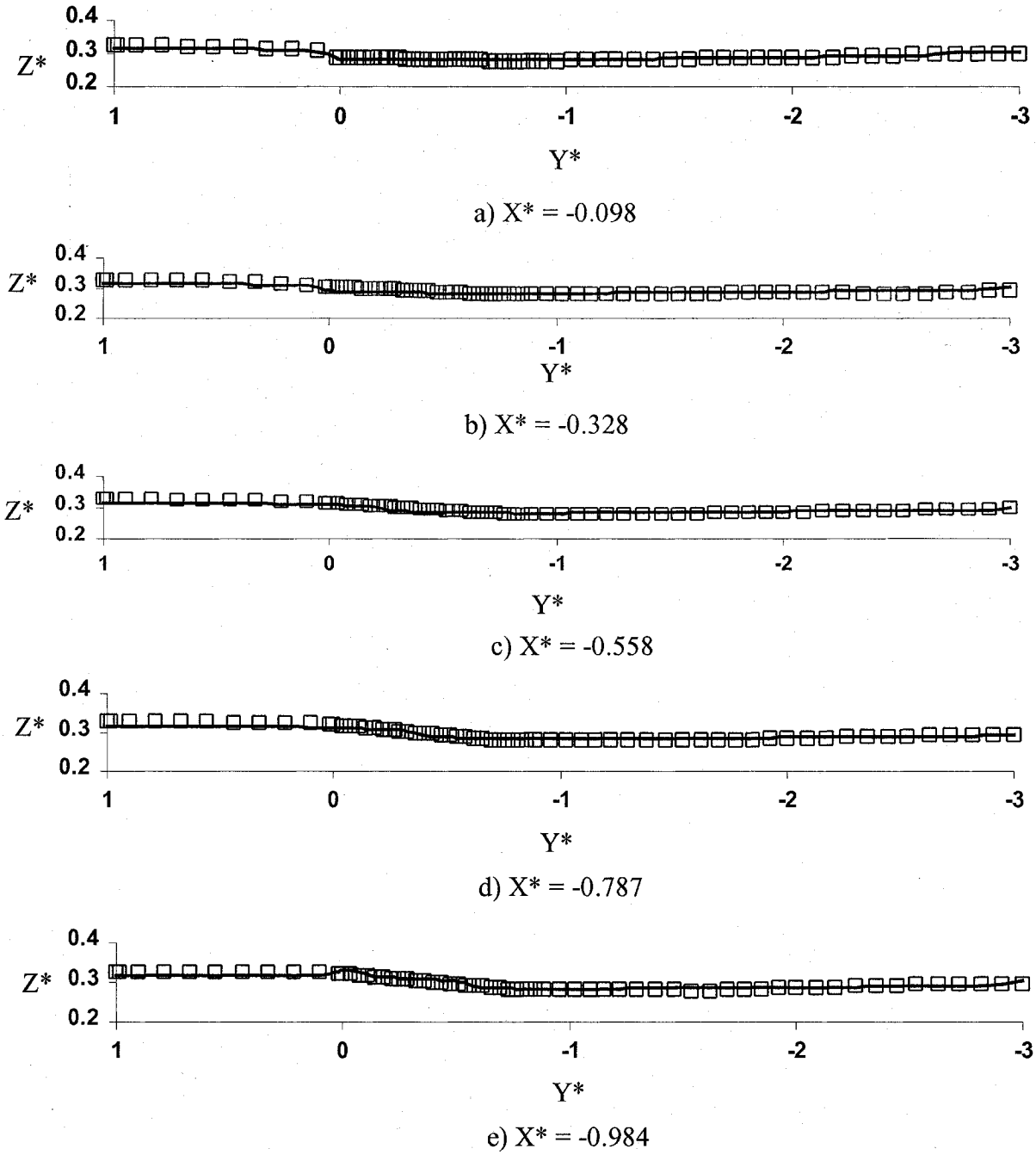

Fig. 10.11 Comparison of water surface profile at several sections
(□ Experimental data —— Numerical data)

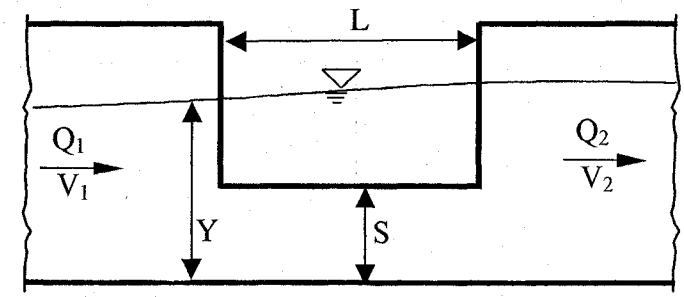

a) Front view

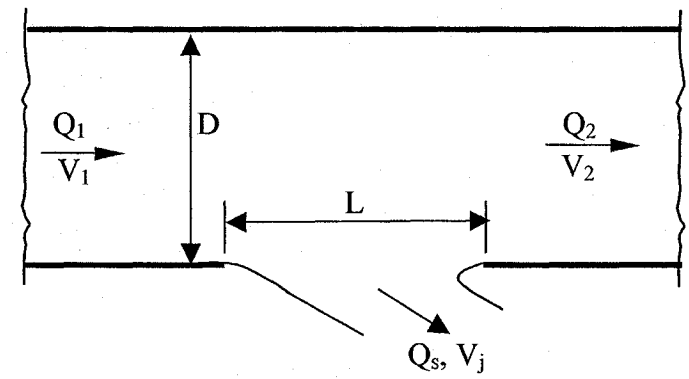

b) Plan view

Fig. 11.1 sketch of side weir

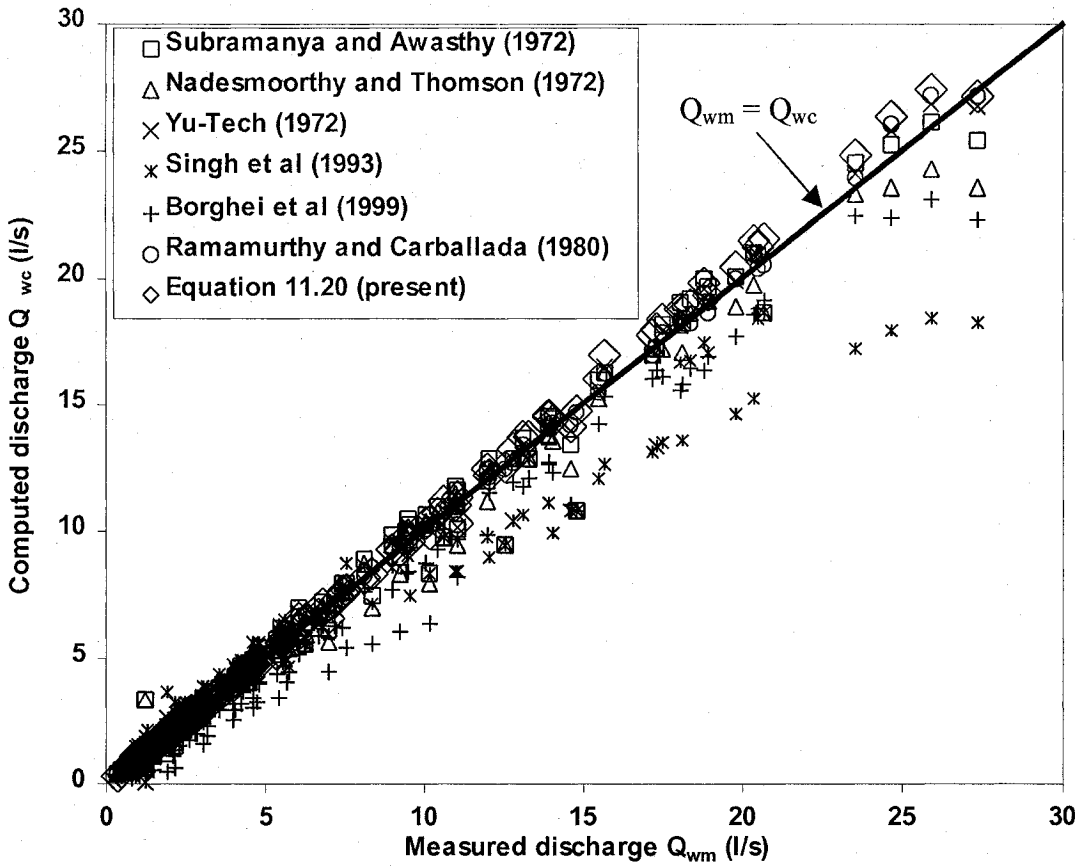

Fig. 11.2 Measured discharge versus computed discharge for a side weir in a rectangular open channel

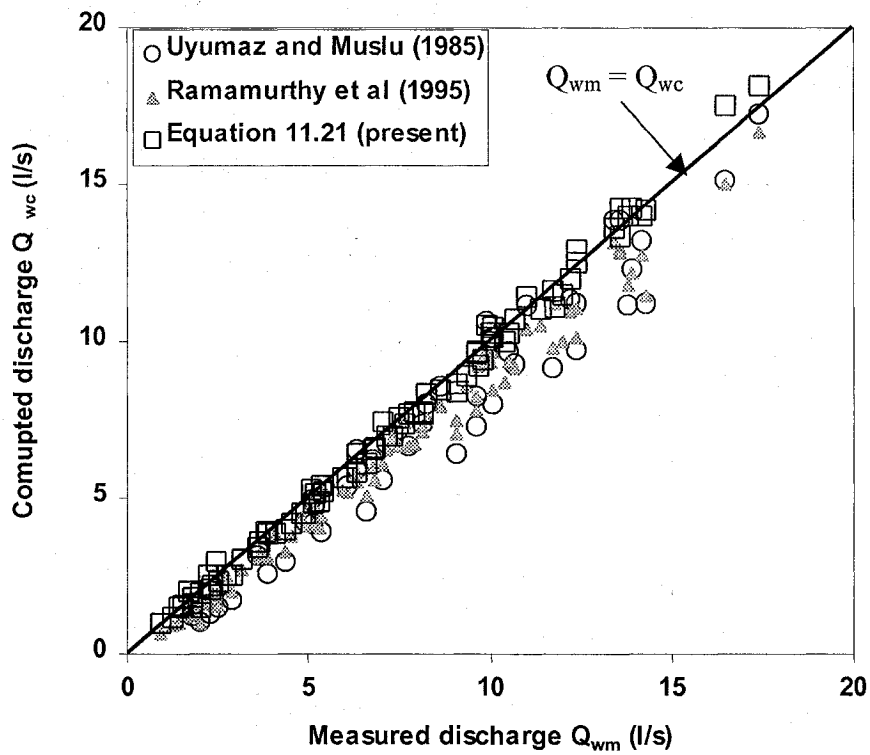

Fig. 11.3 Measured discharge versus computed discharge for a side weir in a circular open channel

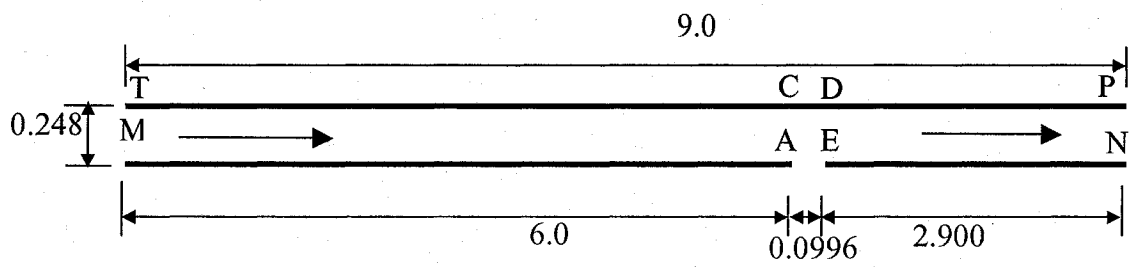

a) Plan view

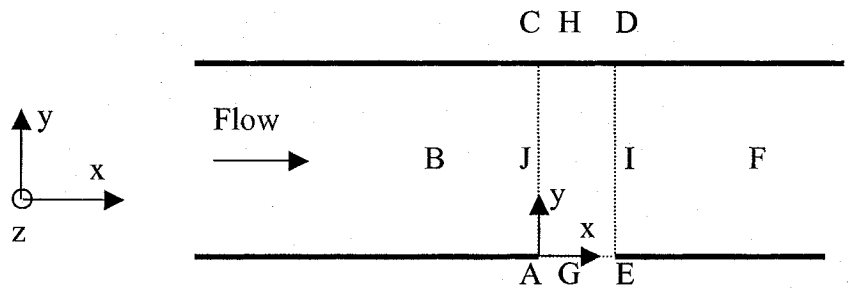

b) Details near the side weir outlet

Fig. 11.4 Computational geometry for the side weir

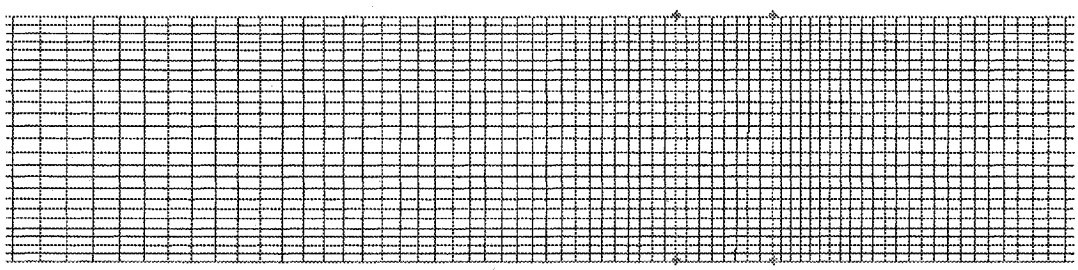

Fig. 11.5 Grid geometry near the weir region

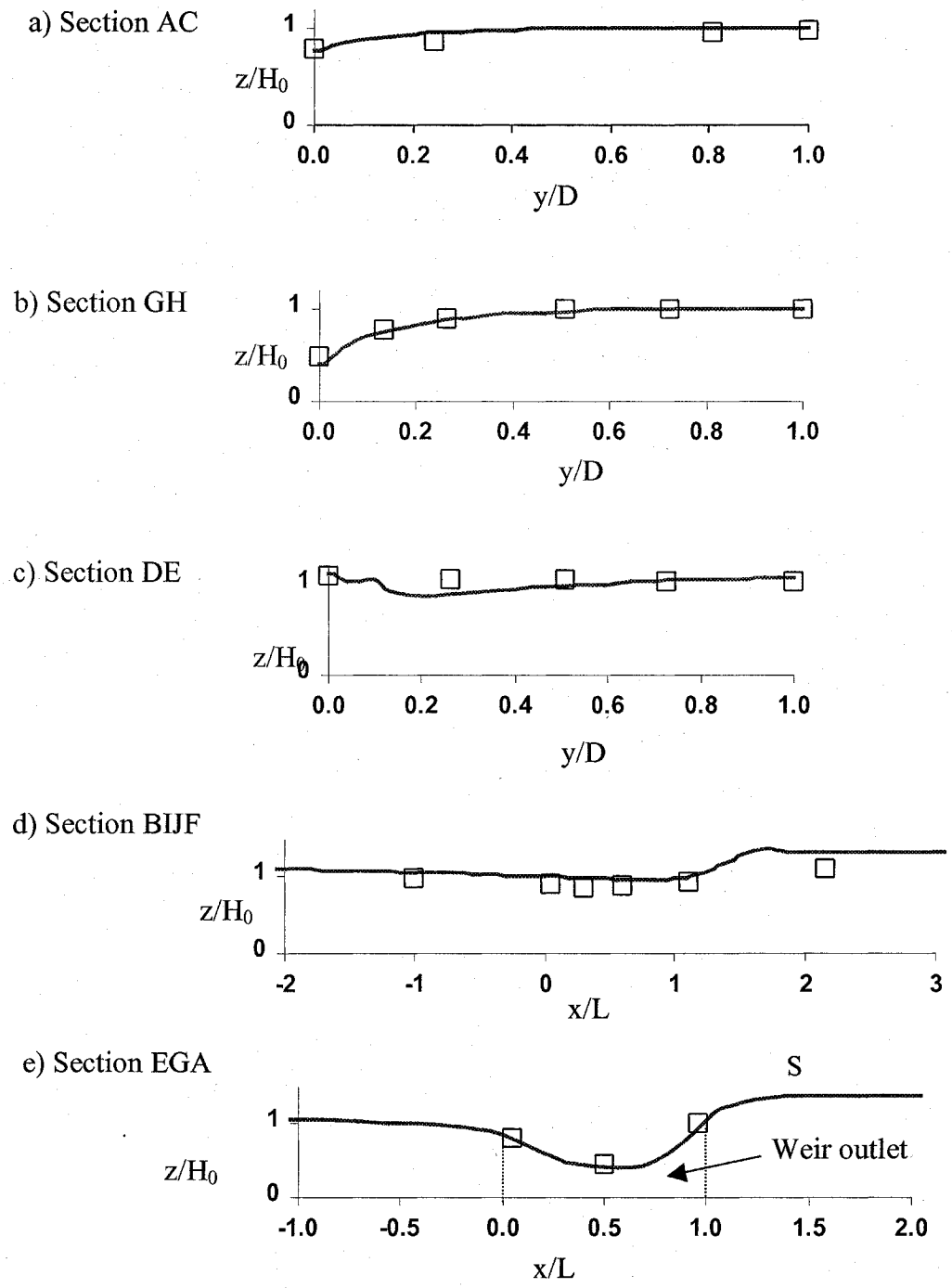

Fig. 11.6 Typical water surface profiles near the weir outlet
□ Experimental data (Subramanya and Awasthy 1972) —— Numerical data

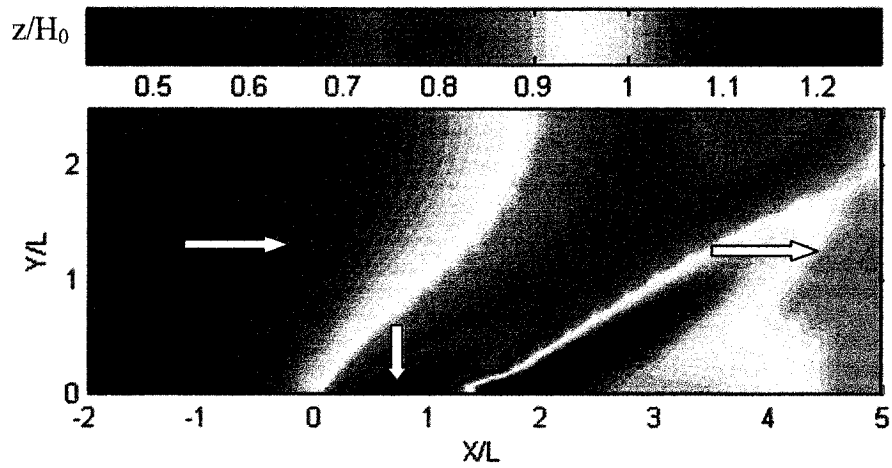

Fig. 11.7 Water surface contour near the weir outlet

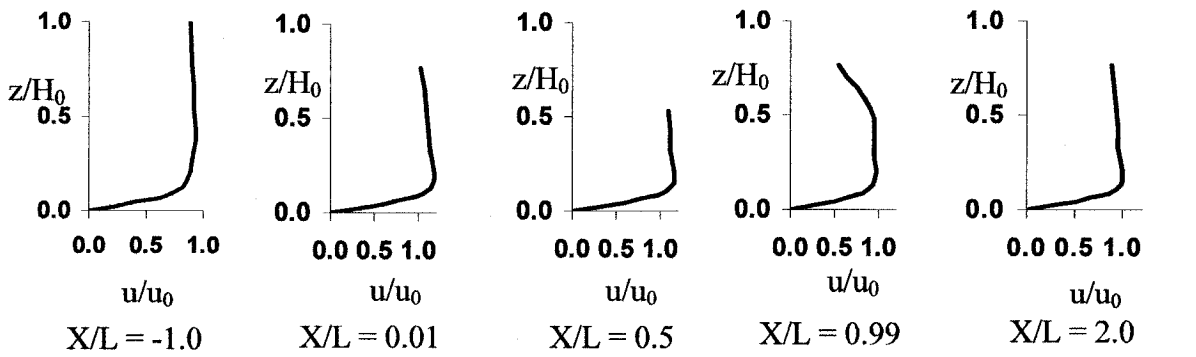

a) Axial velocity u

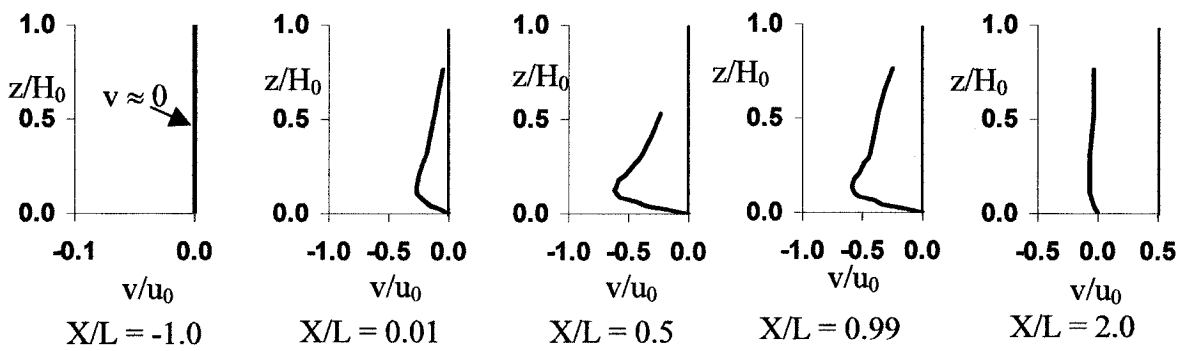

b) Lateral velocity v

Fig. 11.8 Typical velocity distribution near the weir outlet (Y/D = 0.002)

APPENDIX 4 TABLES

Table 3.1. Summary of grid cells

No.	Width (m)	B (m)	L/B	Number of grid cells				
				$X_{upstream}$	$X_{downstream}$	X_{Slot}	Y	Z
SM1	0.0413	0.0915	1.00	200	100	30	20	30
SM2	0.0413	0.0915	0.78	200	100	24	20	30
SM3	0.0413	0.0915	0.11	200	100	12	20	30

Table 4.1. Summary of grid cells

No.	B (m)	L (m)	L/B	Z (m)	Number of grid cells					
					$X_{upstream}$	$X_{downstream}$	X_{branch}	$Y_{main\ conduit}$	Y_{branch}	Z
SM1	0.0915	0.0705	0.77	0.0412	120	100	16	20	70	12

Table 5.1. Summary of grid cells

No.	B (m)	L (m)	L/B	Z (m)	Number of grid cells					
					$X_{upstream}$	$X_{downstream}$	X_{branch}	$Y_{main\ conduit}$	Y_{branch}	Z
SM1	0.0915	0.0915	1.00	0.0412	120	80	24	24	70	12
SM2	0.0915	0.0705	0.77	0.0412	120	80	16	24	70	12
SM3	0.0915	0.0204	0.22	0.0412	120	80	8	24	70	12

Table 5.2. Contraction Coefficient C_c and Average Entry Angle δ for Momentum Transfer for combining conduit flow (L/B = 0.22 and Q_3/Q_2=0.50)

Parameter	Experimental Data	Numerical Data	Remarks
C_c	0.41	0.40	Eq. (8) of Ramamurthy and Zhu (1997)
δ	82.6	84.9	Ramamurthy and Zhu (1997)

Table 6.1. Grid cells and flow parameters

Mesh No.	Slot Width L (m)	Discharge q (m^3/s.m)	Initial Flow Depth H (m)	Fr Number	Number of grid cells			
					$X_{upstream}$	$X_{downstream}$	X_{slot}	$Y_{open\ channel}$
SM1	0.0192	0.1378	0.0766	2.075	120	100	8	30
SM2	0.0400	0.0832	0.0850	1.072	120	100	16	30
SM3	0.0550	0.0850	0.0850	1.096	120	100	20	30
SM4	0.0740	0.0848	0.0850	1.092	120	100	24	30

Table 7.1. Geometric parameters and grid cells

Mesh No.	Slop (S_o)	X_{BC} (m)	X_{JG} (m)	Y_{BM} (m)	Y_{CJ} (m)	Number of grid cells			
						X_{BC}	X_{JG}	Y_{BM}	Y_{CJ}
SM1	0	6	1.0	0.55	0.2	240	100	40	50
SM2	0.0288	6	1.0	0.43	0.2	240	100	36	50

Table 7.2. Flow parameters for simulation

Case No.	Discharge q (m^3/s.m)	Mesh No.	Critical depth y_c (m)	Brink depth y_e (m)	End depth ratio y_e / y_c
1A	0.143	SM1	0.128	0.091	0.715
2A	0.145	SM2	0.129	0.065	0.504
2B	0.286	SM1	0.203	0.131	0.645
2C	1.330	SM1	0.565	0.291	0.515
2D	1.200	SM1	0.572	0.151	0.286

Table 9.1 Experimental flow conditions

Q_u (m^3/s)	Q_b (m^3/s)	Q_r	V_c (m/s)
0.047	0.007	0.149	0.914
0.046	0.014	0.308	0.906
0.046	0.019	0.409	0.907
0.047	0.032	0.672	0.910
0.046	0.038	0.838	0.903

Table 9.2 Water surface profiles for dividing flows in open channels ($Q_r = 0.149$)

X/B	Y/B	Z/B
0.951	0.016	0.307
0.951	0.098	0.309
0.951	0.213	0.301
0.951	0.328	0.308
0.951	0.443	0.297
0.951	0.557	0.305
0.951	0.672	0.295
0.951	0.787	0.302
0.951	0.902	0.307
0.951	0.984	0.306
0.213	0.016	0.294
0.213	0.098	0.306
0.213	0.213	0.297
0.213	0.328	0.296
0.213	0.443	0.299
0.213	0.557	0.307
0.213	0.672	0.308
0.213	0.787	0.296
0.213	0.902	0.295
0.213	0.984	0.301
-0.049	0.016	0.302
-0.049	0.098	0.298
-0.049	0.213	0.300
-0.049	0.328	0.303
-0.049	0.443	0.305
-0.049	0.557	0.301
-0.049	0.672	0.299
-0.049	0.787	0.306
-0.049	0.902	0.309
-0.049	0.984	0.303

X/B	Y/B	Z/B
-0.541	0.016	0.311
-0.541	0.098	0.304
-0.541	0.213	0.299
-0.541	0.328	0.300
-0.541	0.443	0.300
-0.541	0.557	0.303
-0.541	0.672	0.306
-0.541	0.787	0.303
-0.541	0.902	0.301
-0.541	0.984	0.302
-0.787	0.016	0.310
-0.787	0.098	0.299
-0.787	0.213	0.303
-0.787	0.328	0.309
-0.787	0.443	0.301
-0.787	0.557	0.312
-0.787	0.672	0.308
-0.787	0.787	0.304
-0.787	0.902	0.305
-0.787	0.984	0.306
-1.049	0.016	0.305
-1.049	0.098	0.302
-1.049	0.213	0.299
-1.049	0.328	0.301
-1.049	0.443	0.312
-1.049	0.557	0.305
-1.049	0.672	0.309
-1.049	0.787	0.306
-1.049	0.902	0.311
-1.049	0.984	0.297

X/B	Y/B	Z/B
-1.311	0.016	0.306
-1.311	0.098	0.302
-1.311	0.213	0.305
-1.311	0.328	0.296
-1.311	0.443	0.300
-1.311	0.557	0.301
-1.311	0.672	0.305
-1.311	0.787	0.302
-1.311	0.902	0.297
-1.311	0.984	0.307
-1.689	0.016	0.308
-1.689	0.098	0.303
-1.689	0.213	0.309
-1.689	0.328	0.305
-1.689	0.443	0.299
-1.689	0.557	0.307
-1.689	0.672	0.296
-1.689	0.787	0.304
-1.689	0.902	0.303
-1.689	0.984	0.301
-2.131	0.016	0.304
-2.131	0.098	0.300
-2.131	0.213	0.305
-2.131	0.328	0.306
-2.131	0.443	0.303
-2.131	0.557	0.300
-2.131	0.672	0.301
-2.131	0.787	0.310
-2.131	0.902	0.304
-2.131	0.984	0.305

X/B	Y/B	Z/B
-3.000	0.016	0.307
-3.000	0.098	0.306
-3.000	0.213	0.305
-3.000	0.328	0.302
-3.000	0.443	0.300
-3.000	0.557	0.301
-3.000	0.672	0.301
-3.000	0.787	0.300
-3.000	0.902	0.297
-3.000	0.984	0.303

Table 9.2 Water surface profiles for dividing flows in open channels ($Q_r = 0.149$, continued)

X/B	Y/B	Z/B
-0.016	-0.287	0.300
-0.098	-0.287	0.294
-0.213	-0.287	0.293
-0.328	-0.287	0.294
-0.443	-0.287	0.292
-0.557	-0.287	0.289
-0.672	-0.287	0.308
-0.787	-0.287	0.305
-0.902	-0.287	0.303
-0.984	-0.287	0.307
-0.016	-0.730	0.289
-0.098	-0.730	0.290
-0.213	-0.730	0.293
-0.328	-0.730	0.298
-0.443	-0.730	0.303
-0.557	-0.730	0.293
-0.672	-0.730	0.290
-0.787	-0.730	0.299
-0.902	-0.730	0.290
-0.984	-0.730	0.298
-0.016	-1.230	0.282
-0.098	-1.230	0.292
-0.213	-1.230	0.284
-0.328	-1.230	0.289
-0.443	-1.230	0.285
-0.557	-1.230	0.285
-0.672	-1.230	0.278
-0.787	-1.230	0.279
-0.902	-1.230	0.281
-0.984	-1.230	0.295

X/B	Y/B	Z/B
-0.016	-1.639	0.298
-0.098	-1.639	0.296
-0.213	-1.639	0.301
-0.328	-1.639	0.297
-0.443	-1.639	0.302
-0.557	-1.639	0.301
-0.672	-1.639	0.306
-0.787	-1.639	0.293
-0.902	-1.639	0.299
-0.984	-1.639	0.293
-0.016	-1.967	0.301
-0.098	-1.967	0.303
-0.213	-1.967	0.299
-0.328	-1.967	0.300
-0.443	-1.967	0.304
-0.557	-1.967	0.294
-0.672	-1.967	0.295
-0.787	-1.967	0.290
-0.902	-1.967	0.293
-0.984	-1.967	0.285
-0.016	-2.557	0.303
-0.098	-2.557	0.301
-0.213	-2.557	0.301
-0.328	-2.557	0.297
-0.443	-2.557	0.294
-0.557	-2.557	0.302
-0.672	-2.557	0.307
-0.787	-2.557	0.305
-0.902	-2.557	0.294
-0.984	-2.557	0.290

X/B	Y/B	Z/B
-0.016	-2.951	0.293
-0.098	-2.951	0.294
-0.213	-2.951	0.292
-0.328	-2.951	0.292
-0.443	-2.951	0.286
-0.557	-2.951	0.294
-0.672	-2.951	0.292
-0.787	-2.951	0.293
-0.902	-2.951	0.292
-0.984	-2.951	0.295

Table 9.3 Velocity data for dividing flows in open channels ($Q_r = 0.149$)

X/B	Y/B	Z/B	U (m/s)	V (m/s)
0.970	0.098	0.011	-0.400	0.020
0.970	0.098	0.033	-0.406	0.029
0.970	0.098	0.098	-0.437	0.025
0.970	0.098	0.164	-0.406	0.012
0.970	0.098	0.229	-0.389	0.008
0.970	0.213	0.011	-0.410	0.045
0.970	0.213	0.033	-0.441	0.046
0.970	0.213	0.098	-0.425	0.037
0.970	0.213	0.164	-0.411	0.015
0.970	0.213	0.229	-0.391	-0.010
0.970	0.443	0.011	-0.385	0.021
0.970	0.443	0.033	-0.436	0.021
0.970	0.443	0.098	-0.422	0.022
0.970	0.443	0.164	-0.418	-0.009
0.970	0.443	0.229	-0.438	-0.053
0.970	0.672	0.011	-0.470	-0.033
0.970	0.672	0.033	-0.504	-0.037
0.970	0.672	0.098	-0.480	-0.015
0.970	0.672	0.164	-0.480	-0.002
0.970	0.672	0.229	-0.452	0.021
0.970	0.902	0.011	-0.487	-0.020
0.970	0.902	0.033	-0.529	-0.014
0.970	0.902	0.098	-0.533	-0.010
0.970	0.902	0.164	-0.501	0.007
0.970	0.902	0.229	-0.498	0.006
0.220	0.016	0.011	-0.333	-0.002
0.220	0.016	0.033	-0.329	0.023
0.220	0.016	z0.098	-0.344	0.011
0.220	0.016	0.164	-0.352	0.010
0.220	0.016	0.229	-0.326	0.011

X/B	Y/B	Z/B	U (m/s)	V (m/s)
0.220	0.213	0.011	-0.395	0.044
0.220	0.213	0.033	-0.436	0.039
0.220	0.213	0.098	-0.432	0.034
0.220	0.213	0.164	-0.425	0.001
0.220	0.213	0.229	-0.388	-0.024
0.220	0.443	0.011	-0.374	0.039
0.220	0.443	0.033	-0.429	0.047
0.220	0.443	0.098	-0.431	0.025
0.220	0.443	0.164	-0.417	0.005
0.220	0.443	0.229	-0.431	-0.023
0.220	0.672	0.011	-0.464	-0.017
0.220	0.672	0.033	-0.482	-0.015
0.220	0.672	0.098	-0.482	0.000
0.220	0.672	0.164	-0.473	0.012
0.220	0.672	0.229	-0.442	0.019
0.220	0.902	0.011	-0.480	0.003
0.220	0.902	0.033	-0.521	0.003
0.220	0.902	0.098	-0.522	0.010
0.220	0.902	0.164	-0.513	0.013
0.220	0.902	0.229	-0.481	0.014
-0.040	0.016	0.011	-0.333	-0.006
-0.040	0.016	0.033	-0.377	-0.001
-0.040	0.016	0.098	-0.382	-0.004
-0.040	0.016	0.164	-0.415	-0.006
-0.040	0.016	0.229	-0.372	0.015
-0.040	0.213	0.011	-0.413	0.025
-0.040	0.213	0.033	-0.446	0.021
-0.040	0.213	0.098	-0.447	0.015
-0.040	0.213	0.164	-0.441	-0.009
-0.040	0.213	0.229	-0.439	-0.049

Table 9.3 Velocity data for dividing flows in open channels ($Q_r = 0.149$, continued)

X/B	Y/B	Z/B	U (m/s)	V (m/s)
-0.040	0.443	0.011	-0.400	0.001
-0.040	0.443	0.033	-0.417	0.017
-0.040	0.443	0.098	-0.440	0.004
-0.040	0.443	0.164	-0.447	-0.012
-0.040	0.443	0.229	-0.432	-0.043
-0.040	0.672	0.033	-0.499	-0.028
-0.040	0.672	0.098	-0.507	-0.010
-0.040	0.672	0.164	-0.486	-0.001
-0.040	0.672	0.229	-0.469	0.015
-0.040	0.672	0.011	-0.463	-0.021
-0.040	0.902	0.011	-0.467	-0.003
-0.040	0.902	0.033	-0.500	-0.004
-0.040	0.902	0.098	-0.512	-0.002
-0.040	0.902	0.164	-0.504	0.011
-0.040	0.902	0.229	-0.463	0.019
-0.290	0.016	0.011	-0.283	-0.029
-0.290	0.016	0.033	-0.399	-0.041
-0.290	0.016	0.098	-0.423	-0.045
-0.290	0.016	0.164	-0.401	-0.058
-0.290	0.016	0.229	-0.378	0.018
-0.290	0.213	0.011	-0.384	-0.008
-0.290	0.213	0.033	-0.430	0.000
-0.290	0.213	0.098	-0.450	-0.013
-0.290	0.213	0.164	-0.423	-0.035
-0.290	0.213	0.229	-0.443	-0.071
-0.290	0.443	0.011	-0.389	-0.010
-0.290	0.443	0.033	-0.416	0.011
-0.290	0.443	0.098	-0.425	-0.001
-0.290	0.443	0.164	-0.446	-0.020
-0.290	0.443	0.229	-0.436	-0.048

X/B	Y/B	Z/B	U (m/s)	V (m/s)
-0.290	0.672	0.011	-0.426	-0.015
-0.290	0.672	0.033	-0.459	-0.028
-0.290	0.672	0.098	-0.506	-0.029
-0.290	0.672	0.164	-0.486	-0.009
-0.290	0.672	0.229	-0.448	0.013
-0.290	0.902	0.011	-0.483	-0.009
-0.290	0.902	0.033	-0.495	-0.012
-0.290	0.902	0.098	-0.525	0.001
-0.290	0.902	0.164	-0.473	0.011
-0.290	0.902	0.229	-0.438	0.011
-0.800	0.902	0.011	-0.393	-0.008
-0.800	0.902	0.033	-0.429	-0.010
-0.800	0.016	0.011	-0.257	-0.086
-0.800	0.016	0.033	-0.318	-0.095
-0.800	0.016	0.098	-0.323	-0.097
-0.800	0.016	0.164	-0.316	-0.114
-0.800	0.016	0.229	-0.304	-0.116
-0.800	0.213	0.011	-0.289	-0.018
-0.800	0.213	0.033	-0.351	-0.024
-0.800	0.213	0.098	-0.350	-0.021
-0.800	0.213	0.164	-0.368	-0.023
-0.800	0.213	0.229	-0.360	-0.046
-0.800	0.443	0.011	-0.325	-0.011
-0.800	0.443	0.033	-0.349	-0.021
-0.800	0.443	0.098	-0.410	-0.025
-0.800	0.443	0.164	-0.399	-0.027
-0.800	0.443	0.229	-0.402	-0.035
-0.800	0.672	0.011	-0.420	-0.027
-0.800	0.672	0.033	-0.454	-0.032
-0.800	0.672	0.098	-0.436	-0.015

Table 9.3 Velocity data for dividing flows in open channels ($Q_r = 0.149$, continued)

X/B	Y/B	Z/B	U (m/s)	V (m/s)
-0.800	0.902	0.098	-0.461	-0.009
-0.800	0.902	0.164	-0.443	0.001
-0.800	0.902	0.229	-0.436	0.006
-1.040	0.148	0.011	-0.266	0.005
-1.040	0.148	0.033	-0.316	0.003
-1.040	0.148	0.098	-0.290	0.004
-1.040	0.148	0.164	-0.328	-0.005
-1.040	0.148	0.229	-0.274	-0.029
-1.040	0.213	0.011	-0.280	0.014
-1.040	0.213	0.033	-0.317	0.006
-1.040	0.213	0.098	-0.343	-0.010
-1.040	0.213	0.164	-0.329	-0.022
-1.040	0.213	0.229	-0.306	-0.020
-1.040	0.443	0.011	-0.295	-0.032
-1.040	0.443	0.033	-0.335	-0.017
-1.040	0.443	0.098	-0.374	-0.023
-1.040	0.443	0.164	-0.378	-0.036
-1.040	0.443	0.229	-0.375	-0.031
-1.040	0.672	0.011	-0.403	-0.025
-1.040	0.672	0.033	-0.417	-0.031
-1.040	0.672	0.098	-0.438	-0.021
-1.040	0.672	0.164	-0.426	-0.009
-1.040	0.672	0.229	-0.420	0.000
-1.040	0.902	0.011	-0.383	-0.013
-1.040	0.902	0.033	-0.425	-0.007
-1.040	0.902	0.098	-0.423	0.001
-1.040	0.902	0.164	-0.450	0.009
-1.040	0.902	0.229	-0.412	0.014
-0.800	0.902	0.098	-0.461	-0.009
-0.800	0.902	0.164	-0.443	0.001

X/B	Y/B	Z/B	U (m/s)	V (m/s)
-1.700	0.098	0.011	-0.299	0.026
-1.700	0.098	0.033	-0.336	0.020
-1.700	0.098	0.098	-0.343	0.007
-1.700	0.098	0.164	-0.343	-0.003
-1.700	0.098	0.229	-0.358	-0.018
-1.700	0.213	0.011	-0.276	0.040
-1.700	0.213	0.033	-0.307	0.025
-1.700	0.213	0.098	-0.351	0.006
-1.700	0.213	0.164	-0.362	-0.012
-1.700	0.213	0.229	-0.368	-0.025
-1.700	0.443	0.011	-0.301	0.015
-1.700	0.443	0.033	-0.346	0.001
-1.700	0.443	0.098	-0.379	-0.001
-1.700	0.443	0.164	-0.379	-0.001
-1.700	0.443	0.229	-0.388	-0.009
-1.700	0.672	0.011	-0.389	-0.008
-1.700	0.672	0.033	-0.423	-0.008
-1.700	0.672	0.098	-0.425	0.003
-1.700	0.672	0.164	-0.426	0.008
-1.700	0.672	0.229	-0.405	0.025
-1.700	0.902	0.011	-0.382	0.004
-1.700	0.902	0.033	-0.413	0.006
-1.700	0.902	0.098	-0.414	0.006
-1.700	0.902	0.164	-0.426	0.013
-1.700	0.902	0.229	-0.405	0.020
-3.000	0.098	0.011	-0.312	0.022
-3.000	0.098	0.033	-0.351	0.020
-3.000	0.098	0.098	-0.357	0.005
-3.000	0.098	0.164	-0.372	-0.011
-3.000	0.098	0.229	-0.351	-0.014

Table 9.3 Velocity data for dividing flows in open channels ($Q_r = 0.149$, continued)

X/B	Y/B	Z/B	U (m/s)	V (m/s)
-3.000	0.213	0.011	-0.281	0.035
-3.000	0.213	0.033	-0.325	0.025
-3.000	0.213	0.098	-0.329	0.001
-3.000	0.213	0.164	-0.360	-0.011
-3.000	0.213	0.229	-0.387	-0.016
-3.000	0.443	0.011	-0.218	-0.002
-3.000	0.443	0.033	-0.300	0.004
-3.000	0.443	0.098	-0.350	0.006
-3.000	0.443	0.164	-0.396	-0.013
-3.000	0.443	0.229	-0.396	-0.014
-3.000	0.672	0.011	-0.300	-0.008
-3.000	0.672	0.033	-0.360	-0.008
-3.000	0.672	0.098	-0.426	-0.018
-3.000	0.672	0.164	-0.439	-0.018
-3.000	0.672	0.229	-0.408	-0.007
-3.000	0.902	0.011	-0.326	-0.023
-3.000	0.902	0.033	-0.381	-0.018
-3.000	0.902	0.098	-0.381	-0.016
-3.000	0.902	0.164	-0.405	-0.008
-3.000	0.902	0.229	-0.402	0.011
-0.098	-0.030	0.011	-0.018	0.010
-0.098	-0.030	0.033	-0.018	0.032
-0.098	-0.030	0.098	-0.018	0.032
-0.098	-0.030	0.164	-0.018	0.032
-0.098	-0.030	0.229	-0.063	0.032
-0.328	-0.030	0.011	-0.136	-0.046
-0.328	-0.030	0.033	-0.125	-0.036
-0.328	-0.030	0.098	-0.122	-0.049
-0.328	-0.030	0.164	-0.118	-0.036
-0.328	-0.030	0.229	-0.131	-0.032

X/B	Y/B	Z/B	U (m/s)	V (m/s)
-0.557	-0.030	0.011	-0.264	-0.116
-0.557	-0.030	0.033	-0.260	-0.118
-0.557	-0.030	0.098	-0.253	-0.114
-0.557	-0.030	0.164	-0.258	-0.122
-0.557	-0.030	0.229	-0.250	-0.112
-0.787	-0.030	0.011	-0.207	-0.159
-0.787	-0.030	0.033	-0.263	-0.170
-0.787	-0.030	0.098	-0.283	-0.177
-0.787	-0.030	0.164	-0.268	-0.186
-0.787	-0.030	0.229	-0.267	-0.177
-0.902	-0.030	0.011	-0.055	-0.161
-0.902	-0.030	0.033	-0.182	-0.170
-0.902	-0.030	0.098	-0.182	-0.162
-0.902	-0.030	0.164	-0.163	-0.175
-0.902	-0.030	0.229	-0.144	-0.174
-0.098	-0.290	0.011	-0.007	0.016
-0.098	-0.290	0.033	0.001	0.023
-0.098	-0.290	0.098	0.001	0.023
-0.098	-0.290	0.164	0.015	0.267
-0.098	-0.290	0.229	-0.116	0.142
-0.328	-0.290	0.011	0.015	0.034
-0.328	-0.290	0.033	0.015	-0.018
-0.328	-0.290	0.098	-0.029	0.057
-0.328	-0.290	0.164	-0.029	0.057
-0.328	-0.290	0.229	-0.012	0.054
-0.557	-0.290	0.011	-0.001	-0.031
-0.557	-0.290	0.033	-0.045	0.007
-0.557	-0.290	0.098	-0.010	0.009
-0.557	-0.290	0.164	-0.071	-0.051
-0.557	-0.290	0.229	-0.004	0.100

Table 9.3 Velocity data for dividing flows in open channels ($Q_r = 0.149$, continued)

X/B	Y/B	Z/B	U (m/s)	V (m/s)
-0.787	-0.290	0.011	-0.019	-0.269
-0.787	-0.290	0.033	-0.049	-0.229
-0.787	-0.290	0.098	-0.103	-0.252
-0.787	-0.290	0.164	-0.074	-0.223
-0.787	-0.290	0.229	-0.045	-0.227
-0.902	-0.290	0.011	0.069	-0.328
-0.902	-0.290	0.033	-0.086	-0.338
-0.902	-0.290	0.098	-0.080	-0.335
-0.902	-0.290	0.164	-0.070	-0.339
-0.902	-0.290	0.229	-0.049	-0.332
-0.098	-0.730	0.011	0.023	0.013
-0.098	-0.730	0.033	-0.017	0.082
-0.098	-0.730	0.098	-0.001	0.084
-0.098	-0.730	0.164	-0.014	0.037
-0.098	-0.730	0.229	-0.014	0.094
-0.328	-0.730	0.011	0.002	0.017
-0.328	-0.730	0.033	0.027	0.029
-0.328	-0.730	0.098	-0.032	0.078
-0.328	-0.730	0.164	-0.032	0.078
-0.328	-0.730	0.229	-0.034	0.104
-0.557	-0.730	0.011	0.076	-0.095
-0.557	-0.730	0.033	0.045	-0.090
-0.557	-0.730	0.098	0.003	-0.010
-0.557	-0.730	0.164	-0.022	0.013
-0.557	-0.730	0.229	-0.030	0.042
-0.787	-0.730	0.011	0.051	-0.333
-0.787	-0.730	0.033	0.030	-0.300
-0.787	-0.730	0.098	-0.023	-0.243
-0.787	-0.730	0.164	0.005	-0.239
-0.787	-0.730	0.229	0.004	-0.261

X/B	Y/B	Z/B	U (m/s)	V (m/s)
-0.902	-0.730	0.011	0.027	-0.383
-0.902	-0.730	0.033	0.013	-0.363
-0.902	-0.730	0.098	-0.015	-0.375
-0.902	-0.730	0.164	-0.018	-0.369
-0.902	-0.730	0.229	-0.003	-0.359
-0.098	-1.250	0.011	0.051	0.073
-0.098	-1.250	0.033	0.022	0.032
-0.098	-1.250	0.098	0.000	0.089
-0.098	-1.250	0.164	-0.005	0.093
-0.098	-1.250	0.229	-0.024	0.113
-0.328	-1.250	0.011	0.005	-0.002
-0.328	-1.250	0.033	-0.021	0.048
-0.328	-1.250	0.098	0.014	0.028
-0.328	-1.250	0.164	0.000	0.065
-0.328	-1.250	0.229	-0.013	0.080
-0.557	-1.250	0.011	0.014	-0.041
-0.557	-1.250	0.033	0.052	-0.124
-0.557	-1.250	0.098	-0.018	-0.055
-0.557	-1.250	0.164	-0.031	-0.042
-0.557	-1.250	0.229	-0.003	-0.064
-0.787	-1.250	0.011	0.028	-0.300
-0.787	-1.250	0.033	0.032	-0.297
-0.787	-1.250	0.098	-0.014	-0.208
-0.787	-1.250	0.164	-0.030	-0.221
-0.787	-1.250	0.229	0.011	-0.248
-0.902	-1.250	0.011	0.002	-0.375
-0.902	-1.250	0.033	0.017	-0.356
-0.902	-1.250	0.098	-0.019	-0.341
-0.902	-1.250	0.164	-0.012	-0.345
-0.902	-1.250	0.229	0.000	-0.370

Table 9.3 Velocity data for dividing flows in open channels ($Q_r = 0.149$, continued)

X/B	Y/B	Z/B	U (m/s)	V (m/s)
-0.098	-1.620	0.011	0.020	0.037
-0.098	-1.620	0.033	-0.012	0.077
-0.098	-1.620	0.098	-0.008	0.118
-0.098	-1.620	0.164	-0.014	0.126
-0.098	-1.620	0.229	-0.013	0.127
-0.328	-1.620	0.011	0.001	0.015
-0.328	-1.620	0.033	0.063	-0.008
-0.328	-1.620	0.098	-0.027	0.079
-0.328	-1.620	0.164	-0.038	0.075
-0.328	-1.620	0.229	-0.024	0.095
-0.557	-1.620	0.011	0.023	-0.020
-0.557	-1.620	0.033	0.022	-0.086
-0.557	-1.620	0.098	-0.060	0.012
-0.557	-1.620	0.164	0.006	-0.038
-0.557	-1.620	0.229	-0.042	-0.027
-0.787	-1.620	0.011	0.021	-0.267
-0.787	-1.620	0.033	0.033	-0.289
-0.787	-1.620	0.098	-0.005	-0.243
-0.787	-1.620	0.164	-0.021	-0.236
-0.787	-1.620	0.229	-0.001	-0.298
-0.902	-1.620	0.011	0.011	-0.367
-0.902	-1.620	0.033	0.010	-0.375
-0.902	-1.620	0.098	0.000	-0.344
-0.902	-1.620	0.164	-0.031	-0.328
-0.902	-1.620	0.229	-0.003	-0.368
-0.098	-2.500	0.011	0.002	0.008
-0.098	-2.500	0.033	-0.010	0.159
-0.098	-2.500	0.098	0.002	0.174
-0.098	-2.500	0.164	-0.012	0.173
-0.098	-2.500	0.229	-0.003	0.163

X/B	Y/B	Z/B	U (m/s)	V (m/s)
-0.328	-2.500	0.011	-0.024	0.061
-0.328	-2.500	0.033	-0.004	0.159
-0.328	-2.500	0.098	-0.019	0.055
-0.328	-2.500	0.164	-0.019	0.055
-0.328	-2.500	0.229	-0.078	0.160
-0.557	-2.500	0.011	0.000	-0.008
-0.557	-2.500	0.033	0.041	-0.106
-0.557	-2.500	0.098	0.005	-0.107
-0.557	-2.500	0.164	-0.013	-0.122
-0.557	-2.500	0.229	0.025	-0.044
-0.787	-2.500	0.011	0.014	-0.096
-0.787	-2.500	0.033	0.019	-0.264
-0.787	-2.500	0.098	-0.010	-0.273
-0.787	-2.500	0.164	-0.010	-0.273
-0.787	-2.500	0.229	0.020	-0.106
-0.902	-2.500	0.011	-0.002	-0.085
-0.902	-2.500	0.033	0.000	-0.299
-0.902	-2.500	0.098	-0.002	-0.318
-0.902	-2.500	0.164	-0.005	-0.313
-0.902	-2.500	0.229	0.012	-0.224

Table 9.4 Water surface profiles for dividing flows in open channels ($Q_r = 0.308$)

X/B	Y/B	Z/B
0.984	0.016	0.245
0.984	0.033	0.249
0.984	0.098	0.251
0.984	0.328	0.251
0.984	0.443	0.248
0.984	0.557	0.250
0.984	0.672	0.252
0.984	0.787	0.247
0.984	0.902	0.248
0.984	0.984	0.248
0.926	0.016	0.249
0.926	0.098	0.249
0.926	0.213	0.246
0.926	0.328	0.247
0.926	0.443	0.246
0.926	0.557	0.244
0.926	0.672	0.245
0.926	0.787	0.247
0.926	0.902	0.253
0.926	0.984	0.250
0.249	0.016	0.246
0.249	0.033	0.243
0.249	0.098	0.249
0.249	0.328	0.248
0.249	0.443	0.248
0.249	0.557	0.248
0.249	0.672	0.253
0.249	0.787	0.246
0.249	0.902	0.246
0.249	0.984	0.260

X/B	Y/B	Z/B
0.221	0.016	0.248
0.221	0.098	0.252
0.221	0.213	0.249
0.221	0.328	0.248
0.221	0.443	0.251
0.221	0.557	0.249
0.221	0.672	0.245
0.221	0.787	0.247
0.221	0.902	0.248
0.221	0.984	0.250
0.164	0.016	0.243
0.164	0.033	0.242
0.164	0.098	0.236
0.164	0.328	0.242
0.164	0.443	0.246
0.164	0.557	0.249
0.164	0.672	0.252
0.164	0.787	0.250
0.164	0.902	0.251
0.164	0.984	0.250
-0.041	0.016	0.238
-0.041	0.098	0.249
-0.041	0.213	0.245
-0.041	0.328	0.247
-0.041	0.443	0.247
-0.041	0.557	0.247
-0.041	0.672	0.249
-0.041	0.787	0.250
-0.041	0.902	0.250
-0.041	0.984	0.248

X/B	Y/B	Z/B
-0.164	0.016	0.246
-0.164	0.033	0.240
-0.164	0.098	0.244
-0.164	0.328	0.249
-0.164	0.443	0.252
-0.164	0.557	0.249
-0.164	0.672	0.257
-0.164	0.787	0.249
-0.164	0.902	0.252
-0.164	0.984	0.251
-0.287	0.016	0.237
-0.287	0.098	0.253
-0.287	0.213	0.245
-0.287	0.328	0.247
-0.287	0.443	0.250
-0.287	0.557	0.248
-0.287	0.672	0.247
-0.287	0.787	0.249
-0.287	0.902	0.253
-0.287	0.984	0.257
-0.410	0.016	0.243
-0.410	0.033	0.255
-0.410	0.098	0.248
-0.410	0.328	0.252
-0.410	0.443	0.251
-0.410	0.557	0.255
-0.410	0.672	0.254
-0.410	0.787	0.252
-0.410	0.902	0.256
-0.410	0.984	0.255

X/B	Y/B	Z/B
-0.541	0.016	0.247
-0.541	0.098	0.253
-0.541	0.213	0.253
-0.541	0.328	0.251
-0.541	0.443	0.254
-0.541	0.557	0.253
-0.541	0.672	0.256
-0.541	0.787	0.258
-0.541	0.902	0.253
-0.541	0.984	0.256
-0.656	0.016	0.254
-0.656	0.033	0.246
-0.656	0.098	0.239
-0.656	0.328	0.261
-0.656	0.443	0.256
-0.656	0.557	0.254
-0.656	0.672	0.259
-0.656	0.787	0.261
-0.656	0.902	0.258
-0.656	0.984	0.257
-0.795	0.016	0.262
-0.795	0.098	0.265
-0.795	0.213	0.258
-0.795	0.328	0.257
-0.795	0.443	0.258
-0.795	0.557	0.257
-0.795	0.672	0.255
-0.795	0.787	0.257
-0.795	0.902	0.260
-0.795	0.984	0.257

Table 9.4 Water surface profiles for dividing flows in open channels ($Q_r = 0.308$, continued)

X/B	Y/B	Z/B
-0.820	0.016	0.267
-0.820	0.033	0.270
-0.820	0.098	0.274
-0.820	0.328	0.259
-0.820	0.443	0.257
-0.820	0.557	0.257
-0.820	0.672	0.256
-0.820	0.787	0.259
-0.820	0.902	0.262
-0.820	0.984	0.261
-1.041	0.016	0.265
-1.041	0.098	0.264
-1.041	0.213	0.265
-1.041	0.328	0.260
-1.041	0.443	0.261
-1.041	0.557	0.260
-1.041	0.672	0.256
-1.041	0.787	0.257
-1.041	0.902	0.257
-1.041	0.984	0.260
-1.148	0.016	0.270
-1.148	0.033	0.262
-1.148	0.098	0.262
-1.148	0.328	0.263
-1.148	0.443	0.259
-1.148	0.557	0.259
-1.148	0.672	0.257
-1.148	0.787	0.257
-1.148	0.902	0.263
-1.148	0.984	0.261

X/B	Y/B	Z/B
-1.287	0.016	0.262
-1.287	0.098	0.263
-1.287	0.213	0.261
-1.287	0.328	0.260
-1.287	0.443	0.259
-1.287	0.557	0.260
-1.287	0.672	0.263
-1.287	0.787	0.257
-1.287	0.902	0.258
-1.287	0.984	0.264
-1.311	0.016	0.260
-1.311	0.033	0.266
-1.311	0.098	0.264
-1.311	0.328	0.265
-1.311	0.443	0.259
-1.311	0.557	0.263
-1.311	0.672	0.261
-1.311	0.787	0.257
-1.311	0.902	0.261
-1.311	0.984	0.259
-1.697	0.016	0.268
-1.697	0.098	0.262
-1.697	0.213	0.258
-1.697	0.328	0.261
-1.697	0.443	0.259
-1.697	0.557	0.258
-1.697	0.672	0.259
-1.697	0.787	0.258
-1.697	0.902	0.257
-1.697	0.984	0.259

X/B	Y/B	Z/B
-1.803	0.016	0.263
-1.803	0.033	0.263
-1.803	0.098	0.264
-1.803	0.328	0.259
-1.803	0.443	0.265
-1.803	0.557	0.262
-1.803	0.672	0.259
-1.803	0.787	0.259
-1.803	0.902	0.259
-1.803	0.984	0.262
-2.107	0.016	0.262
-2.107	0.098	0.258
-2.107	0.213	0.260
-2.107	0.328	0.259
-2.107	0.443	0.261
-2.107	0.557	0.263
-2.107	0.672	0.264
-2.107	0.787	0.259
-2.107	0.902	0.261
-2.107	0.984	0.260
-2.131	0.016	0.265
-2.131	0.033	0.262
-2.131	0.098	0.258
-2.131	0.328	0.262
-2.131	0.443	0.264
-2.131	0.557	0.260
-2.131	0.672	0.264
-2.131	0.787	0.260
-2.131	0.902	0.260
-2.131	0.984	0.262

X/B	Y/B	Z/B
-3.000	0.016	0.258
-3.000	0.098	0.260
-3.000	0.213	0.257
-3.000	0.328	0.258
-3.000	0.443	0.260
-3.000	0.557	0.262
-3.000	0.672	0.259
-3.000	0.787	0.260
-3.000	0.902	0.263
-3.000	0.984	0.264

Table 9.4 Water surface profiles for dividing flows in open channels ($Q_r = 0.308$, continued)

X/B	Y/B	Z/B
-0.016	0.016	0.240
-0.098	0.016	0.237
-0.213	0.016	0.240
-0.328	0.016	0.238
-0.443	0.016	0.242
-0.557	0.016	0.245
-0.672	0.016	0.251
-0.787	0.016	0.263
-0.902	0.016	0.269
-0.984	0.016	0.275
-0.016	0.000	0.243
-0.098	0.000	0.238
-0.213	0.000	0.231
-0.328	0.000	0.237
-0.443	0.000	0.241
-0.557	0.000	0.250
-0.672	0.000	0.254
-0.787	0.000	0.266
-0.902	0.000	0.267
-0.984	0.000	0.270
-0.016	-0.287	0.238
-0.098	-0.287	0.236
-0.213	-0.287	0.240
-0.328	-0.287	0.239
-0.443	-0.287	0.237
-0.557	-0.287	0.237
-0.672	-0.287	0.241
-0.787	-0.287	0.249
-0.902	-0.287	0.254
-0.984	-0.287	0.255

X/B	Y/B	Z/B
-0.016	-0.730	0.241
-0.098	-0.730	0.241
-0.213	-0.730	0.237
-0.328	-0.730	0.237
-0.443	-0.730	0.237
-0.557	-0.730	0.237
-0.672	-0.730	0.241
-0.787	-0.730	0.236
-0.902	-0.730	0.238
-0.984	-0.730	0.237
-0.016	-0.893	0.239
-0.098	-0.893	0.238
-0.213	-0.893	0.237
-0.328	-0.893	0.234
-0.443	-0.893	0.237
-0.557	-0.893	0.237
-0.672	-0.893	0.241
-0.787	-0.893	0.240
-0.902	-0.893	0.238
-0.984	-0.893	0.237
-0.016	-1.221	0.238
-0.098	-1.221	0.239
-0.213	-1.221	0.239
-0.328	-1.221	0.235
-0.443	-1.221	0.238
-0.557	-1.221	0.241
-0.672	-1.221	0.240
-0.787	-1.221	0.242
-0.902	-1.221	0.236
-0.984	-1.221	0.240

X/B	Y/B	Z/B
-0.016	-1.623	0.241
-0.098	-1.623	0.238
-0.213	-1.623	0.238
-0.328	-1.623	0.237
-0.443	-1.623	0.238
-0.557	-1.623	0.240
-0.672	-1.623	0.240
-0.787	-1.623	0.238
-0.902	-1.623	0.240
-0.984	-1.623	0.238
-0.016	-2.000	0.241
-0.098	-2.000	0.238
-0.213	-2.000	0.238
-0.328	-2.000	0.238
-0.443	-2.000	0.238
-0.557	-2.000	0.239
-0.672	-2.000	0.239
-0.787	-2.000	0.239
-0.902	-2.000	0.240
-0.984	-2.000	0.238
-0.016	-2.533	0.243
-0.098	-2.533	0.238
-0.213	-2.533	0.241
-0.328	-2.533	0.237
-0.443	-2.533	0.237
-0.557	-2.533	0.239
-0.672	-2.533	0.239
-0.787	-2.533	0.246
-0.902	-2.533	0.241
-0.984	-2.533	0.237

X/B	Y/B	Z/B
-0.016	-3.000	0.239
-0.098	-3.000	0.243
-0.213	-3.000	0.236
-0.328	-3.000	0.241
-0.443	-3.000	0.239
-0.557	-3.000	0.242
-0.672	-3.000	0.241
-0.787	-3.000	0.238
-0.902	-3.000	0.236
-0.984	-3.000	0.243

Table 9.5 Velocity data for dividing flows in open channels ($Q_r = 0.308$)

X/B	Y/B	Z/B	U (m/s)	V (m/s)
0.970	0.098	0.007	-0.595	0.017
0.970	0.098	0.033	-0.615	0.022
0.970	0.098	0.131	-0.572	0.002
0.970	0.098	0.197	-0.501	0.005
0.970	0.213	0.007	-0.593	0.046
0.970	0.213	0.033	-0.603	0.051
0.970	0.213	0.131	-0.539	-0.008
0.970	0.213	0.197	-0.465	-0.028
0.970	0.442	0.007	-0.537	0.069
0.970	0.442	0.033	-0.567	0.061
0.970	0.442	0.131	-0.558	-0.010
0.970	0.442	0.197	-0.542	-0.064
0.970	0.672	0.007	-0.591	-0.036
0.970	0.672	0.033	-0.625	-0.037
0.970	0.672	0.131	-0.601	0.007
0.970	0.672	0.197	-0.525	0.023
0.970	0.902	0.007	-0.637	-0.019
0.970	0.902	0.033	-0.652	-0.016
0.970	0.902	0.131	-0.653	0.002
0.970	0.902	0.197	-0.643	-0.077
0.220	0.098	0.007	-0.463	0.016
0.220	0.098	0.033	-0.497	0.017
0.220	0.098	0.131	-0.525	0.011
0.220	0.098	0.197	-0.454	0.005
0.220	0.213	0.007	-0.574	0.041
0.220	0.213	0.033	-0.606	0.038
0.220	0.213	0.131	-0.550	-0.008
0.220	0.213	0.197	-0.504	-0.045
0.220	0.442	0.007	-0.521	0.043
0.220	0.442	0.033	-0.555	0.034

X/B	Y/B	Z/B	U (m/s)	V (m/s)
0.220	0.442	0.131	-0.574	-0.010
0.220	0.442	0.197	-0.535	-0.041
0.220	0.672	0.007	-0.573	-0.018
0.220	0.672	0.033	-0.605	-0.026
0.220	0.672	0.131	-0.589	0.010
0.220	0.672	0.197	-0.511	0.038
0.220	0.902	0.007	-0.635	-0.002
0.220	0.902	0.033	-0.659	-0.004
0.220	0.902	0.131	-0.622	0.017
0.220	0.902	0.197	-0.548	0.015
0.040	0.098	0.007	-0.574	-0.037
0.040	0.098	0.033	-0.589	-0.039
0.040	0.098	0.131	-0.611	-0.044
0.040	0.098	0.197	-0.550	-0.049
0.040	0.213	0.007	-0.585	-0.005
0.040	0.213	0.033	-0.597	-0.017
0.040	0.213	0.131	-0.575	-0.043
0.040	0.213	0.197	-0.552	-0.086
0.040	0.442	0.007	-0.500	0.020
0.040	0.442	0.033	-0.535	0.020
0.040	0.442	0.131	-0.565	-0.010
0.040	0.442	0.197	-0.523	-0.051
0.040	0.672	0.007	-0.577	-0.029
0.040	0.672	0.033	-0.602	-0.022
0.040	0.672	0.131	-0.584	0.012
0.040	0.672	0.197	-0.524	0.021
0.040	0.902	0.007	-0.596	0.007
0.040	0.902	0.033	-0.634	0.007
0.040	0.902	0.131	-0.611	0.024
0.040	0.902	0.197	-0.507	0.018

Table 9.5 Velocity data for dividing flows in open channels ($Q_r = 0.308$, continued)

X/B	Y/B	Z/B	U (m/s)	V (m/s)
-0.290	0.016	0.007	-0.585	-0.137
-0.290	0.016	0.033	-0.619	-0.135
-0.290	0.016	0.131	-0.589	-0.158
-0.290	0.016	0.197	-0.548	-0.138
-0.290	0.147	0.007	-0.569	-0.053
-0.290	0.147	0.033	-0.570	-0.052
-0.290	0.147	0.131	-0.543	-0.139
-0.290	0.147	0.197	-0.529	-0.074
-0.290	0.442	0.007	-0.421	-0.046
-0.290	0.442	0.033	-0.490	-0.026
-0.290	0.442	0.131	-0.530	-0.039
-0.290	0.442	0.197	-0.506	-0.073
-0.290	0.672	0.007	-0.526	-0.050
-0.290	0.672	0.033	-0.567	-0.038
-0.290	0.672	0.131	-0.548	-0.006
-0.290	0.672	0.197	-0.499	0.010
-0.290	0.902	0.007	-0.526	-0.003
-0.290	0.902	0.033	-0.606	0.004
-0.290	0.902	0.131	-0.583	0.013
-0.290	0.902	0.197	-0.509	0.011
-0.800	0.016	0.007	-0.231	-0.170
-0.800	0.016	0.033	-0.346	-0.172
-0.800	0.016	0.131	-0.345	-0.200
-0.800	0.016	0.197	-0.322	-0.231
-0.800	0.147	0.007	-0.212	-0.060
-0.800	0.147	0.033	-0.349	-0.084
-0.800	0.147	0.131	-0.409	-0.116
-0.800	0.147	0.197	-0.392	-0.150
-0.800	0.442	0.007	-0.334	-0.079
-0.800	0.442	0.033	-0.391	-0.073

X/B	Y/B	Z/B	U (m/s)	V (m/s)
-0.800	0.442	0.131	-0.443	-0.051
-0.800	0.442	0.197	-0.429	-0.058
-0.800	0.672	0.007	-0.495	-0.041
-0.800	0.672	0.033	-0.520	-0.038
-0.800	0.672	0.131	-0.486	-0.011
-0.800	0.672	0.197	-0.438	-0.003
-0.800	0.902	0.007	-0.460	0.001
-0.800	0.902	0.033	-0.500	0.004
-0.800	0.902	0.131	-0.532	0.008
-0.800	0.902	0.197	-0.487	0.005
-1.110	0.016	0.007	-0.221	0.030
-1.110	0.016	0.033	-0.339	-0.001
-1.110	0.016	0.131	-0.328	-0.009
-1.110	0.016	0.197	-0.341	0.009
-1.110	0.147	0.007	-0.138	0.035
-1.110	0.147	0.033	-0.229	-0.035
-1.110	0.147	0.131	-0.384	-0.053
-1.110	0.147	0.197	-0.370	-0.069
-1.110	0.442	0.007	-0.321	-0.036
-1.110	0.442	0.033	-0.384	-0.037
-1.110	0.442	0.131	-0.412	-0.018
-1.110	0.442	0.197	-0.395	-0.007
-1.110	0.672	0.007	-0.455	-0.042
-1.110	0.672	0.033	-0.464	-0.043
-1.110	0.672	0.131	-0.451	-0.016
-1.110	0.672	0.197	-0.379	-0.007
-1.110	0.902	0.007	-0.467	-0.037
-1.110	0.902	0.033	-0.512	-0.028
-1.110	0.902	0.131	-0.454	-0.011
-1.110	0.902	0.197	-0.413	0.000

Table 9.5 Velocity data for dividing flows in open channels ($Q_r = 0.308$, continued)

X/B	Y/B	Z/B	U (m/s)	V (m/s)
-1.700	0.098	0.007	-0.355	0.050
-1.700	0.098	0.033	-0.355	0.034
-1.700	0.098	0.131	-0.379	-0.014
-1.700	0.098	0.197	-0.382	-0.028
-1.700	0.213	0.007	-0.283	0.089
-1.700	0.213	0.033	-0.283	0.030
-1.700	0.213	0.131	-0.357	-0.031
-1.700	0.213	0.197	-0.373	-0.041
-1.700	0.442	0.007	-0.321	-0.015
-1.700	0.442	0.033	-0.370	-0.022
-1.700	0.442	0.131	-0.386	-0.012
-1.700	0.442	0.197	-0.374	-0.005
-1.700	0.672	0.007	-0.433	-0.014
-1.700	0.672	0.033	-0.461	-0.015
-1.700	0.672	0.131	-0.447	0.000
-1.700	0.672	0.197	-0.379	0.015
-1.700	0.902	0.007	-0.403	-0.001
-1.700	0.902	0.033	-0.418	0.000
-1.700	0.902	0.131	-0.424	0.009
-1.700	0.902	0.197	-0.380	0.009
-3.000	0.098	0.007	-0.363	0.025
-3.000	0.098	0.033	-0.374	0.017
-3.000	0.098	0.131	-0.387	-0.008
-3.000	0.098	0.197	-0.365	-0.016
-3.000	0.213	0.007	-0.338	0.039
-3.000	0.213	0.033	-0.351	0.034
-3.000	0.213	0.131	-0.357	-0.018
-3.000	0.213	0.197	-0.381	-0.025
-3.000	0.442	0.007	-0.291	0.018
-3.000	0.442	0.033	-0.322	0.009

X/B	Y/B	Z/B	U (m/s)	V (m/s)
-3.000	0.442	0.131	-0.400	-0.016
-3.000	0.442	0.197	-0.388	-0.001
-3.000	0.672	0.007	-0.399	-0.007
-3.000	0.672	0.033	-0.429	-0.009
-3.000	0.672	0.131	-0.436	-0.003
-3.000	0.672	0.197	-0.419	0.008
-3.000	0.902	0.007	-0.360	-0.005
-3.000	0.902	0.033	-0.395	0.004
-3.000	0.902	0.131	-0.402	0.005
-3.000	0.902	0.197	-0.388	0.010
-0.098	-0.290	0.007	0.045	0.097
-0.098	-0.290	0.033	-0.009	0.057
-0.098	-0.290	0.131	0.021	0.129
-0.098	-0.290	0.197	0.034	0.095
-0.328	-0.290	0.007	0.050	-0.001
-0.328	-0.290	0.033	0.054	-0.003
-0.328	-0.290	0.131	0.075	0.081
-0.328	-0.290	0.197	0.039	0.070
-0.558	-0.290	0.007	0.092	-0.160
-0.558	-0.290	0.033	0.107	-0.160
-0.558	-0.290	0.131	0.081	-0.074
-0.558	-0.290	0.197	0.052	-0.038
-0.787	-0.290	0.007	-0.072	-0.395
-0.787	-0.290	0.033	0.236	-0.429
-0.787	-0.290	0.131	0.202	-0.447
-0.787	-0.290	0.197	0.166	-0.434
-0.902	-0.290	0.007	-0.031	-0.377
-0.902	-0.290	0.033	0.134	-0.422
-0.902	-0.290	0.131	0.109	-0.434
-0.902	-0.290	0.197	0.078	-0.429

Table 9.5 Velocity data for dividing flows in open channels ($Q_r = 0.308$, continued)

X/B	Y/B	Z/B	U (m/s)	V (m/s)
-0.098	-0.730	0.007	0.012	0.114
-0.098	-0.730	0.033	0.017	0.135
-0.098	-0.730	0.131	0.017	0.134
-0.098	-0.730	0.197	0.020	0.117
-0.328	-0.730	0.007	-0.040	0.188
-0.328	-0.730	0.033	0.027	0.018
-0.328	-0.730	0.131	0.066	0.097
-0.328	-0.730	0.197	0.041	0.084
-0.558	-0.730	0.007	-0.063	-0.253
-0.558	-0.730	0.033	-0.045	-0.172
-0.558	-0.730	0.131	-0.003	-0.053
-0.558	-0.730	0.197	0.033	0.038
-0.787	-0.730	0.007	-0.110	-0.438
-0.787	-0.730	0.033	0.014	-0.446
-0.787	-0.730	0.131	0.044	-0.448
-0.787	-0.730	0.197	0.025	-0.308
-0.902	-0.730	0.007	-0.003	-0.480
-0.902	-0.730	0.033	0.054	-0.501
-0.902	-0.730	0.131	0.013	-0.257
-0.902	-0.730	0.197	0.040	-0.097
-0.098	-1.220	0.007	-0.018	0.130
-0.098	-1.220	0.033	-0.008	0.197
-0.098	-1.220	0.131	0.005	0.195
-0.098	-1.220	0.197	0.009	0.128
-0.328	-1.220	0.007	-0.078	-0.085
-0.328	-1.220	0.033	-0.035	0.004
-0.328	-1.220	0.131	0.031	0.052
-0.328	-1.220	0.197	0.051	0.102
-0.558	-1.220	0.007	-0.085	-0.246
-0.558	-1.220	0.033	-0.070	-0.235

X/B	Y/B	Z/B	U (m/s)	V (m/s)
-0.558	-1.220	0.131	0.010	-0.038
-0.558	-1.220	0.197	0.049	0.076
-0.787	-1.220	0.007	-0.036	-0.466
-0.787	-1.220	0.033	-0.007	-0.441
-0.787	-1.220	0.131	0.048	-0.414
-0.787	-1.220	0.197	0.041	-0.297
-0.902	-1.220	0.007	0.023	-0.481
-0.902	-1.220	0.033	0.056	-0.480
-0.902	-1.220	0.131	0.030	-0.429
-0.902	-1.220	0.197	-0.009	-0.033
-0.098	-1.620	0.007	0.002	0.102
-0.098	-1.620	0.033	-0.003	0.105
-0.098	-1.620	0.131	0.007	0.115
-0.098	-1.620	0.197	0.027	0.141
-0.328	-1.620	0.007	-0.086	-0.051
-0.328	-1.620	0.033	-0.090	-0.043
-0.328	-1.620	0.131	0.024	0.027
-0.328	-1.620	0.197	0.051	0.119
-0.558	-1.620	0.007	-0.068	-0.200
-0.558	-1.620	0.033	0.002	-0.185
-0.558	-1.620	0.131	0.003	-0.136
-0.558	-1.620	0.197	-0.011	-0.063
-0.787	-1.620	0.007	-0.005	-0.435
-0.787	-1.620	0.033	-0.026	-0.446
-0.787	-1.620	0.131	0.026	-0.414
-0.787	-1.620	0.197	0.004	-0.323
-0.902	-1.620	0.007	0.020	-0.427
-0.902	-1.620	0.033	0.037	-0.483
-0.902	-1.620	0.131	0.021	-0.481
-0.902	-1.620	0.197	-0.017	-0.216

Table 9.5 Velocity data for dividing flows in open channels ($Q_r = 0.308$, continued)

X/B	Y/B	Z/B	U (m/s)	V (m/s)
-0.098	-2.500	0.007	-0.002	0.119
-0.098	-2.500	0.033	0.007	0.112
-0.098	-2.500	0.131	0.018	0.217
-0.098	-2.500	0.197	0.038	0.209
-0.328	-2.500	0.007	-0.061	-0.003
-0.328	-2.500	0.033	-0.020	0.019
-0.328	-2.500	0.131	0.222	0.252
-0.328	-2.500	0.197	0.020	0.333
-0.558	-2.500	0.007	-0.008	-0.028
-0.558	-2.500	0.033	-0.032	-0.278
-0.558	-2.500	0.131	0.032	-0.178
-0.558	-2.500	0.197	0.026	-0.178
-0.787	-2.500	0.007	0.001	-0.428
-0.787	-2.500	0.033	-0.016	-0.410
-0.787	-2.500	0.131	0.015	-0.391
-0.787	-2.500	0.197	0.012	-0.391
-0.902	-2.500	0.007	0.044	-0.395
-0.902	-2.500	0.033	0.038	-0.458
-0.902	-2.500	0.131	0.052	-0.439
-0.902	-2.500	0.197	0.010	-0.422

Table 9.6 Water surface profiles for dividing flows in open channels ($Q_r = 0.409$)

X/B	Y/B	Z/B	X/B	Y/B	Z/B	X/B	Y/B	Z/B	X/B	Y/B	Z/B
0.967	0.016	0.239	-0.287	0.016	0.234	-1.041	0.016	0.268	-2.107	0.016	0.255
0.967	0.098	0.240	-0.287	0.098	0.235	-1.041	0.098	0.263	-2.107	0.098	0.253
0.967	0.213	0.245	-0.287	0.213	0.241	-1.041	0.213	0.260	-2.107	0.213	0.255
0.967	0.328	0.248	-0.287	0.328	0.245	-1.041	0.328	0.258	-2.107	0.328	0.255
0.967	0.443	0.245	-0.287	0.443	0.248	-1.041	0.443	0.257	-2.107	0.443	0.255
0.967	0.557	0.244	-0.287	0.557	0.250	-1.041	0.557	0.257	-2.107	0.557	0.255
0.967	0.672	0.245	-0.287	0.672	0.248	-1.041	0.672	0.256	-2.107	0.672	0.254
0.967	0.787	0.246	-0.287	0.787	0.249	-1.041	0.787	0.255	-2.107	0.787	0.254
0.967	0.902	0.245	-0.287	0.902	0.249	-1.041	0.902	0.254	-2.107	0.902	0.254
0.967	0.984	0.248	-0.287	0.984	0.254	-1.041	0.984	0.255	-2.107	0.984	0.255
0.221	0.016	0.245	-0.541	0.016	0.243	-1.287	0.016	0.263	-3.000	0.016	0.257
0.221	0.098	0.244	-0.541	0.098	0.250	-1.287	0.098	0.259	-3.000	0.098	0.256
0.221	0.213	0.241	-0.541	0.213	0.253	-1.287	0.213	0.258	-3.000	0.213	0.258
0.221	0.328	0.242	-0.541	0.328	0.255	-1.287	0.328	0.257	-3.000	0.328	0.253
0.221	0.443	0.243	-0.541	0.443	0.253	-1.287	0.443	0.257	-3.000	0.443	0.253
0.221	0.557	0.242	-0.541	0.557	0.254	-1.287	0.557	0.257	-3.000	0.557	0.253
0.221	0.672	0.245	-0.541	0.672	0.254	-1.287	0.672	0.257	-3.000	0.672	0.253
0.221	0.787	0.244	-0.541	0.787	0.253	-1.287	0.787	0.256	-3.000	0.787	0.256
0.221	0.902	0.246	-0.541	0.902	0.252	-1.287	0.902	0.256	-3.000	0.902	0.256
0.221	0.984	0.247	-0.541	0.984	0.252	-1.287	0.984	0.254	-3.000	0.984	0.261
-0.041	0.016	0.224	-0.795	0.016	0.259	-1.697	0.016	0.257			
-0.041	0.098	0.235	-0.795	0.098	0.258	-1.697	0.098	0.257			
-0.041	0.213	0.242	-0.795	0.213	0.256	-1.697	0.213	0.256			
-0.041	0.328	0.246	-0.795	0.328	0.255	-1.697	0.328	0.256			
-0.041	0.443	0.245	-0.795	0.443	0.254	-1.697	0.443	0.255			
-0.041	0.557	0.246	-0.795	0.557	0.254	-1.697	0.557	0.255			
-0.041	0.672	0.246	-0.795	0.672	0.254	-1.697	0.672	0.255			
-0.041	0.787	0.246	-0.795	0.787	0.255	-1.697	0.787	0.255			
-0.041	0.902	0.247	-0.795	0.902	0.255	-1.697	0.902	0.255			
-0.041	0.984	0.250	-0.795	0.984	0.254	-1.697	0.984	0.256			

Table 9.6 Water surface profiles for dividing flows in open channels (Q_r = 0.409, continued)

X/B	Y/B	Z/B
-0.016	-0.287	0.222
-0.098	-0.287	0.222
-0.213	-0.287	0.222
-0.328	-0.287	0.223
-0.443	-0.287	0.224
-0.557	-0.287	0.230
-0.672	-0.287	0.235
-0.787	-0.287	0.245
-0.902	-0.287	0.245
-0.984	-0.287	0.251
-0.016	-0.730	0.223
-0.098	-0.730	0.222
-0.213	-0.730	0.222
-0.328	-0.730	0.222
-0.443	-0.730	0.217
-0.557	-0.730	0.221
-0.672	-0.730	0.218
-0.787	-0.730	0.218
-0.902	-0.730	0.220
-0.984	-0.730	0.227
-0.016	-0.893	0.223
-0.098	-0.893	0.222
-0.213	-0.893	0.220
-0.328	-0.893	0.219
-0.443	-0.893	0.218
-0.557	-0.893	0.220
-0.672	-0.893	0.222
-0.787	-0.893	0.219
-0.902	-0.893	0.218
-0.984	-0.893	0.221

X/B	Y/B	Z/B
-0.016	-1.221	0.223
-0.098	-1.221	0.222
-0.213	-1.221	0.223
-0.328	-1.221	0.224
-0.443	-1.221	0.220
-0.557	-1.221	0.220
-0.672	-1.221	0.220
-0.787	-1.221	0.220
-0.902	-1.221	0.216
-0.984	-1.221	0.219
-0.016	-1.623	0.225
-0.098	-1.623	0.225
-0.213	-1.623	0.224
-0.328	-1.623	0.222
-0.443	-1.623	0.222
-0.557	-1.623	0.223
-0.672	-1.623	0.222
-0.787	-1.623	0.221
-0.902	-1.623	0.220
-0.984	-1.623	0.221
-0.016	-2.000	0.228
-0.098	-2.000	0.228
-0.213	-2.000	0.227
-0.328	-2.000	0.227
-0.443	-2.000	0.226
-0.557	-2.000	0.226
-0.672	-2.000	0.224
-0.787	-2.000	0.221
-0.902	-2.000	0.222
-0.984	-2.000	0.225

X/B	Y/B	Z/B
-0.016	-2.533	0.228
-0.098	-2.533	0.230
-0.213	-2.533	0.232
-0.328	-2.533	0.231
-0.443	-2.533	0.232
-0.557	-2.533	0.232
-0.672	-2.533	0.232
-0.787	-2.533	0.228
-0.902	-2.533	0.227
-0.984	-2.533	0.228
-0.016	-3.000	0.234
-0.098	-3.000	0.235
-0.213	-3.000	0.235
-0.328	-3.000	0.234
-0.443	-3.000	0.235
-0.557	-3.000	0.236
-0.672	-3.000	0.235
-0.787	-3.000	0.235
-0.902	-3.000	0.233
-0.984	-3.000	0.234

Table 9.7 Velocity data for dividing flows in open channels ($Q_r = 0.409$)

X/B	Y/B	Z/B	U (m/s)	V (m/s)	W (m/s)
0.970	0.016	0.021	-0.522	0.012	0.000
0.970	0.016	0.043	-0.518	0.016	0.000
0.970	0.016	0.076	-0.571	0.023	0.000
0.970	0.016	0.108	-0.621	0.037	0.000
0.970	0.016	0.141	-0.614	-0.005	0.000
0.970	0.016	0.174	-0.527	0.006	0.000
0.970	0.016	0.207	-0.532	0.016	0.000
0.970	0.016	0.239	-0.531	-0.012	0.000
0.970	0.098	0.021	-0.574	0.044	0.000
0.970	0.098	0.043	-0.624	0.038	0.000
0.970	0.098	0.076	-0.642	0.038	0.000
0.970	0.098	0.108	-0.633	0.027	0.000
0.970	0.098	0.141	-0.637	0.021	0.000
0.970	0.098	0.174	-0.630	0.016	0.000
0.970	0.098	0.207	-0.593	0.005	0.000
0.970	0.098	0.239	-0.535	0.011	0.000
0.970	0.213	0.021	-0.653	0.055	0.000
0.970	0.213	0.043	-0.684	0.034	0.000
0.970	0.213	0.076	-0.677	0.023	0.000
0.970	0.213	0.108	-0.685	0.003	0.000
0.970	0.213	0.141	-0.664	-0.007	0.000
0.970	0.213	0.174	-0.664	-0.009	0.000
0.970	0.213	0.207	-0.600	-0.014	0.000
0.970	0.213	0.239	-0.596	-0.010	0.000
0.970	0.328	0.021	-0.632	0.049	0.000
0.970	0.328	0.043	-0.637	0.036	0.000
0.970	0.328	0.076	-0.632	0.021	0.000
0.970	0.328	0.108	-0.680	0.027	0.000
0.970	0.328	0.141	-0.661	0.015	0.000
0.970	0.328	0.174	-0.642	0.010	0.000

X/B	Y/B	Z/B	U (m/s)	V (m/s)	W (m/s)
0.970	0.328	0.207	-0.530	-0.005	0.000
0.970	0.328	0.239	-0.531	-0.006	0.000
0.970	0.443	0.021	-0.584	0.029	0.000
0.970	0.443	0.043	-0.590	0.028	0.000
0.970	0.443	0.076	-0.620	0.029	0.000
0.970	0.443	0.108	-0.619	0.027	0.000
0.970	0.443	0.141	-0.623	0.018	0.000
0.970	0.443	0.174	-0.628	0.032	0.000
0.970	0.443	0.207	-0.574	0.013	0.000
0.970	0.443	0.239	-0.551	0.003	0.000
0.970	0.557	0.021	-0.511	-0.010	0.000
0.970	0.557	0.043	-0.548	-0.006	0.000
0.970	0.557	0.076	-0.598	0.010	0.000
0.970	0.557	0.108	-0.603	0.021	0.000
0.970	0.557	0.141	-0.609	0.041	0.000
0.970	0.557	0.174	-0.598	0.031	0.000
0.970	0.557	0.207	-0.547	0.030	0.001
0.970	0.557	0.239	-0.538	0.012	0.001
0.970	0.672	0.021	-0.550	-0.019	0.000
0.970	0.672	0.043	-0.579	-0.021	0.000
0.970	0.672	0.076	-0.567	0.014	0.000
0.970	0.672	0.108	-0.582	0.040	0.000
0.970	0.672	0.141	-0.596	0.064	0.000
0.970	0.672	0.174	-0.593	0.071	0.001
0.970	0.672	0.207	-0.540	0.057	0.001
0.970	0.672	0.239	-0.527	0.016	0.001
0.970	0.787	0.021	-0.513	-0.043	0.000
0.970	0.787	0.043	-0.533	-0.013	0.000
0.970	0.787	0.076	-0.555	0.013	0.000
0.970	0.787	0.108	-0.564	0.055	0.000

Table 9.7 Velocity data for dividing flows in open channels (Q_r = 0.409, continued)

X/B	Y/B	Z/B	U (m/s)	V (m/s)	W (m/s)
0.970	0.787	0.141	-0.570	0.055	0.000
0.970	0.787	0.174	-0.562	0.074	0.001
0.970	0.787	0.207	-0.519	0.064	0.001
0.970	0.787	0.239	-0.502	0.027	0.001
0.970	0.902	0.021	-0.509	-0.024	0.000
0.970	0.902	0.043	-0.532	0.003	0.000
0.970	0.902	0.076	-0.533	0.027	0.000
0.970	0.902	0.108	-0.526	0.036	0.000
0.970	0.902	0.141	-0.546	0.063	0.001
0.970	0.902	0.174	-0.490	0.049	0.001
0.970	0.902	0.207	-0.482	0.012	0.001
0.970	0.902	0.239	-0.481	-0.086	0.001
0.970	0.984	0.021	-0.404	0.003	0.000
0.970	0.984	0.043	-0.419	0.006	0.000
0.970	0.984	0.076	-0.458	0.014	0.000
0.970	0.984	0.108	-0.466	0.026	0.001
0.970	0.984	0.141	-0.466	0.026	0.001
0.970	0.984	0.174	-0.466	0.026	0.001
0.970	0.984	0.207	-0.466	0.026	0.001
0.970	0.984	0.239	-0.466	0.026	0.001
0.220	0.016	0.021	-0.555	0.017	-0.001
0.220	0.016	0.043	-0.573	0.023	-0.001
0.220	0.016	0.076	-0.594	0.024	-0.002
0.220	0.016	0.108	-0.612	0.019	-0.003
0.220	0.016	0.141	-0.604	0.010	-0.004
0.220	0.016	0.174	-0.605	0.013	-0.004
0.220	0.016	0.207	-0.538	0.019	-0.005
0.220	0.016	0.239	-0.518	0.012	-0.006
0.220	0.148	0.021	-0.669	0.029	0.000
0.220	0.148	0.043	-0.671	0.022	0.000

X/B	Y/B	Z/B	U (m/s)	V (m/s)	W (m/s)
0.220	0.148	0.076	-0.676	0.015	-0.002
0.220	0.148	0.108	-0.690	0.003	-0.003
0.220	0.148	0.141	-0.670	-0.013	-0.003
0.220	0.148	0.174	-0.662	-0.013	-0.004
0.220	0.148	0.207	-0.598	-0.019	-0.005
0.220	0.148	0.239	-0.579	-0.001	-0.007
0.220	0.213	0.021	-0.639	0.033	0.000
0.220	0.213	0.043	-0.676	0.025	0.000
0.220	0.213	0.076	-0.677	0.011	-0.001
0.220	0.213	0.108	-0.665	0.006	-0.002
0.220	0.213	0.141	-0.674	-0.011	-0.003
0.220	0.213	0.174	-0.654	-0.022	-0.003
0.220	0.213	0.207	-0.601	-0.026	-0.004
0.220	0.213	0.239	-0.606	-0.014	-0.006
0.220	0.328	0.021	-0.590	0.030	0.000
0.220	0.328	0.043	-0.641	0.024	0.000
0.220	0.328	0.076	-0.641	0.016	-0.001
0.220	0.328	0.108	-0.650	0.011	-0.001
0.220	0.328	0.141	-0.646	0.002	-0.001
0.220	0.328	0.174	-0.634	-0.012	-0.002
0.220	0.328	0.207	-0.588	-0.017	-0.003
0.220	0.328	0.239	-0.575	-0.027	-0.004
0.220	0.443	0.021	-0.555	0.007	0.000
0.220	0.443	0.043	-0.597	0.019	0.000
0.220	0.443	0.076	-0.601	0.016	0.000
0.220	0.443	0.108	-0.600	0.007	0.000
0.220	0.443	0.141	-0.609	0.002	-0.001
0.220	0.443	0.174	-0.615	0.001	-0.001
0.220	0.443	0.207	-0.569	0.003	-0.001
0.220	0.443	0.239	-0.542	0.001	-0.002

Table 9.7 Velocity data for dividing flows in open channels ($Q_r = 0.409$, continued)

X/B	Y/B	Z/B	U (m/s)	V (m/s)	W (m/s)
0.220	0.557	0.021	-0.534	-0.014	0.000
0.220	0.557	0.043	-0.572	0.003	0.000
0.220	0.557	0.076	-0.592	0.009	0.000
0.220	0.557	0.108	-0.586	0.011	0.000
0.220	0.557	0.141	-0.588	0.023	0.001
0.220	0.557	0.174	-0.594	0.035	0.001
0.220	0.557	0.207	-0.569	0.026	0.001
0.220	0.557	0.239	-0.556	0.017	0.000
0.220	0.672	0.021	-0.557	-0.049	0.000
0.220	0.672	0.043	-0.586	-0.048	0.000
0.220	0.672	0.076	-0.590	-0.015	0.001
0.220	0.672	0.108	-0.586	0.007	0.001
0.220	0.672	0.141	-0.596	0.020	0.001
0.220	0.672	0.174	-0.574	0.040	0.002
0.220	0.672	0.207	-0.539	0.030	0.002
0.220	0.672	0.239	-0.533	0.018	0.002
0.220	0.787	0.021	-0.518	-0.040	0.000
0.220	0.787	0.043	-0.569	-0.036	0.001
0.220	0.787	0.076	-0.588	-0.014	0.001
0.220	0.787	0.108	-0.600	0.004	0.002
0.220	0.787	0.141	-0.605	0.029	0.002
0.220	0.787	0.174	-0.557	0.038	0.003
0.220	0.787	0.207	-0.519	0.027	0.003
0.220	0.787	0.239	-0.514	0.003	0.004
0.220	0.902	0.021	-0.545	-0.017	0.001
0.220	0.902	0.043	-0.564	-0.007	0.001
0.220	0.902	0.076	-0.574	0.014	0.003
0.220	0.902	0.108	-0.580	0.014	0.003
0.220	0.902	0.141	-0.556	0.029	0.004
0.220	0.902	0.174	-0.500	0.019	0.004

X/B	Y/B	Z/B	U (m/s)	V (m/s)	W (m/s)
0.220	0.902	0.207	-0.505	0.007	0.004
0.220	0.902	0.239	-0.500	-0.003	0.005
0.220	0.984	0.021	-0.423	0.012	0.002
0.220	0.984	0.043	-0.444	0.013	0.003
0.220	0.984	0.076	-0.474	0.019	0.005
0.220	0.984	0.108	-0.501	0.016	0.005
0.220	0.984	0.141	-0.501	0.017	0.005
0.220	0.984	0.174	-0.485	0.014	0.005
0.220	0.984	0.207	-0.440	-0.005	0.005
0.220	0.984	0.239	-0.442	0.004	0.003
-0.040	0.016	0.021	-0.675	-0.043	-0.024
-0.040	0.016	0.043	-0.675	-0.052	-0.030
-0.040	0.016	0.076	-0.685	-0.064	-0.025
-0.040	0.016	0.108	-0.717	-0.062	-0.018
-0.040	0.016	0.141	-0.706	-0.077	-0.014
-0.040	0.016	0.174	-0.706	-0.077	-0.012
-0.040	0.016	0.207	-0.706	-0.077	-0.013
-0.040	0.016	0.239	-0.706	-0.077	-0.013
-0.040	0.148	0.021	-0.680	-0.036	0.000
-0.040	0.148	0.043	-0.728	-0.043	-0.001
-0.040	0.148	0.076	-0.736	-0.046	-0.004
-0.040	0.148	0.108	-0.753	-0.051	-0.006
-0.040	0.148	0.141	-0.712	-0.063	-0.008
-0.040	0.148	0.174	-0.688	-0.068	-0.011
-0.040	0.148	0.207	-0.683	-0.070	-0.017
-0.040	0.148	0.239	-0.573	-0.028	-0.015
-0.040	0.213	0.021	-0.649	-0.029	0.000
-0.040	0.213	0.043	-0.673	-0.027	0.000
-0.040	0.213	0.076	-0.700	-0.043	0.000
-0.040	0.213	0.108	-0.675	-0.051	-0.001

Table 9.7 Velocity data for dividing flows in open channels (Q_r = 0.409, continued)

X/B	Y/B	Z/B	U (m/s)	V (m/s)	W (m/s)
-0.040	0.213	0.141	-0.680	-0.064	-0.002
-0.040	0.213	0.174	-0.674	-0.072	-0.003
-0.040	0.213	0.207	-0.614	-0.079	-0.004
-0.040	0.213	0.239	-0.600	-0.050	-0.008
-0.040	0.328	0.021	-0.575	-0.013	0.000
-0.040	0.328	0.043	-0.609	-0.005	0.001
-0.040	0.328	0.076	-0.639	-0.010	0.001
-0.040	0.328	0.108	-0.639	-0.021	0.001
-0.040	0.328	0.141	-0.623	-0.038	0.000
-0.040	0.328	0.174	-0.634	-0.044	0.000
-0.040	0.328	0.207	-0.588	-0.039	-0.001
-0.040	0.328	0.239	-0.584	-0.025	-0.003
-0.040	0.443	0.021	-0.526	-0.023	0.000
-0.040	0.443	0.043	-0.557	-0.020	0.001
-0.040	0.443	0.076	-0.573	-0.021	0.001
-0.040	0.443	0.108	-0.579	-0.020	0.001
-0.040	0.443	0.141	-0.574	-0.026	0.001
-0.040	0.443	0.174	-0.580	-0.016	0.001
-0.040	0.443	0.207	-0.554	-0.019	0.001
-0.040	0.443	0.239	-0.520	-0.010	-0.001
-0.040	0.557	0.021	-0.498	-0.053	0.001
-0.040	0.557	0.043	-0.529	-0.043	0.001
-0.040	0.557	0.076	-0.556	-0.034	0.002
-0.040	0.557	0.108	-0.560	-0.014	0.002
-0.040	0.557	0.141	-0.550	-0.005	0.002
-0.040	0.557	0.174	-0.569	0.009	0.003
-0.040	0.557	0.207	-0.550	0.014	0.003
-0.040	0.557	0.239	-0.550	0.005	0.003
-0.040	0.672	0.021	-0.524	-0.068	0.001
-0.040	0.672	0.043	-0.575	-0.055	0.001

X/B	Y/B	Z/B	U (m/s)	V (m/s)	W (m/s)
-0.040	0.672	0.076	-0.560	-0.034	0.002
-0.040	0.672	0.108	-0.550	-0.013	0.002
-0.040	0.672	0.141	-0.548	0.013	0.003
-0.040	0.672	0.174	-0.547	0.023	0.004
-0.040	0.672	0.207	-0.535	0.012	0.004
-0.040	0.672	0.239	-0.535	0.012	0.005
-0.040	0.787	0.021	-0.520	-0.047	0.001
-0.040	0.787	0.043	-0.552	-0.034	0.001
-0.040	0.787	0.076	-0.567	-0.021	0.003
-0.040	0.787	0.108	-0.551	-0.005	0.003
-0.040	0.787	0.141	-0.557	0.010	0.004
-0.040	0.787	0.174	-0.534	0.014	0.005
-0.040	0.787	0.207	-0.516	0.030	0.005
-0.040	0.787	0.239	-0.519	0.008	0.005
-0.040	0.902	0.021	-0.539	-0.008	0.002
-0.040	0.902	0.043	-0.543	0.002	0.003
-0.040	0.902	0.076	-0.559	0.011	0.006
-0.040	0.902	0.108	-0.542	0.021	0.006
-0.040	0.902	0.141	-0.534	0.029	0.006
-0.040	0.902	0.174	-0.496	0.025	0.006
-0.040	0.902	0.207	-0.477	0.013	0.005
-0.040	0.902	0.239	-0.497	0.005	0.004
-0.040	0.984	0.021	-0.391	0.014	-0.008
-0.040	0.984	0.043	-0.432	0.017	0.002
-0.040	0.984	0.076	-0.447	0.019	0.011
-0.040	0.984	0.108	-0.498	0.027	0.011
-0.040	0.984	0.141	-0.496	0.027	0.010
-0.040	0.984	0.174	-0.456	0.023	0.008
-0.040	0.984	0.207	-0.343	0.018	0.006
-0.040	0.984	0.239	-0.317	0.013	0.002

Table 9.7 Velocity data for dividing flows in open channels ($Q_r = 0.409$, continued)

X/B	Y/B	Z/B	U (m/s)	V (m/s)	W (m/s)
-0.290	0.016	0.021	-0.685	-0.193	0.005
-0.290	0.016	0.043	-0.676	-0.198	0.006
-0.290	0.016	0.076	-0.677	-0.199	0.005
-0.290	0.016	0.108	-0.682	-0.194	0.003
-0.290	0.016	0.141	-0.692	-0.196	0.002
-0.290	0.016	0.174	-0.683	-0.201	0.002
-0.290	0.016	0.207	-0.632	-0.181	0.005
-0.290	0.016	0.239	-0.625	-0.078	0.005
-0.290	0.148	0.021	-0.624	-0.124	0.003
-0.290	0.148	0.043	-0.652	-0.113	0.004
-0.290	0.148	0.076	-0.655	-0.139	0.006
-0.290	0.148	0.108	-0.651	-0.144	0.006
-0.290	0.148	0.141	-0.631	-0.160	0.006
-0.290	0.148	0.174	-0.630	-0.171	0.007
-0.290	0.148	0.207	-0.592	-0.183	0.011
-0.290	0.148	0.239	-0.504	-0.093	0.003
-0.290	0.213	0.021	-0.585	-0.102	0.002
-0.290	0.213	0.043	-0.610	-0.097	0.003
-0.290	0.213	0.076	-0.653	-0.108	0.006
-0.290	0.213	0.108	-0.640	-0.125	0.007
-0.290	0.213	0.141	-0.629	-0.138	0.008
-0.290	0.213	0.174	-0.612	-0.149	0.009
-0.290	0.213	0.207	-0.580	-0.157	0.009
-0.290	0.213	0.239	-0.555	-0.075	0.004
-0.290	0.328	0.021	-0.523	-0.095	0.002
-0.290	0.328	0.043	-0.548	-0.089	0.003
-0.290	0.328	0.076	-0.570	-0.089	0.005
-0.290	0.328	0.108	-0.582	-0.091	0.007
-0.290	0.328	0.141	-0.589	-0.101	0.008
-0.290	0.328	0.174	-0.581	-0.100	0.009

X/B	Y/B	Z/B	U (m/s)	V (m/s)	W (m/s)
-0.290	0.328	0.207	-0.556	-0.104	0.010
-0.290	0.328	0.239	-0.561	-0.053	0.006
-0.290	0.443	0.021	-0.468	-0.061	0.001
-0.290	0.443	0.043	-0.506	-0.067	0.002
-0.290	0.443	0.076	-0.530	-0.078	0.005
-0.290	0.443	0.108	-0.542	-0.068	0.006
-0.290	0.443	0.141	-0.556	-0.064	0.007
-0.290	0.443	0.174	-0.548	-0.068	0.008
-0.290	0.443	0.207	-0.523	-0.055	0.009
-0.290	0.443	0.239	-0.532	-0.032	0.007
-0.290	0.557	0.021	-0.448	-0.090	0.001
-0.290	0.557	0.043	-0.488	-0.085	0.002
-0.290	0.557	0.076	-0.531	-0.058	0.004
-0.290	0.557	0.108	-0.531	-0.048	0.005
-0.290	0.557	0.141	-0.532	-0.035	0.006
-0.290	0.557	0.174	-0.523	-0.036	0.007
-0.290	0.557	0.207	-0.508	-0.010	0.008
-0.290	0.557	0.239	-0.577	-0.008	0.008
-0.290	0.672	0.021	-0.492	-0.093	0.001
-0.290	0.672	0.043	-0.516	-0.060	0.002
-0.290	0.672	0.076	-0.529	-0.056	0.004
-0.290	0.672	0.108	-0.535	-0.037	0.005
-0.290	0.672	0.141	-0.549	-0.023	0.006
-0.290	0.672	0.174	-0.543	0.001	0.006
-0.290	0.672	0.207	-0.516	-0.005	0.007
-0.290	0.672	0.239	-0.523	-0.005	0.007
-0.290	0.787	0.021	-0.513	-0.054	0.001
-0.290	0.787	0.043	-0.522	-0.048	0.002
-0.290	0.787	0.076	-0.531	-0.039	0.005
-0.290	0.787	0.108	-0.530	-0.018	0.006

Table 9.7 Velocity data for dividing flows in open channels (Q_r = 0.409, continued)

X/B	Y/B	Z/B	U (m/s)	V (m/s)	W (m/s)
-0.290	0.787	0.141	-0.542	-0.005	0.007
-0.290	0.787	0.174	-0.513	-0.006	0.007
-0.290	0.787	0.207	-0.506	-0.006	0.007
-0.290	0.787	0.239	-0.498	-0.004	0.006
-0.290	0.902	0.021	-0.485	-0.019	0.001
-0.290	0.902	0.043	-0.504	-0.008	0.003
-0.290	0.902	0.076	-0.508	0.002	0.009
-0.290	0.902	0.108	-0.515	0.012	0.011
-0.290	0.902	0.141	-0.506	0.011	0.011
-0.290	0.902	0.174	-0.481	0.010	0.010
-0.290	0.902	0.207	-0.430	-0.004	0.008
-0.290	0.902	0.239	-0.411	-0.007	0.006
-0.290	0.984	0.021	-0.320	0.009	0.000
-0.290	0.984	0.043	-0.346	0.013	-0.003
-0.290	0.984	0.076	-0.372	0.011	0.008
-0.290	0.984	0.108	-0.424	0.014	0.013
-0.290	0.984	0.141	-0.406	0.011	0.013
-0.290	0.984	0.174	-0.415	0.010	0.011
-0.290	0.984	0.207	-0.418	-0.003	0.008
-0.290	0.984	0.239	-0.414	0.005	0.003
-0.800	0.016	0.021	-0.283	-0.224	0.010
-0.800	0.016	0.043	-0.313	-0.238	0.014
-0.800	0.016	0.076	-0.426	-0.248	0.020
-0.800	0.016	0.108	-0.408	-0.247	0.020
-0.800	0.016	0.141	-0.391	-0.258	0.020
-0.800	0.016	0.174	-0.376	-0.263	0.020
-0.800	0.016	0.207	-0.351	-0.249	0.021
-0.800	0.016	0.239	-0.335	-0.155	0.029
-0.800	0.148	0.021	-0.217	-0.157	0.007
-0.800	0.148	0.043	-0.327	-0.163	0.011

X/B	Y/B	Z/B	U (m/s)	V (m/s)	W (m/s)
-0.800	0.148	0.076	-0.385	-0.151	0.019
-0.800	0.148	0.108	-0.418	-0.166	0.021
-0.800	0.148	0.141	-0.414	-0.177	0.022
-0.800	0.148	0.174	-0.429	-0.179	0.023
-0.800	0.148	0.207	-0.401	-0.185	0.023
-0.800	0.148	0.239	-0.377	-0.114	0.029
-0.800	0.213	0.021	-0.254	-0.142	0.004
-0.800	0.213	0.043	-0.316	-0.116	0.007
-0.800	0.213	0.076	-0.389	-0.132	0.015
-0.800	0.213	0.108	-0.424	-0.138	0.017
-0.800	0.213	0.141	-0.419	-0.138	0.019
-0.800	0.213	0.174	-0.414	-0.145	0.021
-0.800	0.213	0.207	-0.396	-0.145	0.022
-0.800	0.213	0.239	-0.384	-0.092	0.023
-0.800	0.328	0.021	-0.303	-0.118	0.002
-0.800	0.328	0.043	-0.341	-0.117	0.004
-0.800	0.328	0.076	-0.421	-0.109	0.009
-0.800	0.328	0.108	-0.400	-0.099	0.012
-0.800	0.328	0.141	-0.409	-0.106	0.013
-0.800	0.328	0.174	-0.424	-0.100	0.015
-0.800	0.328	0.207	-0.400	-0.106	0.015
-0.800	0.328	0.239	-0.401	-0.044	0.015
-0.800	0.443	0.021	-0.333	-0.110	0.002
-0.800	0.443	0.043	-0.378	-0.108	0.003
-0.800	0.443	0.076	-0.426	-0.094	0.007
-0.800	0.443	0.108	-0.430	-0.081	0.009
-0.800	0.443	0.141	-0.432	-0.071	0.010
-0.800	0.443	0.174	-0.438	-0.070	0.011
-0.800	0.443	0.207	-0.410	-0.066	0.012
-0.800	0.443	0.239	-0.398	-0.029	0.012

Table 9.7 Velocity data for dividing flows in open channels ($Q_r = 0.409$, continued)

X/B	Y/B	Z/B	U (m/s)	V (m/s)	W (m/s)
-0.800	0.557	0.021	-0.403	-0.095	0.001
-0.800	0.557	0.043	-0.421	-0.097	0.001
-0.800	0.557	0.076	-0.410	-0.083	0.005
-0.800	0.557	0.108	-0.427	-0.065	0.006
-0.800	0.557	0.141	-0.442	-0.056	0.007
-0.800	0.557	0.174	-0.439	-0.051	0.008
-0.800	0.557	0.207	-0.419	-0.039	0.008
-0.800	0.557	0.239	-0.407	-0.009	0.008
-0.800	0.672	0.021	-0.404	-0.064	0.000
-0.800	0.672	0.043	-0.440	-0.054	0.000
-0.800	0.672	0.076	-0.446	-0.044	0.004
-0.800	0.672	0.108	-0.438	-0.029	0.006
-0.800	0.672	0.141	-0.449	-0.016	0.007
-0.800	0.672	0.174	-0.435	-0.012	0.007
-0.800	0.672	0.207	-0.438	-0.006	0.007
-0.800	0.672	0.239	-0.412	-0.007	0.006
-0.800	0.787	0.021	-0.418	-0.036	-0.001
-0.800	0.787	0.043	-0.447	-0.032	-0.001
-0.800	0.787	0.076	-0.440	-0.015	0.003
-0.800	0.787	0.108	-0.436	-0.008	0.006
-0.800	0.787	0.141	-0.429	-0.003	0.008
-0.800	0.787	0.174	-0.403	-0.002	0.008
-0.800	0.787	0.207	-0.413	-0.008	0.006
-0.800	0.787	0.239	-0.393	-0.006	0.004
-0.800	0.902	0.021	-0.376	-0.005	-0.001
-0.800	0.902	0.043	-0.405	0.000	-0.002
-0.800	0.902	0.076	-0.425	0.003	0.000
-0.800	0.902	0.108	-0.431	0.009	0.003
-0.800	0.902	0.141	-0.430	0.012	0.007
-0.800	0.902	0.174	-0.401	0.010	0.009

X/B	Y/B	Z/B	U (m/s)	V (m/s)	W (m/s)
-0.800	0.902	0.207	-0.384	-0.006	0.007
-0.800	0.902	0.239	-0.364	-0.010	0.003
-0.800	0.984	0.021	-0.237	0.019	0.000
-0.800	0.984	0.043	-0.198	0.015	-0.001
-0.800	0.984	0.076	-0.245	0.005	-0.005
-0.800	0.984	0.108	-0.284	0.007	-0.003
-0.800	0.984	0.141	-0.329	0.014	0.002
-0.800	0.984	0.174	-0.293	0.014	0.004
-0.800	0.984	0.207	-0.266	0.013	0.004
-0.800	0.984	0.239	-0.255	-0.001	0.002
-1.040	0.016	0.021	-0.249	0.000	-0.078
-1.040	0.016	0.043	-0.310	-0.010	-0.100
-1.040	0.016	0.076	-0.347	-0.031	-0.098
-1.040	0.016	0.108	-0.387	-0.028	-0.074
-1.040	0.016	0.141	-0.342	0.001	-0.050
-1.040	0.016	0.174	-0.354	-0.023	-0.026
-1.040	0.016	0.207	-0.341	-0.029	-0.001
-1.040	0.016	0.239	-0.314	-0.009	0.025
-1.040	0.148	0.021	-0.084	-0.023	-0.013
-1.040	0.148	0.043	-0.195	-0.077	-0.018
-1.040	0.148	0.076	-0.286	-0.107	-0.023
-1.040	0.148	0.108	-0.342	-0.088	-0.022
-1.040	0.148	0.141	-0.349	-0.079	-0.017
-1.040	0.148	0.174	-0.387	-0.078	-0.012
-1.040	0.148	0.207	-0.375	-0.068	-0.004
-1.040	0.148	0.239	-0.377	-0.039	0.006
-1.040	0.213	0.021	-0.154	-0.026	0.003
-1.040	0.213	0.043	-0.236	-0.071	0.004
-1.040	0.213	0.076	-0.279	-0.079	0.006
-1.040	0.213	0.108	-0.317	-0.085	0.005

Table 9.7 Velocity data for dividing flows in open channels ($Q_r = 0.409$, continued)

X/B	Y/B	Z/B	U (m/s)	V (m/s)	W (m/s)
-1.040	0.213	0.141	-0.368	-0.078	0.004
-1.040	0.213	0.174	-0.378	-0.073	0.002
-1.040	0.213	0.207	-0.373	-0.076	0.000
-1.040	0.213	0.239	-0.371	-0.039	0.006
-1.040	0.328	0.021	-0.250	-0.056	0.001
-1.040	0.328	0.043	-0.274	-0.067	0.002
-1.040	0.328	0.076	-0.323	-0.056	0.005
-1.040	0.328	0.108	-0.349	-0.057	0.005
-1.040	0.328	0.141	-0.355	-0.052	0.005
-1.040	0.328	0.174	-0.374	-0.052	0.004
-1.040	0.328	0.207	-0.371	-0.045	0.002
-1.040	0.328	0.239	-0.361	-0.030	0.004
-1.040	0.443	0.021	-0.309	-0.071	0.000
-1.040	0.443	0.043	-0.343	-0.068	0.001
-1.040	0.443	0.076	-0.362	-0.061	0.003
-1.040	0.443	0.108	-0.381	-0.048	0.004
-1.040	0.443	0.141	-0.397	-0.038	0.004
-1.040	0.443	0.174	-0.378	-0.032	0.004
-1.040	0.443	0.207	-0.393	-0.026	0.004
-1.040	0.443	0.239	-0.385	-0.009	0.003
-1.040	0.557	0.021	-0.389	-0.060	-0.001
-1.040	0.557	0.043	-0.403	-0.049	-0.001
-1.040	0.557	0.076	-0.396	-0.035	0.000
-1.040	0.557	0.108	-0.393	-0.028	0.002
-1.040	0.557	0.141	-0.397	-0.016	0.003
-1.040	0.557	0.174	-0.388	-0.008	0.004
-1.040	0.557	0.207	-0.362	-0.010	0.004
-1.040	0.557	0.239	-0.342	-0.023	0.003
-1.040	0.672	0.021	-0.367	-0.064	-0.001
-1.040	0.672	0.043	-0.398	-0.056	-0.002
-1.040	0.672	0.076	-0.413	-0.048	-0.001
-1.040	0.672	0.108	-0.404	-0.041	0.001
-1.040	0.672	0.141	-0.396	-0.030	0.002
-1.040	0.672	0.174	-0.393	-0.021	0.003
-1.040	0.672	0.207	-0.381	-0.005	0.003
-1.040	0.672	0.239	-0.363	0.002	0.003
-1.040	0.787	0.021	-0.286	-0.013	-0.001
-1.040	0.787	0.043	-0.366	-0.011	-0.002
-1.040	0.787	0.076	-0.394	-0.010	-0.003
-1.040	0.787	0.108	-0.382	-0.013	-0.001
-1.040	0.787	0.141	-0.396	-0.010	0.001
-1.040	0.787	0.174	-0.364	-0.003	0.003
-1.040	0.787	0.207	-0.340	-0.012	0.003
-1.040	0.787	0.239	-0.333	-0.014	0.002
-1.040	0.902	0.021	-0.286	-0.013	-0.002
-1.040	0.902	0.043	-0.366	-0.011	-0.003
-1.040	0.902	0.076	-0.394	-0.010	-0.005
-1.040	0.902	0.108	-0.382	-0.013	-0.004
-1.040	0.902	0.141	-0.396	-0.010	-0.002
-1.040	0.902	0.174	-0.364	-0.003	0.002
-1.040	0.902	0.207	-0.340	-0.012	0.003
-1.040	0.902	0.239	-0.333	-0.014	0.002
-1.040	0.984	0.021	-0.135	0.007	0.000
-1.040	0.984	0.043	-0.173	0.005	-0.002
-1.040	0.984	0.076	-0.195	-0.002	-0.007
-1.040	0.984	0.108	-0.223	-0.001	-0.009
-1.040	0.984	0.141	-0.250	-0.001	-0.007
-1.040	0.984	0.174	-0.248	0.004	-0.003
-1.040	0.984	0.207	-0.232	-0.023	0.000
-1.040	0.984	0.239	-0.222	-0.001	0.001

Table 9.7 Velocity data for dividing flows in open channels (Q_r = 0.409, continued)

X/B	Y/B	Z/B	U (m/s)	V (m/s)	W (m/s)
-1.700	0.016	0.021	-0.339	0.022	-0.016
-1.700	0.016	0.043	-0.386	0.030	-0.024
-1.700	0.016	0.076	-0.386	0.013	-0.034
-1.700	0.016	0.108	-0.390	0.027	-0.030
-1.700	0.016	0.141	-0.400	-0.005	-0.020
-1.700	0.016	0.174	-0.377	0.019	-0.009
-1.700	0.016	0.207	-0.427	0.009	0.001
-1.700	0.016	0.239	-0.396	-0.006	0.006
-1.700	0.098	0.021	-0.349	0.058	-0.007
-1.700	0.098	0.043	-0.366	0.040	-0.010
-1.700	0.098	0.076	-0.362	0.016	-0.018
-1.700	0.098	0.108	-0.375	0.010	-0.018
-1.700	0.098	0.141	-0.375	0.005	-0.015
-1.700	0.098	0.174	-0.369	0.004	-0.009
-1.700	0.098	0.207	-0.368	0.006	-0.004
-1.700	0.098	0.239	-0.343	0.019	-0.003
-1.700	0.213	0.021	-0.257	0.086	-0.002
-1.700	0.213	0.043	-0.272	0.043	-0.004
-1.700	0.213	0.076	-0.307	-0.010	-0.006
-1.700	0.213	0.108	-0.314	-0.018	-0.007
-1.700	0.213	0.141	-0.359	-0.015	-0.007
-1.700	0.213	0.174	-0.370	-0.005	-0.005
-1.700	0.213	0.207	-0.359	0.001	-0.003
-1.700	0.213	0.239	-0.327	0.006	-0.002
-1.700	0.328	0.021	-0.250	0.025	0.001
-1.700	0.328	0.043	-0.266	-0.007	0.001
-1.700	0.328	0.076	-0.288	-0.029	0.001
-1.700	0.328	0.108	-0.331	-0.029	0.001
-1.700	0.328	0.141	-0.347	-0.026	0.000
-1.700	0.328	0.174	-0.360	-0.020	-0.001

X/B	Y/B	Z/B	U (m/s)	V (m/s)	W (m/s)
-1.700	0.328	0.207	-0.335	-0.010	-0.001
-1.700	0.328	0.239	-0.321	-0.006	-0.001
-1.700	0.443	0.021	-0.266	-0.009	0.001
-1.700	0.443	0.043	-0.326	-0.017	0.002
-1.700	0.443	0.076	-0.345	-0.036	0.001
-1.700	0.443	0.108	-0.368	-0.018	0.000
-1.700	0.443	0.141	-0.361	-0.011	0.000
-1.700	0.443	0.174	-0.357	-0.003	-0.001
-1.700	0.443	0.207	-0.358	-0.007	-0.001
-1.700	0.443	0.239	-0.335	0.003	-0.001
-1.700	0.557	0.021	-0.325	-0.022	0.000
-1.700	0.557	0.043	-0.347	-0.023	0.000
-1.700	0.557	0.076	-0.365	-0.012	-0.001
-1.700	0.557	0.108	-0.376	-0.013	-0.002
-1.700	0.557	0.141	-0.386	-0.009	-0.002
-1.700	0.557	0.174	-0.373	0.001	-0.002
-1.700	0.557	0.207	-0.354	0.009	-0.001
-1.700	0.557	0.239	-0.336	0.004	0.000
-1.700	0.672	0.021	-0.310	-0.023	0.000
-1.700	0.672	0.043	-0.353	-0.015	0.000
-1.700	0.672	0.076	-0.362	-0.007	-0.002
-1.700	0.672	0.108	-0.376	-0.002	-0.003
-1.700	0.672	0.141	-0.373	0.002	-0.004
-1.700	0.672	0.174	-0.369	0.004	-0.003
-1.700	0.672	0.207	-0.358	0.006	-0.002
-1.700	0.672	0.239	-0.332	0.005	0.000
-1.700	0.787	0.021	-0.315	-0.006	0.000
-1.700	0.787	0.043	-0.353	-0.006	-0.001
-1.700	0.787	0.076	-0.370	-0.002	-0.003
-1.700	0.787	0.108	-0.383	0.004	-0.004

Table 9.7 Velocity data for dividing flows in open channels (Q_r = 0.409, continued)

X/B	Y/B	Z/B	U (m/s)	V (m/s)	W (m/s)
0.970	0.016	0.021	-0.522	0.012	0.000
0.970	0.016	0.043	-0.518	0.016	0.000
0.970	0.016	0.076	-0.571	0.023	0.000
0.970	0.016	0.108	-0.621	0.037	0.000
0.970	0.016	0.141	-0.614	-0.005	0.000
0.970	0.016	0.174	-0.527	0.006	0.000
0.970	0.016	0.207	-0.532	0.016	0.000
0.970	0.016	0.239	-0.531	-0.012	0.000
0.970	0.098	0.021	-0.574	0.044	0.000
0.970	0.098	0.043	-0.624	0.038	0.000
0.970	0.098	0.076	-0.642	0.038	0.000
0.970	0.098	0.108	-0.633	0.027	0.000
0.970	0.098	0.141	-0.637	0.021	0.000
0.970	0.098	0.174	-0.630	0.016	0.000
0.970	0.098	0.207	-0.593	0.005	0.000
0.970	0.098	0.239	-0.535	0.011	0.000
0.970	0.213	0.021	-0.653	0.055	0.000
0.970	0.213	0.043	-0.684	0.034	0.000
0.970	0.213	0.076	-0.677	0.023	0.000
0.970	0.213	0.108	-0.685	0.003	0.000
0.970	0.213	0.141	-0.664	-0.007	0.000
0.970	0.213	0.174	-0.664	-0.009	0.000
0.970	0.213	0.207	-0.600	-0.014	0.000
0.970	0.213	0.239	-0.596	-0.010	0.000
0.970	0.328	0.021	-0.632	0.049	0.000
0.970	0.328	0.043	-0.637	0.036	0.000
0.970	0.328	0.076	-0.632	0.021	0.000
0.970	0.328	0.108	-0.680	0.027	0.000
0.970	0.328	0.141	-0.661	0.015	0.000
0.970	0.328	0.174	-0.642	0.010	0.000

X/B	Y/B	Z/B	U (m/s)	V (m/s)	W (m/s)
-1.700	0.787	0.141	-0.352	0.002	-0.005
-1.700	0.787	0.174	-0.333	0.012	-0.004
-1.700	0.787	0.207	-0.307	-0.003	-0.003
-1.700	0.787	0.239	-0.283	-0.005	0.000
-1.700	0.902	0.021	-0.290	-0.001	0.000
-1.700	0.902	0.043	-0.299	0.005	-0.001
-1.700	0.902	0.076	-0.320	0.006	-0.002
-1.700	0.902	0.108	-0.339	0.005	-0.003
-1.700	0.902	0.141	-0.320	0.009	-0.004
-1.700	0.902	0.174	-0.310	0.007	-0.004
-1.700	0.902	0.207	-0.281	-0.006	-0.003
-1.700	0.902	0.239	-0.290	-0.012	0.000
-1.700	0.984	0.021	-0.177	0.014	0.000
-1.700	0.984	0.043	-0.198	0.010	0.001
-1.700	0.984	0.076	-0.194	0.003	0.001
-1.700	0.984	0.108	-0.195	0.004	0.000
-1.700	0.984	0.141	-0.216	0.003	-0.002
-1.700	0.984	0.174	-0.178	0.005	-0.003
-1.700	0.984	0.207	-0.182	-0.003	-0.003
-1.700	0.984	0.239	-0.162	-0.003	0.000
-3.000	0.033	0.021	-0.280	0.014	-0.003
-3.000	0.033	0.043	-0.305	0.010	-0.006
-3.000	0.033	0.076	-0.327	0.003	-0.011
-3.000	0.033	0.108	-0.320	0.004	-0.011
-3.000	0.033	0.141	-0.328	0.003	-0.008
-3.000	0.033	0.174	-0.330	0.005	-0.004
-3.000	0.033	0.207	-0.327	-0.003	0.000
-3.000	0.033	0.239	-0.317	-0.003	0.000
-3.000	0.098	0.021	-0.376	0.021	-0.003
-3.000	0.098	0.043	-0.368	0.022	-0.004

Table 9.7 Velocity data for dividing flows in open channels ($Q_r = 0.409$, continued)

X/B	Y/B	Z/B	U (m/s)	V (m/s)	W (m/s)
-3.000	0.098	0.076	-0.368	0.012	-0.007
-3.000	0.098	0.108	-0.364	0.006	-0.008
-3.000	0.098	0.141	-0.377	0.002	-0.007
-3.000	0.098	0.174	-0.364	0.004	-0.005
-3.000	0.098	0.207	-0.375	0.007	-0.003
-3.000	0.098	0.239	-0.351	0.000	-0.002
-3.000	0.213	0.021	-0.334	0.038	-0.001
-3.000	0.213	0.043	-0.325	0.025	-0.002
-3.000	0.213	0.076	-0.337	0.016	-0.004
-3.000	0.213	0.108	-0.323	-0.002	-0.005
-3.000	0.213	0.141	-0.358	-0.002	-0.005
-3.000	0.213	0.174	-0.341	-0.008	-0.004
-3.000	0.213	0.207	-0.346	-0.008	-0.002
-3.000	0.213	0.239	-0.322	-0.001	-0.002
-3.000	0.328	0.021	-0.306	0.050	0.000
-3.000	0.328	0.043	-0.293	0.035	0.000
-3.000	0.328	0.076	-0.312	0.012	-0.001
-3.000	0.328	0.108	-0.326	-0.004	-0.001
-3.000	0.328	0.141	-0.348	-0.005	-0.001
-3.000	0.328	0.174	-0.346	-0.006	-0.001
-3.000	0.328	0.207	-0.333	-0.010	-0.001
-3.000	0.328	0.239	-0.312	-0.006	-0.001
-3.000	0.443	0.021	-0.289	0.019	0.000
-3.000	0.443	0.043	-0.305	0.020	0.001
-3.000	0.443	0.076	-0.327	0.008	0.001
-3.000	0.443	0.108	-0.324	0.002	0.000
-3.000	0.443	0.141	-0.356	0.008	0.000
-3.000	0.443	0.174	-0.357	0.005	0.000
-3.000	0.443	0.207	-0.340	0.004	-0.001
-3.000	0.443	0.239	-0.319	0.004	-0.001

X/B	Y/B	Z/B	U (m/s)	V (m/s)	W (m/s)
-3.000	0.557	0.021	-0.309	0.007	0.001
-3.000	0.557	0.043	-0.330	0.006	0.001
-3.000	0.557	0.076	-0.362	0.003	0.001
-3.000	0.557	0.108	-0.344	0.010	0.001
-3.000	0.557	0.141	-0.364	0.011	0.000
-3.000	0.557	0.174	-0.363	0.010	0.000
-3.000	0.557	0.207	-0.363	0.010	0.000
-3.000	0.557	0.239	-0.363	0.010	-0.001
-3.000	0.672	0.021	-0.315	-0.001	0.001
-3.000	0.672	0.043	-0.350	-0.004	0.001
-3.000	0.672	0.076	-0.366	0.004	0.001
-3.000	0.672	0.108	-0.370	0.002	0.000
-3.000	0.672	0.141	-0.373	0.006	0.000
-3.000	0.672	0.174	-0.361	0.009	0.000
-3.000	0.672	0.207	-0.336	0.004	0.000
-3.000	0.672	0.239	-0.327	-0.005	0.000
-3.000	0.787	0.021	-0.298	-0.003	0.000
-3.000	0.787	0.043	-0.330	0.005	0.001
-3.000	0.787	0.076	-0.354	0.008	0.001
-3.000	0.787	0.108	-0.341	0.014	0.000
-3.000	0.787	0.141	-0.335	0.018	0.000
-3.000	0.787	0.174	-0.328	0.009	0.000
-3.000	0.787	0.207	-0.313	-0.003	0.000
-3.000	0.787	0.239	-0.296	-0.008	0.000
-3.000	0.902	0.021	-0.272	0.003	0.001
-3.000	0.902	0.043	-0.297	0.012	0.001
-3.000	0.902	0.076	-0.313	0.010	0.001
-3.000	0.902	0.108	-0.306	0.010	0.001
-3.000	0.902	0.141	-0.303	0.006	0.001
-3.000	0.902	0.174	-0.279	0.005	0.001

Table 9.7 Velocity data for dividing flows in open channels (Q_r = 0.409, continued)

X/B	Y/B	Z/B	U (m/s)	V (m/s)	W (m/s)
-3.000	0.902	0.207	-0.279	-0.005	0.000
-3.000	0.902	0.239	-0.260	-0.007	0.000
-3.000	0.984	0.021	-0.243	0.000	0.000
-3.000	0.984	0.043	-0.202	0.000	0.001
-3.000	0.984	0.076	-0.207	0.000	0.004
-3.000	0.984	0.108	-0.230	-0.002	0.005
-3.000	0.984	0.141	-0.253	0.003	0.005
-3.000	0.984	0.174	-0.222	-0.097	0.004
-3.000	0.984	0.207	-0.210	-0.017	0.002
-3.000	0.984	0.239	-0.213	-0.001	0.001
-0.016	-0.290	0.011	-0.015	0.007	0.006
-0.016	-0.290	0.033	-0.007	0.006	0.008
-0.016	-0.290	0.066	-0.019	-0.029	0.009
-0.016	-0.290	0.098	-0.004	-0.032	0.007
-0.016	-0.290	0.131	-0.011	0.088	0.006
-0.016	-0.290	0.164	-0.002	0.095	0.004
-0.016	-0.290	0.197	-0.007	0.021	0.002
-0.098	-0.290	0.011	-0.006	0.028	0.003
-0.098	-0.290	0.033	0.004	0.040	0.004
-0.098	-0.290	0.066	0.006	0.030	0.005
-0.098	-0.290	0.098	0.023	0.062	0.004
-0.098	-0.290	0.131	0.007	0.091	0.004
-0.098	-0.290	0.164	0.028	0.057	0.003
-0.098	-0.290	0.197	-0.003	0.029	0.002
-0.213	-0.290	0.011	0.014	0.010	0.002
-0.213	-0.290	0.033	0.039	0.067	0.002
-0.213	-0.290	0.066	0.031	0.046	0.003
-0.213	-0.290	0.098	0.054	0.075	0.003
-0.213	-0.290	0.131	0.052	0.089	0.002
-0.213	-0.290	0.164	0.066	0.104	0.002

X/B	Y/B	Z/B	U (m/s)	V (m/s)	W (m/s)
-0.213	-0.290	0.197	0.025	0.077	0.001
-0.328	-0.290	0.011	0.040	-0.046	0.002
-0.328	-0.290	0.033	0.079	0.013	0.003
-0.328	-0.290	0.066	0.075	0.047	0.004
-0.328	-0.290	0.098	0.063	0.075	0.003
-0.328	-0.290	0.131	0.085	0.075	0.003
-0.328	-0.290	0.164	0.055	0.089	0.001
-0.328	-0.290	0.197	0.031	0.042	0.000
-0.443	-0.290	0.011	0.085	-0.146	0.006
-0.443	-0.290	0.033	0.050	-0.099	0.007
-0.443	-0.290	0.066	0.076	-0.057	0.010
-0.443	-0.290	0.098	0.077	0.008	0.009
-0.443	-0.290	0.131	0.081	-0.006	0.007
-0.443	-0.290	0.164	0.062	0.054	0.004
-0.443	-0.290	0.197	0.025	0.008	0.000
-0.557	-0.290	0.011	0.239	-0.399	0.017
-0.557	-0.290	0.033	0.240	-0.331	0.024
-0.557	-0.290	0.066	0.231	-0.331	0.029
-0.557	-0.290	0.098	0.221	-0.322	0.026
-0.557	-0.290	0.131	0.185	-0.287	0.019
-0.557	-0.290	0.164	0.168	-0.276	0.010
-0.557	-0.290	0.197	0.108	-0.172	-0.001
-0.672	-0.290	0.011	0.190	-0.465	0.026
-0.672	-0.290	0.033	0.299	-0.474	0.037
-0.672	-0.290	0.066	0.335	-0.471	0.041
-0.672	-0.290	0.098	0.334	-0.467	0.034
-0.672	-0.290	0.131	0.325	-0.458	0.024
-0.672	-0.290	0.164	0.308	-0.451	0.011
-0.672	-0.290	0.197	0.226	-0.361	-0.005
-0.787	-0.290	0.011	-0.104	-0.415	0.000

Table 9.7 Velocity data for dividing flows in open channels (Q_r = 0.409, continued)

X/B	Y/B	Z/B	U (m/s)	V (m/s)	W (m/s)
-0.787	-0.290	0.033	0.161	-0.450	0.006
-0.787	-0.290	0.066	0.357	-0.478	0.018
-0.787	-0.290	0.098	0.340	-0.488	0.015
-0.787	-0.290	0.131	0.284	-0.490	0.009
-0.787	-0.290	0.164	0.238	-0.487	0.000
-0.787	-0.290	0.197	0.184	-0.478	-0.010
-0.902	-0.290	0.011	-0.014	-0.460	-0.024
-0.902	-0.290	0.033	0.148	-0.496	-0.036
-0.902	-0.290	0.066	0.174	-0.495	-0.051
-0.902	-0.290	0.098	0.201	-0.508	-0.049
-0.902	-0.290	0.131	0.172	-0.490	-0.045
-0.902	-0.290	0.164	0.155	-0.509	-0.041
-0.902	-0.290	0.197	0.098	-0.442	-0.036
-0.984	-0.290	0.011	-0.010	-0.459	-0.066
-0.984	-0.290	0.033	0.017	-0.466	-0.095
-0.984	-0.290	0.066	0.043	-0.488	-0.130
-0.984	-0.290	0.098	0.036	-0.499	-0.119
-0.984	-0.290	0.131	0.023	-0.496	-0.093
-0.984	-0.290	0.164	0.048	-0.498	-0.062
-0.984	-0.290	0.197	-0.008	-0.463	-0.040
-0.016	-0.730	0.011	-0.001	0.219	0.001
-0.016	-0.730	0.033	-0.010	0.270	0.001
-0.016	-0.730	0.066	0.000	0.286	0.002
-0.016	-0.730	0.098	0.027	0.266	0.002
-0.016	-0.730	0.131	-0.010	0.272	0.001
-0.016	-0.730	0.164	0.003	0.249	0.001
-0.016	-0.730	0.197	-0.001	0.120	0.000
-0.098	-0.730	0.011	-0.003	0.179	0.000
-0.098	-0.730	0.033	0.026	0.189	0.000
-0.098	-0.730	0.066	0.023	0.215	0.000

X/B	Y/B	Z/B	U (m/s)	V (m/s)	W (m/s)
-0.098	-0.730	0.098	0.007	0.219	0.000
-0.098	-0.730	0.131	0.003	0.193	0.000
-0.098	-0.730	0.164	0.004	0.180	0.000
-0.098	-0.730	0.197	0.010	0.173	0.000
-0.213	-0.730	0.011	0.037	0.111	0.000
-0.213	-0.730	0.033	0.059	0.143	0.000
-0.213	-0.730	0.066	0.059	0.134	0.000
-0.213	-0.730	0.098	0.041	0.143	0.000
-0.213	-0.730	0.131	0.064	0.174	0.000
-0.213	-0.730	0.164	0.036	0.163	0.000
-0.213	-0.730	0.197	0.024	0.116	0.000
-0.328	-0.730	0.011	0.033	-0.013	0.000
-0.328	-0.730	0.033	0.096	-0.017	0.000
-0.328	-0.730	0.066	-0.004	-0.018	0.000
-0.328	-0.730	0.098	0.056	0.031	0.000
-0.328	-0.730	0.131	0.098	0.055	0.000
-0.328	-0.730	0.164	0.075	0.043	0.000
-0.328	-0.730	0.197	0.025	0.048	0.000
-0.443	-0.730	0.011	-0.094	-0.211	0.000
-0.443	-0.730	0.033	-0.044	-0.187	0.000
-0.443	-0.730	0.066	-0.010	-0.135	0.000
-0.443	-0.730	0.098	0.083	-0.072	0.000
-0.443	-0.730	0.131	0.068	0.006	0.000
-0.443	-0.730	0.164	0.052	0.074	0.000
-0.443	-0.730	0.197	0.036	0.041	0.000
-0.557	-0.730	0.011	-0.110	-0.380	0.016
-0.557	-0.730	0.033	-0.049	-0.357	0.023
-0.557	-0.730	0.066	-0.005	-0.303	0.020
-0.557	-0.730	0.098	0.066	-0.196	0.014
-0.557	-0.730	0.131	0.097	-0.146	0.009

Table 9.7 Velocity data for dividing flows in open channels (Q_r = 0.409, continued)

X/B	Y/B	Z/B	U (m/s)	V (m/s)	W (m/s)
-0.557	-0.730	0.164	0.092	-0.127	0.004
-0.557	-0.730	0.197	0.011	-0.084	-0.001
-0.672	-0.730	0.011	-0.171	-0.440	0.009
-0.672	-0.730	0.033	-0.038	-0.416	0.016
-0.672	-0.730	0.066	0.061	-0.394	0.023
-0.672	-0.730	0.098	0.084	-0.351	0.018
-0.672	-0.730	0.131	0.064	-0.356	0.011
-0.672	-0.730	0.164	0.039	-0.360	0.004
-0.672	-0.730	0.197	0.018	-0.318	-0.003
-0.787	-0.730	0.011	-0.110	-0.455	-0.005
-0.787	-0.730	0.033	0.021	-0.458	-0.008
-0.787	-0.730	0.066	0.133	-0.460	-0.005
-0.787	-0.730	0.098	0.138	-0.449	-0.002
-0.787	-0.730	0.131	0.134	-0.454	-0.002
-0.787	-0.730	0.164	0.134	-0.454	-0.003
-0.787	-0.730	0.197	0.134	-0.454	-0.005
-0.902	-0.730	0.011	0.014	-0.496	-0.013
-0.902	-0.730	0.033	0.086	-0.506	-0.020
-0.902	-0.730	0.066	0.000	-0.506	-0.032
-0.902	-0.730	0.098	0.011	-0.491	-0.030
-0.902	-0.730	0.131	0.011	-0.491	-0.023
-0.902	-0.730	0.164	0.011	-0.491	-0.015
-0.902	-0.730	0.197	0.011	-0.491	-0.005
-0.984	-0.730	0.011	0.014	-0.496	-0.031
-0.984	-0.730	0.033	0.017	-0.496	-0.047
-0.984	-0.730	0.066	0.017	-0.496	-0.068
-0.984	-0.730	0.098	-0.049	-0.496	-0.062
-0.984	-0.730	0.131	0.034	-0.496	-0.046
-0.984	-0.730	0.164	-0.041	-0.496	-0.025
-0.984	-0.730	0.197	-0.023	-0.496	-0.003

X/B	Y/B	Z/B	U (m/s)	V (m/s)	W (m/s)
-0.016	-1.250	0.011	-0.009	0.281	0.000
-0.016	-1.250	0.033	0.003	0.251	0.000
-0.016	-1.250	0.066	-0.009	0.284	0.001
-0.016	-1.250	0.098	0.012	0.290	0.001
-0.016	-1.250	0.131	-0.004	0.286	0.001
-0.016	-1.250	0.164	0.003	0.285	0.001
-0.016	-1.250	0.197	-0.004	0.216	0.001
-0.098	-1.250	0.011	-0.062	0.141	0.000
-0.098	-1.250	0.033	-0.040	0.117	0.000
-0.098	-1.250	0.066	-0.042	0.219	-0.001
-0.098	-1.250	0.098	-0.047	0.140	-0.001
-0.098	-1.250	0.131	-0.004	0.232	-0.001
-0.098	-1.250	0.164	0.041	0.184	0.000
-0.098	-1.250	0.197	0.033	0.143	0.001
-0.213	-1.250	0.011	-0.066	0.059	-0.001
-0.213	-1.250	0.033	-0.098	-0.001	-0.001
-0.213	-1.250	0.066	-0.078	0.115	-0.001
-0.213	-1.250	0.098	-0.081	0.080	-0.001
-0.213	-1.250	0.131	-0.025	0.164	-0.001
-0.213	-1.250	0.164	0.036	0.183	0.000
-0.213	-1.250	0.197	-0.011	0.111	0.001
-0.328	-1.250	0.011	-0.151	-0.146	0.002
-0.328	-1.250	0.033	-0.124	-0.131	0.003
-0.328	-1.250	0.066	-0.094	-0.113	0.003
-0.328	-1.250	0.098	0.021	-0.021	0.003
-0.328	-1.250	0.131	-0.003	0.045	0.002
-0.328	-1.250	0.164	-0.015	0.086	0.001
-0.328	-1.250	0.197	0.041	0.112	0.000
-0.443	-1.250	0.011	-0.138	-0.258	0.006
-0.443	-1.250	0.033	-0.124	-0.281	0.007

Table 9.7 Velocity data for dividing flows in open channels ($Q_r = 0.409$, continued)

X/B	Y/B	Z/B	U (m/s)	V (m/s)	W (m/s)
-0.443	-1.250	0.066	-0.076	-0.246	0.007
-0.443	-1.250	0.098	-0.033	-0.129	0.005
-0.443	-1.250	0.131	-0.010	-0.028	0.003
-0.443	-1.250	0.164	-0.004	0.029	0.002
-0.443	-1.250	0.197	0.054	0.098	0.000
-0.557	-1.250	0.011	-0.087	-0.362	0.006
-0.557	-1.250	0.033	-0.081	-0.358	0.010
-0.557	-1.250	0.066	-0.051	-0.313	0.013
-0.557	-1.250	0.098	-0.037	-0.257	0.008
-0.557	-1.250	0.131	0.012	-0.257	0.004
-0.557	-1.250	0.164	0.021	-0.257	0.002
-0.557	-1.250	0.197	0.002	-0.257	0.000
-0.672	-1.250	0.011	-0.088	-0.429	0.001
-0.672	-1.250	0.033	-0.043	-0.384	0.001
-0.672	-1.250	0.066	0.002	-0.356	0.004
-0.672	-1.250	0.098	0.032	-0.330	0.003
-0.672	-1.250	0.131	0.057	-0.337	0.001
-0.672	-1.250	0.164	0.017	-0.340	0.000
-0.672	-1.250	0.197	0.017	-0.340	0.000
-0.787	-1.250	0.011	0.003	-0.476	-0.004
-0.787	-1.250	0.033	0.018	-0.448	-0.006
-0.787	-1.250	0.066	0.051	-0.428	-0.008
-0.787	-1.250	0.098	0.062	-0.438	-0.006
-0.787	-1.250	0.131	0.090	-0.440	-0.004
-0.787	-1.250	0.164	0.067	-0.361	-0.002
-0.787	-1.250	0.197	-0.015	-0.361	-0.001
-0.902	-1.250	0.011	0.061	-0.492	-0.007
-0.902	-1.250	0.033	0.061	-0.492	-0.011
-0.902	-1.250	0.066	0.061	-0.492	-0.019
-0.902	-1.250	0.098	0.061	-0.492	-0.018

X/B	Y/B	Z/B	U (m/s)	V (m/s)	W (m/s)
-0.902	-1.250	0.131	0.061	-0.492	-0.014
-0.902	-1.250	0.164	0.061	-0.492	-0.009
-0.902	-1.250	0.197	0.061	-0.492	-0.001
-0.984	-1.250	0.011	-0.014	-0.492	-0.016
-0.984	-1.250	0.033	-0.006	-0.492	-0.025
-0.984	-1.250	0.066	-0.013	-0.492	-0.039
-0.984	-1.250	0.098	-0.012	-0.492	-0.038
-0.984	-1.250	0.131	0.018	-0.492	-0.030
-0.984	-1.250	0.164	-0.006	-0.492	-0.017
-0.984	-1.250	0.197	-0.002	-0.492	-0.002
-0.016	-1.620	0.011	-0.014	0.196	0.000
-0.016	-1.620	0.033	-0.006	0.126	0.000
-0.016	-1.620	0.066	-0.013	0.210	0.001
-0.016	-1.620	0.098	-0.012	0.230	0.001
-0.016	-1.620	0.131	0.018	0.208	0.001
-0.016	-1.620	0.164	-0.006	0.258	0.001
-0.016	-1.620	0.197	-0.002	0.198	0.000
-0.098	-1.620	0.011	-0.043	0.117	0.000
-0.098	-1.620	0.033	-0.043	0.155	0.000
-0.098	-1.620	0.066	-0.021	0.194	-0.001
-0.098	-1.620	0.098	-0.023	0.153	-0.002
-0.098	-1.620	0.131	-0.052	0.165	-0.002
-0.098	-1.620	0.164	-0.014	0.182	-0.001
-0.098	-1.620	0.197	0.006	0.140	0.000
-0.213	-1.620	0.011	-0.104	0.015	-0.001
-0.213	-1.620	0.033	-0.152	-0.054	-0.001
-0.213	-1.620	0.066	-0.034	0.008	-0.002
-0.213	-1.620	0.098	-0.066	0.064	-0.002
-0.213	-1.620	0.131	-0.034	0.071	-0.002
-0.213	-1.620	0.164	0.052	0.174	-0.001

Table 9.7 Velocity data for dividing flows in open channels (Q_r = 0.409, continued)

X/B	Y/B	Z/B	U (m/s)	V (m/s)	W (m/s)
-0.213	-1.620	0.197	0.025	0.101	0.000
-0.328	-1.620	0.011	-0.111	-0.169	0.003
-0.328	-1.620	0.033	-0.125	-0.118	0.004
-0.328	-1.620	0.066	-0.126	-0.139	0.004
-0.328	-1.620	0.098	-0.030	-0.054	0.004
-0.328	-1.620	0.131	-0.013	-0.046	0.003
-0.328	-1.620	0.164	0.058	0.075	0.002
-0.328	-1.620	0.197	0.029	0.088	0.000
-0.443	-1.620	0.011	-0.095	-0.288	0.006
-0.443	-1.620	0.033	-0.088	-0.254	0.009
-0.443	-1.620	0.066	-0.079	-0.264	0.010
-0.443	-1.620	0.098	-0.009	-0.122	0.008
-0.443	-1.620	0.131	0.021	-0.095	0.005
-0.443	-1.620	0.164	0.025	-0.008	0.003
-0.443	-1.620	0.197	0.038	0.049	0.000
-0.557	-1.620	0.011	-0.076	-0.380	0.003
-0.557	-1.620	0.033	-0.046	-0.313	0.006
-0.557	-1.620	0.066	-0.033	-0.300	0.009
-0.557	-1.620	0.098	-0.027	-0.278	0.007
-0.557	-1.620	0.131	0.015	-0.219	0.004
-0.557	-1.620	0.164	0.018	-0.176	0.002
-0.557	-1.620	0.197	0.020	-0.105	0.000
-0.672	-1.620	0.011	-0.051	-0.410	0.000
-0.672	-1.620	0.033	-0.031	-0.401	0.000
-0.672	-1.620	0.066	0.017	-0.356	0.002
-0.672	-1.620	0.098	0.015	-0.343	0.001
-0.672	-1.620	0.131	0.012	-0.327	0.001
-0.672	-1.620	0.164	0.019	-0.341	0.000
-0.672	-1.620	0.197	0.014	-0.472	0.000
-0.787	-1.620	0.011	0.006	-0.472	-0.003

X/B	Y/B	Z/B	U (m/s)	V (m/s)	W (m/s)
-0.787	-1.620	0.033	0.044	-0.452	-0.005
-0.787	-1.620	0.066	0.049	-0.452	-0.007
-0.787	-1.620	0.098	0.072	-0.432	-0.005
-0.787	-1.620	0.131	0.078	-0.445	-0.003
-0.787	-1.620	0.164	0.044	-0.429	-0.002
-0.787	-1.620	0.197	0.044	-0.422	0.000
-0.902	-1.620	0.011	0.001	-0.505	-0.006
-0.902	-1.620	0.033	0.058	-0.505	-0.009
-0.902	-1.620	0.066	0.058	-0.505	-0.014
-0.902	-1.620	0.098	0.027	-0.466	-0.014
-0.902	-1.620	0.131	0.088	-0.479	-0.011
-0.902	-1.620	0.164	-0.042	-0.479	-0.006
-0.902	-1.620	0.197	0.004	-0.479	0.000
-0.984	-1.620	0.011	-0.014	-0.505	-0.012
-0.984	-1.620	0.033	-0.006	-0.505	-0.019
-0.984	-1.620	0.066	-0.013	-0.505	-0.031
-0.984	-1.620	0.098	-0.012	-0.466	-0.031
-0.984	-1.620	0.131	0.018	-0.479	-0.025
-0.984	-1.620	0.164	-0.006	-0.479	-0.013
-0.984	-1.620	0.197	-0.002	-0.479	0.000
-0.016	-2.500	0.011	0.029	0.213	-0.001
-0.016	-2.500	0.033	0.004	0.087	0.000
-0.016	-2.500	0.066	0.004	0.087	0.002
-0.016	-2.500	0.098	0.001	0.144	0.004
-0.016	-2.500	0.131	0.008	0.046	0.004
-0.016	-2.500	0.164	0.008	0.046	0.002
-0.016	-2.500	0.011	0.008	0.046	-0.001
-0.098	-2.500	0.011	-0.037	0.114	0.001
-0.098	-2.500	0.033	0.005	0.123	0.002
-0.098	-2.500	0.066	-0.020	0.111	0.002

Table 9.7 Velocity data for dividing flows in open channels (Q_r = 0.409, continued)

X/B	Y/B	Z/B	U (m/s)	V (m/s)	W (m/s)
-0.098	-2.500	0.098	0.001	0.130	0.002
-0.098	-2.500	0.131	0.007	0.163	0.001
-0.098	-2.500	0.164	0.048	0.226	0.001
-0.098	-2.500	0.197	-0.012	0.195	-0.001
-0.213	-2.500	0.011	0.010	0.101	0.000
-0.213	-2.500	0.033	0.032	0.105	0.000
-0.213	-2.500	0.066	0.032	0.105	-0.001
-0.213	-2.500	0.098	0.017	0.206	-0.001
-0.213	-2.500	0.131	0.017	0.206	-0.001
-0.213	-2.500	0.164	0.011	0.082	-0.001
-0.213	-2.500	0.197	0.002	0.077	0.000
-0.328	-2.500	0.011	-0.026	-0.093	0.003
-0.328	-2.500	0.033	-0.044	0.068	0.004
-0.328	-2.500	0.066	-0.044	0.068	0.005
-0.328	-2.500	0.098	-0.044	0.068	0.004
-0.328	-2.500	0.131	0.024	0.077	0.003
-0.328	-2.500	0.164	-0.025	-0.034	0.001
-0.328	-2.500	0.197	-0.020	0.141	0.000
-0.443	-2.500	0.011	-0.047	-0.124	0.003
-0.443	-2.500	0.033	-0.055	-0.160	0.005
-0.443	-2.500	0.066	-0.019	-0.133	0.008
-0.443	-2.500	0.098	-0.013	-0.126	0.007
-0.443	-2.500	0.131	-0.004	-0.041	0.005
-0.443	-2.500	0.164	0.042	0.001	0.003
-0.443	-2.500	0.197	-0.003	0.039	0.001
-0.557	-2.500	0.011	-0.020	-0.187	0.001
-0.557	-2.500	0.033	-0.028	-0.269	0.003
-0.557	-2.500	0.066	-0.036	-0.254	0.005
-0.557	-2.500	0.098	-0.045	-0.263	0.005
-0.557	-2.500	0.131	-0.023	-0.239	0.005

X/B	Y/B	Z/B	U (m/s)	V (m/s)	W (m/s)
-0.557	-2.500	0.164	0.001	-0.211	0.003
-0.557	-2.500	0.197	0.024	-0.215	0.002
-0.672	-2.500	0.011	-0.032	-0.368	0.000
-0.672	-2.500	0.033	-0.040	-0.349	0.001
-0.672	-2.500	0.066	-0.013	-0.311	0.002
-0.672	-2.500	0.098	-0.017	-0.331	0.003
-0.672	-2.500	0.131	0.001	-0.312	0.003
-0.672	-2.500	0.164	-0.009	-0.296	0.003
-0.672	-2.500	0.197	0.005	-0.280	0.003
-0.787	-2.500	0.011	0.009	-0.423	-0.001
-0.787	-2.500	0.033	-0.003	-0.424	-0.001
-0.787	-2.500	0.066	0.003	-0.433	0.000
-0.787	-2.500	0.098	0.020	-0.445	0.000
-0.787	-2.500	0.131	0.021	-0.377	0.001
-0.787	-2.500	0.164	0.030	-0.377	0.002
-0.787	-2.500	0.197	0.003	-0.377	0.003
-0.902	-2.500	0.011	0.072	-0.423	-0.002
-0.902	-2.500	0.033	0.019	-0.476	-0.004
-0.902	-2.500	0.066	0.049	-0.473	-0.005
-0.902	-2.500	0.098	0.059	-0.494	-0.005
-0.902	-2.500	0.131	0.049	-0.421	-0.003
-0.902	-2.500	0.164	-0.015	-0.381	0.000
-0.902	-2.500	0.197	0.013	-0.381	0.004
-0.984	-2.500	0.011	0.012	-0.459	-0.004
-0.984	-2.500	0.033	0.014	-0.431	-0.008
-0.984	-2.500	0.066	0.001	-0.466	-0.015
-0.984	-2.500	0.098	0.039	-0.466	-0.016
-0.984	-2.500	0.131	0.043	-0.466	-0.012
-0.984	-2.500	0.164	0.025	-0.466	-0.006
-0.984	-2.500	0.197	0.034	-0.466	0.004

Table 9.8 Water surface profiles for dividing flows in open channels ($Q_r = 0.672$)

X/B	Y/B	Z/B
0.926	0.016	0.276
0.926	0.098	0.277
0.926	0.213	0.275
0.926	0.328	0.273
0.926	0.443	0.273
0.926	0.557	0.274
0.926	0.672	0.276
0.926	0.787	0.275
0.926	0.902	0.274
0.926	0.984	0.275
0.221	0.016	0.271
0.221	0.098	0.270
0.221	0.213	0.270
0.221	0.328	0.271
0.221	0.443	0.273
0.221	0.557	0.274
0.221	0.672	0.275
0.221	0.787	0.275
0.221	0.902	0.275
0.221	0.984	0.276
0.090	0.016	0.266
0.090	0.098	0.267
0.090	0.213	0.269
0.090	0.328	0.270
0.090	0.443	0.273
0.090	0.557	0.276
0.090	0.672	0.275
0.090	0.787	0.277
0.090	0.902	0.278
0.090	0.984	0.280

X/B	Y/B	Z/B
-0.041	0.016	0.251
-0.041	0.098	0.262
-0.041	0.213	0.267
-0.041	0.328	0.272
-0.041	0.443	0.275
-0.041	0.557	0.276
-0.041	0.672	0.278
-0.041	0.787	0.279
-0.041	0.902	0.280
-0.041	0.984	0.279
-0.134	0.016	0.244
-0.134	0.098	0.259
-0.134	0.213	0.267
-0.134	0.328	0.269
-0.134	0.443	0.275
-0.134	0.557	0.277
-0.134	0.672	0.278
-0.134	0.787	0.279
-0.134	0.902	0.282
-0.134	0.984	0.280
-0.287	0.016	0.259
-0.287	0.098	0.264
-0.287	0.213	0.270
-0.287	0.328	0.274
-0.287	0.443	0.275
-0.287	0.557	0.280
-0.287	0.672	0.281
-0.287	0.787	0.282
-0.287	0.902	0.283
-0.287	0.984	0.284

X/B	Y/B	Z/B
-0.402	0.016	0.267
-0.402	0.098	0.271
-0.402	0.213	0.275
-0.402	0.328	0.277
-0.402	0.443	0.279
-0.402	0.557	0.281
-0.402	0.672	0.284
-0.402	0.787	0.283
-0.402	0.902	0.285
-0.402	0.984	0.285
-0.541	0.016	0.272
-0.541	0.098	0.275
-0.541	0.213	0.278
-0.541	0.328	0.281
-0.541	0.443	0.281
-0.541	0.557	0.283
-0.541	0.672	0.285
-0.541	0.787	0.286
-0.541	0.902	0.285
-0.541	0.984	0.284
-0.648	0.016	0.278
-0.648	0.098	0.279
-0.648	0.213	0.281
-0.648	0.328	0.282
-0.648	0.443	0.285
-0.648	0.557	0.285
-0.648	0.672	0.285
-0.648	0.787	0.286
-0.648	0.902	0.285
-0.648	0.984	0.285

X/B	Y/B	Z/B
-0.795	0.016	0.284
-0.795	0.098	0.285
-0.795	0.213	0.286
-0.795	0.328	0.286
-0.795	0.443	0.286
-0.795	0.557	0.285
-0.795	0.672	0.286
-0.795	0.787	0.286
-0.795	0.902	0.287
-0.795	0.984	0.287
-0.902	0.016	0.288
-0.902	0.098	0.288
-0.902	0.213	0.289
-0.902	0.328	0.288
-0.902	0.443	0.287
-0.902	0.557	0.286
-0.902	0.672	0.285
-0.902	0.787	0.286
-0.902	0.902	0.286
-0.902	0.984	0.287
-1.041	0.016	0.295
-1.041	0.098	0.290
-1.041	0.213	0.289
-1.041	0.328	0.288
-1.041	0.443	0.289
-1.041	0.557	0.286
-1.041	0.672	0.286
-1.041	0.787	0.286
-1.041	0.902	0.284
-1.041	0.984	0.288

Table 9.8 Water surface profiles for dividing flows in open channels (Q_r = 0.672, continued)

X/B	Y/B	Z/B	X/B	Y/B	Z/B	X/B	Y/B	Z/B	X/B	Y/B	Z/B
-1.131	0.016	0.295	-1.861	0.016	0.287	-3.000	0.016	0.289	-0.016	0.000	0.247
-1.131	0.098	0.291	-1.861	0.098	0.286	-3.000	0.098	0.287	-0.098	0.000	0.246
-1.131	0.213	0.289	-1.861	0.213	0.285	-3.000	0.213	0.288	-0.213	0.000	0.259
-1.131	0.328	0.290	-1.861	0.328	0.283	-3.000	0.328	0.288	-0.328	0.000	0.268
-1.131	0.443	0.290	-1.861	0.443	0.285	-3.000	0.443	0.286	-0.443	0.000	0.271
-1.131	0.557	0.287	-1.861	0.557	0.286	-3.000	0.557	0.288	-0.557	0.000	0.276
-1.131	0.672	0.287	-1.861	0.672	0.284	-3.000	0.672	0.285	-0.672	0.000	0.283
-1.131	0.787	0.285	-1.861	0.787	0.284	-3.000	0.787	0.287	-0.787	0.000	0.286
-1.131	0.902	0.286	-1.861	0.902	0.282	-3.000	0.902	0.287	-0.902	0.000	0.286
-1.131	0.984	0.286	-1.861	0.984	0.284	-3.000	0.984	0.287	-0.984	0.000	0.283
-1.287	0.016	0.289	-2.107	0.016	0.287				-0.016	-0.205	0.254
-1.287	0.098	0.289	-2.107	0.098	0.286				-0.098	-0.205	0.255
-1.287	0.213	0.288	-2.107	0.213	0.287				-0.213	-0.205	0.254
-1.287	0.328	0.287	-2.107	0.328	0.288				-0.328	-0.205	0.258
-1.287	0.443	0.288	-2.107	0.443	0.286				-0.443	-0.205	0.265
-1.287	0.557	0.285	-2.107	0.557	0.283				-0.557	-0.205	0.271
-1.287	0.672	0.283	-2.107	0.672	0.284				-0.672	-0.205	0.277
-1.287	0.787	0.285	-2.107	0.787	0.281				-0.787	-0.205	0.280
-1.287	0.902	0.284	-2.107	0.902	0.284				-0.902	-0.205	0.280
-1.287	0.984	0.283	-2.107	0.984	0.285				-0.984	-0.205	0.284
-1.697	0.016	0.287	-2.623	0.016	0.287				-0.016	-0.287	0.250
-1.697	0.098	0.287	-2.623	0.098	0.287				-0.098	-0.287	0.250
-1.697	0.213	0.285	-2.623	0.213	0.288				-0.213	-0.287	0.251
-1.697	0.328	0.285	-2.623	0.328	0.288				-0.328	-0.287	0.253
-1.697	0.443	0.285	-2.623	0.443	0.287				-0.443	-0.287	0.260
-1.697	0.557	0.285	-2.623	0.557	0.286				-0.557	-0.287	0.266
-1.697	0.672	0.284	-2.623	0.672	0.285				-0.672	-0.287	0.270
-1.697	0.787	0.285	-2.623	0.787	0.286				-0.787	-0.287	0.273
-1.697	0.902	0.284	-2.623	0.902	0.286				-0.902	-0.287	0.273
-1.697	0.984	0.282	-2.623	0.984	0.287				-0.984	-0.287	0.275

Table 9.8 Water surface profiles for dividing flows in open channels (Q_r = 0.672, continued)

X/B	Y/B	Z/B	X/B	Y/B	Z/B	X/B	Y/B	Z/B	X/B	Y/B	Z/B
-0.016	-0.730	0.252	-0.016	-1.025	0.244	-0.016	-1.825	0.248	-0.016	-2.533	0.253
-0.098	-0.730	0.248	-0.098	-1.025	0.240	-0.098	-1.825	0.250	-0.098	-2.533	0.253
-0.213	-0.730	0.249	-0.213	-1.025	0.244	-0.213	-1.825	0.246	-0.213	-2.533	0.254
-0.328	-0.730	0.250	-0.328	-1.025	0.241	-0.328	-1.825	0.251	-0.328	-2.533	0.256
-0.443	-0.730	0.252	-0.443	-1.025	0.247	-0.443	-1.825	0.250	-0.443	-2.533	0.253
-0.557	-0.730	0.254	-0.557	-1.025	0.247	-0.557	-1.825	0.250	-0.557	-2.533	0.254
-0.672	-0.730	0.254	-0.672	-1.025	0.244	-0.672	-1.825	0.249	-0.672	-2.533	0.255
-0.787	-0.730	0.253	-0.787	-1.025	0.246	-0.787	-1.825	0.245	-0.787	-2.533	0.253
-0.902	-0.730	0.253	-0.902	-1.025	0.245	-0.902	-1.825	0.248	-0.902	-2.533	0.252
-0.984	-0.730	0.255	-0.984	-1.025	0.245	-0.984	-1.825	0.249	-0.984	-2.533	0.253
-0.016	-0.811	0.244	-0.016	-1.221	0.244	-0.016	-2.000	0.255	-0.016	-2.738	0.255
-0.098	-0.811	0.244	-0.098	-1.221	0.245	-0.098	-2.000	0.253	-0.098	-2.738	0.252
-0.213	-0.811	0.244	-0.213	-1.221	0.242	-0.213	-2.000	0.252	-0.213	-2.738	0.253
-0.328	-0.811	0.244	-0.328	-1.221	0.243	-0.328	-2.000	0.248	-0.328	-2.738	0.254
-0.443	-0.811	0.245	-0.443	-1.221	0.248	-0.443	-2.000	0.251	-0.443	-2.738	0.255
-0.557	-0.811	0.245	-0.557	-1.221	0.245	-0.557	-2.000	0.247	-0.557	-2.738	0.255
-0.672	-0.811	0.246	-0.672	-1.221	0.245	-0.672	-2.000	0.247	-0.672	-2.738	0.255
-0.787	-0.811	0.249	-0.787	-1.221	0.246	-0.787	-2.000	0.249	-0.787	-2.738	0.255
-0.902	-0.811	0.249	-0.902	-1.221	0.243	-0.902	-2.000	0.247	-0.902	-2.738	0.256
-0.984	-0.811	0.249	-0.984	-1.221	0.245	-0.984	-2.000	0.250	-0.984	-2.738	0.254
-0.016	-0.893	0.244	-0.016	-1.623	0.246	-0.016	-2.131	0.251	-0.016	-3.000	0.255
-0.098	-0.893	0.245	-0.098	-1.623	0.244	-0.098	-2.131	0.248	-0.098	-3.000	0.255
-0.213	-0.893	0.244	-0.213	-1.623	0.245	-0.213	-2.131	0.251	-0.213	-3.000	0.258
-0.328	-0.893	0.243	-0.328	-1.623	0.250	-0.328	-2.131	0.248	-0.328	-3.000	0.257
-0.443	-0.893	0.247	-0.443	-1.623	0.248	-0.443	-2.131	0.250	-0.443	-3.000	0.253
-0.557	-0.893	0.249	-0.557	-1.623	0.248	-0.557	-2.131	0.253	-0.557	-3.000	0.255
-0.672	-0.893	0.248	-0.672	-1.623	0.247	-0.672	-2.131	0.249	-0.672	-3.000	0.255
-0.787	-0.893	0.247	-0.787	-1.623	0.243	-0.787	-2.131	0.249	-0.787	-3.000	0.258
-0.902	-0.893	0.247	-0.902	-1.623	0.241	-0.902	-2.131	0.248	-0.902	-3.000	0.258
-0.984	-0.893	0.248	-0.984	-1.623	0.245	-0.984	-2.131	0.251	-0.984	-3.000	0.258

Table 9.9 Velocity data for dividing flows in open channels ($Q_r = 0.672$)

X/B	Y/B	Z/B	U (m/s)	V (m/s)	W (m/s)
0.970	0.098	0.007	-0.424	0.006	0.000
0.970	0.098	0.033	-0.494	0.035	0.000
0.970	0.098	0.109	-0.506	0.017	0.000
0.970	0.098	0.197	-0.481	0.002	0.000
0.970	0.098	0.262	-0.481	0.002	-0.001
0.970	0.213	0.007	-0.469	0.005	0.000
0.970	0.213	0.033	-0.500	0.066	0.000
0.970	0.213	0.109	-0.506	0.001	0.000
0.970	0.213	0.197	-0.506	-0.011	0.000
0.970	0.213	0.262	-0.506	-0.011	-0.001
0.970	0.442	0.007	-0.411	-0.001	0.000
0.970	0.442	0.033	-0.489	0.075	0.000
0.970	0.442	0.109	-0.517	0.054	0.000
0.970	0.442	0.197	-0.528	-0.036	0.000
0.970	0.442	0.262	-0.528	-0.036	0.000
0.970	0.672	0.007	-0.428	-0.005	0.000
0.970	0.672	0.033	-0.480	0.026	0.000
0.970	0.672	0.109	-0.524	0.038	0.000
0.970	0.672	0.197	-0.526	0.053	0.000
0.970	0.672	0.262	-0.526	0.053	0.000
0.970	0.902	0.007	-0.416	0.011	0.000
0.970	0.902	0.033	-0.570	0.031	0.000
0.970	0.902	0.109	-0.580	0.044	0.000
0.970	0.902	0.197	-0.520	0.054	0.000
0.970	0.902	0.262	-0.520	0.054	0.000
0.220	0.016	0.007	-0.416	0.000	0.000
0.220	0.016	0.033	-0.465	0.015	0.000
0.220	0.016	0.109	-0.508	0.013	-0.004
0.220	0.016	0.197	-0.505	0.017	-0.007
0.220	0.016	0.262	-0.505	0.017	-0.007

X/B	Y/B	Z/B	U (m/s)	V (m/s)	W (m/s)
0.220	0.213	0.007	-0.484	0.027	0.000
0.220	0.213	0.033	-0.554	0.028	0.000
0.220	0.213	0.109	-0.549	-0.005	-0.003
0.220	0.213	0.197	-0.524	-0.048	-0.005
0.220	0.213	0.262	-0.524	-0.048	-0.006
0.220	0.442	0.007	-0.412	0.011	0.000
0.220	0.442	0.033	-0.486	0.028	0.000
0.220	0.442	0.109	-0.521	0.004	0.000
0.220	0.442	0.197	-0.521	-0.050	-0.001
0.220	0.442	0.262	-0.521	-0.050	-0.001
0.220	0.672	0.007	-0.453	-0.029	0.000
0.220	0.672	0.033	-0.505	-0.049	0.001
0.220	0.672	0.109	-0.522	-0.019	0.002
0.220	0.672	0.197	-0.510	-0.003	0.002
0.220	0.672	0.262	-0.510	-0.003	0.001
0.220	0.902	0.007	-0.433	0.007	0.002
0.220	0.902	0.033	-0.495	-0.003	0.004
0.220	0.902	0.109	-0.533	0.010	0.008
0.220	0.902	0.197	-0.505	0.022	0.006
0.220	0.902	0.262	-0.505	0.022	0.005
-0.040	0.016	0.011	-0.647	-0.001	0.001
-0.040	0.016	0.033	-0.685	-0.090	0.000
-0.040	0.016	0.098	-0.716	-0.094	-0.016
-0.040	0.016	0.164	-0.707	-0.096	-0.041
-0.040	0.016	0.230	-0.652	-0.108	-0.045
-0.040	0.213	0.011	-0.503	0.001	0.000
-0.040	0.213	0.033	-0.564	-0.045	0.000
-0.040	0.213	0.098	-0.576	-0.058	-0.005
-0.040	0.213	0.164	-0.573	-0.099	-0.012
-0.040	0.213	0.262	-0.300	-0.063	-0.013

Table 9.9 Velocity data for dividing flows in open channels ($Q_r = 0.672$, continued)

X/B	Y/B	Z/B	U (m/s)	V (m/s)	W (m/s)
-0.040	0.442	0.011	-0.201	-0.048	0.001
-0.040	0.442	0.033	-0.430	-0.057	0.001
-0.040	0.442	0.098	-0.507	-0.047	0.001
-0.040	0.442	0.164	-0.380	-0.089	0.001
-0.040	0.442	0.262	-0.373	-0.083	-0.001
-0.040	0.672	0.011	-0.384	-0.071	0.001
-0.040	0.672	0.033	-0.457	-0.076	0.002
-0.040	0.672	0.098	-0.503	-0.060	0.005
-0.040	0.672	0.164	-0.489	-0.043	0.005
-0.040	0.672	0.262	-0.355	-0.034	0.004
-0.040	0.902	0.011	-0.351	-0.031	0.001
-0.040	0.902	0.033	-0.447	-0.028	0.004
-0.040	0.902	0.098	-0.485	-0.024	0.018
-0.040	0.902	0.164	-0.473	-0.011	0.014
-0.040	0.902	0.262	-0.431	-0.022	0.010
-0.290	0.016	0.011	-0.531	-0.051	0.005
-0.290	0.016	0.033	-0.565	-0.279	0.007
-0.290	0.016	0.098	-0.572	-0.322	0.009
-0.290	0.016	0.164	-0.550	-0.338	0.000
-0.290	0.016	0.230	-0.498	-0.342	0.005
-0.290	0.213	0.011	-0.479	-0.199	0.003
-0.290	0.213	0.033	-0.496	-0.169	0.005
-0.290	0.213	0.098	-0.519	-0.175	0.007
-0.290	0.213	0.164	-0.510	-0.221	0.003
-0.290	0.213	0.230	-0.475	-0.271	0.002
-0.290	0.442	0.011	-0.314	-0.019	0.002
-0.290	0.442	0.033	-0.412	-0.128	0.004
-0.290	0.442	0.098	-0.442	-0.112	0.008
-0.290	0.442	0.164	-0.457	-0.123	0.008
-0.290	0.442	0.230	-0.437	-0.129	0.004

X/B	Y/B	Z/B	U (m/s)	V (m/s)	W (m/s)
-0.290	0.672	0.011	-0.353	-0.110	0.001
-0.290	0.672	0.033	-0.442	-0.117	0.003
-0.290	0.672	0.098	-0.468	-0.104	0.013
-0.290	0.672	0.164	-0.461	-0.086	0.012
-0.290	0.672	0.230	-0.414	-0.074	0.009
-0.290	0.902	0.011	-0.277	-0.053	0.001
-0.290	0.902	0.033	-0.370	-0.043	0.002
-0.290	0.902	0.098	-0.411	-0.043	0.018
-0.290	0.902	0.164	-0.434	-0.033	0.020
-0.290	0.902	0.230	-0.384	-0.039	0.014
-0.800	0.016	0.011	-0.065	-0.321	0.000
-0.800	0.016	0.033	-0.097	-0.356	0.003
-0.800	0.016	0.098	-0.228	-0.345	0.021
-0.800	0.016	0.164	-0.217	-0.336	0.021
-0.800	0.016	0.230	-0.199	-0.338	0.019
-0.800	0.213	0.011	-0.180	-0.255	0.001
-0.800	0.213	0.033	-0.235	-0.266	0.003
-0.800	0.213	0.098	-0.284	-0.257	0.022
-0.800	0.213	0.164	-0.277	-0.237	0.024
-0.800	0.213	0.230	-0.272	-0.227	0.021
-0.800	0.442	0.011	-0.280	0.000	-0.001
-0.800	0.442	0.033	-0.317	-0.199	-0.001
-0.800	0.442	0.098	-0.346	-0.182	0.016
-0.800	0.442	0.164	-0.322	-0.171	0.021
-0.800	0.442	0.230	-0.266	-0.174	0.017
-0.800	0.672	0.011	-0.219	-0.106	0.000
-0.800	0.672	0.033	-0.308	-0.115	0.000
-0.800	0.672	0.098	-0.387	-0.119	0.007
-0.800	0.672	0.164	-0.361	-0.111	0.016
-0.800	0.672	0.230	-0.243	-0.109	0.014

Table 9.9 Velocity data for dividing flows in open channels ($Q_r = 0.672$, continued)

X/B	Y/B	Z/B	U (m/s)	V (m/s)	W (m/s)
-0.800	0.902	0.011	0.017	-0.023	-0.002
-0.800	0.902	0.033	-0.030	-0.049	-0.003
-0.800	0.902	0.098	-0.112	-0.035	-0.003
-0.800	0.902	0.164	-0.213	-0.022	0.003
-0.800	0.902	0.230	-0.135	-0.037	0.004
-1.040	0.016	0.011	0.052	-0.005	-0.016
-1.040	0.016	0.033	-0.053	-0.115	-0.025
-1.040	0.016	0.098	-0.043	-0.089	-0.052
-1.040	0.016	0.164	0.000	0.000	-0.022
-1.040	0.016	0.230	-0.080	-0.067	-0.008
-1.040	0.213	0.011	-0.152	-0.132	0.002
-1.040	0.213	0.033	-0.205	-0.168	0.002
-1.040	0.213	0.098	-0.240	-0.163	0.000
-1.040	0.213	0.164	-0.216	-0.160	0.007
-1.040	0.213	0.230	-0.163	-0.128	0.009
-1.040	0.442	0.011	-0.273	-0.030	-0.002
-1.040	0.442	0.033	-0.158	-0.112	-0.002
-1.040	0.442	0.098	-0.295	-0.161	-0.001
-1.040	0.442	0.164	-0.249	-0.145	0.008
-1.040	0.442	0.230	-0.224	-0.133	0.008
-1.040	0.672	0.011	0.002	-0.002	-0.001
-1.040	0.672	0.033	-0.167	-0.106	-0.002
-1.040	0.672	0.098	-0.268	-0.102	-0.004
-1.040	0.672	0.164	-0.326	-0.090	-0.001
-1.040	0.672	0.230	-0.299	-0.094	0.001
-1.040	0.902	0.011	-0.004	0.011	-0.008
-1.040	0.902	0.033	0.042	-0.021	-0.012
-1.040	0.902	0.098	-0.031	0.008	-0.024
-1.040	0.902	0.164	-0.063	0.002	-0.018
-1.040	0.902	0.230	-0.016	-0.020	-0.012

X/B	Y/B	Z/B	U (m/s)	V (m/s)	W (m/s)
-1.700	0.098	0.011	-0.265	0.062	-0.011
-1.700	0.098	0.033	-0.270	0.017	-0.017
-1.700	0.098	0.098	-0.297	-0.045	-0.040
-1.700	0.098	0.164	-0.287	-0.026	-0.030
-1.700	0.098	0.230	-0.262	0.034	-0.020
-1.700	0.213	0.011	-0.243	0.074	-0.003
-1.700	0.213	0.033	-0.251	0.043	-0.005
-1.700	0.213	0.098	-0.320	-0.047	-0.015
-1.700	0.213	0.164	-0.276	-0.054	-0.014
-1.700	0.213	0.230	-0.229	0.022	-0.010
-1.700	0.442	0.011	-0.235	-0.006	0.002
-1.700	0.442	0.033	-0.254	-0.026	0.003
-1.700	0.442	0.098	-0.295	-0.019	0.002
-1.700	0.442	0.164	-0.289	-0.028	-0.001
-1.700	0.442	0.230	-0.257	-0.009	-0.001
-1.700	0.672	0.011	-0.107	0.018	0.000
-1.700	0.672	0.033	-0.114	0.003	0.000
-1.700	0.672	0.098	-0.057	-0.020	-0.002
-1.700	0.672	0.164	-0.127	-0.001	-0.002
-1.700	0.672	0.230	-0.179	0.007	-0.002
-1.700	0.902	0.011	0.093	-0.012	0.000
-1.700	0.902	0.033	0.084	-0.023	0.000
-1.700	0.902	0.098	0.051	-0.008	0.000
-1.700	0.902	0.164	0.084	0.011	-0.001
-1.700	0.902	0.230	-0.018	0.004	0.000
-3.000	0.098	0.011	-0.296	0.025	-0.004
-3.000	0.098	0.033	-0.293	0.024	-0.006
-3.000	0.098	0.098	-0.275	-0.005	-0.013
-3.000	0.098	0.164	-0.271	0.000	-0.009
-3.000	0.098	0.230	-0.291	0.020	-0.006

Table 9.9 Velocity data for dividing flows in open channels ($Q_r = 0.672$, continued)

X/B	Y/B	Z/B	U (m/s)	V (m/s)	W (m/s)
-3.000	0.213	0.011	-0.239	0.024	-0.001
-3.000	0.213	0.033	-0.270	0.022	-0.001
-3.000	0.213	0.098	-0.261	0.002	-0.003
-3.000	0.213	0.164	-0.284	-0.003	-0.002
-3.000	0.213	0.230	-0.270	0.020	-0.001
-3.000	0.442	0.011	-0.146	-0.027	0.001
-3.000	0.442	0.033	-0.204	0.012	0.001
-3.000	0.442	0.098	-0.199	0.011	0.003
-3.000	0.442	0.164	-0.223	0.035	0.002
-3.000	0.442	0.230	-0.193	-0.053	0.001
-3.000	0.672	0.011	-0.082	0.020	0.001
-3.000	0.672	0.033	-0.098	0.028	0.002
-3.000	0.672	0.098	-0.097	0.007	0.003
-3.000	0.672	0.164	-0.114	0.024	0.002
-3.000	0.672	0.230	-0.122	0.040	0.002
-3.000	0.902	0.011	0.097	-0.017	0.001
-3.000	0.902	0.033	0.030	-0.022	0.002
-3.000	0.902	0.098	-0.006	0.052	0.003
-3.000	0.902	0.164	-0.003	0.038	0.001
-3.000	0.902	0.230	0.052	0.001	0.001
-0.098	-0.030	0.011	-0.209	-0.099	-0.003
-0.098	-0.030	0.033	-0.288	-0.132	-0.006
-0.098	-0.030	0.098	-0.192	-0.068	-0.023
-0.098	-0.030	0.164	-0.192	-0.068	-0.032
-0.098	-0.030	0.219	-0.178	-0.007	-0.003
-0.328	-0.030	0.011	-0.438	-0.365	0.008
-0.328	-0.030	0.033	-0.440	-0.363	0.013
-0.328	-0.030	0.098	-0.498	-0.364	0.016
-0.328	-0.030	0.164	-0.472	-0.379	0.019
-0.328	-0.030	0.219	-0.430	-0.384	0.026

X/B	Y/B	Z/B	U (m/s)	V (m/s)	W (m/s)
-0.443	-0.030	0.011	-0.196	-0.393	0.009
-0.443	-0.030	0.033	-0.304	-0.375	0.014
-0.443	-0.030	0.098	-0.352	-0.374	0.024
-0.443	-0.030	0.164	-0.309	-0.403	0.026
-0.443	-0.030	0.219	-0.284	-0.414	0.032
-0.558	-0.030	0.011	-0.338	-0.381	0.009
-0.558	-0.030	0.033	-0.418	-0.374	0.015
-0.558	-0.030	0.098	-0.417	-0.385	0.028
-0.558	-0.030	0.164	-0.373	-0.410	0.028
-0.558	-0.030	0.219	-0.354	-0.426	0.028
-0.787	-0.030	0.011	-0.053	-0.400	-0.003
-0.787	-0.030	0.033	-0.116	-0.402	-0.001
-0.787	-0.030	0.098	-0.190	-0.381	0.012
-0.787	-0.030	0.164	-0.192	-0.386	0.009
-0.787	-0.030	0.219	-0.165	-0.372	0.009
-0.902	-0.030	0.011	0.010	-0.406	-0.009
-0.902	-0.030	0.033	-0.087	-0.402	-0.015
-0.902	-0.030	0.098	-0.114	-0.396	-0.026
-0.902	-0.030	0.164	-0.119	-0.390	-0.013
-0.902	-0.030	0.219	-0.108	-0.388	0.003
-0.098	-0.290	0.011	0.014	0.022	-0.001
-0.098	-0.290	0.033	0.011	0.010	-0.002
-0.098	-0.290	0.098	-0.032	0.052	-0.007
-0.098	-0.290	0.164	-0.023	0.065	-0.005
-0.098	-0.290	0.230	-0.004	0.032	0.002
-0.328	-0.290	0.011	-0.040	-0.040	0.016
-0.328	-0.290	0.033	-0.117	-0.240	0.022
-0.328	-0.290	0.098	-0.089	-0.130	0.027
-0.328	-0.290	0.164	-0.059	-0.021	0.013
-0.328	-0.290	0.219	-0.045	-0.089	-0.003

Table 9.9 Velocity data for dividing flows in open channels (Q_r = 0.672, continued)

X/B	Y/B	Z/B	U (m/s)	V (m/s)	W (m/s)
-0.443	-0.290	0.011	-0.180	-0.491	0.020
-0.443	-0.290	0.033	-0.350	-0.448	0.029
-0.443	-0.290	0.098	-0.336	-0.479	0.033
-0.443	-0.290	0.164	-0.330	-0.456	0.015
-0.443	-0.290	0.219	-0.300	-0.405	-0.004
-0.558	-0.290	0.011	-0.036	-0.456	0.018
-0.558	-0.290	0.033	-0.285	-0.488	0.029
-0.558	-0.290	0.098	-0.301	-0.499	0.033
-0.558	-0.290	0.164	-0.223	-0.497	0.016
-0.558	-0.290	0.219	-0.244	-0.428	0.000
-0.787	-0.290	0.011	0.027	-0.484	-0.009
-0.787	-0.290	0.033	-0.072	-0.487	-0.014
-0.787	-0.290	0.098	-0.190	-0.491	-0.020
-0.787	-0.290	0.164	-0.156	-0.498	-0.025
-0.787	-0.290	0.219	-0.087	-0.501	-0.025
-0.902	-0.290	0.011	0.036	-0.483	-0.024
-0.902	-0.290	0.033	-0.030	-0.494	-0.038
-0.902	-0.290	0.098	-0.109	-0.496	-0.072
-0.902	-0.290	0.164	-0.109	-0.499	-0.059
-0.902	-0.290	0.219	-0.065	-0.447	-0.047
-0.098	-0.730	0.011	0.026	0.031	-0.001
-0.098	-0.730	0.033	0.046	0.076	-0.002
-0.098	-0.730	0.098	-0.027	0.106	-0.004
-0.098	-0.730	0.164	-0.032	0.151	-0.003
-0.098	-0.730	0.219	-0.020	0.117	-0.001
-0.328	-0.730	0.011	0.063	-0.211	0.001
-0.328	-0.730	0.033	0.061	-0.160	0.001
-0.328	-0.730	0.098	-0.068	0.036	-0.002
-0.328	-0.730	0.164	-0.075	0.042	-0.002
-0.328	-0.730	0.219	-0.004	0.008	-0.001

X/B	Y/B	Z/B	U (m/s)	V (m/s)	W (m/s)
-0.443	-0.730	0.011	0.052	-0.409	0.021
-0.443	-0.730	0.033	-0.024	-0.383	0.029
-0.443	-0.730	0.098	-0.036	-0.262	0.015
-0.443	-0.730	0.164	-0.020	-0.309	0.004
-0.443	-0.730	0.219	0.001	-0.238	-0.003
-0.558	-0.730	0.011	0.120	-0.487	0.007
-0.558	-0.730	0.033	-0.021	-0.476	0.013
-0.558	-0.730	0.098	-0.150	-0.429	0.022
-0.558	-0.730	0.164	-0.186	-0.435	0.005
-0.558	-0.730	0.219	-0.064	-0.432	-0.010
-0.787	-0.730	0.011	0.116	-0.495	-0.011
-0.787	-0.730	0.033	-0.090	-0.493	-0.017
-0.787	-0.730	0.098	-0.090	-0.492	-0.027
-0.787	-0.730	1.640	-0.090	-0.499	-0.021
-0.787	-0.730	0.219	-0.090	-0.481	-0.016
-0.902	-0.730	0.011	-0.090	-0.490	-0.018
-0.902	-0.730	0.033	-0.090	-0.509	-0.029
-0.902	-0.730	0.098	-0.090	-0.505	-0.054
-0.902	-0.730	0.164	-0.090	-0.506	-0.036
-0.902	-0.730	0.219	-0.090	-0.484	-0.020
-0.098	-1.250	0.011	0.066	0.107	-0.002
-0.098	-1.250	0.033	0.077	0.090	-0.003
-0.098	-1.250	0.098	-0.002	0.171	-0.008
-0.098	-1.250	0.164	-0.028	0.188	-0.006
-0.098	-1.250	0.219	-0.006	0.133	-0.001
-0.328	-1.250	0.011	0.049	-0.232	0.009
-0.328	-1.250	0.033	0.098	-0.241	0.012
-0.328	-1.250	0.098	-0.067	-0.114	0.002
-0.328	-1.250	0.164	-0.018	-0.043	0.000
-0.328	-1.250	0.219	0.034	-0.083	0.000

Table 9.9 Velocity data for dividing flows in open channels (Q_r = 0.672, continued)

X/B	Y/B	Z/B	U (m/s)	V (m/s)	W (m/s)
-0.443	-1.250	0.011	0.056	-0.368	0.009
-0.443	-1.250	0.033	0.060	-0.373	0.014
-0.443	-1.250	0.098	-0.031	-0.291	0.009
-0.443	-1.250	0.164	-0.026	-0.287	0.002
-0.443	-1.250	0.219	0.026	-0.250	0.000
-0.558	-1.250	0.011	0.067	-0.427	0.001
-0.558	-1.250	0.033	-0.039	-0.444	0.002
-0.558	-1.250	0.098	-0.088	-0.409	0.008
-0.558	-1.250	0.164	-0.107	-0.378	0.002
-0.558	-1.250	0.219	-0.022	-0.361	-0.001
-0.787	-1.250	0.011	0.120	-0.487	-0.007
-0.787	-1.250	0.033	0.120	-0.493	-0.011
-0.787	-1.250	0.098	0.120	-0.491	-0.020
-0.787	-1.250	0.164	0.120	-0.493	-0.011
-0.787	-1.250	0.219	0.120	-0.477	-0.004
-0.902	-1.250	0.011	0.120	-0.497	-0.011
-0.902	-1.250	0.033	0.120	-0.507	-0.017
-0.902	-1.250	0.098	0.120	-0.512	-0.032
-0.902	-1.250	0.164	0.120	-0.509	-0.019
-0.902	-1.250	0.219	0.120	-0.490	-0.006
-0.098	-1.620	0.011	0.031	0.143	-0.002
-0.098	-1.620	0.033	0.059	0.118	-0.003
-0.098	-1.620	0.098	-0.009	0.188	-0.007
-0.098	-1.620	0.164	-0.029	0.210	-0.006
-0.098	-1.620	0.219	-0.008	0.144	-0.003
-0.328	-1.620	0.011	0.036	-0.197	0.007
-0.328	-1.620	0.033	0.083	-0.227	0.011
-0.328	-1.620	0.098	-0.027	-0.159	0.005
-0.328	-1.620	0.164	0.016	-0.080	0.001
-0.328	-1.620	0.219	0.030	-0.088	0.001

X/B	Y/B	Z/B	U (m/s)	V (m/s)	W (m/s)
-0.443	-1.620	0.011	0.000	-0.368	0.005
-0.443	-1.620	0.033	0.025	-0.384	0.009
-0.443	-1.620	0.098	-0.002	-0.351	0.008
-0.443	-1.620	0.164	-0.020	-0.287	0.003
-0.443	-1.620	0.219	-0.002	-0.273	0.002
-0.558	-1.620	0.011	0.007	-0.428	0.000
-0.558	-1.620	0.033	-0.012	-0.461	0.000
-0.558	-1.620	0.098	-0.063	-0.429	0.005
-0.558	-1.620	0.164	-0.090	-0.427	0.003
-0.558	-1.620	0.219	-0.053	-0.352	0.003
-0.787	-1.620	0.011	0.042	-0.499	-0.005
-0.787	-1.620	0.033	0.042	-0.501	-0.009
-0.787	-1.620	0.098	0.042	-0.510	-0.015
-0.787	-1.620	0.164	0.042	-0.503	-0.005
-0.787	-1.620	0.219	0.042	-0.492	0.003
-0.902	-1.620	0.011	0.042	-0.499	-0.008
-0.902	-1.620	0.033	0.042	-0.501	-0.013
-0.902	-1.620	0.098	0.042	-0.510	-0.024
-0.902	-1.620	0.164	0.042	-0.503	-0.011
-0.902	-1.620	0.219	0.042	-0.492	0.001
-0.098	-2.500	0.011	0.000	0.038	0.005
-0.098	-2.500	0.033	0.016	0.078	0.008
-0.098	-2.500	0.098	0.007	0.065	0.012
-0.098	-2.500	0.164	0.009	0.089	0.006
-0.098	-2.500	0.219	0.023	0.077	-0.002
-0.328	-2.500	0.011	0.021	-0.203	0.003
-0.328	-2.500	0.033	0.021	-0.203	0.005
-0.328	-2.500	0.098	0.021	-0.203	0.007
-0.328	-2.500	0.164	0.021	-0.203	0.003
-0.328	-2.500	0.219	0.021	-0.203	0.000

Table 9.9 Velocity data for dividing flows in open channels ($Q_r = 0.672$, continued)

X/B	Y/B	Z/B	U (m/s)	V (m/s)	W (m/s)
-0.443	-2.500	0.011	0.034	-0.353	0.001
-0.443	-2.500	0.033	0.034	-0.353	0.003
-0.443	-2.500	0.098	0.057	-0.366	0.007
-0.443	-2.500	0.164	0.016	-0.312	0.004
-0.443	-2.500	0.219	0.001	-0.244	0.001
-0.558	-2.500	0.011	-0.001	-0.410	0.000
-0.558	-2.500	0.033	-0.001	-0.410	0.000
-0.558	-2.500	0.098	0.033	-0.426	0.005
-0.558	-2.500	0.164	-0.007	-0.424	0.004
-0.558	-2.500	0.219	-0.007	-0.424	0.003
-0.787	-2.500	0.011	-0.084	-0.483	-0.002
-0.787	-2.500	0.033	-0.084	-0.483	-0.004
-0.787	-2.500	0.098	-0.058	-0.486	-0.006
-0.787	-2.500	0.164	-0.058	-0.486	0.000
-0.787	-2.500	0.219	-0.058	-0.486	0.006
-0.902	-2.500	0.011	-0.058	-0.486	-0.004
-0.902	-2.500	0.033	-0.058	-0.486	-0.007
-0.902	-2.500	0.098	-0.058	-0.486	-0.011
-0.902	-2.500	0.164	-0.058	-0.486	-0.002
-0.902	-2.500	0.219	-0.058	-0.486	0.007

Table 9.10 Water surface profiles for dividing flows in open channels ($Q_r = 0.838$)

X/B	Y/B	Z/B	X/B	Y/B	Z/B	X/B	Y/B	Z/B	X/B	Y/B	Z/B
0.934	0.016	0.311	-0.344	0.016	0.306	-1.148	0.016	0.326	-1.148	0.016	0.326
0.934	0.098	0.308	-0.344	0.098	0.311	-1.148	0.098	0.325	-1.148	0.098	0.325
0.934	0.213	0.309	-0.344	0.213	0.316	-1.148	0.213	0.321	-1.148	0.213	0.321
0.934	0.328	0.309	-0.344	0.328	0.320	-1.148	0.328	0.320	-1.148	0.328	0.320
0.934	0.443	0.307	-0.344	0.443	0.322	-1.148	0.443	0.321	-1.148	0.443	0.321
0.934	0.557	0.311	-0.344	0.557	0.324	-1.148	0.557	0.320	-1.148	0.557	0.320
0.934	0.672	0.309	-0.344	0.672	0.325	-1.148	0.672	0.320	-1.148	0.672	0.320
0.934	0.787	0.308	-0.344	0.787	0.327	-1.148	0.787	0.318	-1.148	0.787	0.318
0.934	0.902	0.308	-0.344	0.902	0.327	-1.148	0.902	0.320	-1.148	0.902	0.320
0.934	0.984	0.307	-0.344	0.984	0.327	-1.148	0.984	0.318	-1.148	0.984	0.318
0.164	0.016	0.312	-0.639	0.016	0.318	-1.672	0.016	0.322	-1.672	0.016	0.322
0.164	0.098	0.311	-0.639	0.098	0.322	-1.672	0.098	0.322	-1.672	0.098	0.322
0.164	0.213	0.314	-0.639	0.213	0.324	-1.672	0.213	0.319	-1.672	0.213	0.319
0.164	0.328	0.314	-0.639	0.328	0.324	-1.672	0.328	0.320	-1.672	0.328	0.320
0.164	0.443	0.316	-0.639	0.443	0.326	-1.672	0.443	0.319	-1.672	0.443	0.319
0.164	0.557	0.318	-0.639	0.557	0.327	-1.672	0.557	0.319	-1.672	0.557	0.319
0.164	0.672	0.319	-0.639	0.672	0.327	-1.672	0.672	0.316	-1.672	0.672	0.316
0.164	0.787	0.319	-0.639	0.787	0.328	-1.672	0.787	0.319	-1.672	0.787	0.319
0.164	0.902	0.321	-0.639	0.902	0.328	-1.672	0.902	0.319	-1.672	0.902	0.319
0.164	0.984	0.322	-0.639	0.984	0.329	-1.672	0.984	0.320	-1.672	0.984	0.320
-0.066	0.016	0.286	-0.934	0.016	0.321	-2.213	0.016	0.320	-2.213	0.016	0.320
-0.066	0.098	0.305	-0.934	0.098	0.328	-2.213	0.098	0.323	-2.213	0.098	0.323
-0.066	0.213	0.311	-0.934	0.213	0.327	-2.213	0.213	0.324	-2.213	0.213	0.324
-0.066	0.328	0.314	-0.934	0.328	0.327	-2.213	0.328	0.326	-2.213	0.328	0.326
-0.066	0.443	0.319	-0.934	0.443	0.327	-2.213	0.443	0.326	-2.213	0.443	0.326
-0.066	0.557	0.320	-0.934	0.557	0.328	-2.213	0.557	0.324	-2.213	0.557	0.324
-0.066	0.672	0.321	-0.934	0.672	0.329	-2.213	0.672	0.323	-2.213	0.672	0.323
-0.066	0.787	0.322	-0.934	0.787	0.328	-2.213	0.787	0.324	-2.213	0.787	0.324
-0.066	0.902	0.323	-0.934	0.902	0.328	-2.213	0.902	0.323	-2.213	0.902	0.323
-0.066	0.984	0.323	-0.934	0.984	0.328	-2.213	0.984	0.324	-2.213	0.984	0.324

Table 9.10 Water surface profiles for dividing flows in open channels ($Q_r = 0.838$, continued)

X/B	Y/B	Z/B
-0.016	-0.311	0.278
-0.098	-0.311	0.277
-0.213	-0.311	0.278
-0.328	-0.311	0.280
-0.443	-0.311	0.291
-0.557	-0.311	0.292
-0.672	-0.311	0.296
-0.787	-0.311	0.297
-0.902	-0.311	0.298
-0.984	-0.311	0.303
-0.016	-0.705	0.278
-0.098	-0.705	0.277
-0.213	-0.705	0.280
-0.328	-0.705	0.279
-0.443	-0.705	0.281
-0.557	-0.705	0.283
-0.672	-0.705	0.284
-0.787	-0.705	0.281
-0.902	-0.705	0.282
-0.984	-0.705	0.285
-0.016	-0.902	0.282
-0.098	-0.902	0.278
-0.213	-0.902	0.275
-0.328	-0.902	0.279
-0.443	-0.902	0.276
-0.557	-0.902	0.280
-0.672	-0.902	0.280
-0.787	-0.902	0.280
-0.902	-0.902	0.283
-0.984	-0.902	0.283

X/B	Y/B	Z/B
-0.016	-1.230	0.280
-0.098	-1.230	0.279
-0.213	-1.230	0.280
-0.328	-1.230	0.278
-0.443	-1.230	0.282
-0.557	-1.230	0.282
-0.672	-1.230	0.280
-0.787	-1.230	0.280
-0.902	-1.230	0.279
-0.984	-1.230	0.282
-0.016	-1.607	0.284
-0.098	-1.607	0.284
-0.213	-1.607	0.280
-0.328	-1.607	0.281
-0.443	-1.607	0.284
-0.557	-1.607	0.282
-0.672	-1.607	0.281
-0.787	-1.607	0.280
-0.902	-1.607	0.279
-0.984	-1.607	0.280
-0.016	-2.000	0.286
-0.098	-2.000	0.286
-0.213	-2.000	0.286
-0.328	-2.000	0.287
-0.443	-2.000	0.285
-0.557	-2.000	0.286
-0.672	-2.000	0.284
-0.787	-2.000	0.283
-0.902	-2.000	0.285
-0.984	-2.000	0.286

X/B	Y/B	Z/B
-0.016	-2.541	0.293
-0.098	-2.541	0.295
-0.213	-2.541	0.294
-0.328	-2.541	0.280
-0.443	-2.541	0.295
-0.557	-2.541	0.292
-0.672	-2.541	0.293
-0.787	-2.541	0.291
-0.902	-2.541	0.293
-0.984	-2.541	0.294
-0.016	-3.000	0.298
-0.098	-3.000	0.297
-0.213	-3.000	0.298
-0.328	-3.000	0.294
-0.443	-3.000	0.297
-0.557	-3.000	0.298
-0.672	-3.000	0.296
-0.787	-3.000	0.295
-0.902	-3.000	0.294
-0.984	-3.000	0.297

Table 9.11 Velocity data for dividing flows in open channels ($Q_r = 0.838$)

X/B	Y/B	Z/B	U (m/s)	V (m/s)	W (m/s)
0.970	0.098	0.011	-0.406	0.013	0.000
0.970	0.098	0.033	-0.409	0.014	0.000
0.970	0.098	0.098	-0.432	0.008	0.000
0.970	0.098	0.164	-0.405	-0.007	0.000
0.970	0.098	0.229	-0.393	-0.012	0.000
0.970	0.213	0.011	-0.330	0.022	0.000
0.970	0.213	0.033	-0.409	0.031	0.000
0.970	0.213	0.098	-0.413	0.025	0.000
0.970	0.213	0.164	-0.393	0.006	0.000
0.970	0.213	0.229	-0.368	-0.025	0.000
0.970	0.443	0.011	-0.356	0.013	0.000
0.970	0.443	0.033	-0.408	0.026	0.000
0.970	0.443	0.098	-0.424	0.030	0.000
0.970	0.443	0.164	-0.411	0.004	0.000
0.970	0.443	0.229	-0.416	-0.028	0.000
0.970	0.672	0.011	-0.424	-0.021	0.000
0.970	0.672	0.033	-0.471	-0.024	0.000
0.970	0.672	0.098	-0.461	-0.008	0.000
0.970	0.672	0.164	-0.457	0.000	0.000
0.970	0.672	0.229	-0.446	0.010	0.000
0.970	0.902	0.011	-0.450	-0.020	0.000
0.970	0.902	0.033	-0.495	-0.010	0.000
0.970	0.902	0.098	-0.491	-0.008	0.000
0.970	0.902	0.164	-0.483	0.006	0.000
0.970	0.902	0.229	-0.458	0.020	0.000

X/B	Y/B	Z/B	U (m/s)	V (m/s)	W (m/s)
0.220	0.016	0.011	-0.408	-0.001	0.001
0.220	0.016	0.033	-0.412	0.001	0.000
0.220	0.016	0.098	-0.418	0.002	-0.001
0.220	0.016	0.164	-0.420	-0.001	-0.003
0.220	0.016	0.229	-0.412	-0.005	-0.005
0.220	0.213	0.011	-0.270	-0.003	0.000
0.220	0.213	0.033	-0.444	0.001	0.000
0.220	0.213	0.098	-0.450	-0.008	0.000
0.220	0.213	0.164	-0.443	-0.019	-0.002
0.220	0.213	0.229	-0.439	-0.059	-0.004
0.220	0.443	0.011	-0.093	-0.034	0.000
0.220	0.443	0.033	-0.388	-0.038	0.001
0.220	0.443	0.098	-0.428	-0.040	0.001
0.220	0.443	0.164	-0.426	-0.056	0.000
0.220	0.443	0.229	-0.426	-0.073	-0.001
0.220	0.672	0.011	-0.371	-0.059	0.001
0.220	0.672	0.033	-0.443	-0.056	0.001
0.220	0.672	0.098	-0.463	-0.044	0.002
0.220	0.672	0.164	-0.444	-0.034	0.002
0.220	0.672	0.229	-0.429	-0.020	0.002
0.220	0.902	0.011	-0.289	-0.014	0.002
0.220	0.902	0.033	-0.417	-0.020	0.005
0.220	0.902	0.098	-0.440	-0.018	0.007
0.220	0.902	0.164	-0.442	-0.007	0.007
0.220	0.902	0.229	-0.428	0.001	0.004

Table 9.11 Velocity data for dividing flows in open channels ($Q_r = 0.838$, continued)

X/B	Y/B	Z/B	U (m/s)	V (m/s)	W (m/s)
-0.040	0.016	0.011	-0.225	-0.028	0.013
-0.040	0.016	0.033	-0.605	-0.147	0.013
-0.040	0.016	0.098	-0.629	-0.147	0.010
-0.040	0.016	0.164	-0.623	-0.156	0.013
-0.040	0.016	0.229	-0.614	-0.157	0.074
-0.040	0.213	0.011	-0.393	-0.086	-0.021
-0.040	0.213	0.033	-0.455	-0.114	-0.021
-0.040	0.213	0.098	-0.470	-0.107	-0.016
-0.040	0.213	0.164	-0.467	-0.126	-0.010
-0.040	0.213	0.229	-0.459	-0.168	-0.002
-0.040	0.443	0.011	-0.273	-0.073	-0.027
-0.040	0.443	0.033	-0.364	-0.114	-0.027
-0.040	0.443	0.098	-0.412	-0.115	-0.029
-0.040	0.443	0.164	-0.414	-0.114	-0.023
-0.040	0.443	0.229	-0.410	-0.124	-0.009
-0.040	0.672	0.011	-0.323	-0.099	-0.015
-0.040	0.672	0.033	-0.401	-0.100	-0.015
-0.040	0.672	0.098	-0.429	-0.089	-0.021
-0.040	0.672	0.164	-0.409	-0.077	-0.017
-0.040	0.672	0.229	-0.394	-0.061	-0.005
-0.040	0.902	0.011	-0.264	-0.025	-0.003
-0.040	0.902	0.033	-0.354	-0.039	-0.003
-0.040	0.902	0.098	-0.389	-0.034	-0.020
-0.040	0.902	0.164	-0.388	-0.027	-0.017
-0.040	0.902	0.229	-0.359	-0.018	-0.019

X/B	Y/B	Z/B	U (m/s)	V (m/s)	W (m/s)
-0.290	0.016	0.011	-0.376	-0.338	0.006
-0.290	0.016	0.033	-0.437	-0.336	0.012
-0.290	0.016	0.098	-0.450	-0.337	0.016
-0.290	0.016	0.164	-0.445	-0.353	0.012
-0.290	0.016	0.229	-0.433	-0.007	0.006
-0.290	0.213	0.011	-0.295	-0.256	0.005
-0.290	0.213	0.033	-0.361	-0.212	0.010
-0.290	0.213	0.098	-0.415	-0.213	0.013
-0.290	0.213	0.164	-0.395	-0.233	0.010
-0.290	0.213	0.229	-0.404	-0.261	0.001
-0.290	0.443	0.011	-0.296	-0.193	0.003
-0.290	0.443	0.033	-0.340	-0.176	0.008
-0.290	0.443	0.098	-0.386	-0.166	0.013
-0.290	0.443	0.164	-0.385	-0.168	0.011
-0.290	0.443	0.229	-0.366	-0.162	0.005
-0.290	0.672	0.011	-0.295	-0.143	0.003
-0.290	0.672	0.033	-0.363	-0.127	0.008
-0.290	0.672	0.098	-0.405	-0.115	0.017
-0.290	0.672	0.164	-0.366	-0.110	0.015
-0.290	0.672	0.229	-0.344	-0.098	0.007
-0.290	0.902	0.011	-0.186	-0.042	0.002
-0.290	0.902	0.033	-0.203	-0.042	0.005
-0.290	0.902	0.098	-0.272	-0.068	0.006
-0.290	0.902	0.164	-0.298	-0.050	0.004
-0.290	0.902	0.229	-0.319	-0.035	0.000

Table 9.11 Velocity data for dividing flows in open channels ($Q_r = 0.838$, continued)

X/B	Y/B	Z/B	U (m/s)	V (m/s)	W (m/s)
-0.800	0.016	0.011	-0.044	-0.370	-0.006
-0.800	0.016	0.033	-0.053	-0.390	-0.006
-0.800	0.016	0.098	-0.174	-0.382	0.016
-0.800	0.016	0.164	-0.190	-0.380	0.002
-0.800	0.016	0.229	-0.128	-0.353	0.002
-0.800	0.213	0.011	-0.002	-0.247	0.001
-0.800	0.213	0.033	-0.158	-0.285	0.001
-0.800	0.213	0.098	-0.209	-0.287	-0.016
-0.800	0.213	0.164	-0.220	-0.273	0.026
-0.800	0.213	0.229	-0.225	-0.267	0.003
-0.800	0.443	0.011	-0.150	-0.221	-0.001
-0.800	0.443	0.033	-0.145	-0.221	-0.001
-0.800	0.443	0.098	-0.288	-0.220	-0.027
-0.800	0.443	0.164	-0.256	-0.213	-0.046
-0.800	0.443	0.229	-0.212	-0.189	-0.026
-0.800	0.672	0.011	-0.028	-0.092	0.003
-0.800	0.672	0.033	-0.046	-0.124	0.003
-0.800	0.672	0.098	-0.240	-0.121	-0.018
-0.800	0.672	0.164	-0.258	-0.137	-0.020
-0.800	0.672	0.229	-0.227	-0.122	-0.046
-0.800	0.902	0.011	0.081	-0.018	-0.017
-0.800	0.902	0.033	0.096	0.006	-0.017
-0.800	0.902	0.098	0.002	-0.014	-0.017
-0.800	0.902	0.164	-0.008	-0.001	0.011
-0.800	0.902	0.229	-0.074	-0.039	0.030

X/B	Y/B	Z/B	U (m/s)	V (m/s)	W (m/s)
-1.040	0.148	0.011	-0.025	-0.106	-0.013
-1.040	0.148	0.033	-0.103	-0.131	-0.029
-1.040	0.148	0.098	-0.177	-0.232	-0.061
-1.040	0.148	0.164	-0.165	-0.226	-0.057
-1.040	0.148	0.229	-0.142	-0.210	-0.012
-1.040	0.213	0.011	-0.036	-0.158	0.000
-1.040	0.213	0.033	-0.138	-0.195	-0.003
-1.040	0.213	0.098	-0.186	-0.213	-0.014
-1.040	0.213	0.164	-0.207	-0.217	-0.017
-1.040	0.213	0.229	-0.147	-0.200	-0.002
-1.040	0.443	0.011	-0.096	-0.144	-0.007
-1.040	0.443	0.033	-0.080	-0.156	-0.015
-1.040	0.443	0.098	-0.175	-0.147	-0.027
-1.040	0.443	0.164	-0.183	-0.160	-0.025
-1.040	0.443	0.229	-0.197	-0.166	-0.007
-1.040	0.672	0.011	-0.056	-0.054	-0.007
-1.040	0.672	0.033	-0.040	-0.038	-0.014
-1.040	0.672	0.098	-0.155	-0.090	-0.024
-1.040	0.672	0.164	-0.049	-0.089	-0.020
-1.040	0.672	0.229	-0.138	-0.060	-0.005
-1.040	0.902	0.011	0.070	-0.003	0.000
-1.040	0.902	0.033	0.067	-0.012	0.001
-1.040	0.902	0.098	0.066	0.001	0.001
-1.040	0.902	0.164	0.065	-0.003	0.000
-1.040	0.902	0.229	-0.052	-0.001	0.000

Table 9.11 Velocity data for dividing flows in open channels ($Q_r = 0.838$, continued)

X/B	Y/B	Z/B	U (m/s)	V (m/s)	W (m/s)
-1.700	0.098	0.011	-0.267	0.037	-0.009
-1.700	0.098	0.033	-0.223	0.032	-0.019
-1.700	0.098	0.098	-0.210	-0.033	-0.032
-1.700	0.098	0.164	-0.225	-0.034	-0.029
-1.700	0.098	0.229	-0.261	-0.032	-0.012
-1.700	0.213	0.011	-0.192	0.062	-0.001
-1.700	0.213	0.033	-0.192	0.015	-0.003
-1.700	0.213	0.098	-0.192	-0.034	-0.005
-1.700	0.213	0.164	-0.172	-0.048	-0.007
-1.700	0.213	0.229	-0.193	-0.042	-0.004
-1.700	0.443	0.011	-0.145	0.043	0.004
-1.700	0.443	0.033	-0.105	0.015	0.007
-1.700	0.443	0.098	-0.103	0.010	0.010
-1.700	0.443	0.164	-0.105	-0.003	0.008
-1.700	0.443	0.229	-0.178	-0.005	0.003
-1.700	0.672	0.011	-0.035	0.006	0.000
-1.700	0.672	0.033	0.007	0.021	0.000
-1.700	0.672	0.098	0.066	-0.035	0.001
-1.700	0.672	0.164	0.042	0.007	0.001
-1.700	0.672	0.229	-0.077	-0.043	0.000
-1.700	0.902	0.011	0.063	-0.019	0.001
-1.700	0.902	0.033	0.074	0.005	0.001
-1.700	0.902	0.098	0.088	-0.007	0.001
-1.700	0.902	0.164	0.087	0.000	0.001
-1.700	0.902	0.229	0.077	0.008	0.001

X/B	Y/B	Z/B	U (m/s)	V (m/s)	W (m/s)
-3.000	0.098	0.011	-0.240	0.010	-0.003
-3.000	0.098	0.033	-0.212	0.006	-0.005
-3.000	0.098	0.098	-0.197	-0.001	-0.009
-3.000	0.098	0.164	-0.186	0.001	-0.008
-3.000	0.098	0.229	-0.183	-0.003	-0.003
-3.000	0.213	0.011	-0.162	0.012	-0.001
-3.000	0.213	0.033	-0.191	0.027	-0.001
-3.000	0.213	0.098	-0.173	0.011	-0.001
-3.000	0.213	0.164	-0.139	-0.009	-0.001
-3.000	0.213	0.229	-0.159	-0.002	0.000
-3.000	0.443	0.011	-0.089	0.027	0.001
-3.000	0.443	0.033	-0.080	0.035	0.002
-3.000	0.443	0.098	-0.087	0.017	0.004
-3.000	0.443	0.164	-0.075	0.009	0.003
-3.000	0.443	0.229	-0.103	0.019	0.001
-3.000	0.672	0.011	-0.014	0.038	0.001
-3.000	0.672	0.033	0.056	0.005	0.001
-3.000	0.672	0.098	0.009	-0.013	0.002
-3.000	0.672	0.164	0.063	-0.035	0.001
-3.000	0.672	0.229	0.015	0.018	0.000
-3.000	0.902	0.011	0.069	-0.005	0.002
-3.000	0.902	0.033	0.072	-0.020	0.004
-3.000	0.902	0.098	0.030	0.011	0.007
-3.000	0.902	0.164	0.025	0.002	0.007
-3.000	0.902	0.229	0.053	0.004	0.003

Table 9.11 Velocity data for dividing flows in open channels ($Q_r = 0.838$, continued)

X/B	Y/B	Z/B	U (m/s)	V (m/s)	W (m/s)
-0.098	-0.290	0.011	-0.014	0.034	0.000
-0.098	-0.290	0.033	0.000	0.060	0.001
-0.098	-0.290	0.098	-0.025	0.070	0.002
-0.098	-0.290	0.164	-0.031	0.080	0.003
-0.098	-0.290	0.229	-0.014	0.060	0.002
-0.328	-0.290	0.011	-0.242	-0.339	0.019
-0.328	-0.290	0.033	-0.241	-0.319	0.032
-0.328	-0.290	0.098	-0.239	-0.307	0.034
-0.328	-0.290	0.164	-0.229	-0.287	0.022
-0.328	-0.290	0.229	-0.203	-0.240	-0.001
-0.557	-0.290	0.011	-0.105	-0.385	0.002
-0.557	-0.290	0.033	-0.217	-0.430	0.017
-0.557	-0.290	0.098	-0.242	-0.453	0.036
-0.557	-0.290	0.164	-0.208	-0.467	0.025
-0.557	-0.290	0.229	-0.171	-0.442	0.001
-0.787	-0.290	0.011	-0.060	-0.429	0.007
-0.787	-0.290	0.033	-0.054	-0.482	0.015
-0.787	-0.290	0.098	-0.175	-0.496	0.025
-0.787	-0.290	0.164	-0.173	-0.494	-0.025
-0.787	-0.290	0.229	-0.120	-0.469	-0.022
-0.902	-0.290	0.011	0.027	-0.466	0.021
-0.902	-0.290	0.033	0.082	-0.485	0.046
-0.902	-0.290	0.098	0.116	-0.505	0.083
-0.902	-0.290	0.164	0.111	-0.509	-0.074
-0.902	-0.290	0.229	0.086	-0.477	-0.039

X/B	Y/B	Z/B	U (m/s)	V (m/s)	W (m/s)
-0.098	-0.730	0.011	0.049	0.108	-0.003
-0.098	-0.730	0.033	0.079	0.137	-0.007
-0.098	-0.730	0.098	-0.030	0.165	-0.010
-0.098	-0.730	0.164	-0.083	0.170	-0.009
-0.098	-0.730	0.229	-0.044	0.180	0.000
-0.328	-0.730	0.011	0.057	-0.286	0.022
-0.328	-0.730	0.033	0.005	-0.296	0.033
-0.328	-0.730	0.098	-0.027	-0.247	0.026
-0.328	-0.730	0.164	-0.039	-0.227	0.014
-0.328	-0.730	0.229	-0.032	-0.180	0.002
-0.557	-0.730	0.011	-0.117	-0.472	0.002
-0.557	-0.730	0.033	-0.058	-0.487	0.006
-0.557	-0.730	0.098	-0.089	-0.468	0.027
-0.557	-0.730	0.164	-0.192	-0.464	0.021
-0.557	-0.730	0.229	-0.178	-0.411	-0.003
-0.787	-0.730	0.011	0.013	-0.412	0.009
-0.787	-0.730	0.033	0.100	-0.489	0.019
-0.787	-0.730	0.098	0.194	-0.490	0.034
-0.787	-0.730	0.164	0.194	-0.490	-0.027
-0.787	-0.730	0.229	-0.036	-0.429	-0.009
-0.902	-0.730	0.011	0.070	-0.442	0.018
-0.902	-0.730	0.033	0.070	-0.491	0.040
-0.902	-0.730	0.098	0.070	-0.502	0.068
-0.902	-0.730	0.164	0.070	-0.510	-0.056
-0.902	-0.730	0.229	0.070	-0.472	-0.015

Table 9.11 Velocity data for dividing flows in open channels ($Q_r = 0.838$, continued)

X/B	Y/B	Z/B	U (m/s)	V (m/s)	W (m/s)
-0.098	-1.250	0.011	0.055	0.090	0.006
-0.098	-1.250	0.033	0.029	0.107	0.012
-0.098	-1.250	0.098	-0.022	0.116	0.017
-0.098	-1.250	0.164	-0.048	0.123	-0.017
-0.098	-1.250	0.229	-0.038	0.131	-0.002
-0.328	-1.250	0.011	0.066	-0.286	0.009
-0.328	-1.250	0.033	0.090	-0.311	0.021
-0.328	-1.250	0.098	0.022	-0.260	0.020
-0.328	-1.250	0.164	-0.011	-0.212	0.007
-0.328	-1.250	0.229	-0.016	-0.190	0.015
-0.557	-1.250	0.011	0.075	-0.366	0.001
-0.557	-1.250	0.033	0.032	-0.420	0.003
-0.557	-1.250	0.098	-0.047	-0.453	0.012
-0.557	-1.250	0.164	-0.080	-0.459	0.013
-0.557	-1.250	0.229	-0.039	-0.408	0.005
-0.787	-1.250	0.011	0.056	-0.429	0.006
-0.787	-1.250	0.033	0.098	-0.482	0.015
-0.787	-1.250	0.098	0.098	-0.496	-0.026
-0.787	-1.250	0.164	-0.058	-0.494	-0.018
-0.787	-1.250	0.229	-0.026	-0.469	0.004
-0.902	-1.250	0.011	0.036	-0.466	0.012
-0.902	-1.250	0.033	0.036	-0.499	0.025
-0.902	-1.250	0.098	0.036	-0.505	-0.043
-0.902	-1.250	0.164	0.036	-0.509	-0.032
-0.902	-1.250	0.229	0.006	-0.477	-0.003

X/B	Y/B	Z/B	U (m/s)	V (m/s)	W (m/s)
-0.098	-1.620	0.011	0.037	-0.132	0.003
-0.098	-1.620	0.033	0.053	-0.102	0.004
-0.098	-1.620	0.098	-0.059	-0.065	0.003
-0.098	-1.620	0.164	-0.007	0.126	0.000
-0.098	-1.620	0.229	-0.015	0.163	-0.005
-0.328	-1.620	0.011	0.094	-0.303	0.004
-0.328	-1.620	0.033	0.078	-0.297	0.010
-0.328	-1.620	0.098	0.072	-0.270	0.012
-0.328	-1.620	0.164	-0.017	-0.239	-0.001
-0.328	-1.620	0.229	-0.028	-0.229	-0.004
-0.557	-1.620	0.011	0.053	-0.432	0.000
-0.557	-1.620	0.033	-0.054	-0.462	0.001
-0.557	-1.620	0.098	-0.034	-0.464	0.005
-0.557	-1.620	0.164	-0.070	-0.440	0.007
-0.557	-1.620	0.229	-0.095	-0.435	0.001
-0.787	-1.620	0.011	0.005	-0.401	-0.006
-0.787	-1.620	0.033	0.057	-0.497	-0.013
-0.787	-1.620	0.098	-0.038	-0.498	-0.024
-0.787	-1.620	0.164	-0.053	-0.506	-0.019
-0.787	-1.620	0.229	-0.018	-0.506	-0.004
-0.902	-1.620	0.011	0.013	-0.486	0.010
-0.902	-1.620	0.033	0.022	-0.506	0.021
-0.902	-1.620	0.098	-0.022	-0.506	-0.036
-0.902	-1.620	0.164	-0.022	-0.506	-0.030
-0.902	-1.620	0.229	-0.022	-0.506	-0.008

Table 9.11 Velocity data for dividing flows in open channels ($Q_r = 0.838$, continued)

X/B	Y/B	Z/B	U (m/s)	V (m/s)	W (m/s)
-0.098	-2.500	0.011	0.007	-0.220	0.012
-0.098	-2.500	0.033	0.035	-0.194	0.027
-0.098	-2.500	0.098	0.062	-0.172	0.045
-0.098	-2.500	0.164	0.064	-0.142	0.047
-0.098	-2.500	0.229	-0.045	-0.095	0.022
-0.328	-2.500	0.011	0.049	-0.309	0.000
-0.328	-2.500	0.033	0.081	-0.323	0.000
-0.328	-2.500	0.098	0.073	-0.345	0.002
-0.328	-2.500	0.164	-0.087	-0.349	-0.002
-0.328	-2.500	0.229	-0.067	-0.319	-0.003
-0.557	-2.500	0.011	0.007	-0.404	-0.001
-0.557	-2.500	0.033	0.052	-0.444	-0.002
-0.557	-2.500	0.098	0.044	-0.461	-0.002
-0.557	-2.500	0.164	0.030	-0.471	-0.001
-0.557	-2.500	0.229	0.018	-0.441	0.000
-0.787	-2.500	0.011	-0.001	-0.433	0.003
-0.787	-2.500	0.033	-0.005	-0.481	0.007
-0.787	-2.500	0.098	-0.003	-0.491	-0.014
-0.787	-2.500	0.164	-0.038	-0.496	-0.013
-0.787	-2.500	0.229	-0.038	-0.481	-0.003
-0.902	-2.500	0.011	0.004	-0.450	0.005
-0.902	-2.500	0.033	0.039	-0.492	0.012
-0.902	-2.500	0.098	0.029	-0.502	0.020
-0.902	-2.500	0.164	-0.044	-0.502	-0.017
-0.902	-2.500	0.229	-0.002	-0.482	-0.004